PRESSURE SHIFTS IN CARBON DIOXIDE AND ITS ISOTOPES

by

Kie L SooHoo

B.S. New Mexico State University
(1978)
B.S.EE New Mexico State University
(1978)

Submitted to the Department of
Nuclear Engineering
in Partial Fulfillment of the
Requirements of the
Degree of

DOCTOR OF PHILOSOPHY

at the

MASSACHUSETTS INSTITUTE OF TECHNOLOGY

January 1984

Signature of Author _____
Department of Nuclear Engineering

Certified by _____
Thesis Supervisor

Accepted by _____
Head PhD.Committee

PRESSURE SHIFTS IN CARBON DIOXIDE AND ITS ISOTOPES

by

KIE L SOOHOO

Submitted to the Department of Nuclear Engineering

in partial fulfillment of the requirements of the Degree of Doctor of Philosophy in Nuclear Engineering

ABSTRACT

The theory of pressure broadening and pressure shifts of emission and absorption lines has been developed over the years. Only recently has it been possible to use Doppler-free techniques to measure the linewidths and lineshifts within the resolution of the homogeneous linewidths. Pressure shifts in the 9 and 10 μm lasing transition in CO_2 is measured using a two channel 4.3μ saturated fluorescence stabilized CO_2 laser heterodyne system. These pressure shift measurements are unique because the J dependence and vibrational dependence (relating to the different Fermi resonances in the different CO_2 isotopes) can studied using this saturated fluorescence technique. They are also important in providing an estimate of the reproducibility of the many CO_2 lasing transitions for use as a secondary infrared frequency standard and for providing another bound on the uncertainty of several other 'absolute' measurements in which the CO_2 laser was another frequency source in the frequency chain.

Phase locked, frequency locked lineshape scans were also taken to determine the pressure broadening coefficient. Various power scans and fluorescence linescans were also taken to obtain estimates of the various laser linewidths, Doppler widths and other physical parameters of the system. The linewidths were fitted to a saturated absorption lineshape obtained from using a two level rate equation analysis. Existing offsets and shifts such as the recoil, transit time, curvature, and slope effects were calculated and minimized in order to obtain a true pressure shift. The major problem due to the background power slope, which gave a pressure squared error dependence, was effectively nulled and monitored in the experiment.

After all these corrections and adjustments, pressure shifts were taken over a wide range of J in the I and II bands for four different CO_2 isotopes and as a function of several perturbers including Xe, N_2, Ar, He, H_2 and CH_3F. The pressure shift measurements showed very little J dependence and practically no P or R dependence for all the isotopes. The measured shifts were less than 100 KHz/torr blue shifted at pressures less than 100 mtorr but appeared red shifted at pressures between 1 to 10 torr. In contrast, the traditional pressure broadening theory predicted a red shift based on the dephasing of the vibrational isotropic potentials due to the anharmonicities (Fermi resonance) in the lasing levels. The shifts taken with the perturber gases were blue, scaling approximately with their respective Van der Waals constants, except for He and H_2which yielded red shift data.

It turns out that another nonlinear pressure shift taken with HeNe stabilized on the CH_4 resonance were also blue shifted while being red shifted at very high pressures. Such similarities point to the possibility of velocity changing collisions in the low pressure Lamb dip experiments versus the standard phase changing collisions at the high pressure linear absorption measurements.

Thesis Supervisor: Herman A. Haus

Title: Professor of Electrical Engineering

The experimental portion of this
thesis was performed at MIT Lincoln Laboratory.
This project was supported by a
National Science Foundation
Research Grant and
a Graduate Fellowship.

ACKNOWLEDGEMENTS

ACKNOWLEDGEMENTS
Ratiocinations Cerebrations
COGITATIONS Ruminations
ξξψκινλ σηιτασσηρωε

The successful completion of this thesis can be partially attributed to several factors, both animate and inanimate, human and nonhuman, physical and psychological, all of which need further expatiation and some background material. Primordially, who, what, how, when and all those querulous adverbs concerning the initialization, formulation, evolution and now dismantling (demise?) of the thesis committee must be elucidated henceforth.

I unequivocally am enrolled in the Nuclear Engineering department at MIT. Instead of an indigenous thesis committee, the primary members of this 'exotic' band included Herman A. Haus from the EE department, John E. Thomas initially from Aero and Astro but now from the MIT Spectroscopy Lab, and Charles Freed from MIT Lincoln Laboratory; S.H. Chen was the official reader from the Nuclear Engineering department. Of course, I was the cynosure of every 'board of inquiry' that expired of which

all official extant transcripts have been fumigated and excoriated. Thus the need for this section.

I would like to thank Herman Haus, the thesis advisor for all his patience and unrequited tolerance; from his past experiences, it always seemed he knew what the next step was (ie. finish the thesis) and always pushed for the correct thing to do in the maze of red tape. I would like to thank Charles Freed, who was willing, to the ineffable astonishment of all, to undertake such a tyro, buffoon as I and attempted to transmigrate the bumpkinlike troglodyte, while exercising his paternal congenial coercion (subliminal intimation), to some semblance of a graduated graduate. Charlie somehow always seemed to have the "right stuff" (sometimes even brand new) or else through subtle means of persuasion, justified long term interminable borrowing (in a jovial mendicant, mendacious, prevaricating sort of way) to replace any dilapidated, moribund, or defunct extant equipment. This, of course, included all the power supplies, dewars, glass tubes, etc. ad nauseum, that inexplicably blew up, malfunctioned or deformed and lost its structural embodiment in an unfathomable, eldritch sort of way, expedited by a lack of sleight of hand or presdigitation or a surfeit of gaucheness.

Special mention should be made of John Thomas since this will be the only unofficial MIT record of his 'collusion'. He served as the laison between the experimental and theoretical portions of this project and was a special boon in the sense he had worked on a similar project for his graduate thesis work (CO_2 laser setup) and hence knew many of the pitfalls and dangers that were gratis for the novice. He was especially aghasted and petrified (or was it disbelieving) when I supplicated to be his first thesis employer (ie. on his first committee) for free. It should be noted that he also applied himself to the collision theory portion of the problem and henceforth alleviated much of the tribulations that could have precipitated. It must be added post mortem that all three committee members perused this thesis, a magnaminous gesture unheard of in the annuals of MIT thesis committee insignifica.+

There were several other people who alleviated, and assuaged the termination of this thesis; these people

---

+Though this endeavor, almost all semantic and typographical errors were corrected so the ultmost in orthography and calligraphy was achieved; any subsequent error can be attributed to a cybernetic malfunction due to exceeding the input buffer capacity, commonly known as a computer error.

exemplified that banal syllogism: a tech in need is a tech indeed. First Robert O'Donnell contributed his expertise in the CO_2 laser lab and provided the initial instruction and technique in how the original measurements were taken. Later on, Joe Bielinski supplied his talents to the problem along with his millenium of precaution, safety procedures and implementations as a concerned lifesaver. A foremost example or gesture of his concern revolved around his obtaining a flat 1.5" x 6'x2.5' piece of polyvinyl which prevented any nocturnal somnambulant activity and presented a means to a end of the all night stands.

There were also several other people who gave exemplary assistance when needed. Foremost among these was Richard Brower who contributed immensely in terms of the lockin system and a newly designed servo electronic feedback system. I have to apologize in the sense of my harassment or imitation of a termigant, harrigan or shrew in the quest to obtain an operational servo system before the commencement date. But such is the behavior of mice and men and also desperate, obsequious, ingratiating, genuflecting and transmogrified graduate students. In the end, after all that G-Student brutality (technical assistance) ad infinitum, Brower delivered a well engineered operational

system whose specs provided enough confidence in the subsequent measurements to ignore drift or DC offset errors.

I would also like to thank Timothy Stephens for providing the lockbox used in the linescan measurements. He had also helped to adapt his box to lock our system by "waving his wand and sprinkling some electrical water over the system" * I would also like to thank Walter Belanger for spending several days helping me with some printed circuit board work. I am grateful to the PAR representative who let me play with the 5301 microprocessor controlled lockin; Figures 54 and 55 were made possible using this phase tracking lockin. I would also like to thank the other participating members of the thesis defense committee, especially those I had asked for overnight service (Perusal not Federal); these included Michael Feld and David Pritchard from the Physics department and Alan Nelson from the Nuclear Engineering department.

I would like to express my thanks to my parents for the inordinate amount of patience they have shown throughout and for allowing me come to MIT away from the doting umbrage or domicile control. Thanks for believing it was the machine at

---

* Heard while inadvertently eavesdropping on an unknown lab employee

fault(what machine?), it broke down(another years delay), again, it don't work (what, again?), when are your going to finish (lets shoot for next June), you said that last year (things just drag on and on), are you coming home for Christmas(I got to finish), you're partying too much (I know, I know), etc.

I would like to thank all the other inanimate, known or unbeknownst to me, who have made this thesis possible. As it turns out, this is the time to elucidate and evaluate a lot of the experiences that has expired. The diurnal and nocturnal part of this thesis was done at Lincoln Labs; there was the best of everything, supplies, lasers and access to almost anything. Special thanks goes to Charlie for letting me work with an almost brand new HP computer, measurement system; without this, much of the results would have never been recorded or analyzed. Special thanks also goes to the existing 4.3 μm InSn detectors for surviving throughout my entire tenure without dying on me but were so infantile and boorish that they required around the clock liquid nitrogren feedings for the entire term. Also thanks to the servo electronics, power supplies, and actual laser setup that allowed 24, or 48 to 72 hour runs without getting too tired or blowing up that frequently. I would also like to express my gratitude toward the Xerox copier at Lincoln

Lab and MIT Magnet Lab for nonpareil, unadulterated service of which much of the literature awareness is based.

One of the most important things I learned or developed was Self Reliance;, self reliance during the dark and dreary or whatever precipitation that was present along the road to the lab. This concerns not the one night stand: but the Tale of One Thousand New England Nights that were made possible by the piece of polyvinyl, air conditioning, bicycle and two legs; this included the 120 consecutive stands that beget a hirsute countenance, much to the consternation of my progenitors. This also gave meaning to the double-entendre three or four day weekend, school vacation or the phrase running from the lab to class or to work. There is meaning to a cyclist that cars have a right of way or else there is life after Boston and a simple fractured fibula; for Boston just means running to the lab and then turning back because you remembered that its time to get vicariously inebriated at a bacchanal gathering at MIT. But then, as euphemisms goes, these are just Games People Play.

Note that I can attest to the probity or veracity of these ruminations; there was no salacious or libelous intent albeit there appeared lugubrious expatiation in the droll manner to give credit where it belongs.

This work was supported by a National Science Foundation Research Grant for the past two years. I would like to thank the National Science Foundation for this support and the support of a National Science Foundation Graduate Fellowship during the course of this experiment.

TABLE OF CONTENTS

TABLE OF CONTENTS

TABLE OF CONTENTS

TABLE OF CONTENTS

LIST OF TABLES AND FIGURES

FIGURES

TABLES

CHAPTER 1 INTRODUCTION

The emission or absorption lineshape of isolated spectral lines have been studied ever since Michelson and Lorentz [281] attempted to model the process with hard sphere collisions. Over the years, pressure broadened theories of the lineshape[281-301] have evolved that attempted to explain the broadening and pressure shift resulting from perturbers colliding with an excited radiator and disrupting its radiation. This broadening and shift has the following simple physical picture.

Consider a two level system, labeled a and b with $\omega_a > \omega_b$ and $\omega_o = \omega_a - \omega_b$. Assume a coherence is excited between the two states such that the system emits or absorbs radiation at ω_o and that a perturber collides with the system with a time duration

$$\tau_d = b/v \simeq 10A^\circ/10^4 cm/s \simeq 10^{-12} sec.$$

During the collision, the energy levels are perturbed from their original positions and consequently the system will radiate at a different ω_o' before returning to the original ω_o level. A pressure shift depending on the number of collisions and hence dependent on the pressure of the

perturbers, will occur if the average ω_o' during this τ_d is different from the original resonance ω_o. Even so, there will be a net broadening since the emitted radiation will have a spread around ω_o due to the collisions. In terms of the energy levels E between the initial and final states as a function of the interaction distance R,

$[E_f(\infty)-E_f(R)]- [E_i(\infty)-E_i(R)]= V(\infty)-V(R) = \Delta V(R)$

Thus the shift is proportional to the difference in the scalar potential functions V(R) during the collision for a distance of closest approach R.

Most of the spectral lineshape studies measure the pressure broadening instead of the pressure shift. This is mainly due to the resolution available and the difficulty in resolving or deconvolving the true lineshape obtained using conventional optical linear spectroscopy and the associated spectrometers or interferometers. This was especially true in the infrared and visible regime where the Doppler response of the radiator severely limited the resolution of the measurements. Part of this problem was resolved with the advent of the laser which provided a single intense coherent frequency source as a probe or tool in optical spectroscopy. Over the years, several methods have been developed to circumvent the Doppler limitations so as to

obtain ultrahigh resolution; these techniques include atomic or molecular beams, the method of saturated absorption, two photon resonances in a standing wave field and resonances in separate optical fields. By eliminating the influence of Doppler broadening, the resolution of the resonances is ultimately limited by the interaction time between the system and the laser field.

Of these Doppler free methods, the nonlinear saturation absorption technique[307-328] has been widely used to improve frequency measurements. In saturation spectroscopy, a saturating beam with frequency ω interacts only with the velocity group ($\pm v$) of molecules that are Doppler shifted into resonance

$$\omega_o = \omega \pm k.v$$

A probe beam experiences a dip in the absorption of the Doppler profile at the frequency of the saturating beam. The Lamb dip or the standing wave saturated resonance occurs when the two dips due to the +v and -v coalesce for v=0 when the laser is exactly on resonance $\omega = \omega_o$. This dip is homogeneously broadened in contrast to the Doppler broadened ensemble response of the resonance and accordingly offers a means to probe or pick the exact ω_o with the resolution of the homogeneous linewidth. Thus, using this saturated

absorption technique, new levels of temporal or frequency stability and reproducibility have been obtained; this has been applied to the measurements of the speed of light and new standards of length and time[132-134] besides providing several secondary infrared frequency standards[147]. In all of these measurements, a laser servo locked to the center of the Lamb dip can provide a coherent IR or visible frequency source with stabilities up to 10^{-13} or 10^{-14}[151-177]. This level of stability is very important in our work since a very small 50 to 100 KHz/torr pressure shift[634-640] (small compared to the 7-8 MHz/torr FWHM[602-618]) line broadening was measured in our experiment.

The purpose of this experiment is to measure the pressure shift in the 9 and 10 μm lasing transition of CO_2. Pressure shifts have been measured for rotational microwave transitions and in the vibrational-rotational hydrogen halide transitions[419-460] to determine the vibrational and J dependence using conventional linear spectroscopy. What makes this experiment unique is that the actual shifts are not measured within the resolution of a spectrometer or interferometer but rather the Lamb dip stabilized laser frequency is heterodyned with another stabilized laser down to the microwave frequency range so that the KHz shifts are

counted using an ordinary electronic counter. This heterodyne technique is possible for any Lamb dip stabilized laser but in most instances the laser can only be locked to one nearby molecular transition. In these lasers (HeNe stabilized on CH_4[178-189] or I_2[195-200], Ar stabilized on I_2[209], and CO_2 stabilized on SF_6 or OsO_4[124-131]) there exist only a few molecular transitions with which the laser output frequency coincides. In contrast, in our CO_2 system, the lasing medium and the molecular absorber are the same so that all J of the P and R branches for the lasing transitions can be investigated as a function of different vibrational Fermi resonances for the different CO_2 isotopes. These measurements provide an unique opportunity to study the pressure shifts as a function of J and as a function of the vibrational dependence (Fermi resonance) using the ultrahigh resolution possible with the heterodyne spectroscopic techniques. The pressure shift for these lasing transitions is also important because of the many lasing lines (P and R branches of several different isotope lasers) provide a wide range of lines of high spectral purity, high frequency stability and resettability in the 9 and 10 μm range which are suitable for high resolution spectroscopy or as a secondary frequency standard in heterodyne spectroscopy. Since CO_2 was one of the

stabilized sources in the frequency chain used in making several 'absolute'[135-147] measurements referenced to the Cs standard, the pressure shift measurements will provide another bound on the absolute error and reproducibility of these measurements, especially since CO_2 on its own right, can easily provide a highly accurate secondary infrared frequency source. The temperature dependence of the shift will not be considered in this experiment since the means and the existing equipment were not available to obtain reliable temperature dependent shifts.

Chapter 2 gives a brief overview of the vibrational modes, existing energy levels, and allowed rotation-vibrational transitions in CO_2. It should be especially noted that the Fermi levels[21-30] in CO_2 had been erroneously labeled in past literature but the correct level assignments[31-35] are still not very well known or emphasized.

A brief overview of the laser is given in Chapter 3. The emphasis in this chapter is not on a detailed description of the system but rather on some of the usual or unusal features or precautions taken in terms or equipment and techniques (plus suggestions for improvement) that would

comprise an ultra-stable system. The existing system is unique in the sense that a wide range of CO_2 isotopes can be studied by interchanging different gas fills in the laser tube and in the absorption cell. Short term stability is determined by the laser structure and components while long term stability is determined by the feedback servo system. The most important variable in long term stability and reproducibility is the S/N of the detector. Given that the ultimate limit in stability is determined by the detector, a different electronic detection and servo system was built to eliminate as much of the electrical drift, errors and offsets in the system. Finally root mean square deviation (σ) vs time (τ) plots and drift runs were taken as a measure of the stability and reproducibility of the system.

A two level rate equation analysis of the standing wave saturated resonance is given in Chapter 4. Essentially, this analysis follows that of Kelly[280] and Thomas[279] in their evaluation of the 4.3 μm fluorescence signal. The expression for the linewidth, depth and percentage depth given in terms of the two level signal and a gaussian intensity averaged signal is used in the later chapters in analyzing the errors or fits in the pressure shift data.

One of the primary results and conclusions obtained from earlier CO_2 4.3 μm fluorescence lineshape studies was the observation that the pressure broadening of the nonlinear resonance dip was not linear at the lower absorption cell pressures (less than 30 mtorr). First Meyer[267], in his high intensity, internal cell studies and then Kelly[280] Thomas[279] with their expanded beam, external cell studies observed this effect. In their work, Kelly and Thomas attributed this nonlinear pressure broadening to a difference in the contributions of the fluorescence signal from the wings of the Gaussian distribution at the lower pressures; there is less power broadening in the wings so the overall linewidth narrows. A similar but weaker effect could also come from the M degeneracy of the rotational states where the weaker transitions contribute more at lower pressures. Linescans of the fluorescence signals were taken in this experiment to verify that the linebroadening coefficient was still about 7.5 MHz/torr FWHM in our experimental setup; extensive measurements were not taken at the lower pressures since our setup was not optimized for it. These linescans were different from the usual linescans since the variable frequency laser was phase and frequency locked to a local oscillator while its frequency output was being scanned. All data, including the frequency readings

and amplitude readings were digitized and stored on tape for later evaluation. It turned out that these linescans were very important in tracking down a power slope contribution to the lineshape that gave rise to the most significant source of error in this experiment.

The 4.3 μm fluorescence system is unique in the sense that the absorber resonance and the peak laser power lies almost on top of each other in frequency space and accordingly the system does not have to depend on any accidental resonances or external external frequency adjustment to provide a lock signal. Because the laser gain and its frequency output is dependent on the overall net dispersion of the entire laser, the peak of the laser's power output will almost never exactly coincide (within the homogeneous width) with the low pressure resonance dip. This has been a major and annoying problem in much of the previous work using saturated absorption in which absolute frequencies or secondary standards were required. This power error was even seen in the earliest as well as current saturated absorption experiments in the form of an asymmetric dip[239-248], skewed off center from the background peak; accordingly, several reasons were proposed to account for this asymmetry. In reality, the 4.3 μm

fluoresence signal is the result of convolving the laser power profile with the absorber's velocity dependent response. Since there is no preferred +v or -v velocities, the molecular response is symmetric in frequency space; the asymmetry of the resonance dip is composed primarily of the nonzero laser power slope which 'adds' a nonzero slope to the existing signal. Thus the servo electronics will lock to this pressure dependent offset zero. This gives rise to the erroneous 'instrumental' error which can account for almost all the nonlinear pressure shift observed at the higher pressures. It turns out that this error is proportional to the power slope and is proportional to pressure squared with a slight power dependence due to the saturation depth and width of the resonance dip.

The linescans and subsequent power scans described in Chapter 5 provide visual evidence that there is a nonzero power slope contribution to the linewidth. This power error plus other offset errors are discribed in Chapter 6. Physically,

$$\omega=\omega_o(t)[1+v_z/c -v^2/2c^2 \pm \hbar\omega_o/(2mc^2)$$

where the terms in the brackets represent the frequency, the first order Doppler shift along the laser propagation direction, the second order Doppler shift and the recoil

shift, respectively. The frequency $\omega_o(t)$ is represented as a function of time (and is also a function of pressure) since it depends on the number and type of collisions. Since the pressure shift measurements reveal approximately a 100 Hz/mtorr change, it was shown that these physical terms are negligible compared to the pressure shift, especially since they do not depend on pressure. It was also shown that transit time effects, wave front curvature (diverging wavefronts mismatched inside the absorption cavity) did not affect the measured shift and is negligible above 20 mtorr. Even diffractive or beam effects due to where the radiation is sampled along the gaussian beam profile is eliminated since spontaneous fluorescence is observed (isotropic in 4π steradian) and not saturated absorption so that this type of asymmetry in the derivative signal is effectively eliminated.

Finally, a non-electrical means of correcting for this power slope was discovered and used to correct for this power slope. (Electronic corrections were avoided since the power variation and electronic error were so small at the zero lock point that any correction would add more to the instability of the system than any correction that it would provide). By adjusting the diffraction grating within the

tuning range of the laser gain while the laser is locked on the resonance dip, the output gain profile can be distorted until a local zero power slope point at the resonance dip is reached.

Calibration runs (with large slope errors) and tests showed that the pressure shift could be 'tuned' red or blue by almost any magnitude just by judiciously adjusting the grating which changes the power slope. Pressure shift measurements for four different CO_2 isotopes were taken after correcting for the power slope. Chapters 6 and 7 describe these tests and measurements. Perturber gas pressure shifts were also taken using the same setup for Xe, Ar, N_2, H_2, He, and CH_3Fl. Pressure shifts were also taken at the relatively higher pressures between 100 and 200 mtorr; these were nonoptimum pressures since the Lamb dip is getting wiped out at these pressures and all the errors and offsets increase dramatically at these higher pressures (error is proportional to pressure squared). An estimate of the sign and magnitude of the pressure shift at large pressures (> 1 torr) was also made by comparing absorption signals as the laser beam passed through two different pressure cells.

These final measurements were made because the pressure shift, as measured using the 4.3 μm fluorescence technique, turned out to be blue, instead of red as predicted by linear spectroscopy theory. At the extremely high pressures (> 1 torr), the pressure shift reversed and became red. Even the perturber data showed this blue and red variation among the heavy and light perturbers, respectively; this indicated that polarizability or the Van der Waals potential could possibly be the dominate term in the lineshift calculatio

A semiclassical perturbative impact approximation of the lineshape theory is outlined and used to evaluate the shift in Chapter 8. Nonzero shifts arise due to the vibrational mixing of the normal harmonic vibrations in each participating level. Thus the shift could depend on the Fermi resonance in the lower lasing levels. But these semiclassical theories predicted a red shift for a linear absorption experiment. But our nonlinear absorption experiment, just as the pressure shifts measured in the CH_4 absorption cell stabilized to a HeNe transition using the same saturation absorption technique, gave a blue shift[189] at low pressures while a red shift was measured at higher pressures[190](in the same transition in CH_4 using a linear absorption technique). In the case of the methane

measurements, the workers apparently were not aware of this discrepancy.

It appears that there is a fundamental difference between linear and nonlinear spectroscopy that could possibly arise from the presence of velocity changing collisions. One physical consequence of the effect of velocity changing collisions, as applied to the nonlinear linewidth dependence [266-280] seen in several saturated absorption experiments, revolves around the concept of velocity changing collisions kicking the molecule out of the homogeneous hole in frequency space. If the average change in velocity Δvcan remove the molecule from effectively interacting with the laser field, (the homogenous width $\Gamma$is smaller than the Doppler shift $k\Delta v$) then that molecule will not contribute further to the broadening or shift. If the opposite occurs, then the molecule will continue interacting with the field. Thus a change or inflection point will occur in the pressure dependence of the shift width when the pressure broadened homogeneous linewidth equals the Doppler shift due to velocity changing collisions.. These explanations, theoretical calculations and conclusions are explored in Chapter 8 and 9.

During the course of this thesis, many of the existing lineshape theories were evaluated and surveyed to try to find which theory would best fit our experiment. Thus, as a final note, Chapter 10 gives a brief overview of the different lineshape theories currently in use along with many of the recent references. A brief survey of the work involving pressure shifts is also included in this chapter.

CHAPTER 2 CARBON DIOXIDE

INTRODUCTION -

Carbon dioxide is a classic example of a linear, symmetric triatomic molecule belonging to the $D_{\infty h}$ group. Spectroscopically, two strong IR absorption bands at 667.3 and 2349.3 cm^{-1} and a strong Raman band at 1340 cm^{-1} represent the three (3N-5, singly degenerate) fundamental vibrational modes that exist in linear triatomics.

The ν_1, ν_2^1, and ν_3 normal vibrational modes shown in Figure 1 are called the symmetric stretch, the bending mode and the asymmetric stretch respectively. The ν_2 mode is doubly degenerate since the molecule can bend in two directions (x or y) perpendicular to the axis of symmetry (z). The superscript l ($l=0,1,2..\nu_2$) represents the vibrational angular momentum about the molecular axis. A sample of the vibrational energy levels (ν_1, ν_2, ν_3) of the ground ^1X electronic state is shown in Figure 2.

Since CO_2 can not have a permanent dipole but does have a nonzero quadrupole moment, the IR ν_3 and ν_2 bands arise

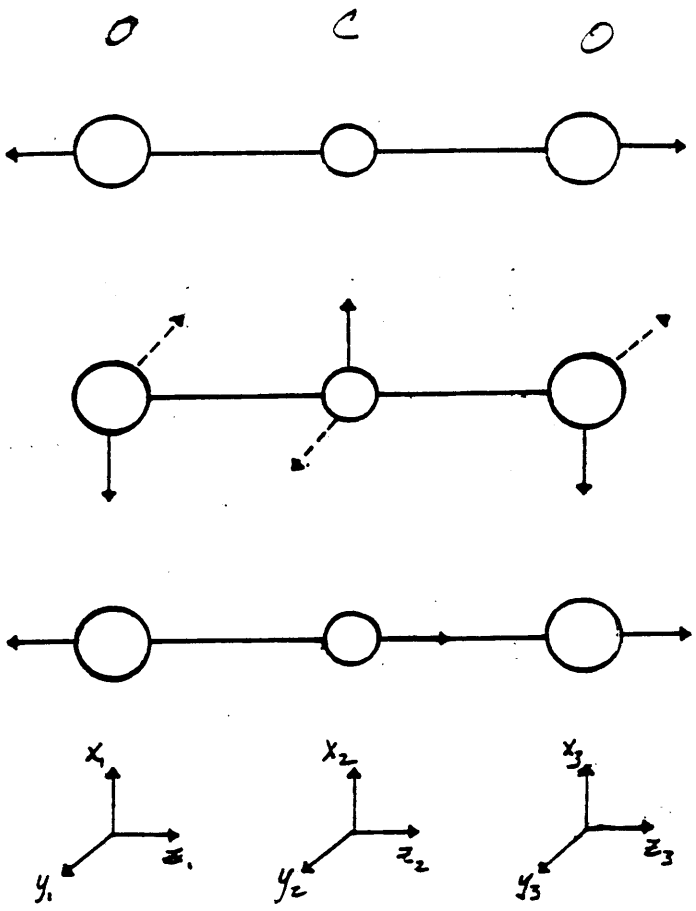

Figure 1
Carbon Dioxide

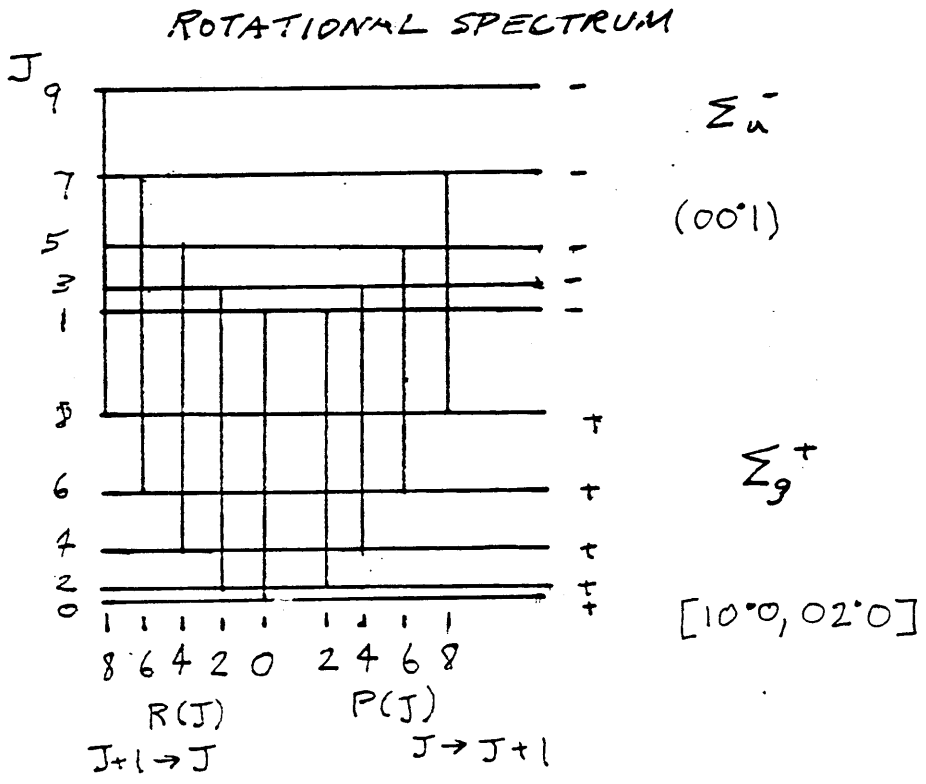

from induced dipole moments while the ν_1 mode gives rise to the Raman spectra. From similar symmetry arguments, the first derivative of the polarizability with respect to the normal coordinates will be nonzero in the ν_1 mode while the first derivative of the dipole and the second derivative of the polarizability and quadrupole moments are nonzero only in the ν_2 and ν_3 vibrational modes; this fact will be very important in the theoretical evaluation of the pressure shifts in Chapter 8.

The most common lasing action [3] occurs between the upper ν_3 level and a lower level doublet. This dyad is the most well known example of Fermi resonance.[21-30] Here the two levels are very close in energy, $\nu_1 \simeq 2\nu_2$ and consequently significant mixing and the corresponding energy repulsion of the two levels occur. The dipole moment ($\simeq$0.018 Debye) and the absorption coefficient ($\simeq 3\times10^{-6}$ cm^{-1} torr^{-1}) for the lasing transitions are very small compared to that of the ground state absorber ν_3 4.3 μm level. The low absorption coefficient follows from the statistical population distribution of the lasing levels. The relative populations of the two ν_3 and ν_1 levels are 1.24×10^{-5} and 1.26×10^{-3} times that of the ground state. Consequently absorption is very small and the upper lasing level population can be

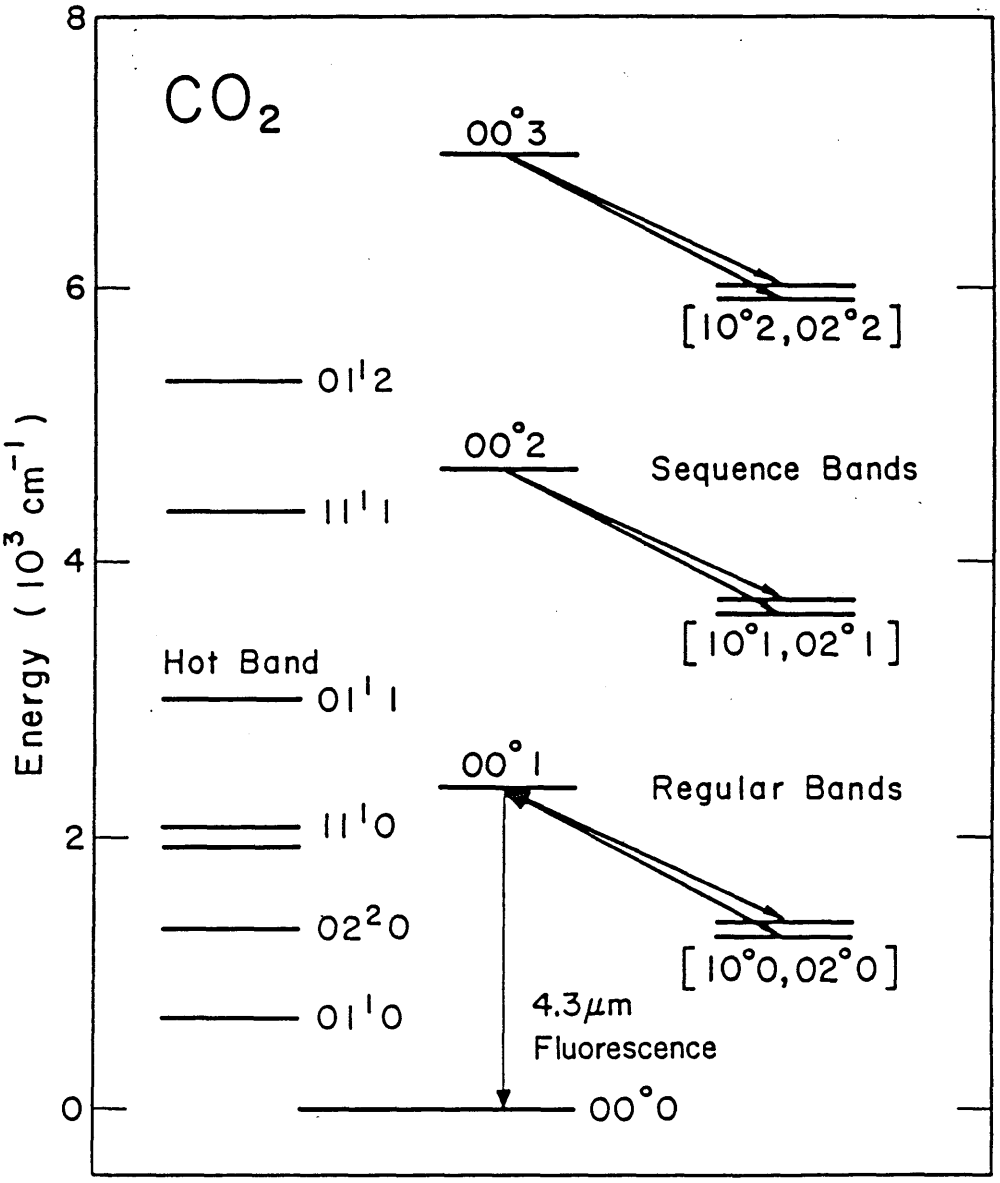

Figure 2 Vibrational Energy Levels

considered to be neglible compared to the lower level population. The Einstein A coefficients for the 4.3μm, 10.6 μm, and 9.6μm transitions are 200.0, 0.33 and 0.2 sec^{-1} respectively. The lasing action does not depend on the slow spontaneous lifetime of the participating levels but rather on the vibrational and rotational relaxation between the levels [83-105] The 4.3μm spontaneous emission can be influenced by its frequency response and by such effects as radiation trapping [76-82], since CO_2 is a ground state absorber at 4.3μm.

SPECTROSCOPIC TRANSITIONS

The symmetry properties of the total molecular eigenfunction and the symmetry properties of the $D_{\infty h}$ group to which CO_2 belongs determine what energy levels exist and what transitions are dipole allowable.

Consider CO_2 in its ground state. To a very good approximation the total molecular eigenfunction can be represented as a product of the individual electronic, vibrational and rotational eigenfunctions:

$$\Psi \simeq \Psi_e \Psi_v \Psi_r$$

where Ψ_e is the electronic eigenfunction

where Ψ_v is the anharmonic oscillator eigenfunction and where Ψ_r is the nonrigid rotor wavefunction:

$$\sim P_J^m \cos(\theta) e^{im\phi}$$

Hence

$$\Psi \simeq \Psi_v(r-r_e)\ \Psi_r(\theta,\phi)\ \Psi_e(r)$$

Initially the effect of nuclear spin can be disregarded if zero nuclear spin atoms ,e.g. O^{16} or O^{18} are considered.

One important way to differentiate between levels or eigenfunctions is to consider the effect of inversion or reflection of the system about the origin: $(\theta \to \pi-\theta\ ,\phi \to \pi+\phi)$

Since Ψ_v is normally unaffected by inversion, the parity of the total eigenfunction is determined by $\Psi_e\Psi_r$. In the case of Ψ_r ,inversion results in

$$\Psi_r \to (-1)^J \Psi_r$$

so each rotational level can be labeled as being even (+) or odd (-) parity. Accordingly, the rotational transition rule $\Delta J=\pm 1$ follows since parity must change to be dipole allowable. Thus considering just the Σ^+ vibrational levels, the even J levels are labeled + and the odd J levels are labeled - , while for the Σ^- vibrational levels, the even J levels are - and the odd J levels are +.

Whenever there is a center of symmetry for a linear molecule, ie. the $D_{\infty h}$ point group, there is also an exchange symmetry where the system is either symmetric or antisymmetric with respect to a complete exchange of identical nuclei (oxygen in this case). The total eigenfunction will either remain unchanged or change sign under this exchange. This nuclear exchange can be considered as a reflection of all nuclei followed by the reflection of all the electrons about the center of symmetry (carbon atom). Consequently the different symmetry (a,s) and different parity (+,-) lead to $2\times 2=4$ possible classifications of each rotational level. Since gerade (g) and ungerade (u) refer exactly to ± under $\mathbf{r} \rightarrow -\mathbf{r}$, the rotational designations for the vibrational states in $D_{\infty h}$ molecules correspond to:

$\Sigma^+_g, \Sigma^-_g, \Pi_g, \Delta_g$ are (s,+) or (a,-)

and

Σ^+_u, Σ^-_u are (a,+) or (s,-)

where specifically for the following cases

Table 1

Σ^+_g	(s,+)	J=even
Σ^+_u	(a,+)	J=even

The reverse holds for the Σ^-_g and the Σ^-_u levels. Here nonzero dipole transitions are allowed if $\Delta J=\pm 1$, parity changes, symmetry types do not change and (g,u) change.

Now consider the influence of nuclear spin which gives rise to the alternation of intensities and the para and ortho modification in homonuclear diatomics. Essentially these two effects depend on whether the symmetric nuclei behave as bosons or fermions. The rotational weights 2J+1 are modified to include the different nuclear spins I_1 and I_2 so that the new weights to be summed over and averaged are of the form $(2I_1+1)(2I_2+1)(2J+1)$.
This arises because the total eigenfunction must now include a nuclear spin function $\Psi = \Psi_r\Psi_v\Psi_e\Psi_I$. When the contributions of the nuclear spin to each rotational level are included, an alternation of intensities occurs. The ratio of symmetric to antisymmetric intensities is given as R in the following table.

Table 2

		Σ^+_u	Σ^-_g
BOSONS	R=I+1 / I	J=odd / J=even	J=even / J=odd
FERMIONS	R= I / I+1	J=odd / J=even	J=even / J=odd

The spin and parity for each atom in the normal $D_{\infty h}$ CO_2 molecule for the various isotopes are given as $^{12}C(0+)$, $^{13}C(1/2-)$ and $^{16}O(0+)$ and $^{18}O(0+)$. Thus the symmetric atoms have zero nuclear spin and are bosons. Since R=1/0= ∞ the antisymmetric J levels will be missing. This means that the even J levels will be missing in the upper (001) Σ^+_u level and the odd J levels will be missing in the lower (100,020) Σ^+_g level. Thus for the usual $D_{\infty h}$ molecules (O-C-O) 16-12-16, 16-13-16, 18-12-18, and 18-13-18 only even P and R rotational lines will be present.

On the other hand, for the isotopically substituted CO_2 18-12-16, 18-13-16, etc. the exchange symmetry (a,s) and the

(g,u) distinction does not exist and there is statistically no difference in the resulting $C_{\infty v}$ molecule and there is no alternation of weights in even or odd J. Thus all even and odd J occur in the P and R branches of 18-12-16,18-13-16, etc.

We have recently completed measurements of the CO_2 molecule 17-12-17 in which the oxygen atom has a nonzero nuclear spin (5/2+). From the statistical arguments, the oxygen behaves as a fermion and the ratio R of symmetric to antisymmetric intensities is R=5/7. From previous evaluations, the antisymmetric upper state with even J values dominates meaning the odd J in the P and R branches will have the largest intensities and correspondingly will prevail in the laser gain or single mode operation of the laser. This was experimentally verified where the odd J's dominated over adjacent lines, especially in the midband gain.

ANHARMONIC POTENTIAL ENERGY FUNCTION

In the above analysis, a harmonic potential function was assumed for all three vibrational modes. But this is not actually true as seen spectroscopically, especially

since CO_2 is the most well known molecule that exhibits Fermi resonance,[21-45] plus other anharmonicities[6-20] including centrifugal distortions, Coriolis interaction, and l- type doubling. To account for these anharmonicities, the potential function is Taylor expanded in terms of the normal coordinates:

$$V=V_e+\frac{\partial V}{\partial q}\Big|q+\frac{\partial^2 V}{\partial q^2}\Big|q^2+\cdots\cdots$$

where V_e is the reference energy and the first derivative of the potential expanded about its minimum is zero and $V\simeq kq^2/2$ is the leading term. By adding higher order terms, including mixing of the various normal modes as allowed by symmetry, a perturbative expansion of the potential energy can be obtained to as high an order as desired. This way, the energy mixing due to the Fermi resonance $q_1q_2^2$ (122) can be accurately predicted if terms up to 5th order, ie (12233), are included. Here for example, the terms (2233) and f_{2233} refer to the partial derivatives coefficients of the Taylor expansion term $q_2^2q_3^2$.

Fortunately, the energy eigenvalue problem, including the anharmonic terms have been studied extensively by several people using two different methods. Basically the Hamiltonian is diagonalized and the energy eigenvalues and

eigenfunctions are obtained. The energy eigenvlues are compared with the measured spectroscopic values,the potential functions are least square adjusted and the process reiterated until the desired convergence between theory and experiment is reached. On one hand Suzuki[10-13] attacked the problem using a direct diagonalization technique using the anharmonic potentials and the direct harmonic oscillator functions as the basis. Chedin[1,6-9] had also worked on this problem for several years by using a perturbative Van Vleck or contact transformation approach,expanding the Hamiltonian as

$$H=H_o+\lambda H_1+\lambda^2 H_2+ \ldots.$$

The contact transformation T, changes the Hamiltonian:

$$H'=THT^{-1} \qquad T=\exp(iS)$$

where S and T are Hermitian. Now H' retains all the diagonal elements of H but will yield no nondiagonal elements in $\lambda H'_1$ but can possibly have nondiagonal elements in higher orders. Thus successive contact transformations diagonalizes the perturbative Hamiltonian to higher orders but introduces other nondiagonal terms or energy resonances in the next higher order energy perturbation. These energy resonances include Fermi type resonances, Coriolis interactions and l-type interactions.

Chedin used two contact transformations to reduce a fourth order Hamiltonian from 28 potential functions to just twelve different matrix evaluations. He attacked the diagonalization problem using a vibrational rotational basis for ten different CO_2 isotopes. Quite impressively,[1] his energies converged with all the spectroscopic results. A list of the anharmonic potential values and the spectroscopic constants appears in Appendix 1. These values were used to obtain the harmonic oscillator decomposition of several energy levels since this wavefunction 'mixing' is important when computing various harmonic oscillator matrix elements.

FERMI DOUBLET NOTATION

The Fermi doublet has been traditionally labeled the (100) ν_1 level corresponding to the 10.6μm radiation and the (02°0) $2\nu_2$ level corresponding to the 9.6μm radiation. This notation began with Patel's original work with CO_2 and became firmly established in industry by the notation used in the Optics Engineering CO_2 spectrometer. In reality, as was pointed out by Amat and Pimbert[26], the energy levels are actually reversed in the standard CO_2 isotope 16-12-16 and in the isotope 16-13-16 where the (02°0) level is

located above the (100) level; in the 18-12-18 and 18-13-18 isotopes, the Fermi levels are in the "normal" order. Even with this order both levels are strongly mixed and the best notation that has been suggested is to label the 10.6μm band as the I band and to label the 9.6μm band as the II band.

Table 3

Level Assignments for $^{12}C\ ^{16}O_2$

Level	Old	New	Notation
1335 cm^{-1} (10 μm)	(10°0)	(02°0)	$(10°0,02°0)_I$
1295 cm^{-1} (9 μm)	(02°0)	(10°0)	$(10°0,02°0)_{II}$

As a final note, for standard 16-12-16, the energy ordering for each level of the Fermi dyad had been traced as CO_2 changed from dilute gas to liquid and to solid[31-35]. Amazingly enough, the Fermi dyad does revert back to the "normal" energy level ordering for standard 16-12-16. Initially the "inverted" levels diverge in energy but then cross over to the "normal" ordering in the dense gas or

liquid phase as the pressures and phase vary[31] . For spectroscopic purposes,in the low pressure regime, the levels will always be referred to as I or II(or 1 or 2) bands and are designated as in Table 3.

CHAPTER 3 DESIGN OF THE LASER SYSTEM

REQUIREMENTS

The laser output frequency must be stabilized and locked with as little drift and jitter as possible to a fixed molecular resonance. Both short term and long term stability are needed to measure the pressure shifts as reliably and reproducibly as possible.

Short term stability is achieved by designing the system with precise, carefully designed, rigid components and by eliminating as much environmental disturbances as possible. The key factor in passive short term stability is the mechanical stability of the laser cavity and the isolation of the laser from external factors such as power supply ripple, acoustic oscillations,thermal drift, or other physical disturbances. For long term stability, drift must be eliminated or compensated by using some active stabilization technique. This long term stability is achieved by correcting the laser frequency output by using a set molecular resonance as an external reference. By locking the laser output to the energy difference of a two

level system, the drifts and variations in the frequency output of the laser can be effectively reduced. Then the ultimate precision is determined by how well the reference molecule resonance can be detected and tracked by the active feedback servo loop and how well other extraneous errors including alignment,focusing, geometry and dispersion, etc. can be eliminated.

Besides reproducibility, it is very important to have component interchangeability, both in terms of mechanical maintenance and in variation of physical parameters including pressure,and various laser lines. This is very important since measurements were taken using four different CO_2 isotopes on both I and II bands over a wide range of J values, meaning that several different isotope combinations were used in the two channel system just to cover this range of data. This was easily done, since sealed-off CO_2 gas lasers were used instead of a flowing gas system, and because the system was well maintained, adequate powers (1 to 2 watts) were obtainable in most of the lines, with each laser gas fill lasting around a month of CW operation before power output dropped below a level required for good stability. Modularity also meant that the power supplies and discharge tubes could be easily replaced when needed.

The ultrastable, single longitudinal mode TEM $_{00}$, high beam quality, sealed-off CO_2 lasers were developed and described in a series of papers by C. Freed[116-121] . This particular two channel system along with the stabilization cells has been discussed in detail[122] and therefore only the highlights or unique features of this system will be discussed.

The laser cavity consists of two granite endplates connected by four invar rods to form a 1.5 meter optical cavity. These invar rods are acoustically, thermally and electromagnetically shielded by covering them with conetic, mu metal, lead foam and aluminum foil. The entire optical cavity, including the mirrors, PZT, and diffraction grating are internal to the vacuum system which also includes a reservoir bulb to hold more gas in the sealed-off laser. The semiconfocal cavity is defined by a curved mirror (R=3m) on one end and an 80 groove/mm diffraction grating on the other. Behind the curved mirror, a PZT stack and a PZT cylinder assembly is attached to provide the fine cavity length control. The diffraction grating is adjusted by a stable, high precision micrometer that controls a spring loaded plunger that contacts a sapphire ball which tilts the grating; this mechanical design contributes to the long term

trouble-free usage, reproducibity and resettability of the grating position based on the micrometer readings. The TEM $_{oo}$ mode is obtained using two limiting apertures. The output is linearly polarized and coupled through the zeroth order of the diffraction grating. The mode radius w_o defined at the diffraction grating is .23 cm with a corresponding beam half angle divergence of 1.5 mradian. The actual laser cavity is completed by a fused quartz discharge tube with an i.d. of 13 mm for the gas discharge and is sealed with glass to metal bellows to the cavity frame. The inner gas discharge tube is surrounded by a water jacket for convection cooling. The discharge tube has platinum anodes at each end with a nickel cathode at the center to provide two equal-armed discharge paths. This was very convenient because either side or both sides of the laser could be fired up to create three different power outputs with the same optics.

This equal-armed plasma discharge is made possible by using the electrical wiring scheme as shown in Figure 3. The cathode (-6 KV) and the anode(+4 KV) voltages are supplied by two Northeast Scientific voltage regulated power supplies which have their respective "low" DC terminals connected to ground. The positive power supply splits its

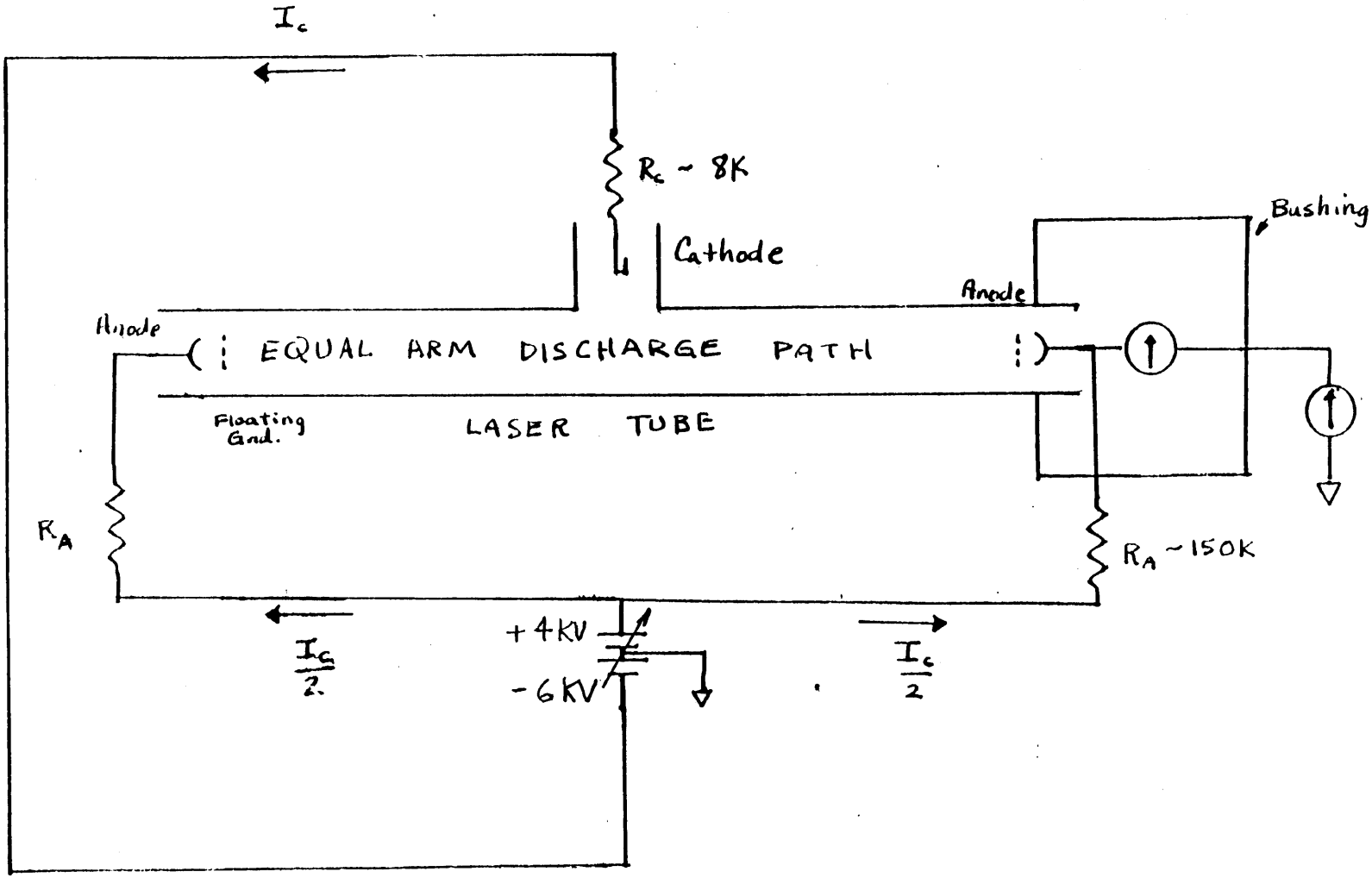

Figure 3 Electrical Discharge Circuit

current between the two anodes via two special, noninductive, high voltage, oil-cooled 150K to 200K ballast resistors. The total discharge current returns through a noninductive 8K ballast resistor on the cathode side. The actual voltage drop between the anodes and the floating laser frame startup and normal discharge conditions is monitored using two microammeters which are protected by 2MΩ resistors. One meter is connected from the anode to the laser vacuum frame (bushing) while the other meter is connected from the bushing to the DC ground (table, power supply). The laser is actually floating due to the granite endplates. Because of this electrical setup, the laser can be discharged with significantly lower discharge voltage power supplies than in a more conventional end-to-end discharged system. The total discharge current follows from V= IR/2 or with V= 4KV, I is approximately 40 to 50 mA; lower current translates into higher gain at lower J lines and a correspondingly wider range of lasing lines.

The laser is tuned using a PZT stack and cylinder arrangement. A small sinusoidal voltage ($10 \leq V \leq 25V$ p-p) at the desired reference frequency is applied to the PZT stack to frequency modulate (dither) the laser output. This frequency deviation of the stack corresponds to

approximately 18 KHz/Volt but the most important point is to get enough signal with as little distortion or parasitic amplitude modulation as possible. The actual servo tuning voltage (0 to -400 V) is applied to the cylinder (200 KHz/Volt);the response of the cylinder is sufficient to tune the laser gain from one longitudinal mode to ($\nu_m = c/2L \simeq$ 100 MHz) mode.

Table 4

Laser Gas Fill

Gas	Pressure (Torr)
Xe	1.1
CO_2	2.3
N_2	3.0
H_2	0.15
He	8.3
Total	14.85

In sealed-off systems, the gas mixture is important in determining the gain and output power. The gas mixture normally used for each laser is shown in Table 4. This doesn't mean that this mixture of gases will give the maximum power but rather the gain for a wide range of J lines is adequate or near optimum at the total operating gas pressure (14.85 torr). At this pressure regime, pressure broadening dominates the lineshape and this pressure also turns out to be near optimum in terms of midband gain power output.

FEEDBACK STABILIZATION

Feedback stabiization is obtained by using an external absorption cell rather than an internal cell (inside the laser cavity). In this setup, the laser output is directed into a specially designed absorption cell and reflected back, slightly misaligned, off a flat (r=.99) mirror to create a resonant standing wave inside the cell. As in the laser cavity, the entire optical assembly in the absorption cell, including the one inch diameter ZnSn input window, absorption cavity and the back reflecting mirror is under a single vacuum enclosure to eliminate any extraneous disturbances. The 4.3 μ m fluorescence signal is focused

onto a special liquid nitrogen cooled InSn detector either by using an ellipsoidal focus to focus arrangement or a curved spherical mirror arrangement. A sapphire window and a liquid nitrogen cooled bandpass filter, is placed before the InSn detector (responsivity 3.5 to 5 μm) to improve the signal to noise ratio. There were two differently configured absorption cells and two different InSn detectors in the two channel system. On the left laser channel (Laser GP 157) a half inch diameter Spectronics detector with an internal resistance of 4K was used while in the right laser channel (Laser GP 153), three 2.25 mm diameter Raytheon detectors connected in parallel with a combined resistance of 25K were used. Both detectors operated in the photovoltaic mode such that the output was current mode amplified and synchronously detected.

When using external cells, care must be taken not to allow any optical feedback from the reflected wave back into the laser; numerous isolation techniques have been tried or suggested to get around this problem including quarter wave plates, Fresnel rhombs, Faraday rotators and different isolators. But this experiment required a wavelength insensitive solution which was most readily provided by beam misalignment and appropriate limiting apertures. Another

small external cell was sometimes used to attenuate the laser power going into the detection cell. This portable cell contained dimethyl ether $(CH_3)_2O$ at pressures of 10 to 100 torr; at these pressures the linewidth was essentially Doppler broadened flat over the 10μm regime but measurements showed it was not flat at 9.6μm. Dimethyl ether was very convenient since the pressure could be adjusted by freezing out portions of the gas into a cold finger with liquid nitrogen and thus provided an autonomous external, variable power attenuator.

Approximately 70-90% ,depending on the wavelength, of the laser beam is directed to the fluorescence cell. The rest of the laser beam of both lasers is combined on a 50% beam splitter and directed onto a very fast liquid nitrogen cooled HgCdTe varactor diode. This detector yields the beat frequency between the two lasers which is subsequently amplified, frequency counted and recorded. All three detectors were kept under vacuum at LN temperatures 24 hours a day for the entire duration of the experiment. The shortest time between refilling the detectors was approximately 16 hours.

All the lasers and optical components and detectors were located on top of a 12 foot honeycomb optical table which is normally kept floating on airmount during operation. Even then, there existed a very low frequency (2 to 10 Hz) acoustic resonance between the shock mounts of the table and the air conditioner. All the data acquisition equipment and rack were kept ten feet away from this table to minimize any electrical or mechanical disturbance to the beat signal.

After everything was lined up as carefully as possible and the signals maximized as much as possible without any 'visible' (heat monitored) clipping or distortion, the laser beam profiles were checked at all the critical points in the optical setup to make sure that there was no significant physical distortion of the beam by any of the optical elements. This was made possible by an unique Inframetrics IR beam profile scanner which displayed either a 1D or 2D beam intensity contour 'map' on a video display (similar to an PAR Optical MultiChannel Analyzer operating in intensity space, not frequency space). Thus the entire beam profile could be monitored as it passed through the various mirrors and absorption cells or Brewster angle polarizers and as it was reflected backed through the absorption cell. The beam profile was also monitored as the grating scanned through

the P and R branches of the various bands to determine beam deviation from the TEM_{oo} pattern and correct laser cavity alignment. This 'unique' real time intensity profile display showed the entire system was well aligned with no beam distortion or clipping due to the mirrors or windows.

SYSTEM DEVELOPMENT

The underlying theme in this experiment was to make the measurements as well as could be done with the available equipment. This meant that all precautions had to be taken to obtain a stable and reproducible laser frequency output with minimun extraneous error from drift and offsets in the servo loop.

First of all, the + and - power supplies were unique in the sense they had very low ripple and spiking at the operating output levels due to the care in winding the shielded transformers. This ripple varied from 4-5mV p-p for the Model RQE 7506 (0 - 7.5 KV) negative supply to 2-3 mV p-p ripple for the Model RQE 5006 (0 - 5KV) positive power supply. Concurrently, all the ballast resistors were very stable, noninductively wound, high wattage resistors.

On the servo side of the system, best stability is achieved with the largest S/N detector signal and as small an offset or drift in the electronics as possible. Since the fluorescence signal is spontaneously emitted, the largest signal is achieved with as large an active volume (ideally with telescope expanders into large volumes of some cell equipped with signal collecting optics) as possible with this emission directed on as large an area, shot-noise limited detector as possible. The InSn detector is essentially a photodiode operated at exactly zero bias by means of a current mode amplifier. The initial stage of detection and amplification is the most critical in terms of bandwidth and noise; here an ultralow ripple (ripple less than 60 μV p-p, due to a special wound transformer) ±15V power supply used with the specially designed Spectronics SPX current mode preamplifier. The output of the preamp is then voltage amplified and fed into the Brower 261 preamplifier and Brower 131 lockin system. In both the detector and the current mode preamp and the 131 lockin detection stage, separation of signal ground versus power and chassis ground were extremely important and were separated in the signal processing. A vivid example of this occured in the lockin detection where the reference signal and its corresponding grounds had to be isolated in a

separate chassis away from the synchronous demodulation and servo amplifier chassis. A short description of the entire servo system is given in Appendix 3 where the unique features and precautions taken in the custom built unit are summarized. It should be noted that the objective of the design and construction of this servo system was to eliminate output drift and offset on the mV (100 Hz) level for the dc chopper stablized high voltage (0 to -400 V) PZT output while emphasizing reproducibility and stability of the servo system.

Care must also be taken in analyzing the laser beat signal. The HgCdTe beat detector is DC-current biased using a microwave biasing tee. Then the beat signal (RF) is fed into a wideband 2 - 18 GHz double balanced mixer and combined with the LO from the HP 8672A microwave synthesizer. The 8672A output is phase locked to a HP 3325A synthesizer for a LO stability of ±1 Hz instead of the usual ±1 KHz stability of the 8672A. The mixer IF signal is then fed into a bandpass (peaked at 320 MHz) ultralow noise (NF= 2db) Trontech L320 amplifier which has a gain of 37 db. Next, it is fed into a K & L Microwave Cavity Filter centered at 320.2 MHz (with a 3 MHz bandwidth) to cut out the wideband noise. This step was essential because it

lowered the S/N requirements for the microwave counter and enhanced the rejection of spurious noise counts. Then the signal is finally amplified with an Avantek (250-500 MHz) 30 db gain amplifier that saturated at +5 db. Normally, further amplification is not needed and the signal is fed directly into the 5345A electronic counter.

Which amplifiers or filters are used and in what order they were situated in the amplifying chain is very important in obtaining the best S/N ratio into the counter. As a minimum, the HP counter required at least S > -30 db with S/N> 25 db or noise spikes were counted. Note that this is an improvement over the specs of the HP counter which can be partially attributed to the counter and the cavity filter that eliminated so much broadband noise. Using this amplifying scheme, for laser beat signals in the 2 to 4 GHz range, signals of the order +0 to +5 db and S/N > 60 to 70 db could be obtained. Similar high level signals could be obtained for beat frequencies greater than 4 GHz but there exist a S/N degradation at beat frequencies greater than 14 GHz due to the frequency rolloff in the coaxial cable, microwave output and detector response. See Figure 35 for a comparison of two such beat signals.

The vacuum in the absorption cell was kept as clean and uncontaminated (of foreign gas) as possible. All external cell pressures were measured using a MKS Baratron capacitance pressure gauge, Type 911-5005; this head was factory rebuilt and calibrated before it was used in the experiment. Two CVC Pirani gauges were also used as a rough monitor of the gas pressure in each external cell and their readings compared and calibrated with the absolute MKS meter. One side of the MKS meter was connected to a Varian 8 liter/sec vacion pump; pressures on the vacuum side were the order of 10^{-8} torr and this pump was also used in the final pumpdown for both external absorption cells. (As an example of the achievable vacuum, the MKS output ranged from 0.2 V to -1.5 mV as the pressure varied from 200 mtorr to vacion vacuum.) Each absorption cell also has a cold finger so that CO_2 could be frozen out and whatever residue gases (about 3 mtorr) could be pumped out between data runs without refilling and repumping the absorption cell with Carbon dioxide. Again, emphasis was on keeping the absorption cell as clean as possible and especially free of traces of whatever isotope gas that was previously used in the absorption cell. Similar precautions were taken with the laser cavity by H_2-He firing the lasers between different isotope fills.

STABILITY AND FREQUENCY PRECAUTIONS

The most important factor that limits the stability of the system, as measured by the standard deviation of the beat frequency (σ), is the detector S/N. The upper limit on how well the system can lock is determined by the magnitude of the fluorescence signal in the feedback loop. Thus, given a shot noise limited detection system and given the existing absorption cell configurations, the only thing left to do is to eliminate detection and feedback servo error and drift. Note that due to the nature of the absorption cell optics, the incoming and outgoing laser wavefronts are both diverging (a flat relecting mirror was used in the cell) and the reflected beam was deliberately misaligned slightly to avoid optical feedback. This can be an important source of error and will be considered later.

One source of error that became evident while developing the new feedback servo system was due to the frequency at which the PZT stack was modulated. Essentially, the lockin system recovers the 4.3μm fluorescence signal by phase sensitive detecting at the modulation frequency. For the (001) level, the Einstein A coefficient is about 200 to 300 sec^{-1}, meaning the spontaneous lifetime is in the msec

regime; thus the modulation frequency must be slow enough such that the molecules in the upper ν_3 level have enough time to fluoresce down to the ground state but this modulation frequency must be high enough to avoid the 1/f noise regime of the InSn detector as well as 30 and 60 cycle harmonics. Accordingly, since it was mentioned that CO_2 is a very strong ground state absorber at the 4.3 μm, radiation trapping[76,78] will show up by as a variation of the relative phase between the reference modulation and the fluorescence signal as the pressure is varied.

Normally if there were no radiation trapping, one would expect that the relative phasing between excitation and response signals would decrease as the pressure is increased since the rate of collisions and interactions would speed up the response. On the other hand, if radiation trapping was dominant, the relative phasing should increase as the pressure increases because there are more molecules to trap the 4.3μm radiation and therefore hinder the response. This phase lag due to radiation trapping was confirmed by displaying both excitation and response signals on an externally triggered dual trace oscilloscope. Furthermore the phase lag is a function of the modulation frequency; the lower the modulation frequency, the smaller is the phase

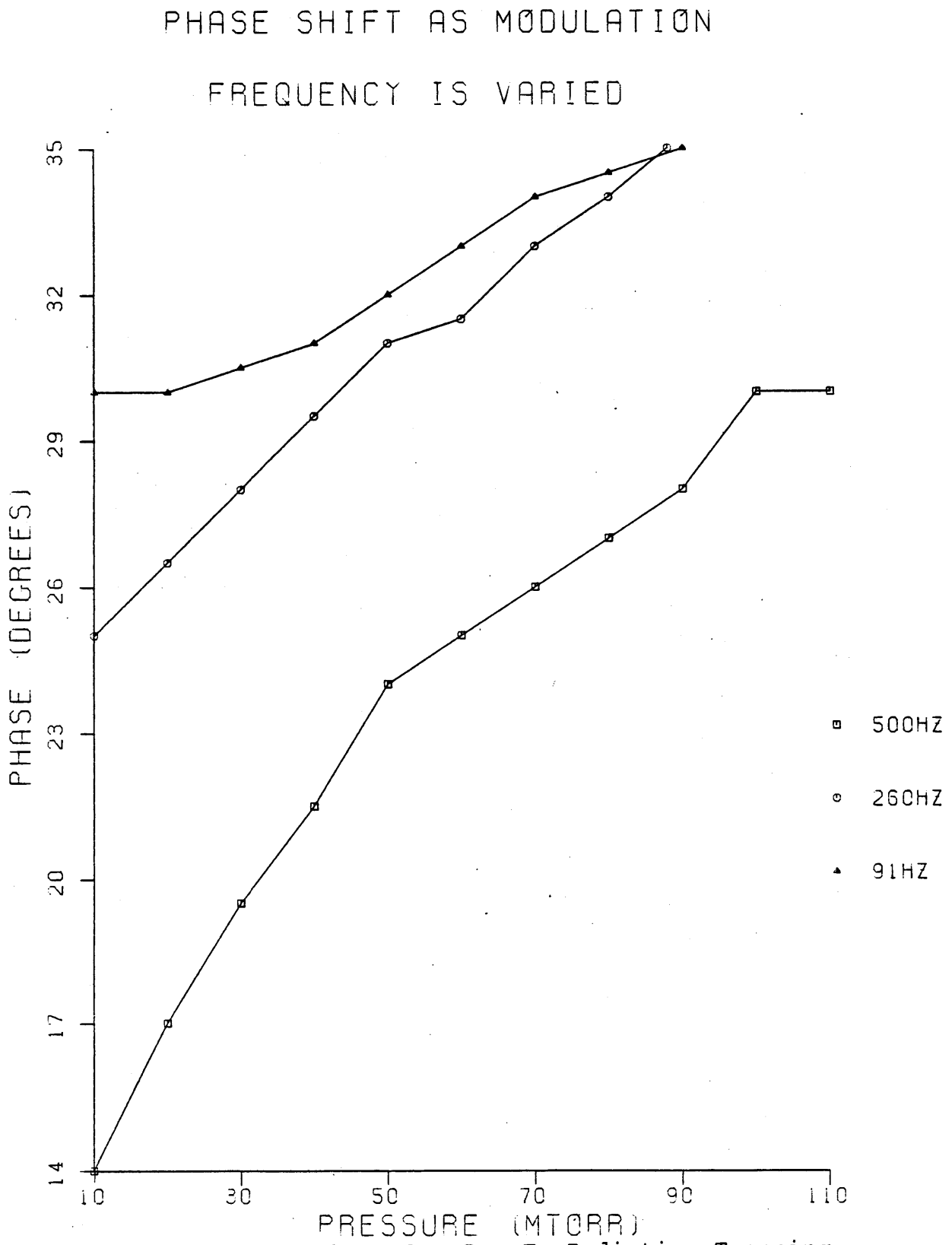

Figure 4 Phase Lag Due To Radiation Trapping

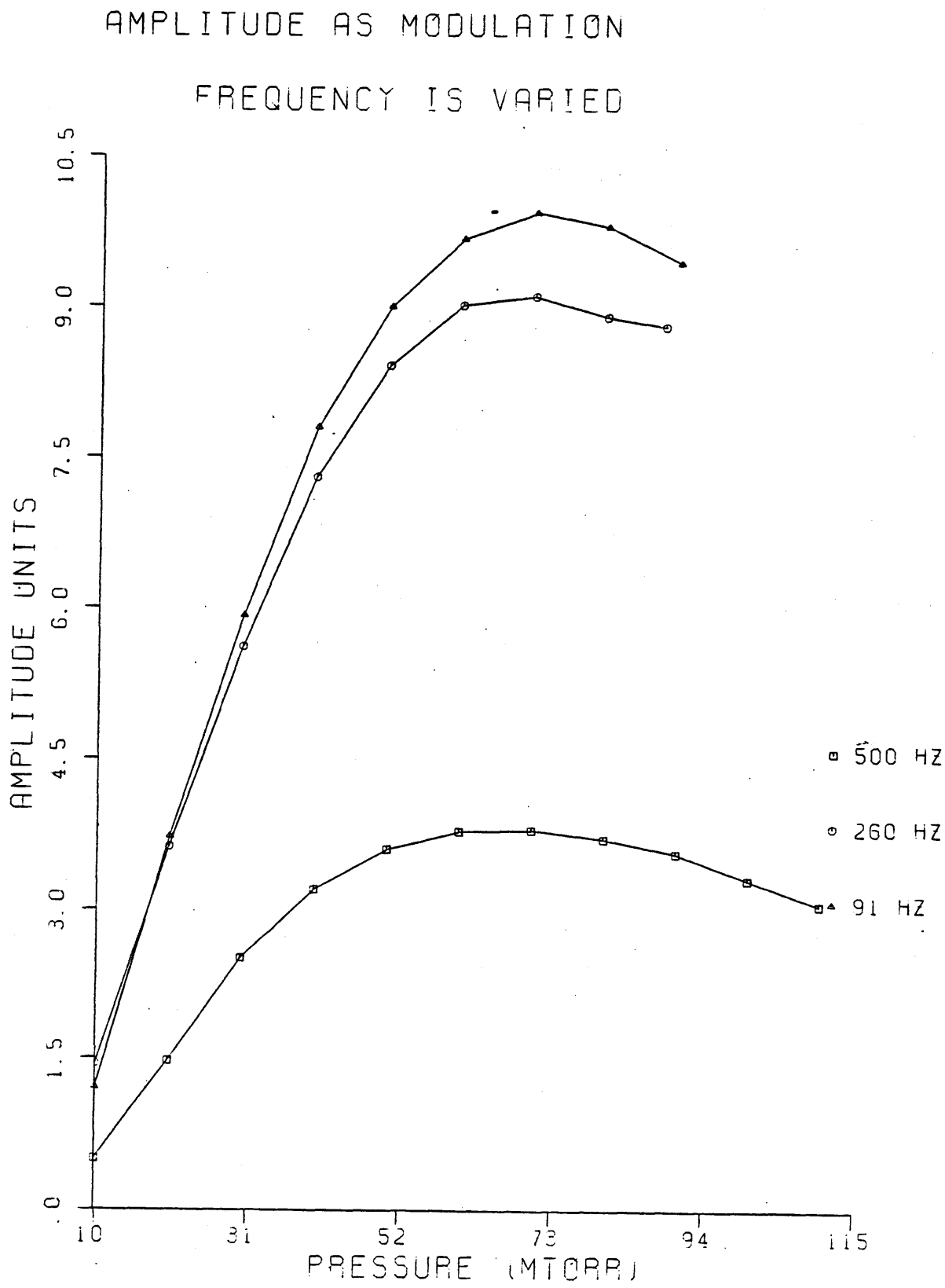

Figure 5 Peak Derivative Signal

lag. The amplitude and phase response of the 4.3 μm fluorescence signal, measured by the lockin amplifier is plotted in Figures 4 and 5 for several modulation frequencies. As expected, the smallest modulation frequency produced the largest amplitude response with the smallest phase lag as the pressure was varied. Likewise, Figures 6 and 7 show the phase and amplitude as a function of power at a fixed 91 Hz modulation frequency. Figure 8 shows the phase response at a modulation frequency of 130 Hz as the pressure is increased to several torr. Note that radiation trapping does not become important at high pressures since then collisions begin to dominate and the phase lag begins to reverse. Kovacs[76] had found that radiation trapping "saturated" (the collisional relaxation rate decreased to a constant value) at a few torr but others[78] postulated that this is due to radiation trapping from other 'hot' band levels. Considering all the above measurements, the servo system was reconfigured to operate at 130 Hz reference and modulation frequency as a compromise.

Even considering all these frequency response arguments, the pressure shift should not depend on the modulation frequency; the stability of the lock or the response time of the servo system could conceivably depend on the

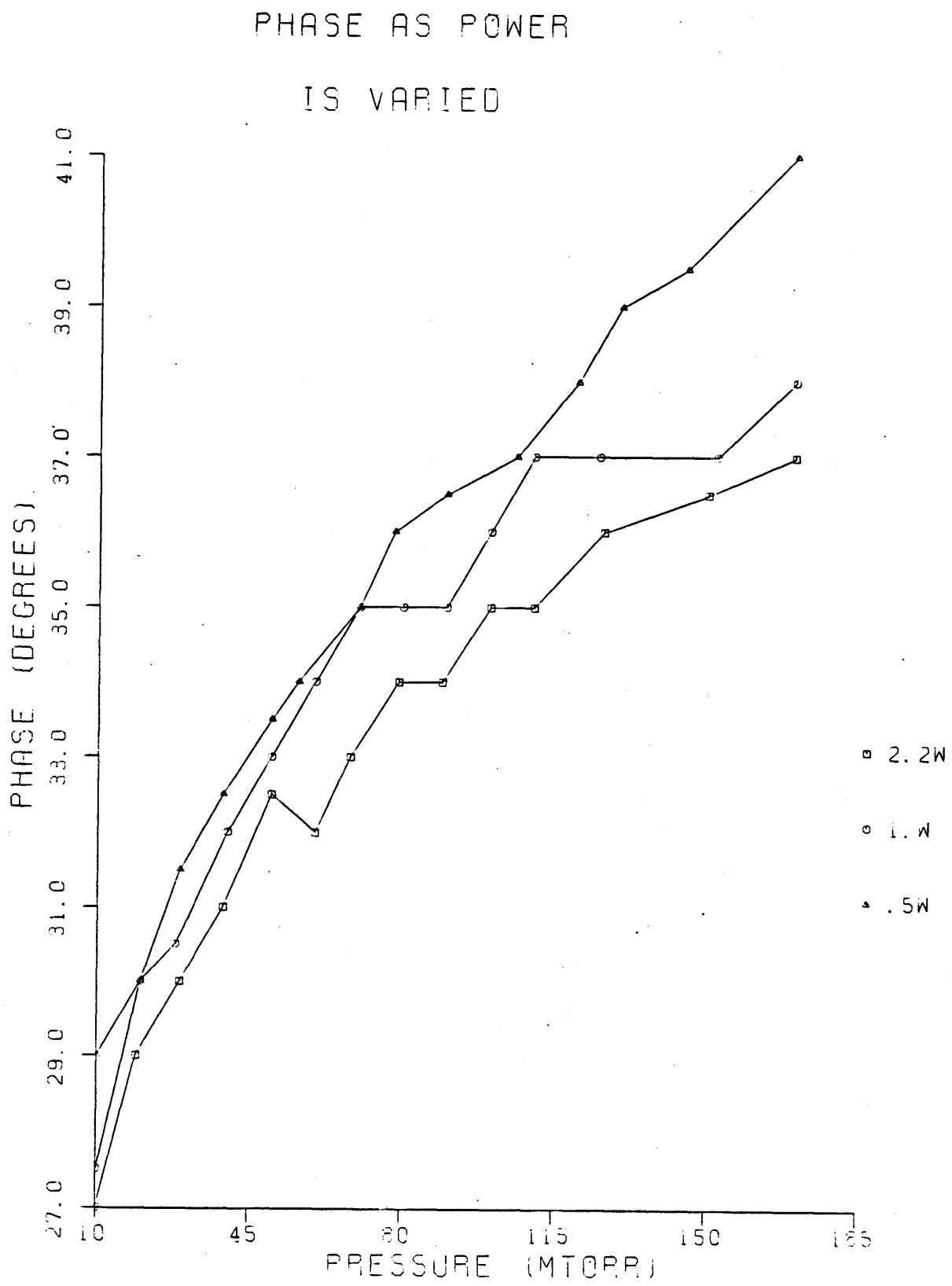

Figure 6 Phase Lag of Derivative Signal

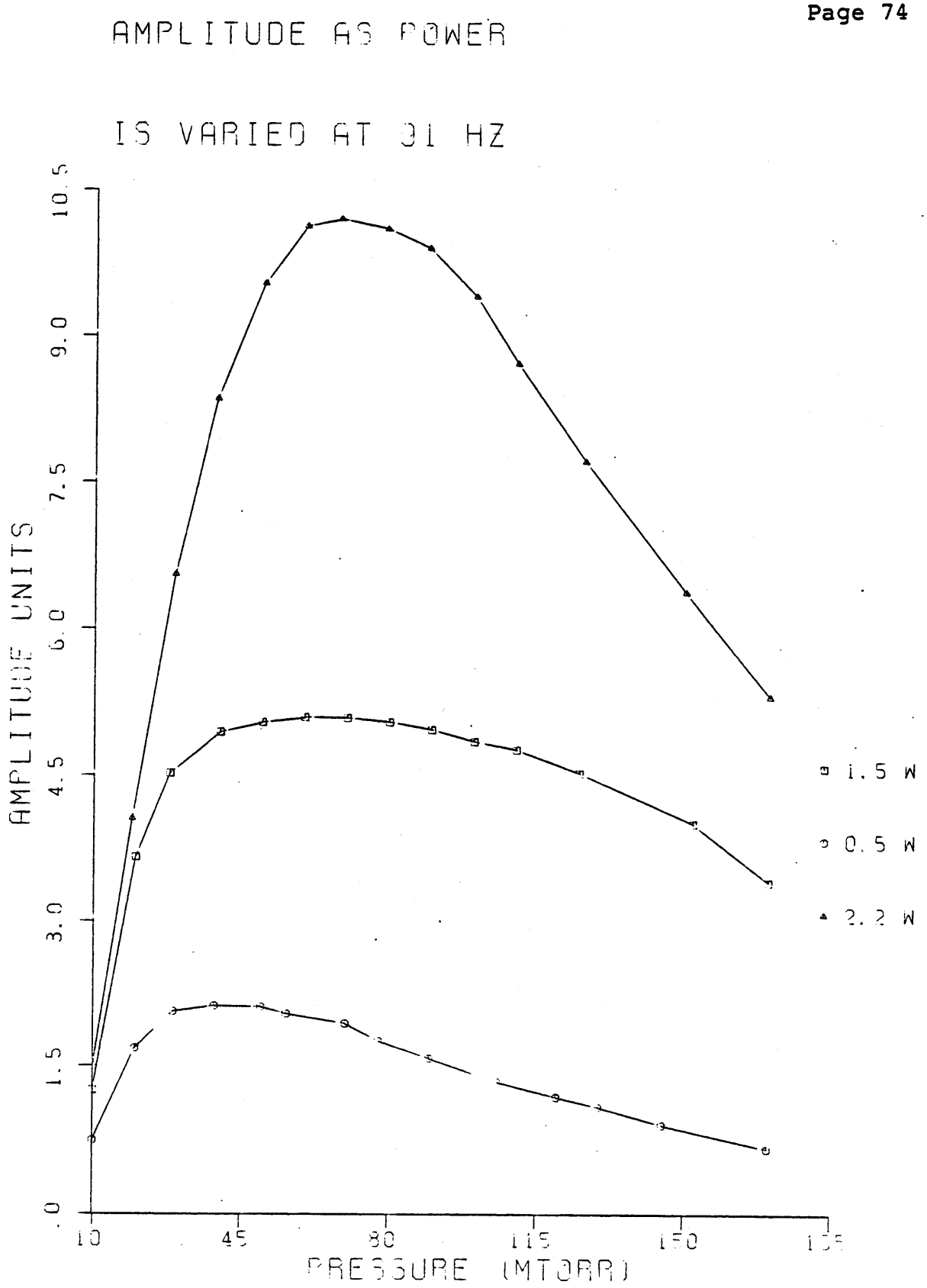

Figure 7 Peak Derivative Signal

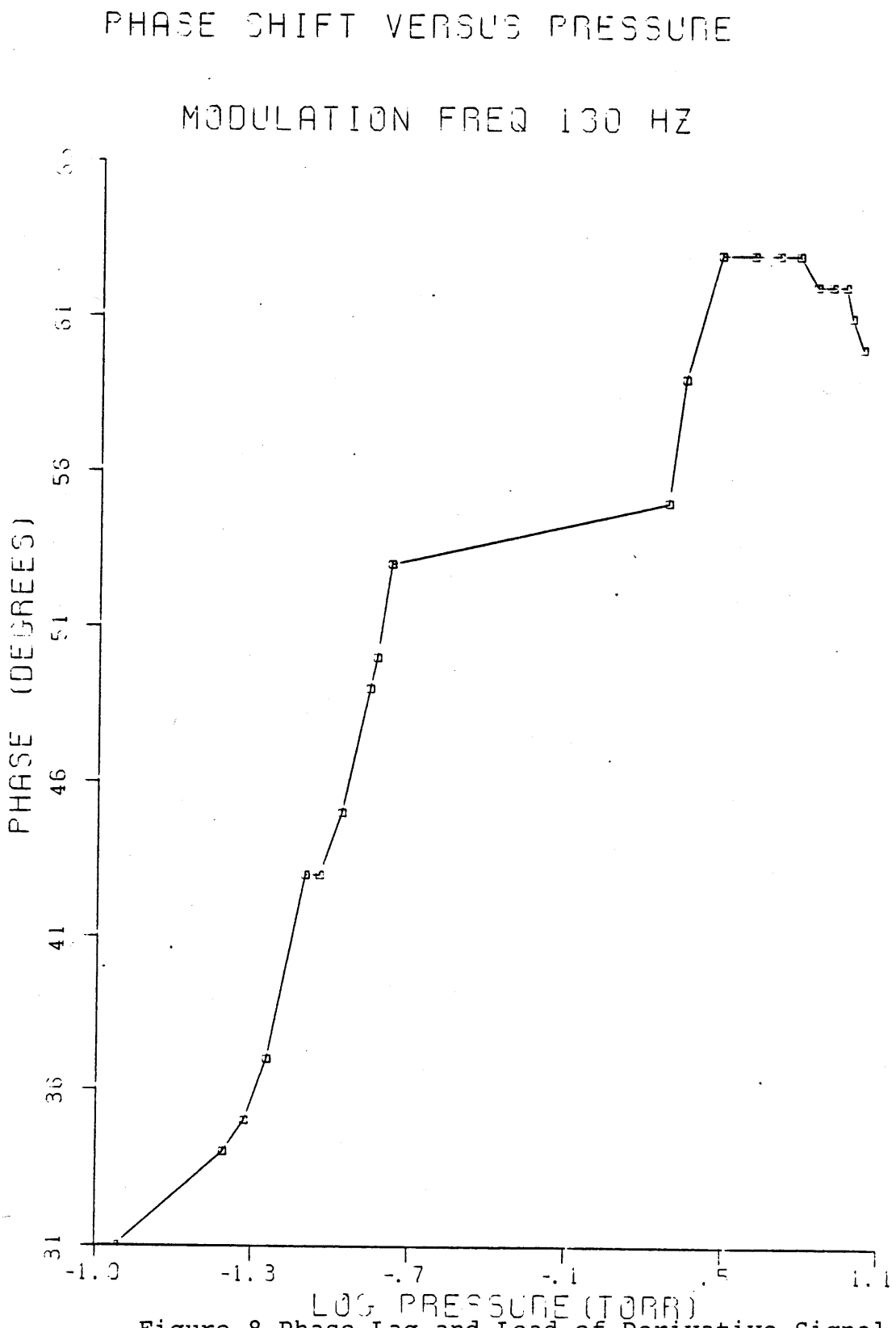

Figure 8 Phase Lag and Lead of Derivative Signal

frequency of modulation. The above analysis showed it is better to use a smaller modulation frequency to avoid phasing errors as the pressure is varied from 10 to 100 mtorr. Figure 9 shows consecutive pressure shift runs as the modulation frequency is varied from 500 to 260 to 91 Hz; remarkably enough, the value of the shift appears to be the same for all modulation frequencies. An older feedback servo loop system and amplifiers were used in these data runs since the reference frequency of the synchronous detector could be varied quite easily in this system. The only real variables in these different data runs were just drift, PZT hysteresis and time to take the runs; accordingly, there were slight absolute frequency displacements as the modulation frequency was changed from run to run. Overall, this showed that the frequency of modulation does not affect the pressure shift, within the errors and standard deviation of the experiment.

After all these precautions, it appeared that a small (3 to 7°) phase error did not affect the stability of the system or else the change was imperceptible in terms of frequency and in terms of the standard deviation of the beat signal. This was seen by deliberately 'misphasing' the lockin system a few degrees and comparing the resulting

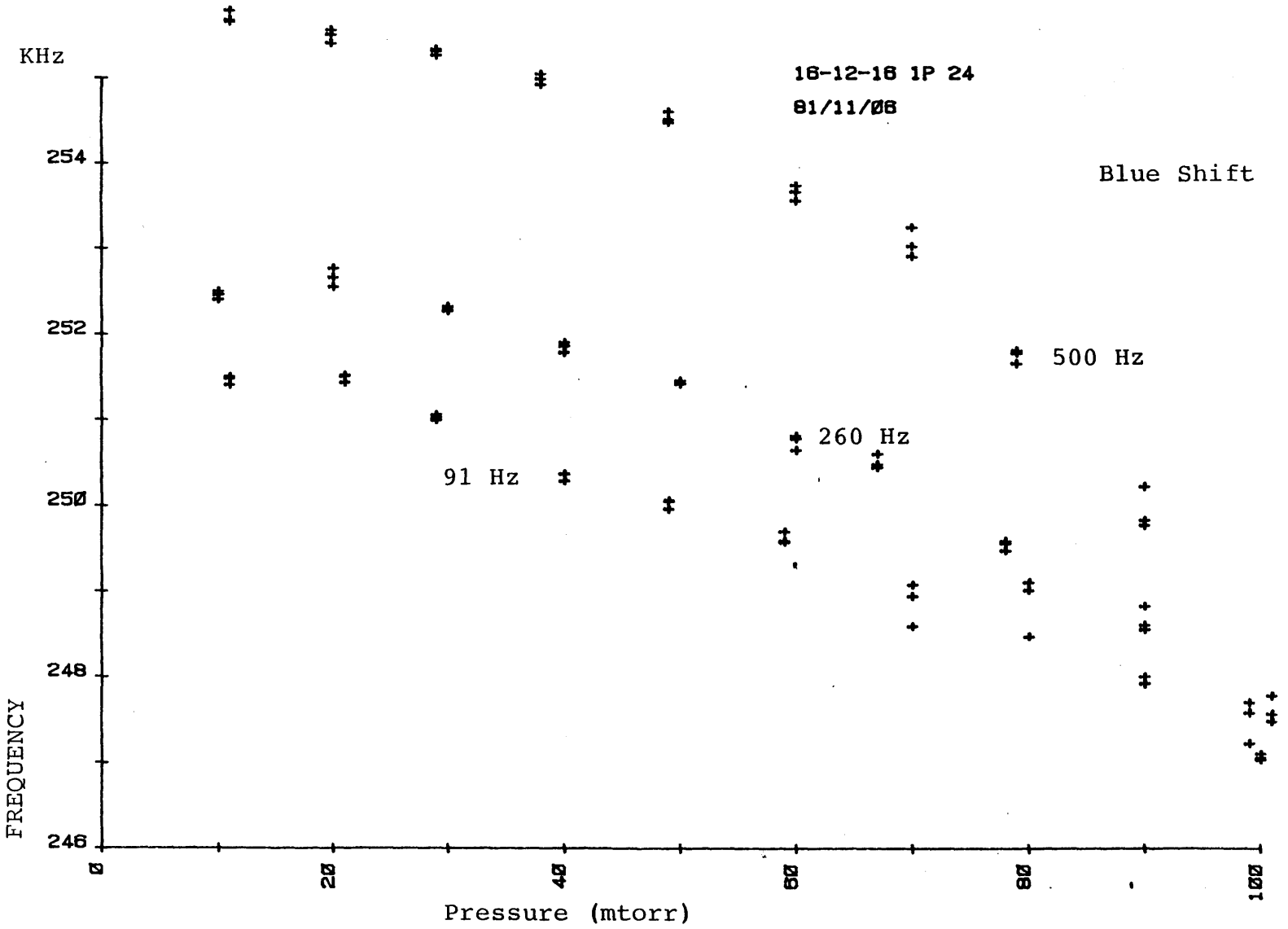

Figure 9 Pressure Shifts for Different Modulation Frequencies

frequency count with that of a correctly phased count. Essentially, a slight misphasing just decreases the lockin signal, A sin ϕ, a small amount which is fed back into the servo loop; this results in an incorrectly phased signal leading to a smaller feedback signal injected into the loop so that the loop takes a little longer time to come to equilibrium.

Besides optimizing the frequency at which to modulate the PZT stack, the amplitude of the modulation (the frequency excursion due to the dithering) must also be considered. The modulation amplitude must be large enough such that the fluorescence signal is detectable (quasi-optimum S/N) but the amplitude must be kept reasonably small to avoid all unnecessary parasitic amplitude modulation, nonlinearities in the PZT response and to avoid distorting the 4.3μm Lorentzian. The maximum derivative signal is obtained if the peak to peak frequency excursion equals 0.7 FWHM (full width half max) of the Lorentzian. But such a large excursion should be avoided based on the likelihood of a significant frequency shift due to prolonged excursions away from line center. A compromise modulation amplitude based on obtaining sufficient S/N for most J lines was used for all the pressure shift measurement. Figure 10 shows the

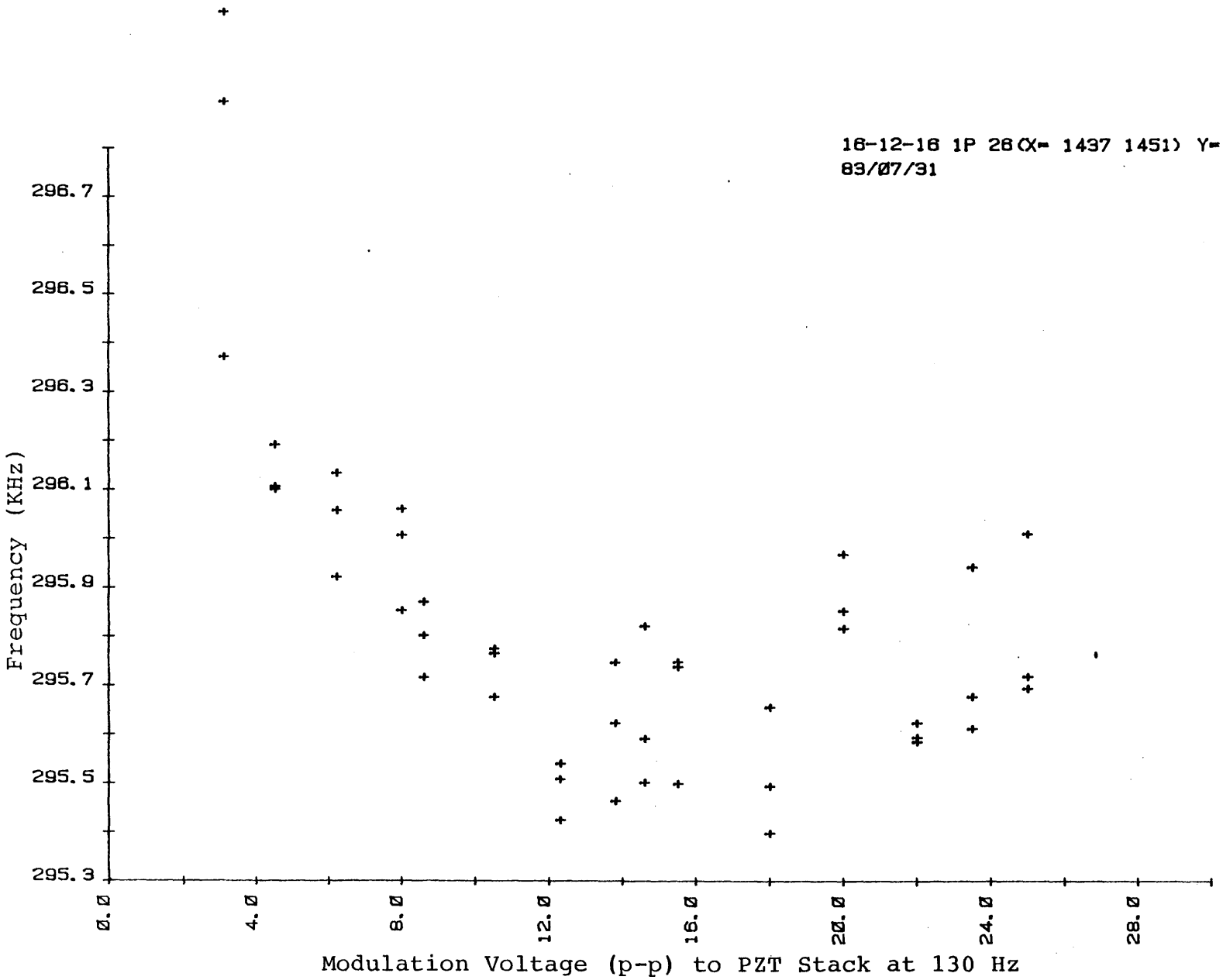

Figure 10 Frequency Shifts at Different Modulation Depths

frequency readings at fixed pressures as the modulation voltage was varied. Fortuitously, the modulation amplitude used throughout this experiment coincided with the minimum frequency deviation shown in the figure; this voltage (≃ 17 V p-p) corresponded to a frequency deviation of 310 KHz peak to peak (as measured on the spectrum analyzer) on a Lorentzian with a FWHM of 1 to 2 MHz. In reality, the frequency deviation due to the different p-p modulation amplitude is a function of several parameters including the applied cylinder voltage, hysteresis in the PZT and amplitude modulation at different grating positions. Note that the 'slope' error (see Chapter 6) was least for the 0-16 V region in Figure 10 while the 'slope' drift increased for voltages greater than 20 V.

STABILITY

After all these preparations and precautions, the question remains as to the stability and reproducibility of the system. This question was answered by taking several stability and drift runs. By examining the beat frequency over several months, the estimated month to month frequency reproducibility, at a given pressure level and approximate power level for a midband line, is probably better than 4

KHz. Depending on how much power there is and how well the lock is and how much external environmental influence there is, the standard deviation for the strongest midband line in 16-12-16 can easily be 100 Hz or less for absorption cell pressures between 20 and 70 mtorr.

Long term drift can be measured by taking time sequential frequency measurements over a period of several hours. These drift measurements (one example is given in Table 5 in the next page) with the time (hr,min,sec) printed out, normally show a maximum drift of less than 1 to 2 KHz over several hours after the system has been stabilized for several hours. The measurements can deviate from these near optimum values for different J or power levels.

Normally a σ vs. τ plot is taken to compare the frequency stability of the system with other systems. In the time domain, the frequency stability has been understood to refer to the square root of the two sample variance or Allan variance $\sigma^2_y(\tau) = \langle (y_{k+1}-y_k)^2/2 \rangle$; the Allan variance is an infinite time average of two frequency readings y_k and y_{k+1}, each of time duration τ. Of course, to realistically compute the Allan variance, only a finite number M, of

Tau(s)	Time		Frequency (Hz)		Standard Deviation (Hz)
10.00	03,02,51	Freq	3.20300867747E 08	Sigma	1.80338140246E 02
10.00	03,03,52	Freq	3.20301007693E 08	Sigma	1.71525401493E 02
10.00	03,04,52	Freq	3.20301044555E 08	Sigma	7.49534941180E 01
10.00	03,05,52	Freq	3.20301234047E 08	Sigma	2.57336179903E 02
10.00	03,06,53	Freq	3.20301115679E 08	Sigma	3.22020010179E 02
10.00	03,07,53	Freq	3.20301269391E 08	Sigma	2.61263334001E 02
10.00	03,08,54	Freq	3.20301390960E 08	Sigma	2.64091996958E 02
10.00	03,09,54	Freq	3.20301591310E 08	Sigma	2.90690657235E 02
10.00	03,10,55	Freq	3.20301547495E 08	Sigma	3.50492540821E 02
10.00	03,11,55	Freq	3.20301578297E 08	Sigma	2.67035946649E 02
10.00	03,12,56	Freq	3.20301259940E 08	Sigma	1.17296641975E 02
10.00	03,13,56	Freq	3.20301541883E 08	Sigma	1.05838797185E 02
10.00	03,14,57	Freq	3.20301811651E 08	Sigma	4.33508167627E 02
10.00	03,15,57	Freq	3.20301789775E 08	Sigma	2.20703723145E 02
10.00	03,16,58	Freq	3.20301894105E 08	Sigma	1.53895946499E 02
10.00	03,17,58	Freq	3.20301908693E 08	Sigma	1.70661875345E 02
10.00	03,18,59	Freq	3.20301042247E 08	Sigma	2.51667139167E 02
10.00	03,19,59	Freq	3.20300751367E 08	Sigma	6.85909470775E 01
10.00	03,21,00	Freq	3.20300876815E 08	Sigma	1.03778515681E 02
10.00	03,22,00	Freq	3.20300052293E 08	Sigma	7.84486089740E 01
10.00	03,23,01	Freq	3.20300958887E 08	Sigma	4.66266828449E 01
10.00	03,24,01	Freq	3.20301043177E 08	Sigma	1.83137798997E 02
10.00	03,25,02	Freq	3.20301395133E 08	Sigma	1.75070447106E 02
10.00	03,26,02	Freq	3.20301436901E 08	Sigma	1.56823022986E 02
10.00	03,27,03	Freq	3.20301370073E 08	Sigma	1.26073198706E 02
10.00	03,28,03	Freq	3.20301344559E 08	Sigma	4.47328537497E 01
10.00	03,29,04	Freq	3.20301254155E 08	Sigma	8.27565100460E 01
10.00	03,30,04	Freq	3.20301266223E 08	Sigma	1.66330010862E 02
10.00	03,31,05	Freq	3.20301150653E 08	Sigma	1.87691789142E 02
10.00	03,32,05	Freq	3.20301142623E 08	Sigma	1.87025210141E 02
10.00	03,33,06	Freq	3.20301150633E 08	Sigma	1.71755404883E 02
10.00	03,34,06	Freq	3.20301225965E 08	Sigma	1.62409438549E 02
10.00	03,35,07	Freq	3.20301157003E 08	Sigma	1.24149581379E 02
10.00	03,36,07	Freq	3.20301362097E 08	Sigma	5.34103014500E 01
10.00	03,37,08	Freq	3.20301418131E 08	Sigma	1.15792340657E 02
10.00	03,38,08	Freq	3.20301728300E 08	Sigma	7.04535548850E 01
10.00	03,39,09	Freq	3.20301790590E 08	Sigma	1.03059443243E 02
10.00	03,40,09	Freq	3.20301926093E 08	Sigma	1.26765557635E 02
10.00	03,41,10	Freq	3.20302026951E 08	Sigma	2.31871365585E 02
10.00	03,42,10	Freq	3.20301917849E 08	Sigma	1.48337216463E 02
10.00	03,43,10	Freq	3.20301974025E 08	Sigma	9.90771588610E 01
10.00	03,44,11	Freq	3.20301769831E 08	Sigma	7.45195589220E 01
10.00	03,45,11	Freq	3.20301852897E 08	Sigma	7.27317684990E 01
10.00	03,46,12	Freq	3.20301613459E 08	Sigma	6.60023245385E 01
10.00	03,47,12	Freq	3.20301621703E 08	Sigma	1.18085965341E 02
10.00	03,48,13	Freq	3.20301492467E 08	Sigma	2.02236360510E 02
10.00	03,49,13	Freq	3.20301383037E 08	Sigma	1.24459260451E 02
10.00	03,50,14	Freq	3.20301560837E 08	Sigma	1.39872111895E 02
10.00	03,51,14	Freq	3.20301515497E 08	Sigma	6.56549515725E 01
10.00	03,52,15	Freq	3.20301464047E 08	Sigma	1.47245607549E 02
10.00	03,53,15	Freq	3.20301519109E 08	Sigma	2.12979486702E 02
10.00	03,54,16	Freq	3.20301451391E 08	Sigma	6.12945773700E 01
10.00	03,55,16	Freq	3.20301435477E 08	Sigma	6.38662202455E 01
10.00	03,56,17	Freq	3.20301362843E 08	Sigma	9.73161337805E 01
10.00	03,57,17	Freq	3.20301323311E 08	Sigma	1.02136408190E 02
10.00	03,58,18	Freq	3.20301184589E 08	Sigma	2.20473013343E 02

Table 5 Drift Measurements

trials is taken such that the Allan variance can be approximated as

$$\sigma^2(M,\tau) \simeq 1/(2(M-1)) \; \Sigma_k{}^M (y_{k+1}-y_k)^2$$

Normally

$$y(t) = \nu_o + 2\pi d\phi(t)/dt$$

where ν_o is the center frequency and $\phi(t)$ is the instantaneous phase deviation. Then the Allan variance is really the fractional frequency deviation defined as

$$\sigma(\tau) \simeq (\phi(t+\tau)-\phi(t))/\; 2\pi\nu_o\tau \simeq \delta\nu_o/\nu_o$$

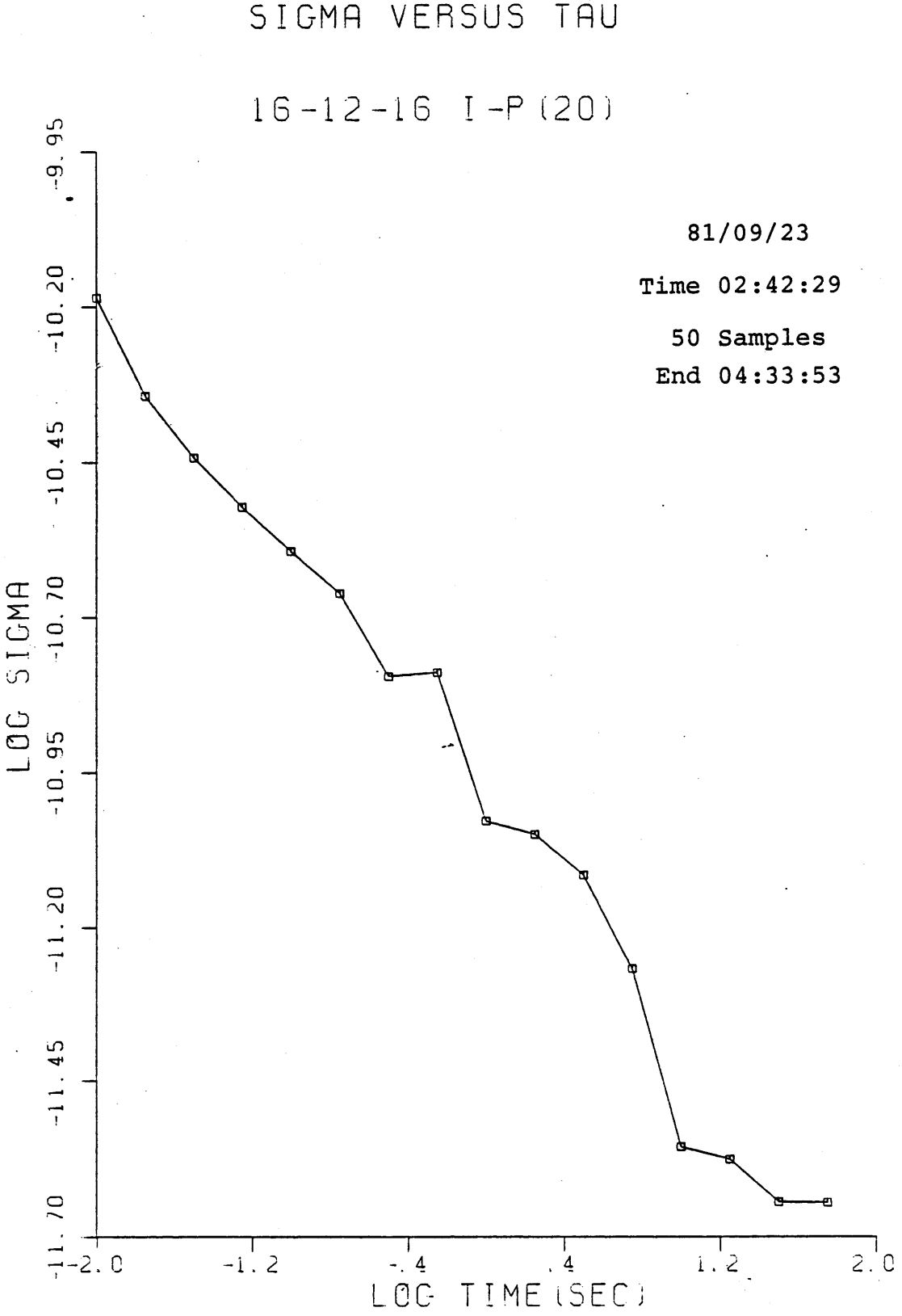

Figure 11 Sigma vs Tau Plot

Table 5
Sigma vs Tau
81/09/23
Time 2:42:29

Time τ	Sigma σ
0.01	6.524E-11
0.0178	4.536E-11
0.0316	3.608E-11
0.0562	3.006E-11
0.100	2.547E-11
0.1778	2.179E-11
0.3162	1.598E-11
0.5623	1.622E-11
1.000	9.366E-12
1.7783	8.894E-12
3.1623	7.657E-12
5.6234	5.382E-12
10.000	2.771E-12
17.7828	2.646E-12
31.6228	2.264E-12
56.2341	2.259E-12

The σ vs τ plot initially decreases with increasing τ to the influence of white noise, eventually it flattens out and increases as flicker and random walk noise dominates when τ is increased beyond a certain value. Using the HP 9345 Frequency Stability Measurement System, which was especially designed to measure the σ vs τ for stable oscillators, several plots were taken to measure the stability of the system. Two of these plots, taken several months apart are shown in Figures 11 and 12 and the actual values are shown

in Tables 6 and 7. These σ vs.τ plots show the characteristic decrease due to white noise and then the flattening out for longer time periods.

From these graphs, one can pick the best sampling interval to average over while remembering that this sampling interval must be reasonable enough so that the data runs will never last (drift) "too long". Since the interval from 10 to 50 seconds was the most reasonable in terms of fractional frequency stability and in time duration, all sampling intervals τ were taken to be 10 seconds where the 'maximum' possible standard deviation is

$$\sigma \simeq 2\times 10^{-12} \simeq \delta\nu/\nu_o \simeq 60 \text{ Hz}$$

in this experiment.

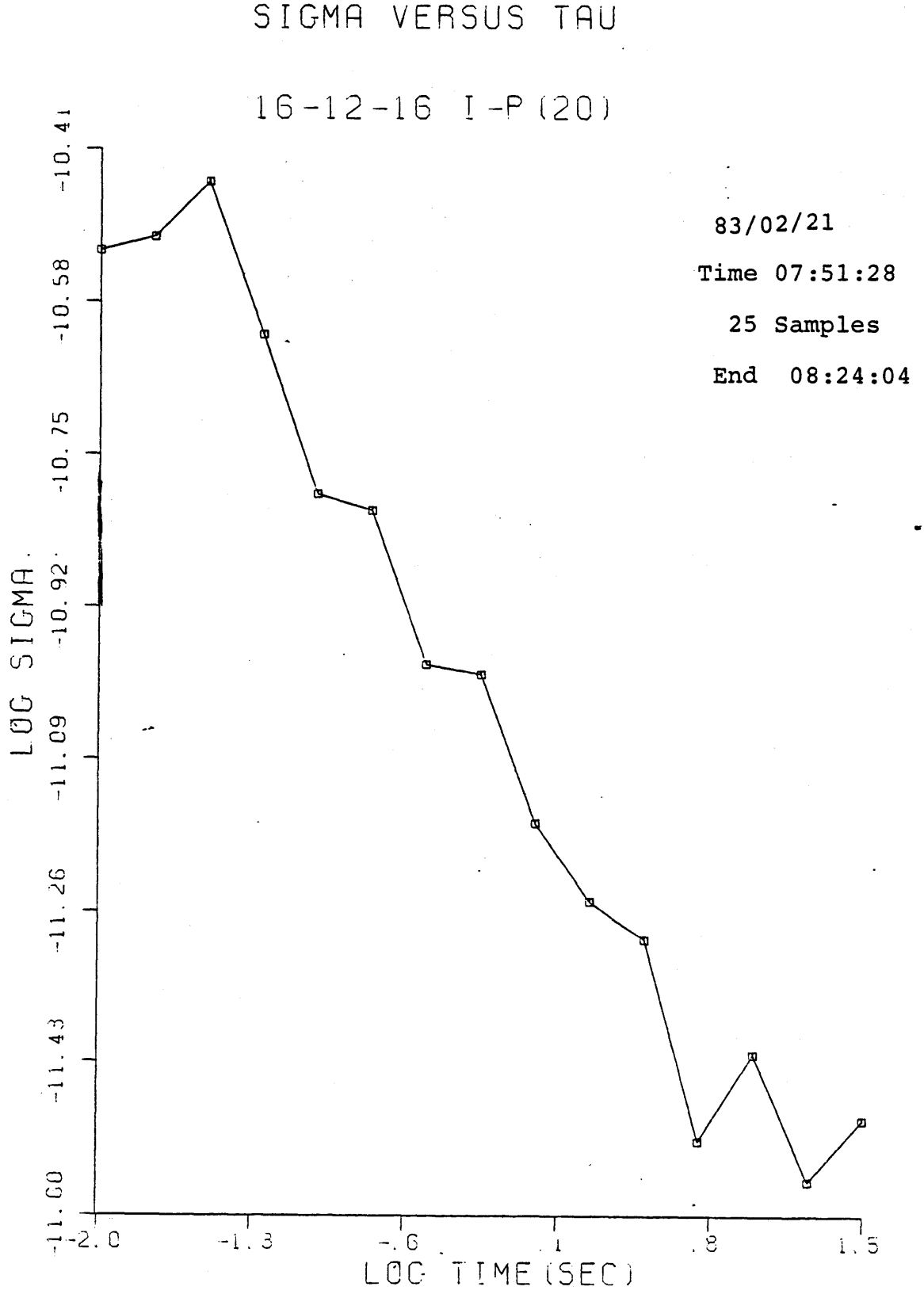

Figure 12 Sigma vs Tau Plot

Table 6
Sigma vs Tau
83/02/21
Time 7:51:28

Time τ	Sigma σ
0.01	2.998E-11
0.0178	3.106E-11
0.0316	3.578E-11
0.0562	2.419E-11
0.100	1.604E-11
0.1778	1.537E-11
0.3162	1.036E-11
0.5623	1.010E-11
1.000	6.888E-12
1.7783	5.644E-12
3.1623	5.109E-12
5.6234	3.031E-12
10.000	3.788E-12
17.7828	2.737E-12
31.6228	3.199E-12

CHAPTER 4 THE STANDING WAVE SATURATED RESONANCE

PHYSICAL ORIGIN

The method of saturated resonances is a well established technique to obtain homogeneous or near natural linewidth accuracy and stability. Saturated absorption spectroscopy or in our case, saturated fluorescence spectroscopy, is a universal technique that makes possible optical and infrared stability and standards (10^{-14} or 10^{-15}) [132-134,157-177] almost unheard of 15 years ago; examples of these techniques include vast improvements in the definition of the meter, second, and the speed of light[132] besides establishing secondary frequency standards by making absolute measurements[135-156] (relative to the cesium standard) in the infrared and quite recently, in the visible [153-155].

Physically, the response of an ensemble of two level systems moving with a velocity v and interacting with a laser field has a homogenous Lorentzian lineshape. A Doppler-broadened medium is obtained by adding these homogeneous responses of the ensemble of molecules with

their molecular velocities distributed according to a Maxwellian. In saturated resonance, an intense standing wave laser field picks a single homogeneous linewidth out of the Doppler broadened profile. In the case of CO_2, this homogeneous linewidth can be less than 1 MHz compared to the 52 MHz FWHM Doppler profile.

The laser standing wave can be decomposed into two counterpropagating traveling waves. Each wave interacts only with molecules which have a thermal velocity component along the field propagation direction sufficient to be Doppler shifted into resonance. Thus the resonance condition in the molecules frame of reference for the forward and backward traveling waves is

$$\omega_o = \omega \pm \mathbf{k}.\mathbf{v}$$

where ω_o is the two level resonance, ω is the laser frequency and $\mathbf{k}.\mathbf{v}$ is the first order Doppler shift. For intense laser fields, the transition between the two levels is fully saturated and half the lower level population is placed in the upper level. Thus the saturated resonance signal will normally be composed of contributions from the +v and -v homogeneous velocity groups for a given laser frequency ω .

When $\omega_o=\omega$ the resonant molecules are at rest in the propagation direction and both forward and backward waves saturate the same velocity group and a "Lamb dip" or a drop in the resonance signal occurs. This dip occurs because now only one velocity group contributes to the signal instead of the two +v or -v groups when the system is off resonance and because the response of the system saturates with intensity. Thus this dip in the signal serves as a fixed independent, physical reference to which the output of the laser can be locked.

In the case of CO_2, laser radiation is absorbed in the 10 and 9μm bands, creating a population inversion in the upper ν_3 level. Radiation from the upper level fluoresces down to the ground level, creating a 4.3 μm signal with insignificant background noise. By using saturated fluorescence, the Lamb dip or the first derivative of the homogeneous linewidth is recovered using phase sensitive detection. Saturated fluorescence, as initially demonstrated by Freed and Javan[119], gives a much better lock in CO_2 than that obtained with saturated absorption at 10 μm where the small ($\simeq 10^{-5}$) absorption signal has to compete with the huge background laser signal; saturated absorption has been used with heated cells[636,648,649]

operating at pressures of 1 to 10 torr to frequency stabilize the CO_2 laser but this method has never rivaled the stability obtained with saturated fluorescence.

LINESHAPE FOR STANDING WAVE SATURATED RESONANCE

There exists several analyses of the two level lineshape for a standing wave saturated resonance, ranging from a weak field to a high intensity solutions[315-328]. The actual lineshape function used to evaluate the linescans and pressure shifts in this experiment follows a rate equation solution of the two level standing wave saturation resonance as given by Kelly[280] and Thomas[279]. The rate equation approach is slightly modified to include rotational relaxation and velocity cross relaxation as measured by Granek[114] for CO_2. Here it is assumed that all dephasing collisions and inelastic collisions are lumped into one decay parameter γ. Instead of using a two level population equation, a semiclassical treatment is taken where the field is treated classically and the response of the medium is treated quantum mechanically in terms of a density matrix formulism ρ

$$d\rho/dt = i/\hbar[\rho, H]$$

where H is the Hamiltonian $H=H_o - \mu E$

and μ is the dipole moment and E is the laser field.

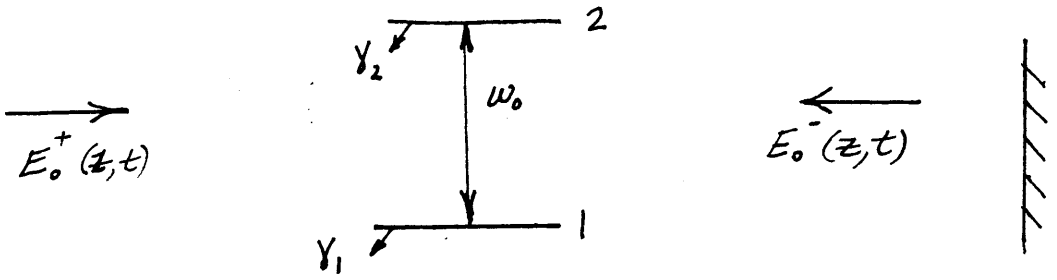

Figure 13 Energy Levels

Here $d/dt = (\partial/\partial t + v.\nabla)$ is the hydrodynamic derivative. Thus the equations for the two level system becomes with $E_2 - E_1 = \hbar\omega_o$

$$(\partial/\partial t + v\partial/\partial z)\rho_{11} = -\gamma_1(\rho_{11}-\rho^o_{11}) - (i/\hbar)V_{12}(\rho_{21} - \rho_{12}) - \int W(v\to v')\,\rho_{11}(v)\,dv' + \int W(v'\to v)\,\rho_{11}(v')\,dv' \qquad (4.1)$$

$$(\partial/\partial t + v\partial/\partial z)\rho_{22} = -\gamma_1(\rho_{22}-\rho^o_{22}) - (i/\hbar)V_{12}(\rho_{21} - \rho_{12}) - \int W(v\to v')\,\rho_{22}(v)\,dv' + \int W(v'\to v)\,\rho_{22}(v')\,dv'$$

$$(\partial/\partial t + v\partial/\partial z + i\omega_o + \gamma_t)\rho_{12} = -i/\hbar(\rho_{22} - \rho_{11})V_{12} + \int W_{12}(v'\to v)\,\rho_{12}(v')\,dv'$$

Here $\rho_{12}=\rho_{21}^*$, and $V_{12} = -\mu_{12}E(z,t)$ with $E(z,t) = 2E_o \sin kz \cos\omega t$ since the laser is considered to propagate only in the z direction. Here γ_1 and γ_2 are the

dephasing rates for levels 1 and 2 respectively while γ_t is the total coherence relaxation rate for the system including effects such as dephasing, rotational relaxation and wall effects.

$W(v \rightarrow v')$ represents the population collision kernels associated with the velocity change and $W_{12}(v \rightarrow v')$ represents the coherence kernels associated with the velocity change. Assuming there is no spatial population variations, $\partial/\partial z = 0$ and assuming that the coherence follows the field such that it can be separated into a slowly varying part and a rapidly varying part

$$\rho_{12}(v,t) \simeq \exp(-i\omega t)[\lambda^{+}_{12}(v)\, e^{ikz} + \lambda^{-}_{12}(v) e^{-ikz}]$$

and the velocity changing coherence dephasing term becomes

$$\int W_{12}(v' \rightarrow v) e^{-ik(v-v')t}\, \lambda_{12}(v')dv'$$

In traditional pressure broadening theory, as was pointed out by Berman[683], λ_{12} is slowly varying compared to W_{12} such that λ_{12} can be factored out of the integral as $\lambda_{12}(v)$. Assuming the same is true for CO_2, the velocity changing coherence term becomes $\Gamma^{vc}\lambda_{12}(v)$ where Γ^{vc} is the effective velocity changing collision relaxation rate. Then the

effective rate due to collisions becomes the usual dephasing relaxation rate

$$\gamma_{12} = \Gamma^{ph} = \Gamma^{t} - \Gamma^{vc} .$$

This approximation to γ_{12} is made in this rate equation analysis and hence only velocity changing effects on the population levels will be considered. In equilibrium, the populations ρ^{o} are assumed to follow a Maxwellian distribution

$$f_e(v) = 1/(u\sqrt{\pi})\exp(-(v/u)^2) \text{ where } u=\sqrt{(2\kappa T/m)} \text{ and}$$

$$\int f_e(v)\, dv = 1 \text{ so that } \rho_{11}^{o} = N_o f_e(v) \text{ and } \rho_{22}^{o} \simeq 0$$

Then, using the principle of detailed balance and also assuming complete randomization for every collision, the collision kernels become

$$W(v\rightarrow v')f_e(v) = W(v'\rightarrow v)f_e(v') = 1/\tau f_e(v)f_e(v')$$

where $1/\tau$ is an effective velocity collision rate. Assuming $\gamma = \gamma_1 = \gamma_2$ and using the above approximations, the equations for the population sum becomes

$$-\gamma(\rho_{11}+\rho_{22}) - (\rho_{11}+\rho_{22})/\tau + f_e(v)/\tau \int (\rho_{11}+\rho_{22})(v')\, dv' + \gamma(\rho_{11}^{o}+\rho_{22}^{o}) = 0$$

or $$\rho_{11}+\rho_{22} = \rho_{11}^{o}+\rho_{22}^{o} = N_o f_e(v)$$

The difference equation becomes

$$-\gamma(\rho_{22}-\rho_{11})-(\rho_{22}-\rho_{11})/\tau + f_e(v)/\tau \int(\rho_{22}-\rho_{11}(v')dv'$$
$$+\gamma(\rho_{22}^{\circ}-\rho_{11}^{\circ})-(\mu E/\hbar)^2(L^+ + L^-)(\rho_{22}-\rho_{11})=0$$

where $x=\omega_o-\omega$ is the detuning and

$$L^{\pm} = \frac{\gamma_{12}^2}{(x\pm kv_z)^2+\gamma_{12}^2}$$

Let $S = \dfrac{(\mu E/\hbar)^2}{\gamma_{12}(\gamma+1/\tau)}$

Then solving for the difference populations

$$\{1+S[L^+ + L^-]\}(\rho_{22}-\rho_{11}) = \frac{\gamma(\rho_{22}^{\circ}-\rho_{11}^{\circ})}{(\gamma+1/\tau)} + \frac{f_e(v)\int(\rho_{22}-\rho_{11})(v')dv'}{\tau(\gamma+1/\tau)}$$

Then dividing by $\{1+S[L^+ + L^-]\}$ and by integrating over $\int dv$ on both sides and collecting terms

$$[1-F/(\tau(\gamma+1/\tau))]\int(\rho_{22}-\rho_{11})(v)dv = -\gamma N_o F/(\gamma+1/\tau)$$

where F and G are the standard integrals that come up so often in the standing wave resonances.

$$1 - F = G = \int \frac{f_e(v) S\,[L^+ + L^-]\,dv}{1 + S[L^+ + L^-]} \qquad (4.2)$$

Since the signal intensity $I(x) \propto \rho_{22} = \int \rho_{22}(v)dv$ and $\rho_{11} = \int \rho_{11}(v)dv$ with

$\rho_{22} + \rho_{11} = N_o$ the signal becomes, after substituting in these definitions

$$\rho_{22} = I(x) = \frac{N_o/2\,[1 + -\gamma F/(\gamma + 1/\tau)]}{1 - F/(\tau(\gamma + 1/\tau))} \qquad (4.3)$$

Clearing fractions and plugging in G = 1 - F

$$I(x) = \frac{N_o\, G(1+\tau\gamma)}{2\,(G+\tau\gamma)} = \frac{N_o\,(\gamma+1/\tau)G}{2\,\gamma(1+G/\tau\gamma)} \qquad (4.4)$$

The values of γ and τ as measured by Granek[114] are

$\gamma = 5\times10^6$ sec^{-1}-$torr^{-1}$ = 795.7 KHz/torr (rotational relaxation)

$\tau = .83\times10^{-7}$ sec^{-1}-torr = 1.91 MHz/torr (velocity cross relaxation)

Since G is approximately γ/ku, $\simeq$ 0.01 to 0.05 near the line core and $1/(\gamma\tau)$ = 2.4, the fluorescence signal is essentially independent of the effects of the velocity cross relaxation and rotational terms assuming no coherence velocity relaxation. Hence the signal is

$$I(x) \simeq N_o(\gamma+1/\tau)\ /(2\gamma)$$

In the Doppler limit, in which G can be evaluated in closed form, the Maxwellian $f_e(v)$ is considered so broad compared to the Lorentzian terms that the Maxwellian is factored out of the integral and evaluated at kv=x. Then the integral becomes, as given by Kelly and Thomas[279,280]

$$G(x) \propto \frac{\gamma_{12}^2 \exp(-(x/ku)^2)}{ku\sqrt{[x^2+\gamma^2(1+2S)]}} \times \frac{\sqrt{\{x^2+(1+S)\gamma^2_{12}+\sqrt{(x^2+\gamma^2_{12})\ [x^2+\gamma^2_{12}\ (1+2S)]}\}}}{\{-x^2+(1+S)\gamma^2_{12}+\sqrt{(x^2+\gamma^2_{12})\ [x^2+\gamma^2_{12}(1+S)]}\}} \qquad (4.5)$$

Taking the limits for $x \to 0$ and $x \to \infty$, the depth is

$$\propto \gamma_{12} N_o S\ \{1/\sqrt{(1+S)} - 1/\sqrt{(1+2S)}\}/ku \qquad (4.6)$$

and the percentage dip is

$$\%\text{Depth} \simeq \frac{\sqrt{(1+S)}}{\sqrt{(1+2S)}} \qquad (4.7)$$

An expression for the lineshape by intensity averaging over a Gaussian beam profile was also obtained by Kelly and Thomas. Here the saturation parameter is evaluated as $S = S_o \exp(-(r/R_o)^2)$. Thus the integral, averaging the previous lineshape which is now a function of x and r and S, $I(x,S(r))$, over the beam cross sectional area becomes

$$F(x) \propto \pi R_o^2 N_o/ku \times \times \{\sqrt{[2\gamma^2_{12}(1+S_o) + 2(x^2+\gamma^2_{12}) \times [1+2\gamma^2_{12}S_o/(x^2+\gamma^2_{12})]^{1/2} - 2x^2] - 2\gamma_{12}\}} \quad (4.8)$$

Here the FWHM is given by

$$\Gamma = \text{FWHM} = \gamma_{12}\sqrt{\{4S^2/[4(1+S)-(H+2)]^2 - (H+2)^2\}} \quad (4.9)$$

where $H+2=1/2\{1+2\sqrt{(1+S)} + \sqrt{(1+2S)}\}$

Then the depth is proportional to

$$D \propto \pi \Gamma^2_o N_o \gamma_{12}/(ku) \times \{2(\sqrt{(1+S_o)} - 1) - (\sqrt{(1+2S_o)} - 1)\} \quad (4.10)$$

and the fractional depth is

$$\%\text{Depth} \simeq \frac{2(\sqrt{(1+S_o)} - 1)}{\sqrt{(1+2S_o)} - 1} \quad (4.11)$$

These formulas for the dip and the fractional depth will be used in fitting the pressure shifts and the linescans with the proper error corrections in Chapters 5,6 and 7.

CHAPTER 5 LINESHAPE

INTRODUCTION

The primary purpose of the experiment reported in this thesis is to measure the pressure shift for the CO_2 lasing transitons. Figure 14 is a block diagram summarizing the two channel heterodyne system where each laser is locked to its own resonance in its own absorption cell. Part of the beams from both lasers are combined on a fast beat detector; the beat frequency is then heterodyned down to microwave frequencies using a HP 8672A microwave oscillator phase locked to a HP 3325A frequency synthesizer as the local oscillator.

In the pressure shift measurements, the pressure in the reference cell (referred to as the cell belonging to Laser 2) is kept fixed at a near optimum value (around 40 to 60 mtorr). The pressure is then varied in the first cell (referred to as the cell belonging to Laser 1) and the beat signal $\nu_1-\nu_2$ is counted on the HP 5345A counter where the 1 and 2 subscripts refer to Laser 1 and Laser 2 respectively. By using this convention, the frequency associated with

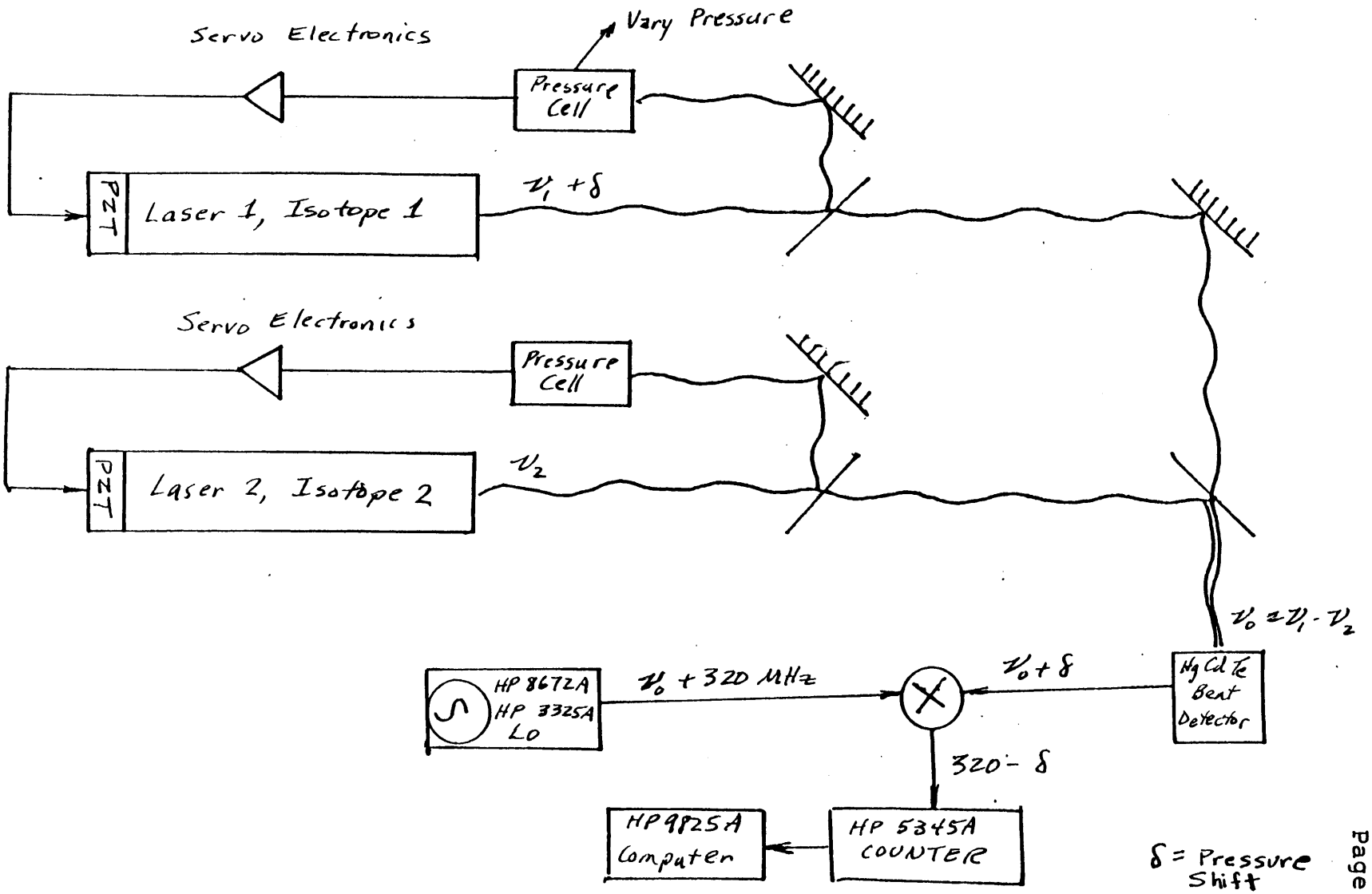

Figure 14 Block Diagram of Pressure Shift Measurements

Laser 1 is always pressure shifted and hence the beat frequency can be plus or minus; one needs to know the sign of the beat frequency to determine whether the shift is blue or red. Note that Laser 1 and Laser 2 can be either the left GP 157 or the right laser GP 153 but it is always Laser 1 that is pressure shifted.

Information on the variation of the linewidth of the Lamb dip resonance with pressure is very useful in formulating the lineshape theory. Normally it is the linewidth that is always measured in the majority of lineshape studies. While lineshift[516-551] studies have been rare, their corresponding theoretical fits have not been as good as those with the linewidths. This will be discussed later in the review of lineshape theory in Chapter 10 but suffice it to say that linewidths are not as sensitive to the theory as lineshifts are and accordingly, rough fits to the linewidths are usually easily obtained. To measure the linewidth a different setup, shown in the block diagram in Figure 15, is necessary to obtain a controlled frequency scan of the the Lamb dip. The unique aspect of this locking scheme is that the ordinate or frequency is counted exactly in contrast to the usual method of feeding a ramp voltage to the PZT cylinder and then

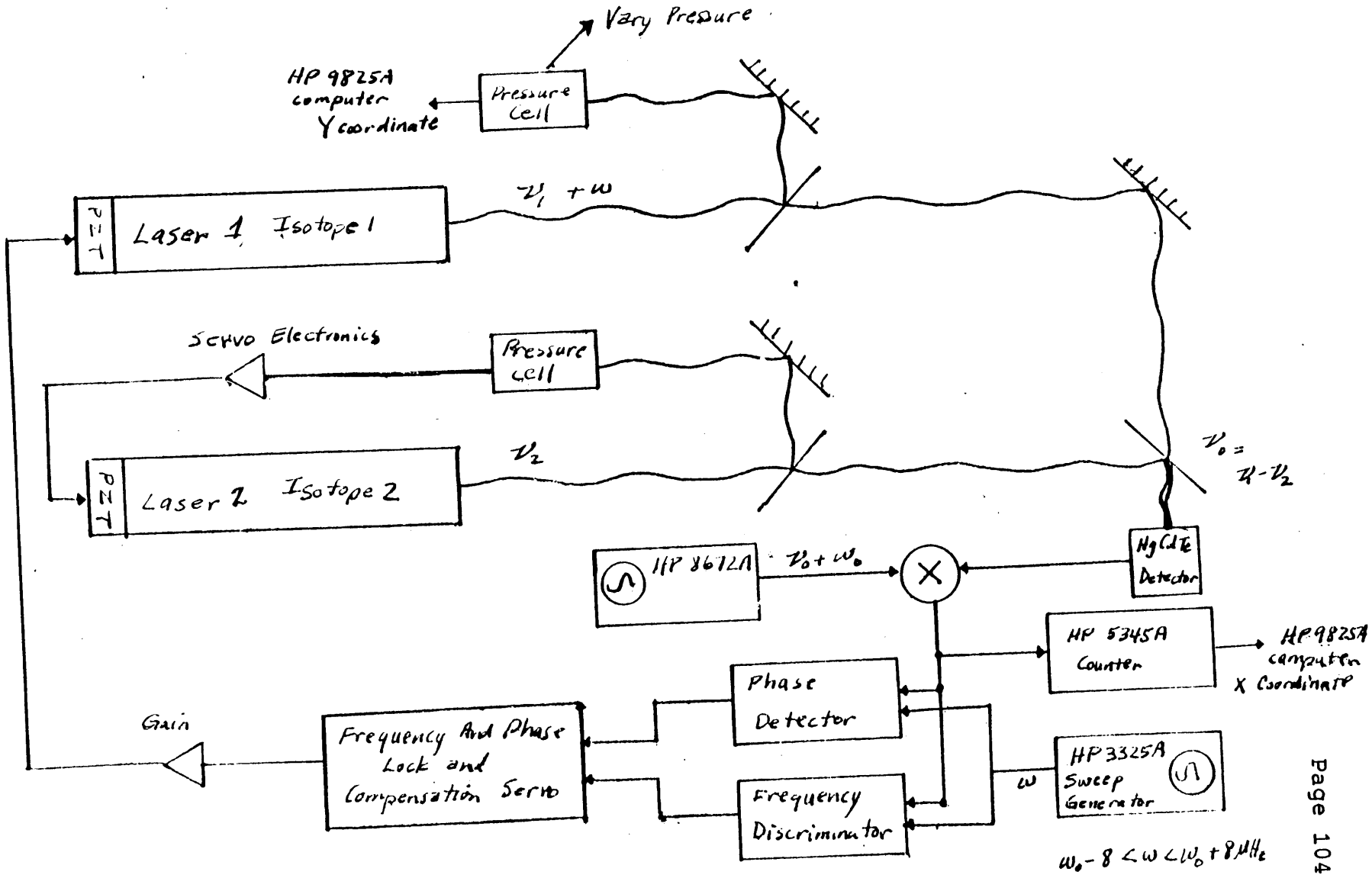

Figure 15 Block Diagram of Linewidth Measurements

expecting a quasilinear frequency scan from the PZT, hysteresis and all. In the lineshape scan technique, the reference laser (called Laser 2) is locked independently to its own Lamb dip and serves only as a reference from which the beat frequency can vary. The primary laser (Laser 1) is initially locked to line center. Now the beat frequency (RF) is heterodyned with the HP 8672A microwave LO source (±1 KHz) to give an IF of 17 to 18 MHz; thus the laser is initially offset locked at 18 MHz through this heterodyne technique. This offset 'beat' signal centered around 18 MHz is amplified and power split through a tee to go either to the HP 5345A electronic counter or else to the 'lock' box. This lock box, outlined in Appendix 3, provides the servo signal necessary to phase lock and frequency lock Laser 1 in the servo loop. In the lock box, the 18 MHz heterodyned laser beat frequency is digitally compared with the frequency doubled output of the HP 3325A synthesizer. The servo phase error is transformer coupled with the modulation voltage to the PZT stack so that both lasers will be synchronous in phase; this is the fast loop portion of the lock since Laser 1 must follow the instantaneous phase variations of Laser 2 such that the phase noise will cancel in the beat detector. The servo frequency error from the lockbox is used as a ramp voltage input; this error replaces

the normal feedback signal that controls the PZT cylinder voltage and consequently determines what frequency offset the laser is locked. Thus, as the output of the HP 3325A varies a few MHz, the cylinder input voltage follows this frequency excursion and consequently the laser output scans in frequency space, phase locked and frequency locked (the offset locked laser is frequency locked to the local oscillator and the frequency of the reference laser and is phase locked to the phases of both local oscillator and reference laser via the beat signal) to the local oscillator (HP 3325A). Of course, as the laser scans, the corresponding portion of the 4.3 μm fluorescence Doppler profile, including the Lamb dip, is probed and detected on the 131 lockin. Then by varying the pressure in the Laser 1 absorption cell, various linewidths as a function of pressure can be obtained. The entire linescan operation is under computer control once the laser has been phase and frequency locked to line center. Everything, including frequency measurements and voltage measurements are digitized and recorded under the HP 9825A computer control.

The timing sequence in which all these instruments operate is very important in obtaining the correct results. Assuming the laser has been phase and frequency locked to

the LO frequency, the 3325A then incrementally sweeps to a different frequency and halts. The 5345 counter takes a ten second average of the frequency and a HP3438A Digital Multimeter simultaneously records the amplitude of the derivative signal as the ordinate and abscissa values, respectively. Then the 3325A continues its discrete digital sweeps and the process continues. Usually 275 discrete, staggered frequency data points are taken for each line sweep and the results stored on cassette tape. Though this is a very different method of recording lineshapes in the sense that actual frequency values are measured, it suffers from being a very long, time consuming process that could suffer from drift errors. Each frequency sweep lasts for about thirty to forty five minutes depending on how many points are scannned. This method is perfectly satisfactory for recording or examining a few lineshapes but because it is time consuming, it is not ideal to use in numerous lineshape scans as a normal ramp voltage method can yield similar but quicker results. In our experiment the emphasis is on pressure shifts; linewidths just serve to complement and clarify the issue and also to reveal what physical parameters are involved in our particular laser system.

Initially several lineshape scans as a function of pressure were taken using both the left and right lasers. It became apparent that in our system the smallest linewidths were of the order of 700 KHz to 800 KHZ FWHM (full width half max); our setup was not designed for ultranarrow linewidths since we did not operate at very low pressures nor did we use expanded beams. This residual linewidth is predominately due to power broadening and some residual geometric broadening.

Most of the linescans concentrated on recording the derivative signal recovered by the 131 lockin amplifier. At almost all the pressures for which linescans were taken, the derivative signal and corresponding S/N looked almost textbook picture perfect; the first derivative signal is a high contrast signal centered about zero with a large plus or minus discriminator curve. Thus the long scan times did not affect the derivative signal such that the noise from each discrete point averaged out except for those points at which very poor lock conditions were present due to very high pressures or at the edges of the linescans. All derivatives scan were least squares fitted to their theoretical Lamb dip on top of a Gaussian. Details of this method are described in Appendix 2. Information about the

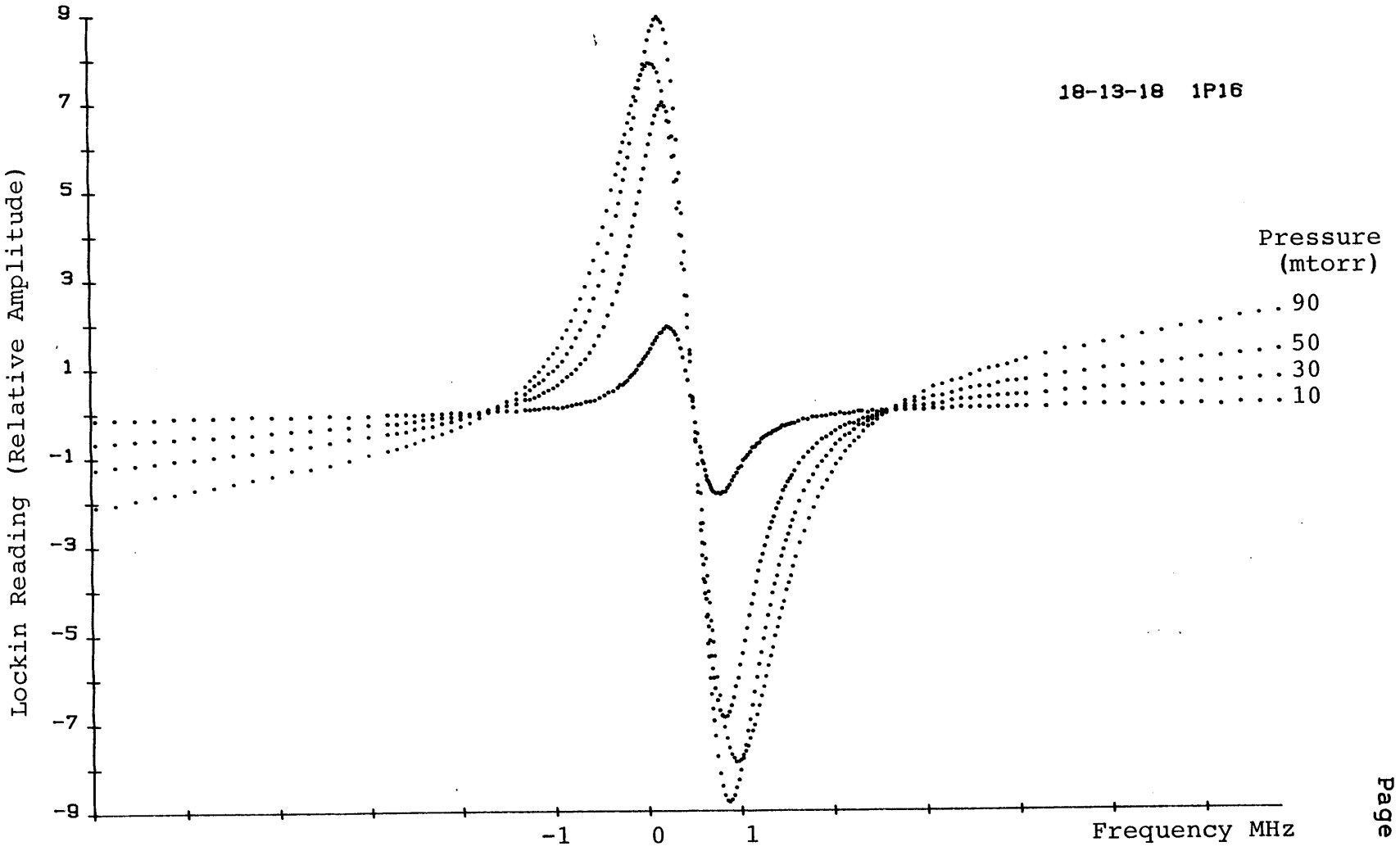

Figure 16 Derivative Signals for Different Pressures

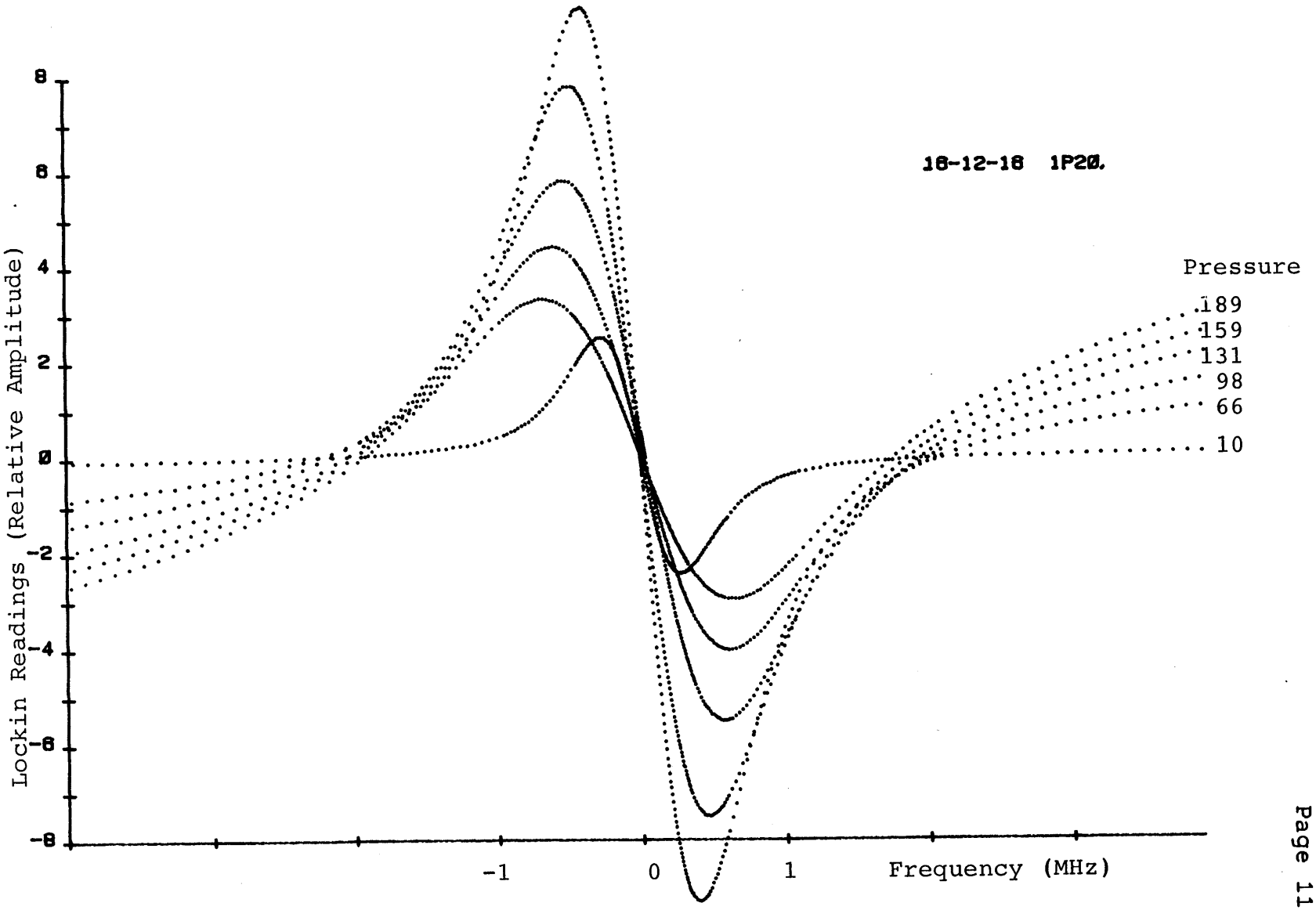

Figure 17 Derivative Signals for Different Pressures

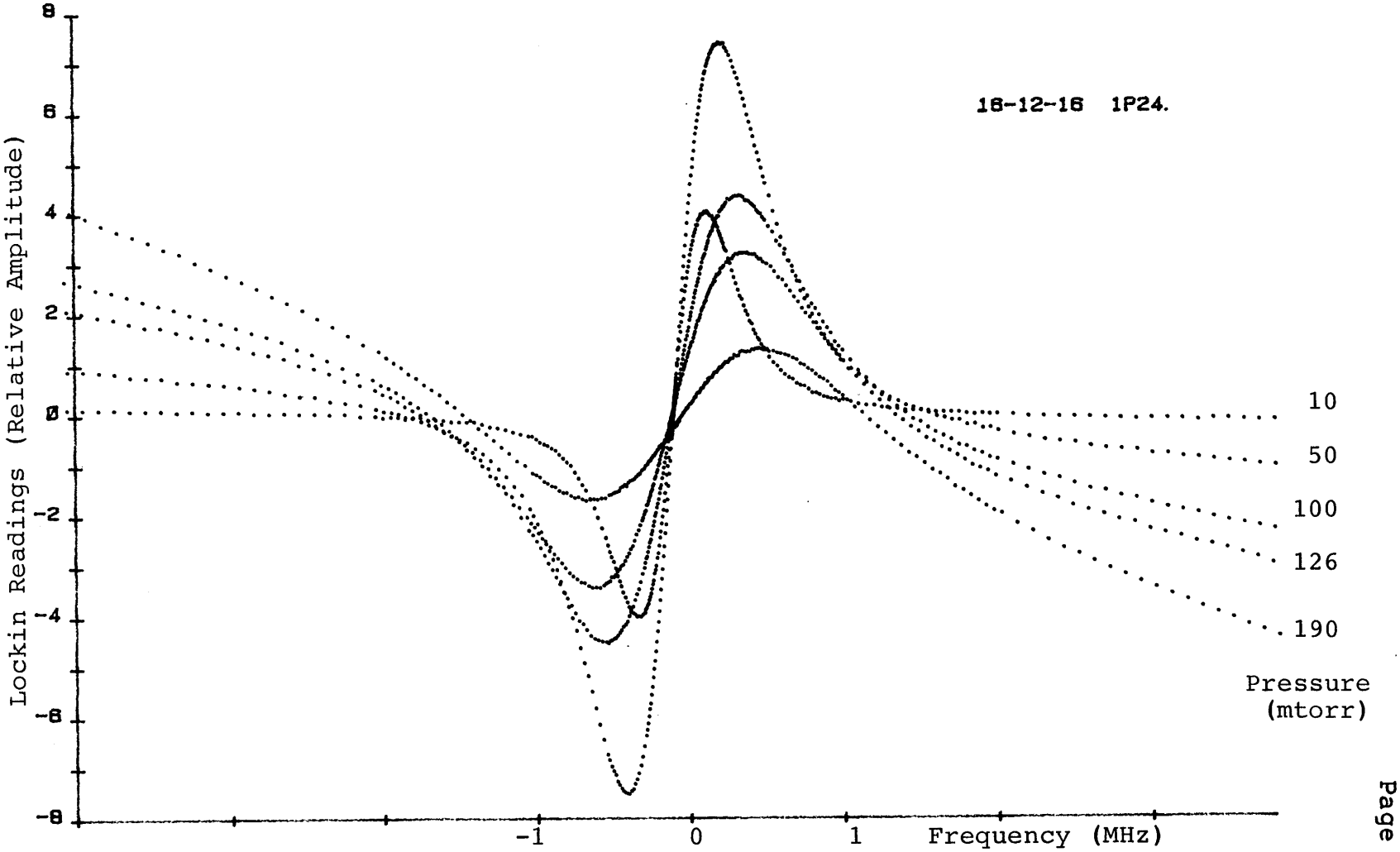

Figure 18 Derivative Signals for Different Pressures

background slope, FWHM and possible offset errors as a function of pressure could be derived from these least squares fits. Correspondingly, these derivative scans can be integrated to yield yet another textbook example of the Lamb dip on top of a Gaussian profile. Figures 16,17 and 18 show several of these 'perfect' derivative scans as a function of pressure; note the variation of the background slope with pressure. The integrated lineshapes in Figures 19 and 20 were least squares fitted to a parabolic background with a Lorentzian dip in the middle. For clarity the fit are not shown in these figures, but the correlation and fit are very good on the scale of the figures.

On the other hand, the actual or what was referred to as the 'integrated' signal can also be obtained by placing a chopper wheel in front of the absorption cell and synchronously detecting the fluorescence signal using the chopper frequency as the external reference. The same linescan procedures and computer programs were used to record the amplitude modulated signal. Now the discrete nature of the signal is very evident since the change due to the Lamb dip is only a small portion of the total signal. For higher cell pressures, not only does this percentage dip

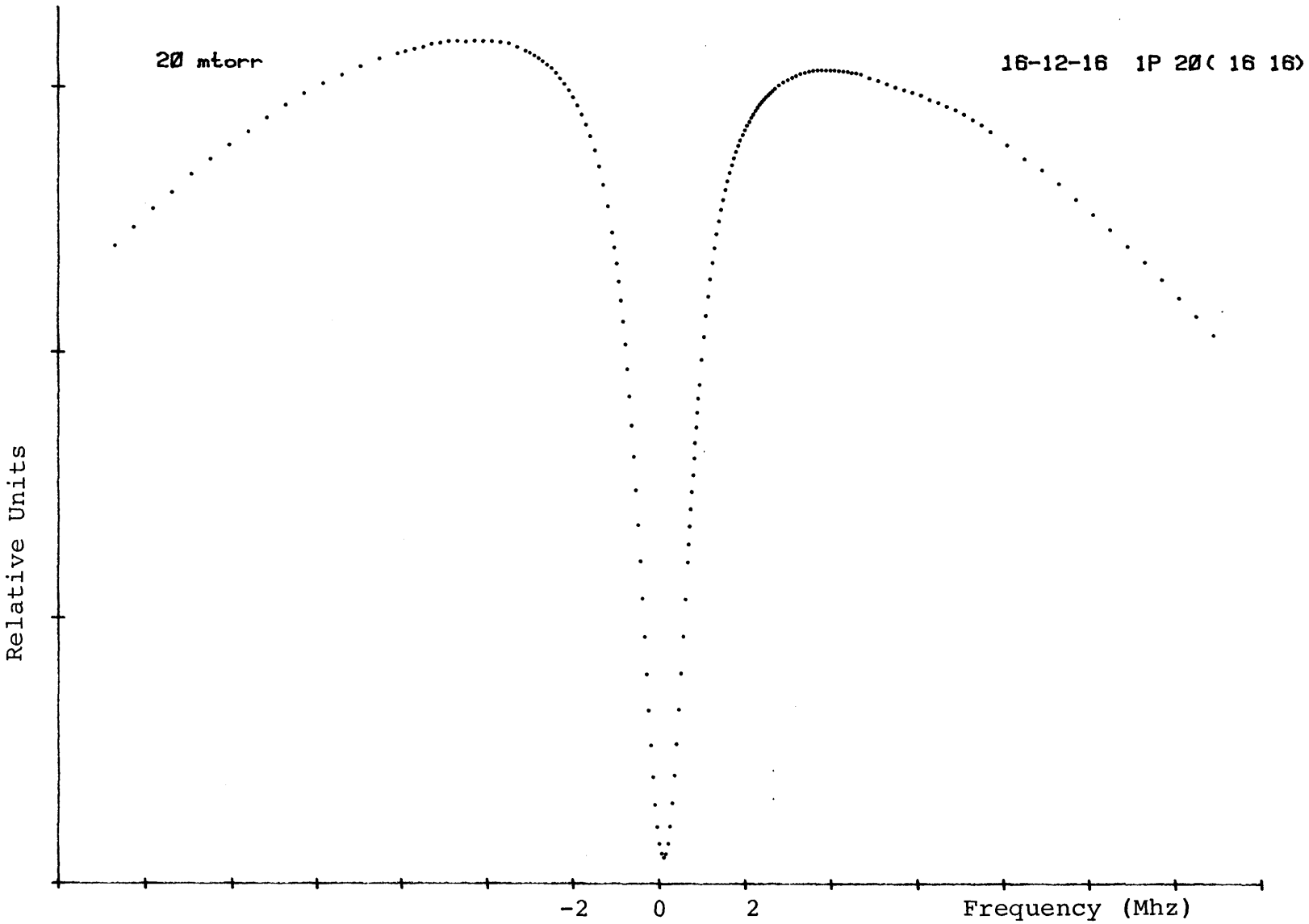

Figure 19 Integrated Fluorescence Signal

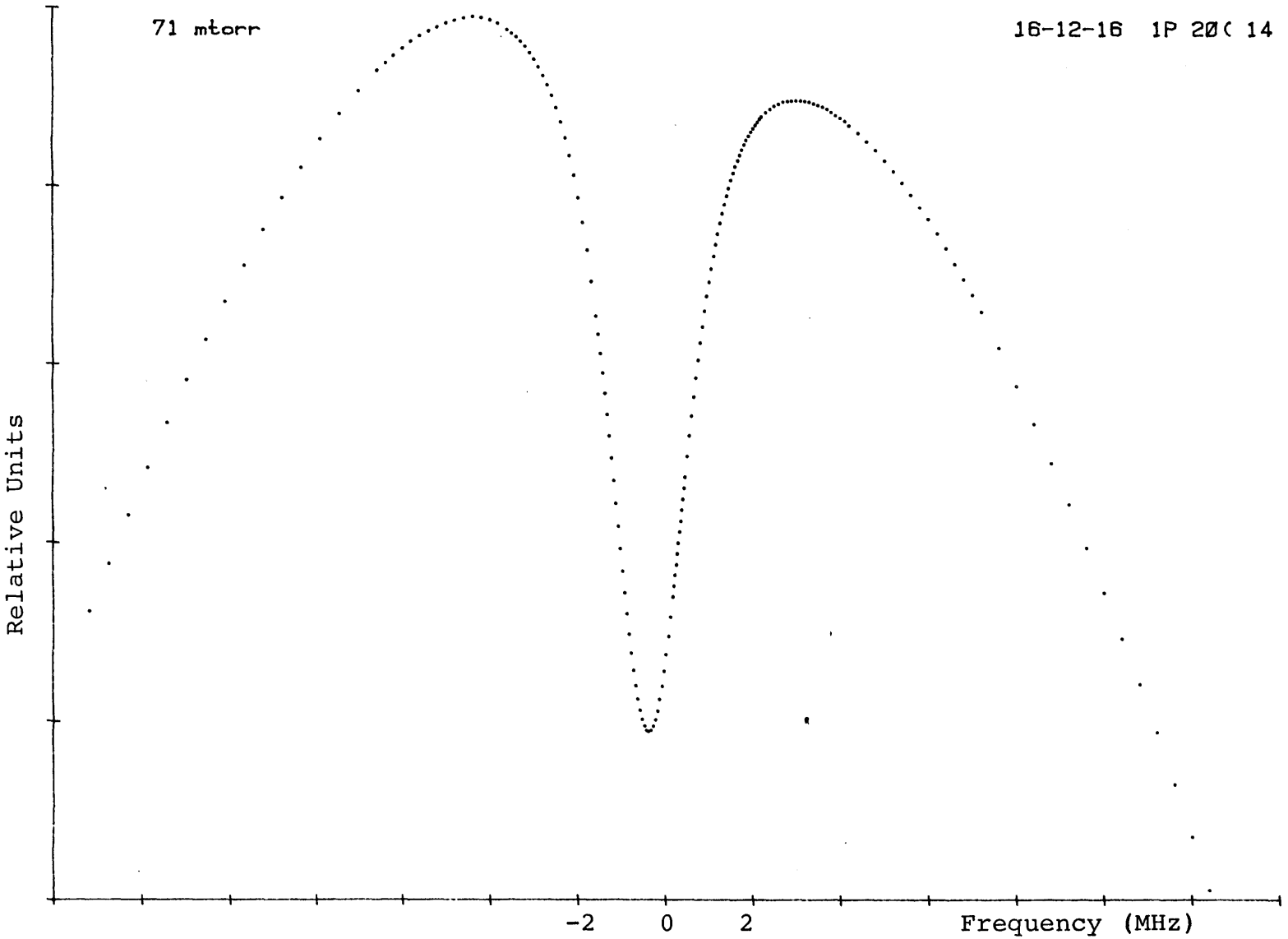

Figure 20 Integrated Fluorescence Signal

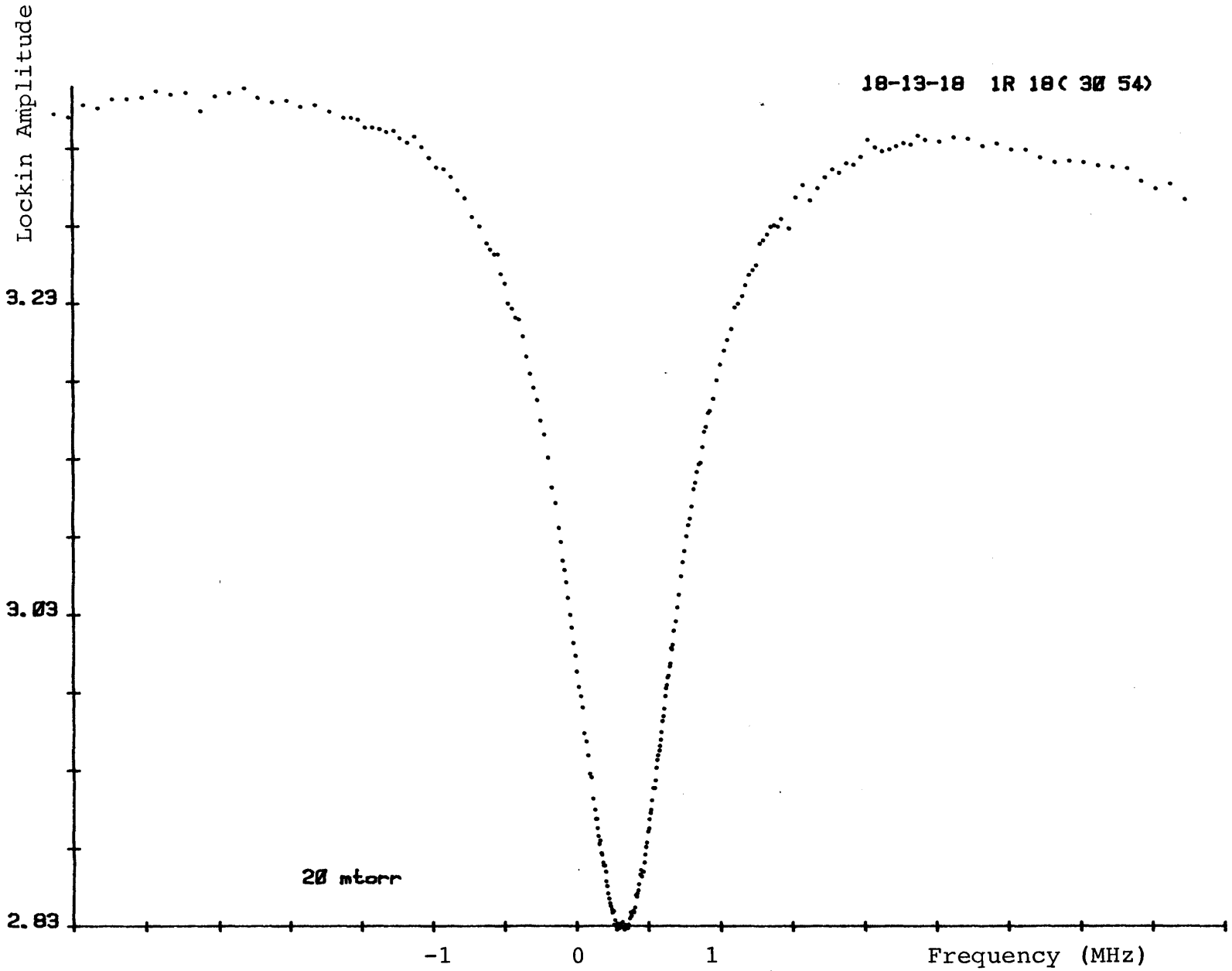

Figure 21 Chopped Fluorescence Signal

decrease, but the signal to noise also gets worse as seen in Figures 21,22,and 23.

Several other important laser parameters were measured in trying to find out the importance of the power slope. Figure 24 shows the fluorescence signal at two different pressures but made by a traveling wave and by a standing wave in the same absorption cell; an independent back reflecting mirror in an independent absorption cell was removed to create the traveling wave signal. The purpose of this test was to make sure the cells were operating correctly since the traveling wave signal should be around half the background standing wave signal. Another experiment involved inserting a Brewster angle attenuator in front of the cell and measuring the signals as the attenuator rotated from 0 to 90 to 180°. As expected, there was no strange polarizing effect as the fluorescence signal decreased proportionally as the linearly polarized laser field was attenuated by the Brewster angle attenuator.

The actual intensity profiles for both left and right laser beams were measured to determine if there was any spatial asymmetries in the spatial power profiles. In this measurement, a Scientech Power Meter 360001 measured the

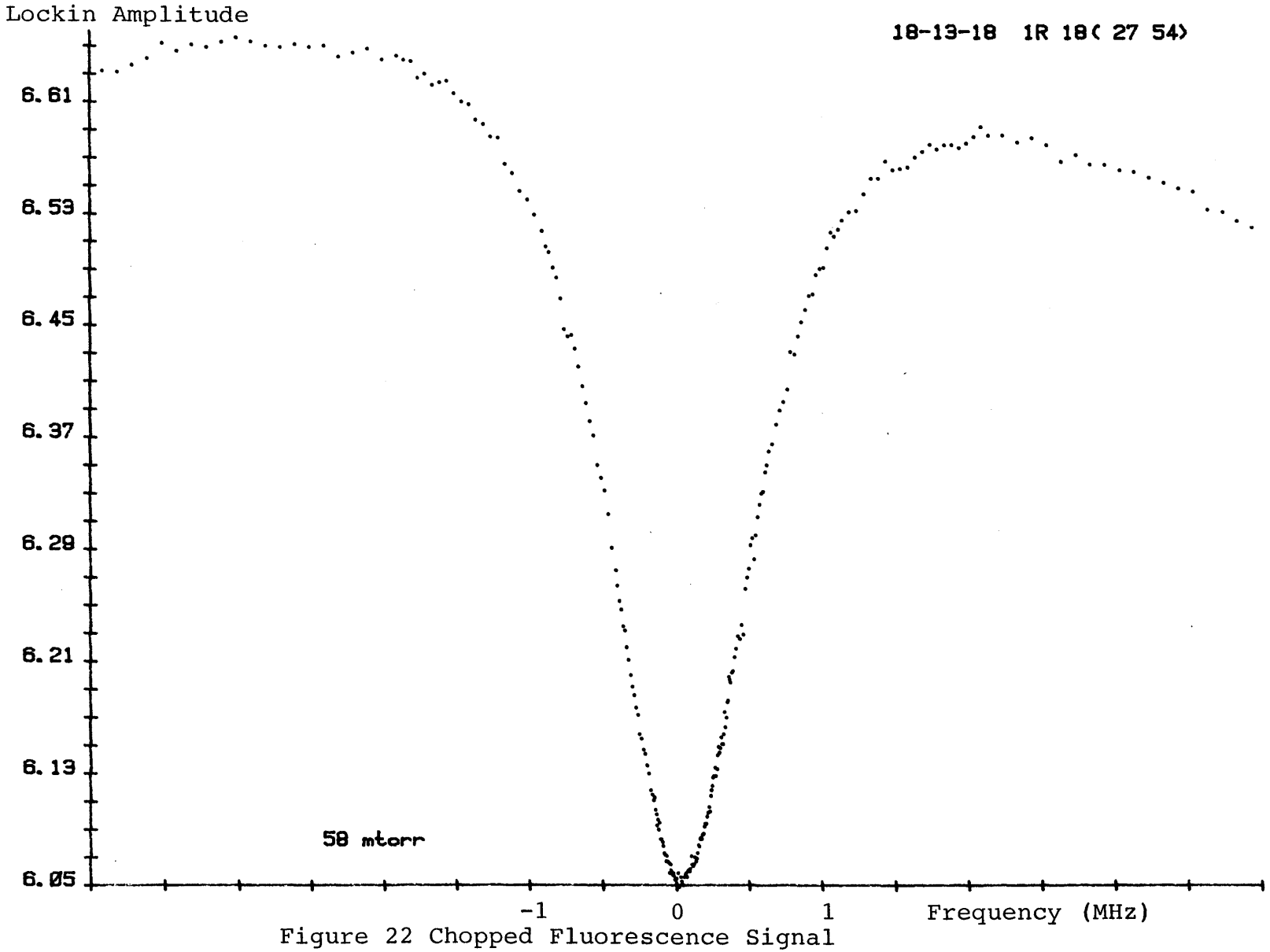

Figure 22 Chopped Fluorescence Signal

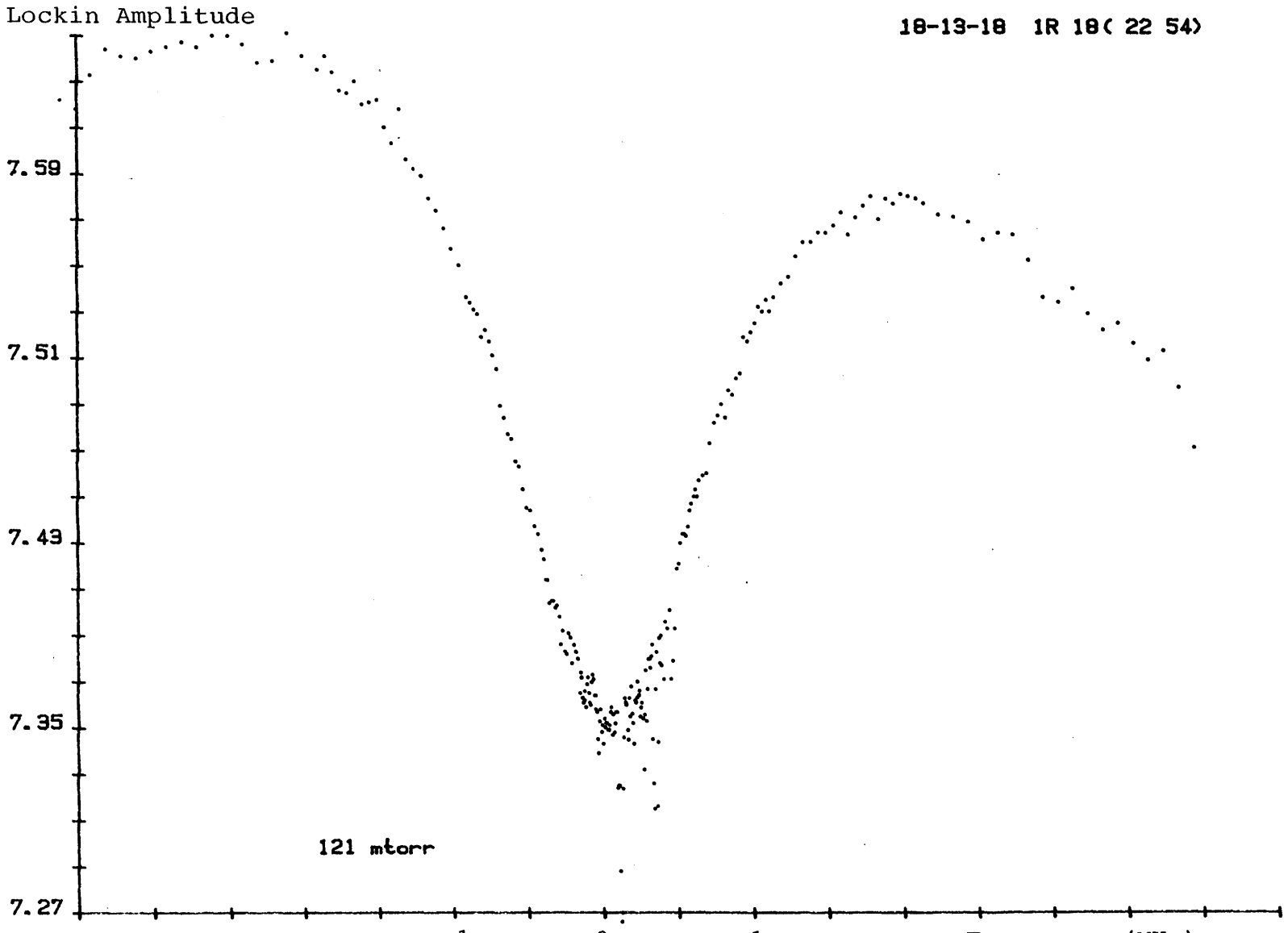

Figure 23 Chopped Fluorescence Signal

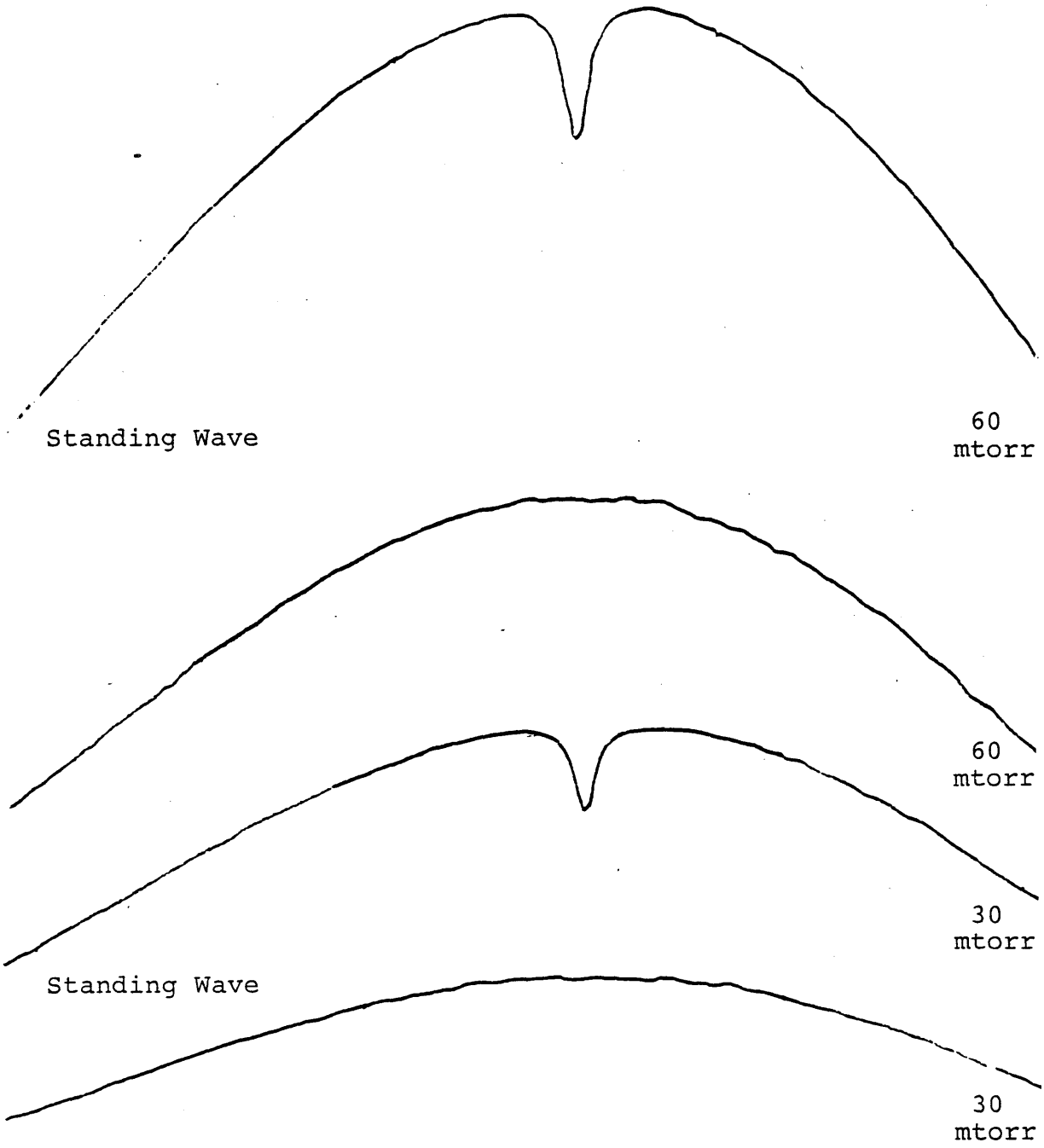

Figure 24 Traveling Wave and Standing Wave Signals

laser power after the laser beam passed through a beam limiting aperture. By varying the size of the beam limiting apertures, the power profile for the right and left lasers were recorded as shown in Figures 25 and 26. The continuous lines show the actual least squares intensity fit,

$$I=I_o\exp(-(r/r_o)^2)$$

where r_o is the 1/e intensity radius. The measured intensity radius was .48 and .43 cm for the left and right lasers respectively.

Besides taking line scans to measure the FWHM for several J values, a set of linewidths were taken at several power levels as the pressure was varied. Thus FWHM and background slope versus pressure for four different power levels were measured from these linescans for the same line. The FWHM and background slope is is plotted in Figures 27 and 28. From these graphs, one can see the residual (as the pressure goes to zero) FWHM is predominantly power broadened (with some misalignment broadening) while the background slope due to the Gaussian profile is also power dependent. Similar plots for the dip depth and percentage depth versus pressure for several different power levels were also taken. In this case, the phase and frequency locked depth measurements were plotted on a chart recorder, instead of being digitized and

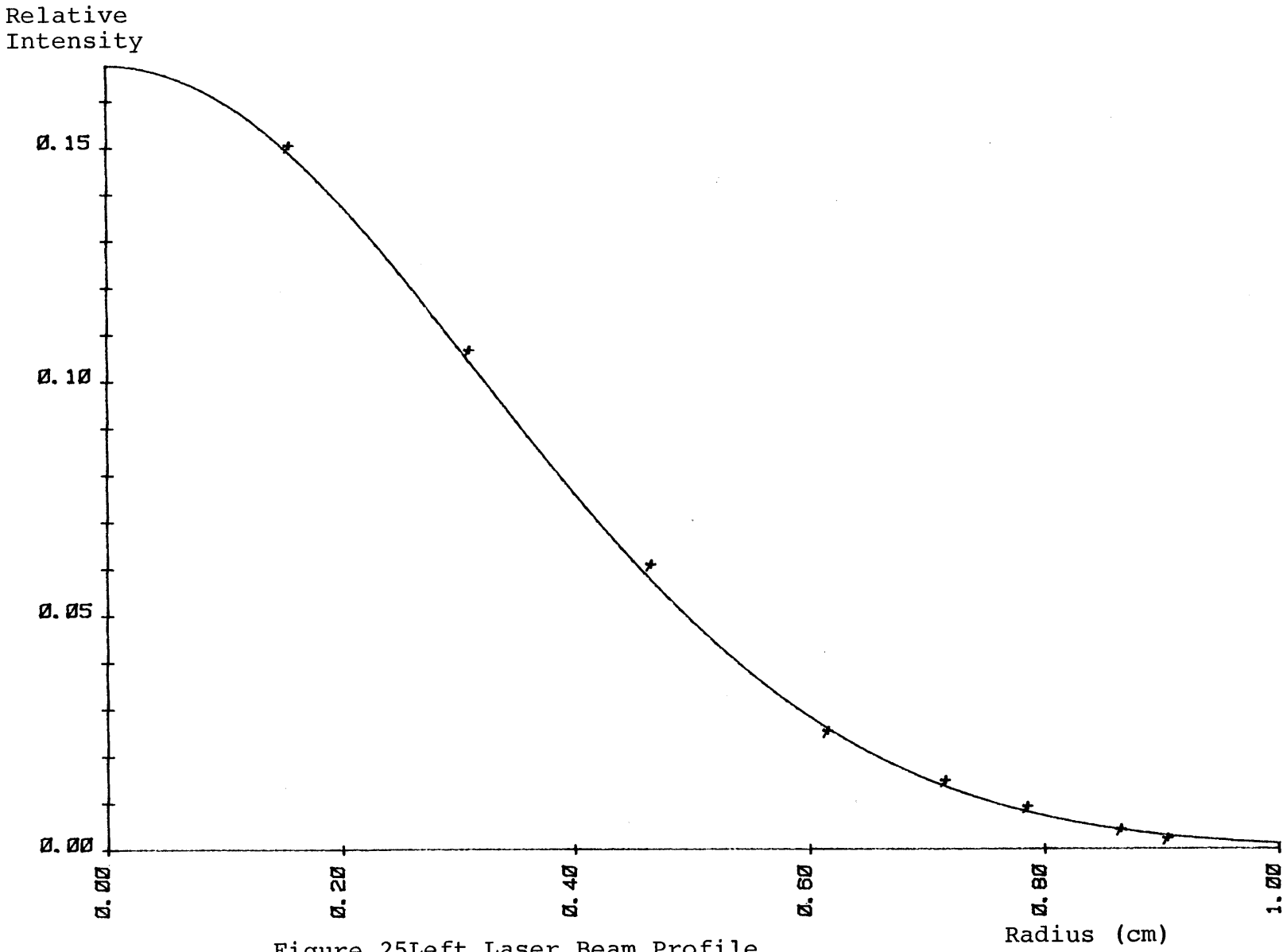

Figure 25Left Laser Beam Profile

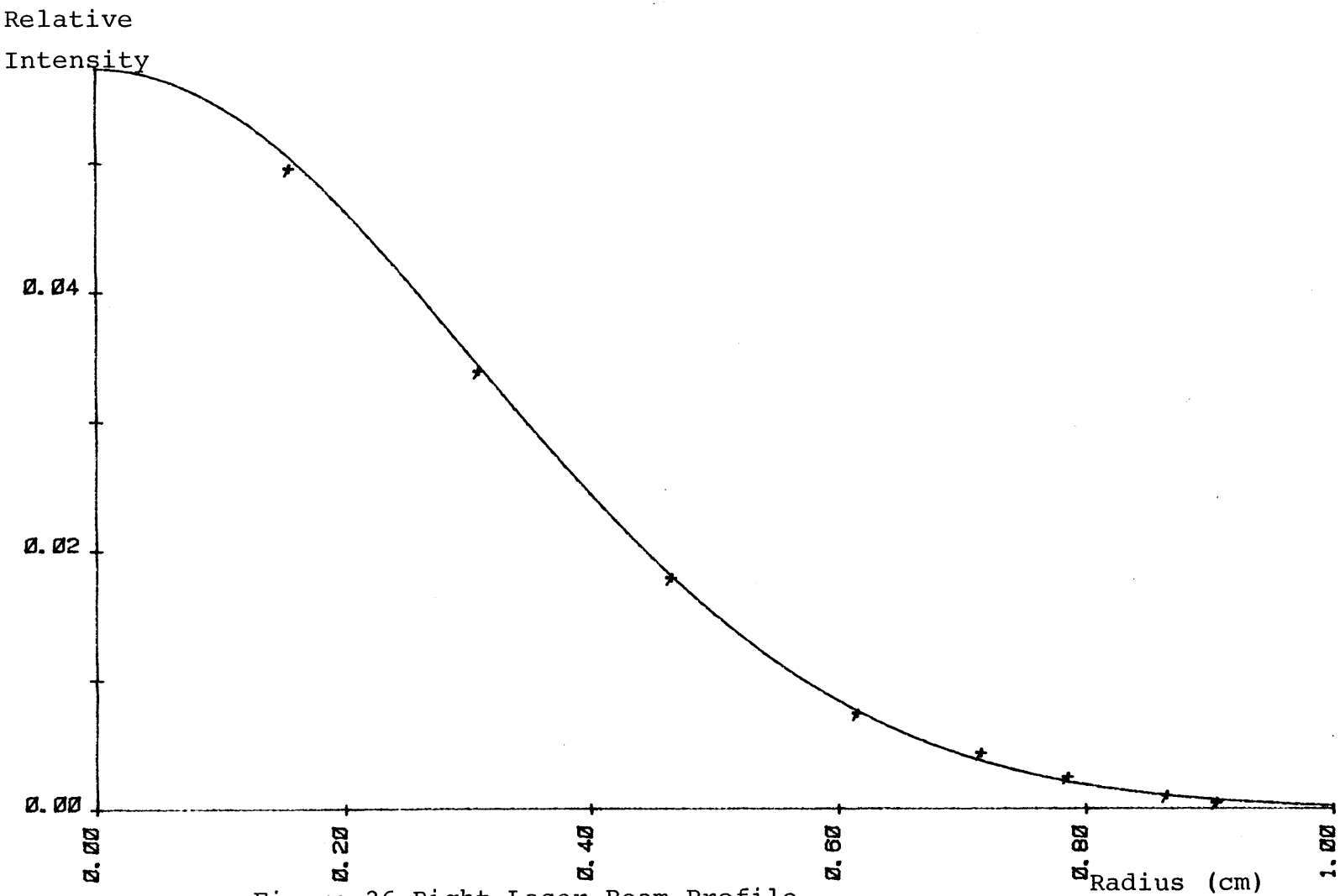

Figure 26 Right Laser Beam Profile

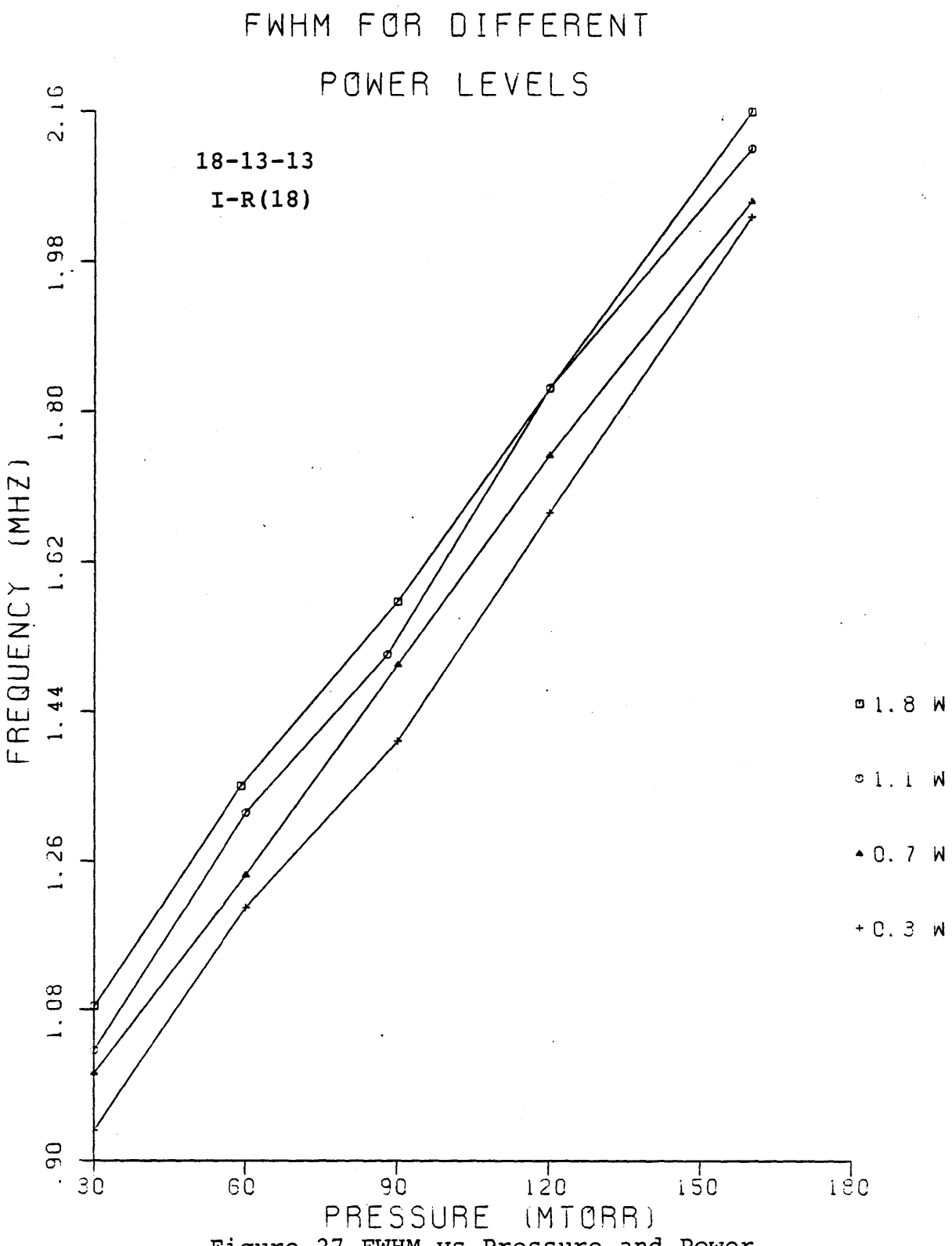

Figure 27 FWHM vs Pressure and Power

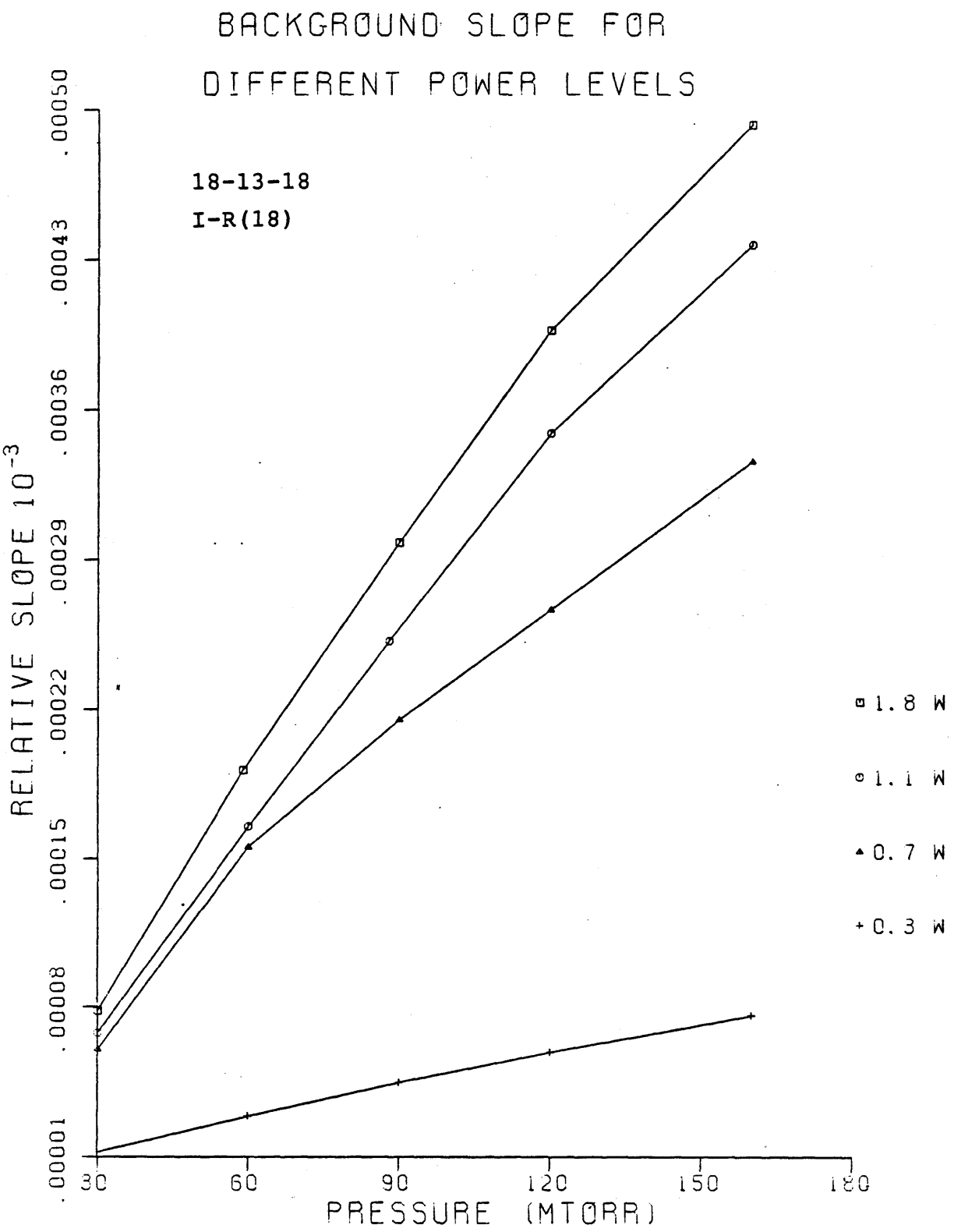

Figure 28 Background Slope vs Pressure and Power

save on casette tape. These plots were just single sweep (90 second sweep) phase locked 10 MHz linescans where the dip depths were just estimated from the plots. Figures 29 and 30 show the dip depth and percentage depth results; these plots follow the general shape and trend as predicted by the rate equation analysis in Chapter 4 but again the S/N due to these single sweeps does not allow a complete analytical fit, especially as a function of power.

The actual fluorescence signal, composed of the Doppler continuum and the Lamb dip in the middle, spans at least 50 MHz for the FWHM of the gaussian background. This scan width is much too large to phase or frequency lock over its entire range but a very accurate (±100 KHz on 500 KHz interval between points) fluorescence scan was taken by scanning the PZT voltage manually while noting the scan frequency on the HP 8555A Spectrum Analyzer. Thus, by using a chopper wheel to amplitude modulate the laser beam, a complete, discrete digitally recorded 4.3 μm fluorescence profile was taken and plotted in Figure 31. The least squares fit revealed a gaussian with a Doppler FWHM width of about 54 MHz with a 1 MHz Lamb dip in 16-12-16 I-P(20). Note, even on this large a frequency scale, the Lamb dip is

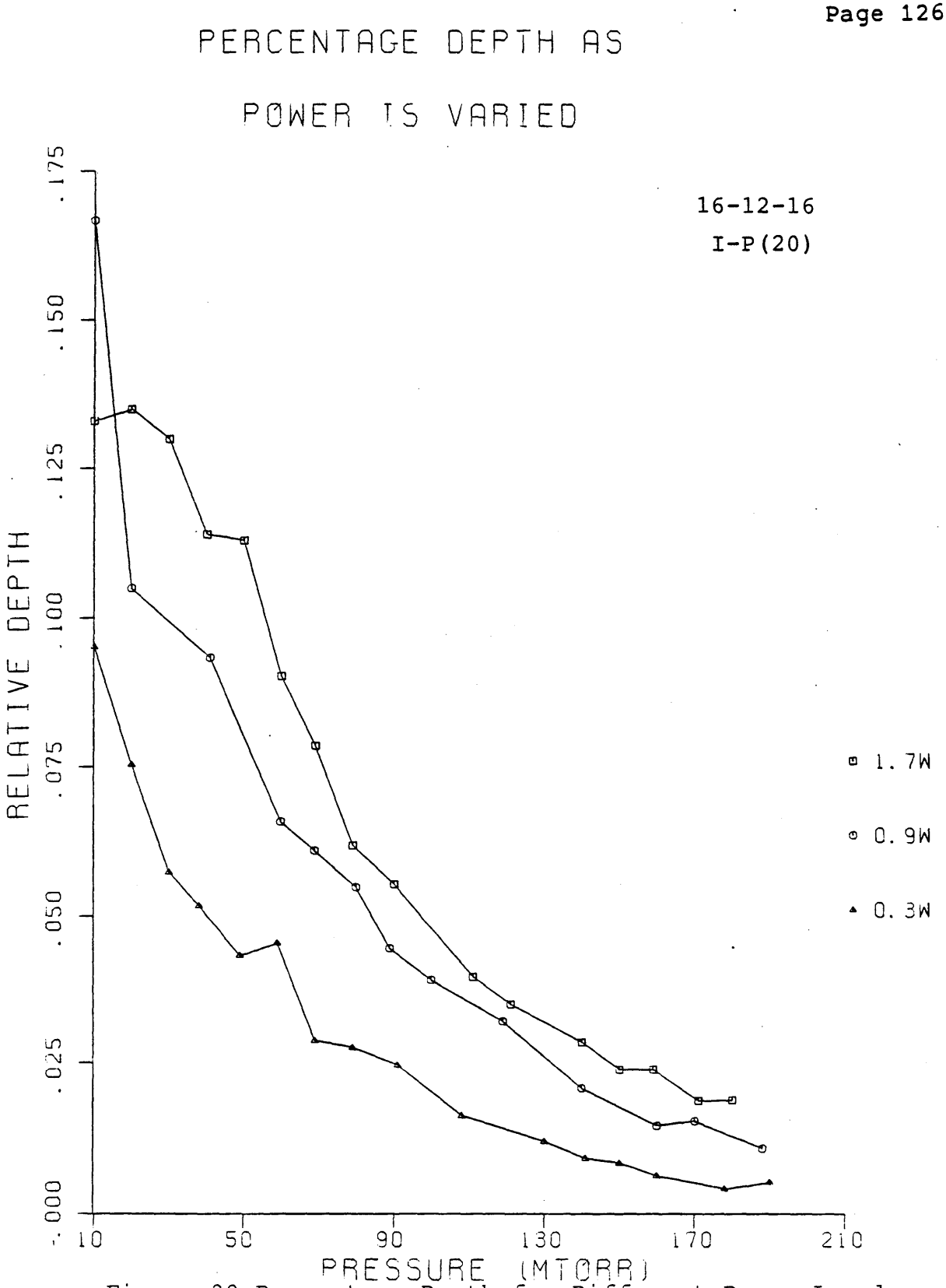

Figure 29 Percentage Depth for Different Power Levels

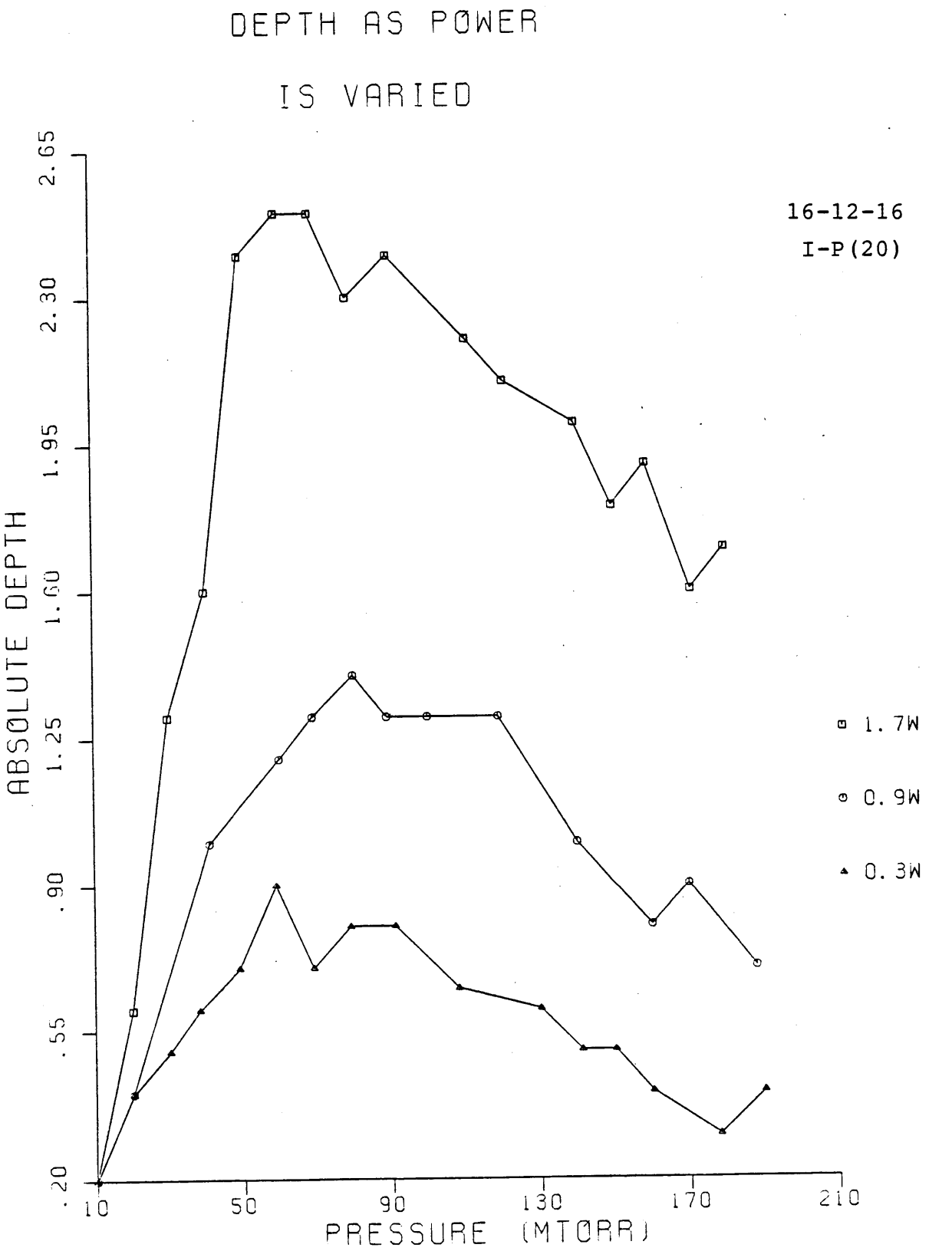

Figure 30 Absolute Depth of Dip for Various Powers

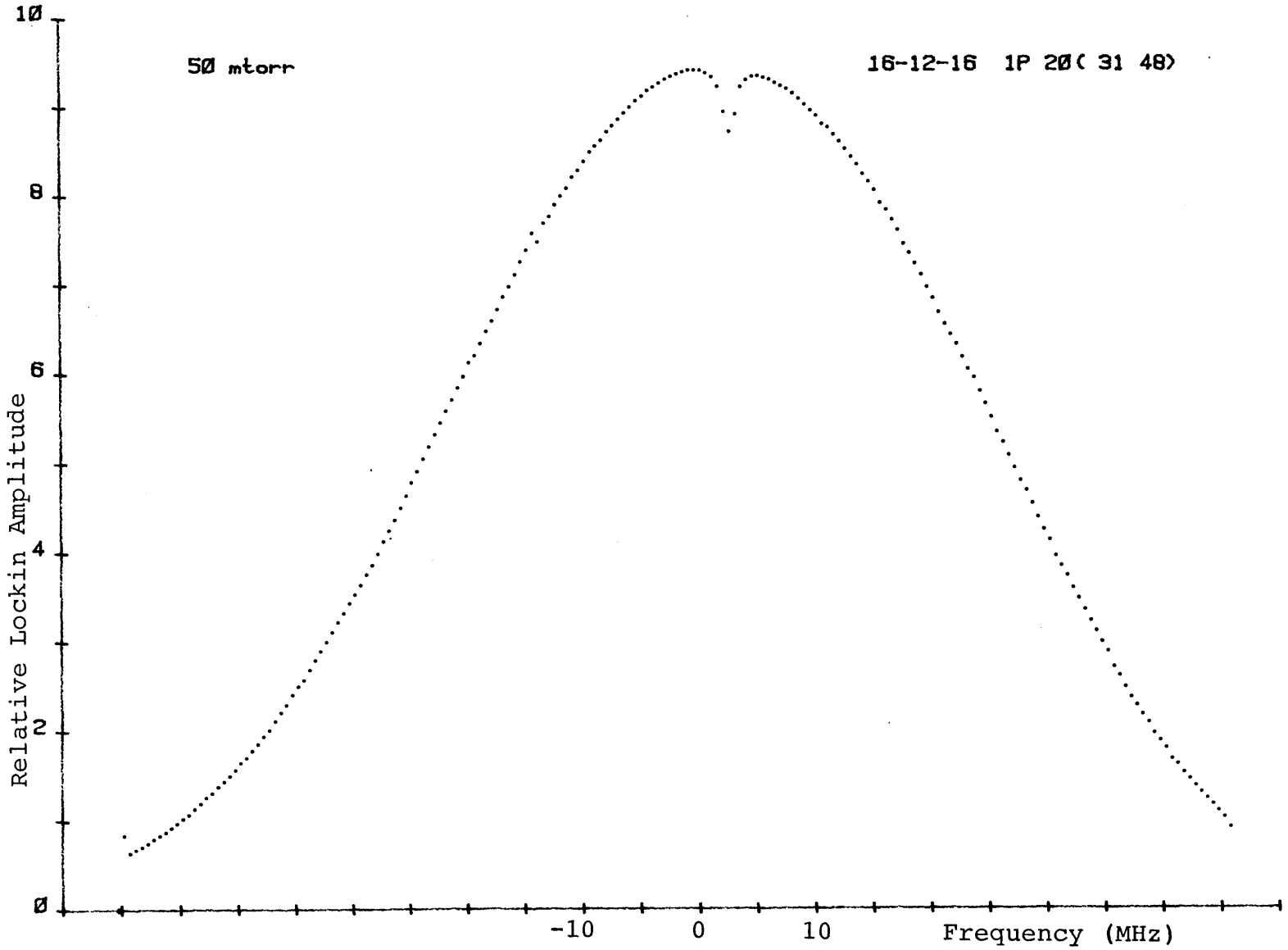

Figure 31 Fluorescence Signal-Doppler Profile

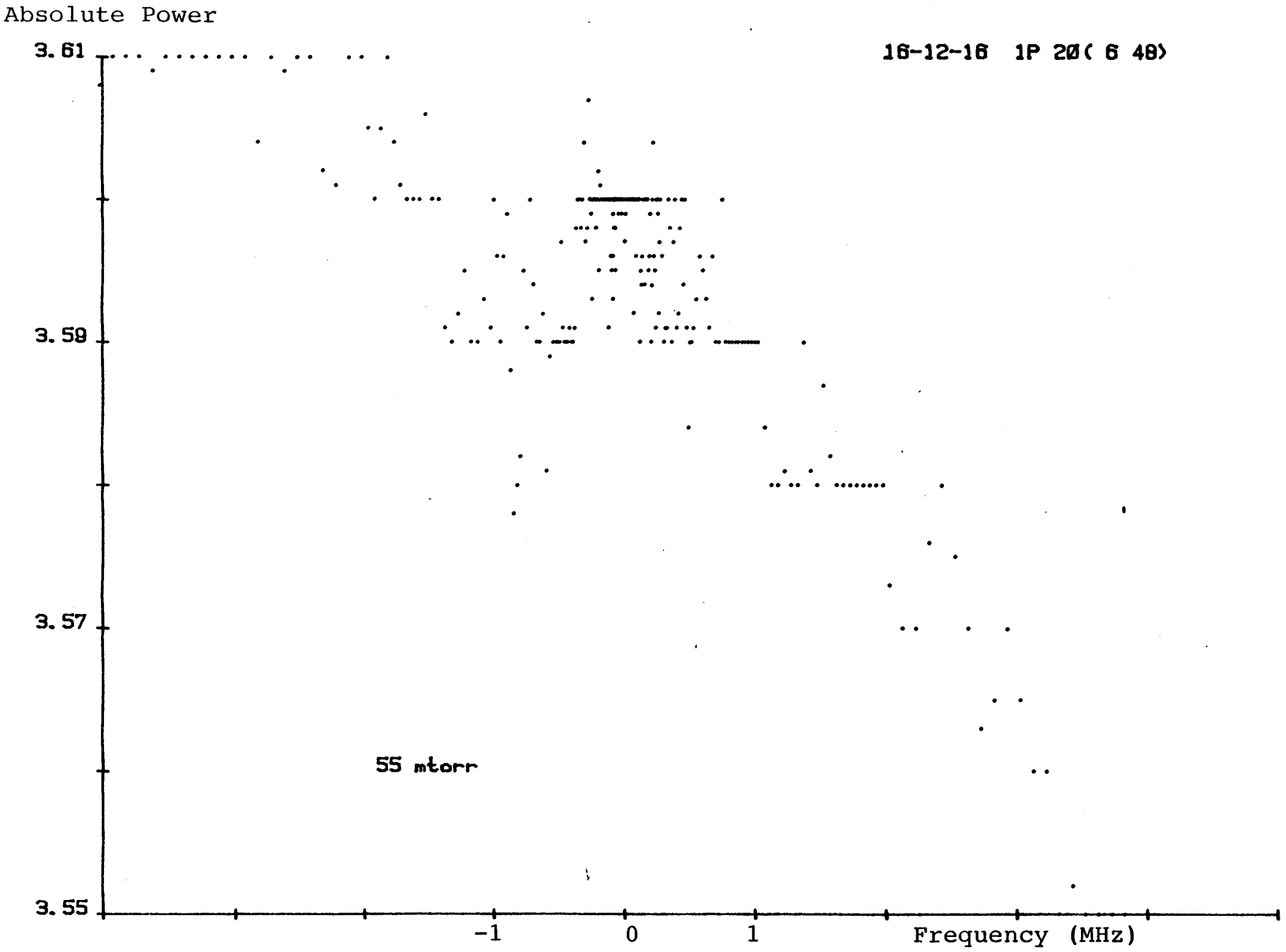

Figure 32 Laser Output Power Slope

still asymmetrically located on top of the gaussian background.

Because the laser power profile is so important, several plots of the output laser power were taken using the frequency lock system. Here the discrete, shot noise fluctuations dominate the linescan. The typical power variation over a 250 or 275 point 6 or 8 MHz linescan centered about the resonance dip is normally only a few tenths of a percent as measured by the Scientech Power meter (thermopile). Thus the digital voltmeter is averaging over quantum fluctuations in the power meter response as the phase and frequency locked servo system scans the lineshape. Even so, in Figure 32, which is a power scan over the exact frequency range as that in the frequency scans in Figures 17 and 18, there is a noticeable slope among the scatter of data points across the normal linescan frequencies. Besides just locking and measuring the power profile over a typical frequency linescan, the entire laser power profile of a single longitudinal mode was also obtained by placing the power meter in front of the absorption cell and manually adjusting the PZT cylinder voltage to scan across the laser gain profile while keeping track of the scan frequency on the spectrum analyzer. In Figure 33, the Scientech power

meter was used to obtain a laser profile; a parabola was least squared fitted to the power profile and revealed an estimated FWHM of about 95 MHz on 16-12-16 I-P(20).

Several other laser profiles power plots were also taken using a Molecutron AP-3 single element pyroelectric detector instead of the thermopile. This was an added precaution since the response time of the pyroelectric is infinitesimal compared with the drift possible in the thermopile. In this measurement, less than 10mW of laser power was directed onto the pyroelectric; the laser was chopper modulated and the signal was synchronously detected on the 131 lockin. Though this method did not suffer from the quantum fluctuations associated with the thermopile, there were still noise problems associated with the bandwidth and shielding in the detection scheme, as shown in the power profile in Figures 34. The most important thing to note in all of these power measurements is that the Lamb dip is somehow always located away from the flat power center of the laser output. The problems associated with this offset will be addressed in Chapter 6.

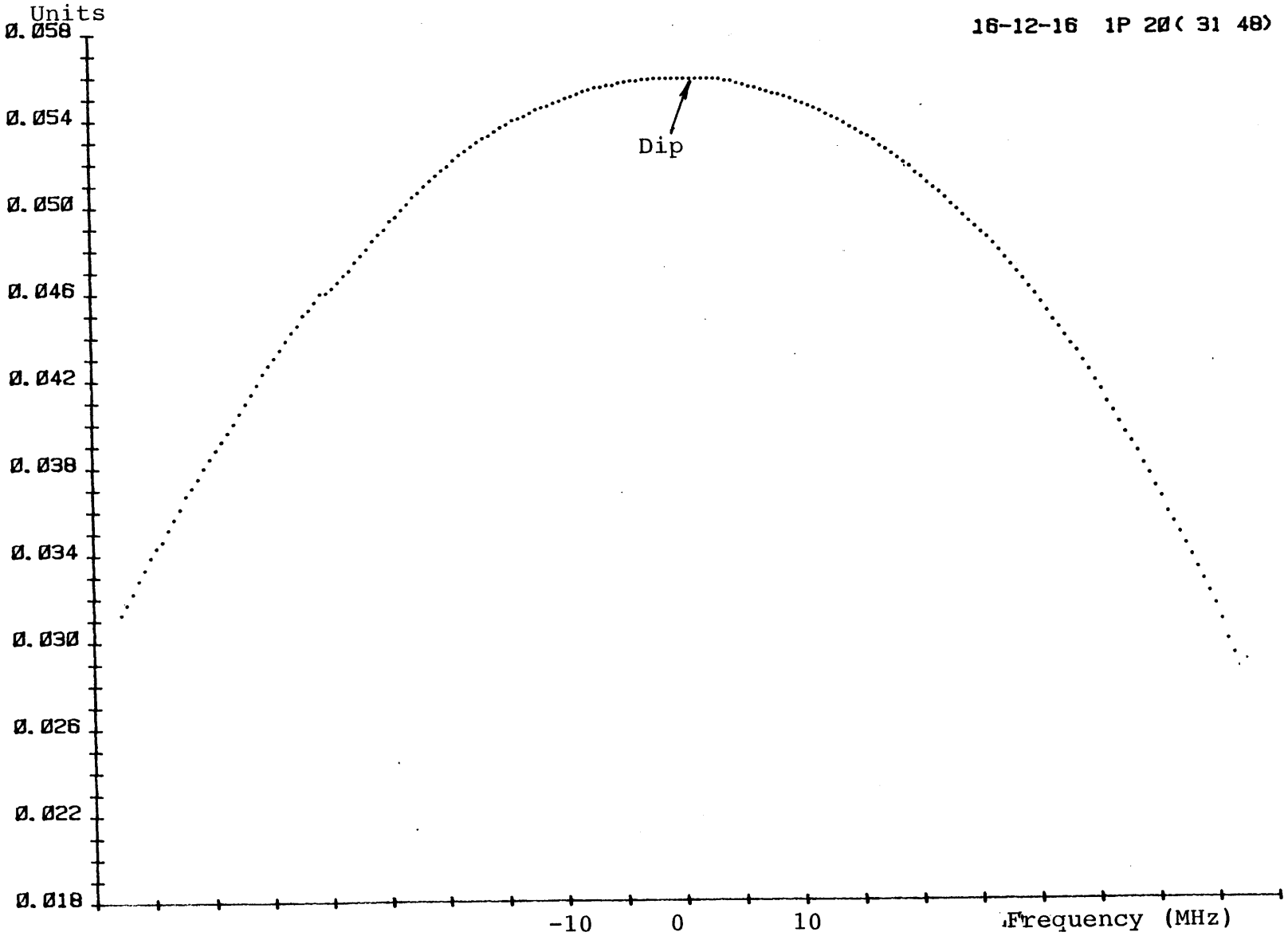

Figure 33 Laser Power Gain Profile, Thermopile

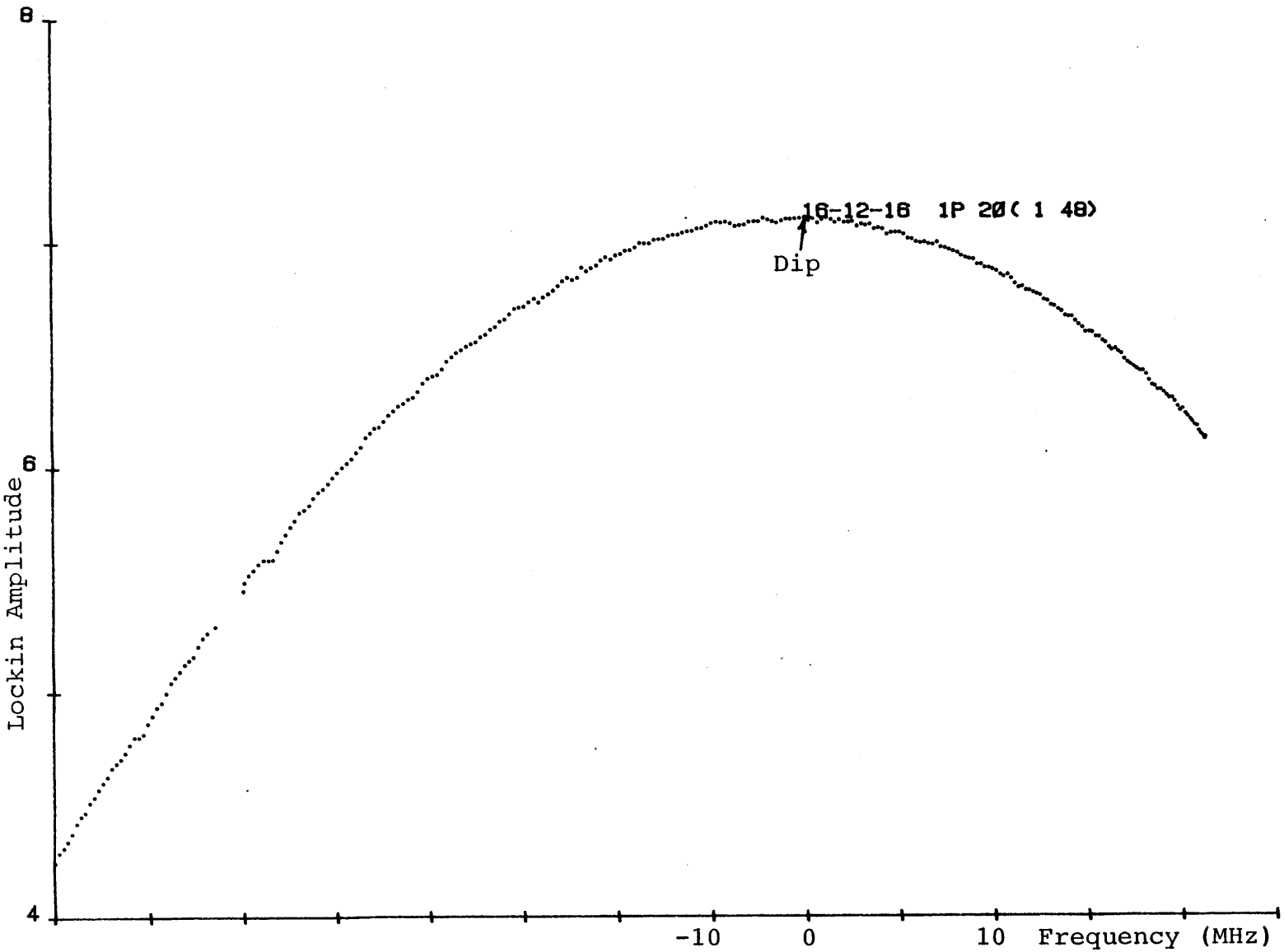

Figure 34 Laser Power Gain Profile, Pyroelectric

CHAPTER 6 FREQUENCY ERRORS, ESTIMATES, AND CORRECTIONS

The primary purpose of this experiment is to measure the pressure shift of the lasing transition of CO_2 as a function of J for several different isotopes. A description of the experimental setup and a block diagram was given in Chapter 5. This chapter will describe some of the possible errors and give an estimate along with steps taken to correct for these errors in the system.

The pressure shift has been measured for CO_2 in the I-P20 transition in 16-12-16 by several different groups[634-640] obtaining such results as -80[634], -120[121], -350[637], -20[639] red and +200[636] blue shifts. Several of these measurements have been taken using an external absorption cell technique at low pressures[636](<100 mtorr); one measurement was taken using an atmospheric pressure[639] laser (TEA) arrangement. Notice that all these measurements were not extensive repeated measurements, but rather single shot or single set of trials; there were problems of drift and reliability in all of these measurements. This follows from the fact that pressure shift measurements suffer enormously from drift, reproducibility and external changes

in the laser cavity or cell from data run to data run. Thus, even if the optimum cell, detector and servo electronics were available, some means of reducing this random 'drift' error must be taken or else the major source of error must be understood and eliminated.

Before any measurements are described, the physical limitations and other possible sources of error in this measurement will be discussed relative to other frequency stabilized techniques. Huge cells and beams have been employed by Borde[655-657] with his 80 cm diameter and 20 m path length cell used in Ramsey fringe studies. Russians workers have utilized such huge absorption cells in their ultimate HeNe CH_4 stabilized absorption cells. These cells range from 3 meter long, 5 cm diameter external cell to an internal telescope expanded[188] 20 cm diameter absorption cell. Thus, by operating at 20 to 100 μtorr range, ultranarrow CH_4 absorption resonances with tremendous resolution and S/N can be obtained with such setups. Methane is ideal because it is essentially a ground state absorber with a large absorption coefficient (.2 $cm^{-1}torr^{-1}$) so that saturated absorption[178-194], instead of fluorescence can be used to obtain high contrast, 100 KHz FWHM signals. Correspondingly, the HeNe laser, stabilized

on the 3.39 μm transition, holds the laser record for stability (10^{-15}) and reproducibility[157-177].

Experimentally, as expounded by Kelly[280] in his CO_2 studies, the ideal experimental configuration would consist of a large diameter internal cell with the internal laser beam parabolically reflected and expanded to fill as large an active absorption volume in the internal cell as possible to create the largest signal with the least amount of noise. Kelly had proposed a large internal absorption cell for several reasons. To obtain the best reproducibility and stability, a derivative signal with as large a contrast (discriminator curve) as posssible is desired. This means the resonance dip must be as narrow as is feasible considering the S/N and with a percentage dip as close to the theoretical maximum (30 percent) as possible. The signal increases while the power saturation effects are reduced with the increased cell diameter. Kelly had also experienced problems with diffraction and feedback coupling originating from the telescope expander; thus a parabolic reflector would work much better as a beam expander. Optical feedback is the major problem associated with an external absorption cell. This is a serious problem since a wavelength independent solution is desired; the magnitude

and asymmetry associated with the derivative signal depends on how this feedback problem is solved and whether misalignment is used to eliminate this feedback. Again, in the case of an internal cell, feedback and alignment is not a problem while a wider range of absorption cell pressures can be used since there is more than enough saturation power inside the laser cavity to provide adequate signal for lockin detection. Unfortunately, power saturation effects tend to be very important as in the case of Meyer's internal cell CO_2 lineshape studies[651] but these effects should be less of a problem with expanded internal cells.

The other important factor that determines the size of the signal is the detector itself and the collection configuration. Since saturated fluorescence provides the discriminator curve signal, there is more signal if more fluorescence radiated into 4π steradians is directed by some optical cell configuration onto the detector. Signal to noise is enhanced greatly if the active background volume is cooled to at least liquid nitrogen temperature (since the normal 300° blackbody radiation peaks near 10μm) and if a cooled bandpass filter is placed over the detector so that only the 4.3μm fluorescence is detected.

As mentioned in Chapter 3, we are using an external cell along with a laser beam whose 1/e radius is .46 cm. As much of the previously mentioned features have been incorporated in the cell so that a satisfactory signal is obtained with a very small (100 Hz) standard deviation at the optimum lock. Lucid examples of the stability of the lock include the drift measurements, the σ vs. τ plots in Chapter 3 and in the beat frequency pictures shown in Figure 35. These pictures are single sweep shots of the 320 MHz beat frequency taken at 10 or 20 KHz/cm with an IF bandwidth of 3 or 10 KHz. Note that there is still a residual modulation in these pictures present from the dithering of the PZT stack at 130 Hz. This is more a function of the PZT hysteresis than any other external disturbances. On the other hand, similar beat frequency pictures taken during the morning when there is significantly more human activity shows noticeably less stability.

SOURCES OF ERROR

Given the existing experimental equipment and configuration, the question still is what other physical mechanisms can broaden and/or shift the nonlinear resonances from their true molecular values. First of all, CO_2 is

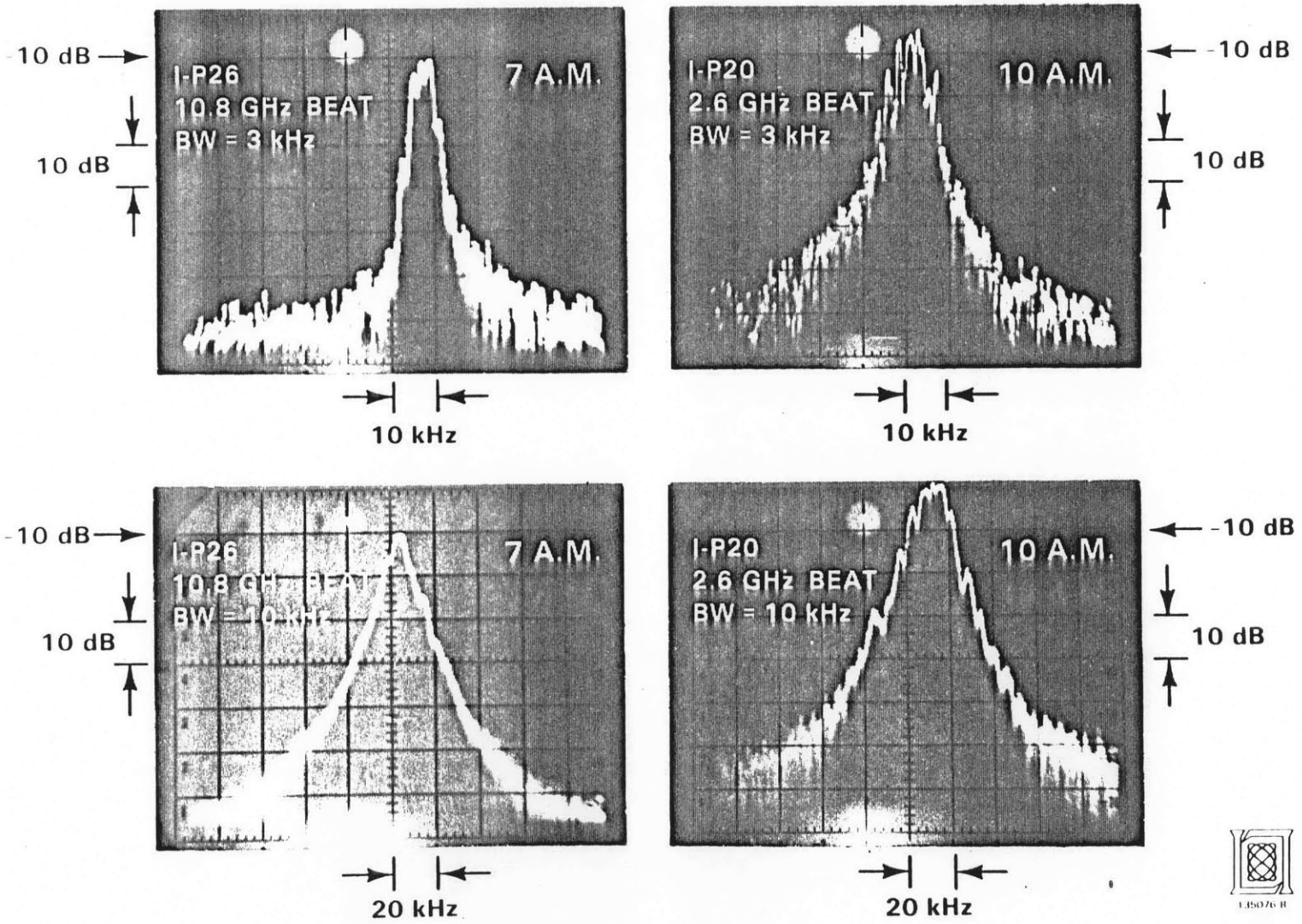

Figure 35 Beat Frequencies

unique among most of the frequency stabilized lasers in that the laser frequency output falls almost exactly on top of the molecular resonance for all the 9 and 10 μm lasing lines (regular band and "hot" bands but not the sequence bands) in all the different isotopes (with, of course, the corresponding isotope in the absorption cell). Thus there is no Stark or Zeeman detuning nor is there just a limited number of accidental resonances, nor as in the case of CH_4, is there the problem of hyperfine splitting[227-232], recoil splitting[208-212], transit time[208-212] or power effects [213-226]. The CO_2 laser power profile easily overlaps the resonance dip but more significantly, the laser power peak usually lies within 1 to 2 MHz of the resonance dip. The FWHM of this resonance dip in our experimental setup usually averaged 700 to 800 KHz at the lowest pressures (10 mtorr) in constrast to the 100 to 200 KHz FWHM dip obtained by Kelly in his expanded cell at the ultralow pressure regimes. The resonance dip is pressure broadened from the residual 700 KHz (due to power and misalignment) to between 1 and 2 MHz FWHM as the pressure increases above 100 mtorr.

Actually there are several mechanisms involved that must be taken into account before the pressure shifts can be considered. Basically, what effect do wavefront curvature,

transit time, diffraction, diffusion, wall effects, and alignment or rather misalignment have on the broadening and shift of the resonance dip? Fortunately, estimates can be made of the contributions to the broadening by these effects. Misalignment broadening has been estimated[280] as

$$\Delta\nu = \Delta\nu_{Doppler}\,\phi\sqrt{\ln 2} \simeq 35 \text{ KHz/mr}$$

where $\Delta\nu_{Doppler}$ is the Doppler width of the signal (52 MHz). In our system the misalignment ϕ, used to prevent feedback is at least 5 mradian; this misalignment broadening results in a residual broadening of at least 100 KHz and up to 300 KHz. On the other hand, the maximum transit time broadening can be estimated by the time needed to traverse the laser beam. This time is

$$T_{tr} = w_o/u = .5\text{cm}/3.3\times10^4 = 1.148\times10^{-5} \text{ sec.}$$

Thus the transit time broadening is $\omega_{tr}/2\pi$ =10.7 KHz HWHM. This HWHM is negligible relative to our total dip width. Geometric and diffractive broadening due to beam curvature and transit time effects have been extensively studied by Hall and Borde[223] where an exact analytical expression has been calculated for the effects of curvature and transit time effects across a gaussian beam profile. Note that in our system, both forward and backward traveling waves are diverging beams since the beams were not mode matched in the absorption cell; a flat mirror was used as the standing wave

mirror. According to Borde and Hall, diverging beams give rise to an extraneous blue shift if the transit time becomes a significant factor in the linewidth. Fortunately, as seen from Figure 5 of their paper[223] and since the relaxation parameter $\eta=\gamma T_r$ is large (>10), especially at pressures greater than 10 mtorr, this transit time frequency shift does not become significant (the shift is at most 1 KHz at the lowest operating pressure and virtually disappears at larger pressures). This conclusion also follows when the lineshape expression (eqn. 89, 90 of Reference 223) was also evaluated with our distances, beam size and confocal parameters. Thus, the contribution of a transit time blue shift to the actual pressure shift measurements is negilible for pressures greater than 20 mtorr.

On the other hand, two additional relativistic frequency shifts must be considered to make sure that they do not affect the actual shift measurements. Using relativistic mechanics, it can be shown that in addition to the normal Doppler shift, $\mathbf{k}.\mathbf{v}$, there exist a second order or transverse Doppler shift and a recoil shift due to the emission or absorption of a photon. Both of these effects have been measured in the HeNe-CH_4 stabilized system

(233-238) and have been significant when an absolute reference was desired.

The shift due to the second order Doppler effect is given as

$$\delta_2=\omega_o u^2/2c^2=111 \text{ rad} =17 \text{ Hz}$$

for CO_2 as opposed to 133 Hz for CH_4. This second order effect can also be considered as a temperature shift and has been measured as such for methane(186) . This red shift is then

$\delta_2= -kT\omega_o/mc^2 =.0566T$ Hz/°K where T is in absolute kelvin. This temperature shift is negligible for CO_2 since the gas in the absorption cell does not absorb very much power. The only heating problem that could arise is if the background warmed up due to the mirror absorption or due to a change of laser power in the cell; this would only change the absolute locking frequency point since the InSb detector would see a different background but the absolute frequency shift would be very small and would be pressure independent once equilibrium power levels are established.

The recoil shift given as

$$\pm\hbar\omega_o^2/2mc^2$$

is 40.3 Hz for CO_2 versus 1.08 KHz for methane. The recoil shift is negligible in CO_2 but is a very big factor in methane, especially since all three hyperfine lines exhibit

this recoil effect such that any resulting lineshape will be slightly skewed by the relative combination of the recoil and hyperfine splitting[208-212].

POWER SLOPE ERROR

The most important source of error in this experiment follows from the fact that the laser power output peak did not exactly coincide with the molecular resonance. This is ironic because the CO_2 laser output and the CO_2 absorption resonance are unique because the two components almost coincide with each other in contrast to the other stabilization techniques that involve SF_6 or OsO_4[124-131], I_2[195-200], or CH_4[178-194]. After much hindsight, it was evident that people were aware of this power slope error, or instrumental shift as was initially referred to by the microwave spectroscopists[461-463].

A nonzero background slope on top of the resonance dip can easily create an asymmetric derivative curve with unequal + and - lobes and accordingly would raise or lower the true zero crossing point on the discriminator curve; hence the lockin detects a shifted zero and the servo system locks onto this 'instrumental' shift. This was a very

significant error in microwave spectroscopy[461-463] since it was 'discovered' during the time that unusally small (10 to 100 KHz/torr) pressure shifts were observed when no shift had been expected or seen before. Now, in microwave spectroscopy[461-495], as in infrared and visible spectroscopy, a nonzero pressure shift has been measured in many transitions and remains at the forefront in which theory and experiment still disagree.

The slope problem has become very important in the IR or visible transitions when saturated absorption spectroscopy demonstrated that frequencies could be resolved well beyond their Doppler uncertainty. This was especially important in establishing an absolute frequency standard or in trying to measure a fundamental constant like the speed of light, since reproducibility and stability limits how well these measurements can be taken. Stability is achieved by using the ultranarrow saturated resonances but reproducibility is hampered by many factors including power drift, operating power levels, pressure, external E or B fields, laser operating characteristics including current discharge and power output and the inherent background slope problem.

Graphically, there is ample evidence that the asymmetry of the fluorescence signal is due to the power slope. Besides the asymmetry seen in Figures 18-22, Figures 36 and 37 which are 40 to 50 MHz laser linescans of the fluorescence signals; these are just successive linescans (not frequency locked) in which a ramp voltage is applied to the PZT cylinder such that the laser gain almost sweeps through an entire longitudinal mode. Figure 38 is a smaller linescan showing the same effect. Figure 37 is unique because it shows the fluoresence signal at a fixed pressure and at peak output power as a function of different J lines; this shows that the gain profile for each J has a different degree of asymmetry depending on the cavity configuration and the dispersion of the grating for that particular line.

The background slope problem was realized quite early by Letokhov[327] and in the work in stabilizing the HeNe and CO_2 lasers. The basic question is how much of the error is the offset error, how can it be corrected, and does it affect the reproducibility of the measurements? Unfortunately, in the ultra-high resolution work, almost any background is noticeable because of its variation across the

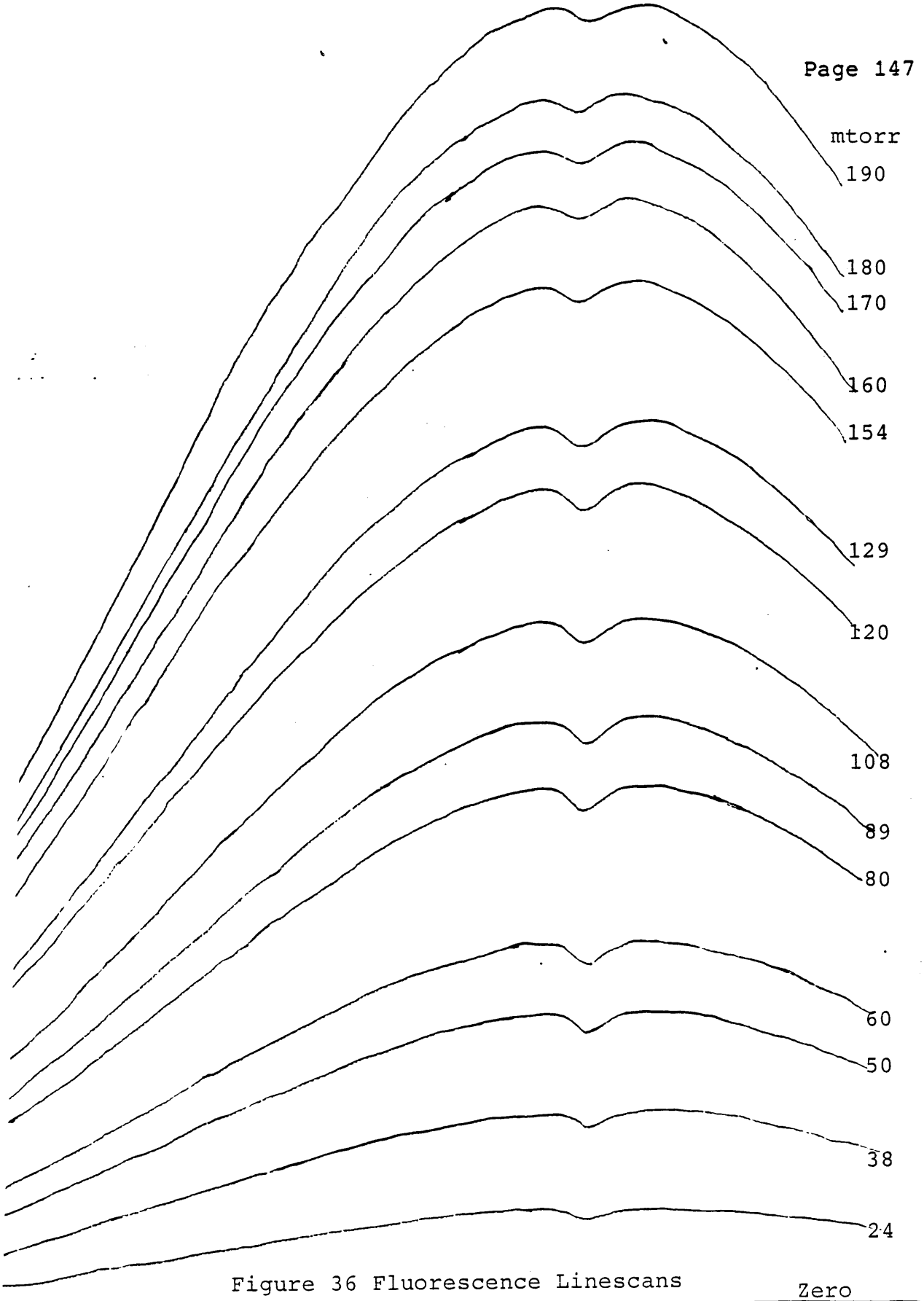

Figure 36 Fluorescence Linescans

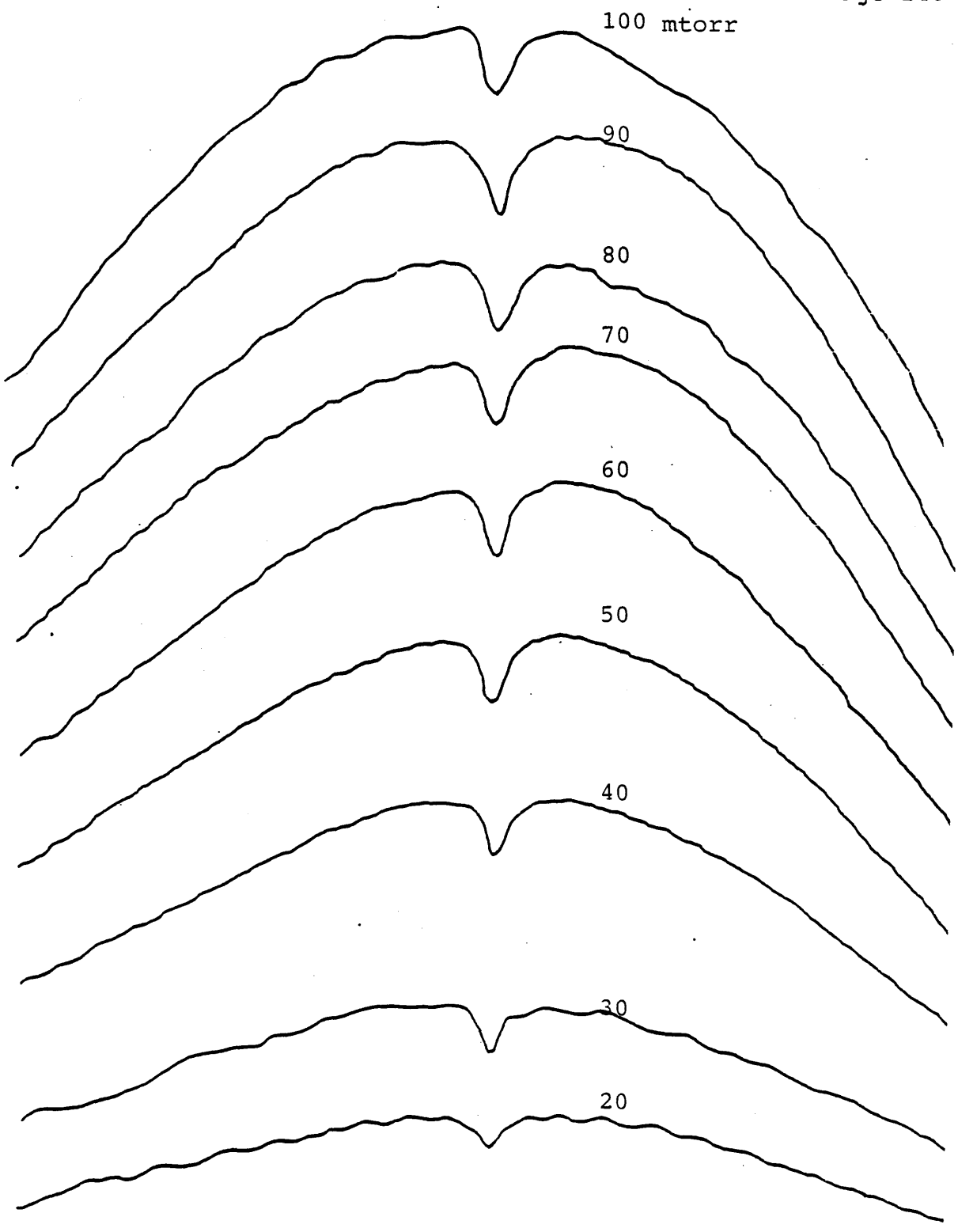

Figure 37 Fluorescence Linescans

resonance and hence any high resolution measurement using saturated absorption techniques[249-255] will have this uncertainty. In some cases, including in the speed of light measurement[132] and in an absolute frequency[154,155] measurement, the offset error was just estimated to be so large by just visually estimating the background slope relative to the steepness of the derivative signal on the lockin detector. People[140] have also tried to electronically correct for slope by adding a supposed correction voltage to the detector output. The major problem with an electronic means of correction is that the power variation is so small that any analog division of the discriminator curve by the power profile would be very tricky and any injected counter offset would be even more uncertain since one would not know what the real error is at the 'zero' lock position. In essence, any electronic means of correcting for this offset error would probably distort the actual signal or else create a different offset; hence slope corrections using some electronic means have not been tried very much and were not very successful so that, many reported frequency measurements simply gave an 'eyeball' (how perpendicular is the background slope relative to the derivative slope) estimate of this error.

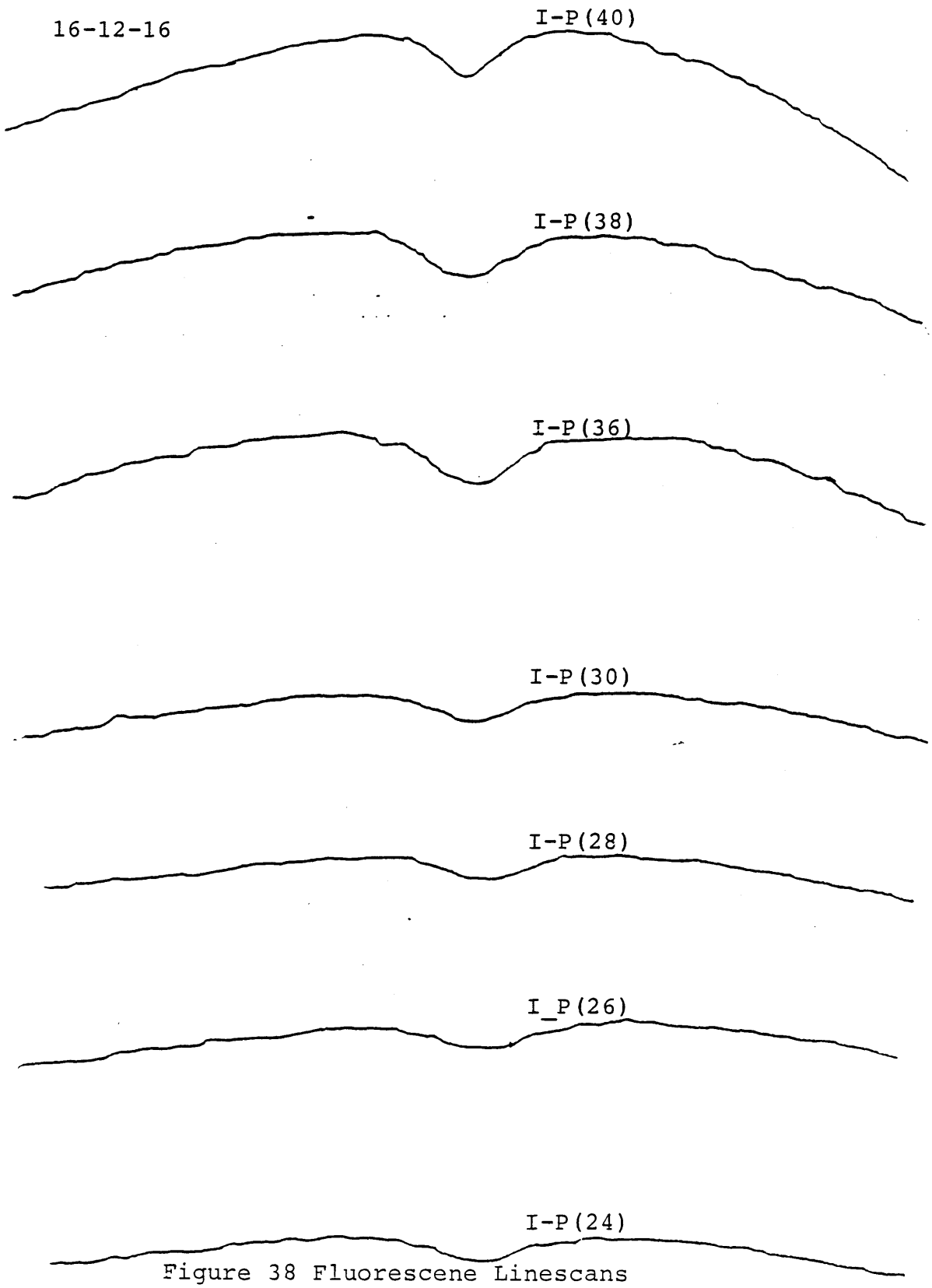

Figure 38 Fluorescene Linescans

It is possible to get rid of this background slope error by using another detection technique that does not add any extraneous electronic correction signal. In most saturation detection schemes, the laser signal is modulated either by frequency modulating the laser output or amplitude modulating the laser signal. In frequency modulation, the first derivative is detected as a discriminator curve to be used in the feedback network. Mathematically, the laser output frequency ω as a result of frequency modulating about the center frequency ω_o with a frequency excursion $a<\gamma/2$ (γ= FWHM) at modulation frequency Ω is

$$I_L(\omega)=I_L(\omega_o+a \sin \Omega t)$$

Using a Taylor series expansion

$$I_L(\omega)=I_L(\omega_o)+a \sin \Omega t\ I^{(1)}(\omega_o)+a^2/2 \sin^2\Omega t\ I^{(2)}(\omega_o)+...$$

where $I^{(i)}$ signifies the ith derivative with respect to ω evaluated at ω_o. Collecting terms, this becomes

$$=I_L(\omega_o) + a^2/4\ I^2(\omega_o) + ...$$
$$+\{a\ I^{(1)} + a^3/8\ \ I^{(3)}+..\} \sin \Omega t$$
$$+\{-a^2/4\ \ I^{(2)}-a^4/48I^{(4)} +..\} \sin 2\Omega t$$
$$+\{-a^3/24\ \ I^{(3)}-a^5/384I^{(5)} +..\} \sin 3\Omega t$$

Thus by assuming a is very small, synchronous detection of the first harmonic Ω component recovers the first derivative signal and synchronous detection of the 2nd harmonic 2Ω

recovers the 2nd derivative signal and so on. Now if the actual signal is on a background slope the net signal can be easily approximated as

$$I(x) = Ax^2 + Bx + C + D/\Gamma$$

where $\Gamma = x^2 + \gamma^2$, $x=\omega - \omega_o$ and γ is the HWHM.

Then the derivatives, with respect to x or ω become

$$I^{(1)}=2Ax + B - 2Dx/\Gamma^2$$

$$I^{(2)}= 2A+ (6Dx^2 - 2\gamma^2 D)/\Gamma^3$$

$$I^{(3)}= 24Dx(\gamma^2 - x^2)/\Gamma^4$$

(6.1)

Thus one possible solution to the background slope problem is to use a third harmonic detection scheme in which the background slope disappears and a much sharper, narrower discriminator curve is used in the servo loop [256-265]. This method has been utilized to stabilize several kinds of lasers, including the HeNe-CH_4 and CO_2-OsO_4 lasers [126-131]. But these applications of the third harmonic detection have occurred in situations in which there is enough S/N and the lock is better than the first derivative lock in terms of stability and reproducibility. In the case of CH_4 and OsO_4, there is enough absorption signal to lock on the third harmonic and accordingly, the best reproducibility occurs with these locks. In both of

these molecules a vary large absorption signal plus very narrow resonances (<100 KHz due to fine structures in OsO_4 or SF_6 and CH_4 unlike CO_2 which is usually limited in its FWHM to several hundred KHz) accounts for their ultrahigh stability.

Even if the third harmonic detection scheme works and sufficient third harmonic signal is detected, special care must be taken to ensure that this is the third harmonic signal from the resonance absorption and not from any other sources[256-265]. Just as 3f is a manifestation of the FM spectrum, there are numerous other sources of 3f error that can possibly be generated thoughout the system and accordingly can create an erroneous 3f signal. Nonlinearities in the PZT, laser cavity, feedback, and any 3f signal in the 1f modulation voltage, can easily create extraneous 3f signal and swamp out the desired laser signal. If there is also a significant dispersion across the resonance dip, 3f cannot eliminate this error[260] but could enhance the error.

For a first derivative lock, the + and - discriminator peaks are located at $x_{max}=\pm\gamma/\sqrt{3}$ where γ is the FWHM. The

peak signal $I^{(1)}(x_{max})= 0.649$ in relative units. In the case of the 3f lock $x_{max}=\pm\sqrt{(1-2/\sqrt{3})}$ so that

$$I^{(3)}(x_{max})= 0.0018.$$

Thus, given the maximum signal at the maximum modulation, the absolute signal is about 300 times smaller than the maximum 1f signal. Such a decrease in fluorescence signal would be much more difficult to detect using the 4.3 μm system, in view of the already small signal due to the 10^{-5} absorption coefficient and especially when all the other nonlinearities in the system add in their 3f contribution. The maximum 3f signal occurs for a frequency excursion of ±1.6 FWHM which is also undesirable from a frequency stability point of view. Nevertheless, we tried to detect the 3f signal in system just to see whether it was feasible or not. Figure 39 shows a very rough discriminator curve of the 3f signal; it is swamped by noise at the highest gain of the lockin amplifier. The biggest source of noise was the dominant 1f signal that was also present in the system. Third harmonic lock was possible and was achieved but the S/N was so bad that the stability was in the ±1 KHz range meaning that the 3f scheme was just not adequate for measuring the pressure shifts.

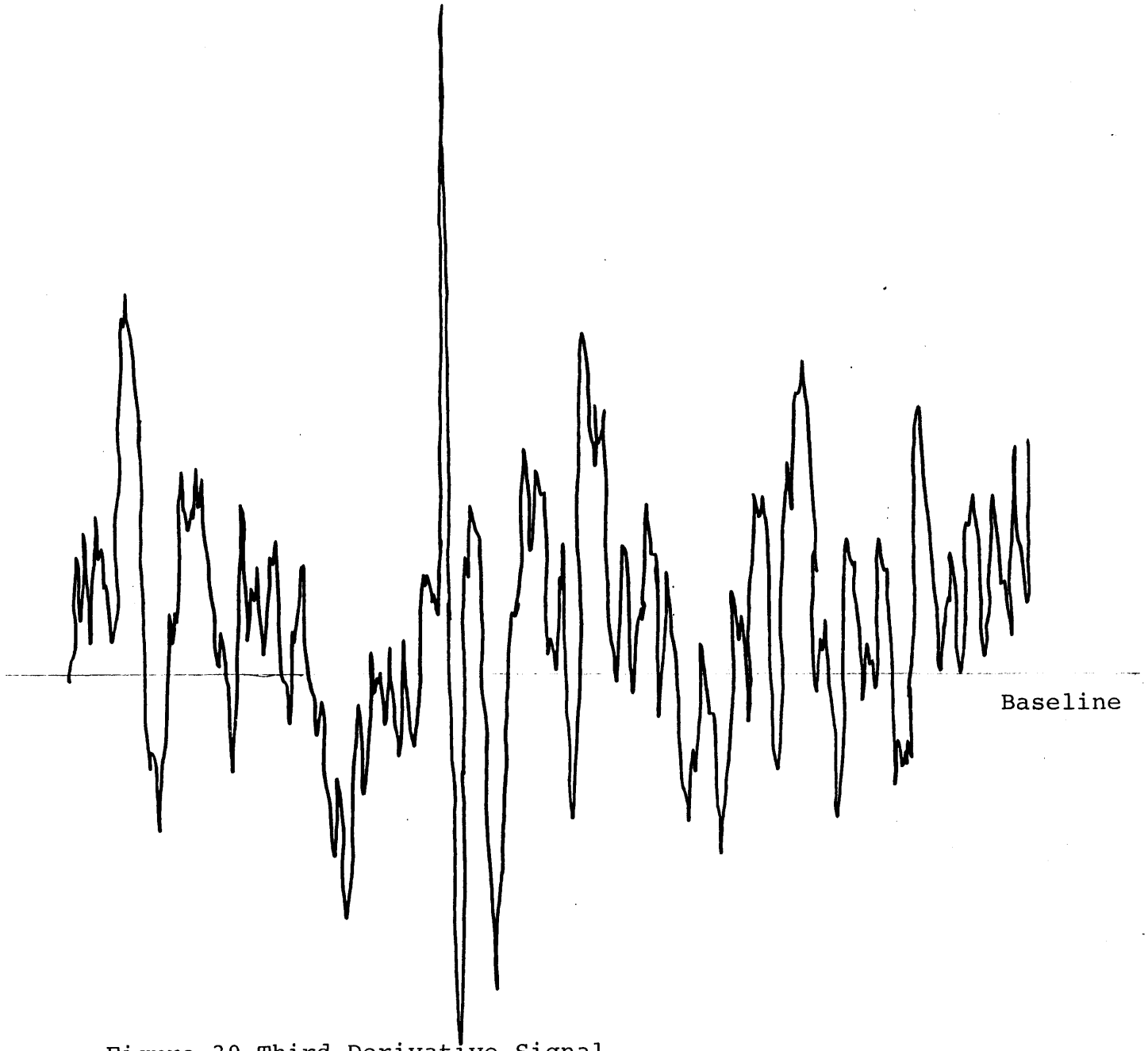

Figure 39 Third Derivative Signal

After all this discussion about the power slope, there still is the question whether or not a slope error will cause an asymmetric lineshape. The asymmetry in the Lamb dip has been observed by many people on many different laser system ever since it was first observed by Szoke and Javan in 1963. There have been numerous explanations[239-248] and numerous possibilities have been offered to explain such anomalous asymmetries, including the possibilities of weak collisions and different dephasing collisions with corresponding different relaxation rates. Nevertheless, for a normal saturation experiment, the lineshape is perfectly symmetric in velocity space such that the resulting Doppler response is also symmetric in frequency space, provided there is no preferred direction in velocity space. Therefore the asymmetry originates from all the dispersive effects associated with the laser configuration, components and lasing medium[250-255]. The dispersion is most noticeable in terms of a net output power or gain profile. This output gain profile can be attributed to the actual dispersion (or index of refraction) effects due to the laser gain medium and/or it could be due to the cavity and its components, especially the mirrors and the diffraction grating. Even with an 'ideal' cavity configuration, there are physical and mechanical limits on designing and building

a perfectly centered and a perfectly aligned laser cavity. How parallel and on axis can the mirrors, grating and endplates be lined up and adjusted and how can one measure the 'perfect' alignment? This is especially questionable since the PZT, with a nonlinear response to any symmetric signal, can easily distort any alignment of the cavity as a function of the voltage applied across it. In our CO_2 system, the diffraction grating together with the frequency tuning PZT cylinder is the frequency dispersive device used to select the different J lines inside the laser cavity. This diffraction grating rotates about a pivot point centered on the cavity axis. Thus, even the laser cavity can minutely change as the grating is rotated from one J line to another J line and hence different cavity gain profiles will emerge from J line to J line. This means that the frequency output is definitely dispersion dependent and the output power profile changes from line to line and any power correction or compensation must be able to detect this J dependent change and correct for it.

The laser power peak for any J line will almost never not coincide with the corresponding resonance Lamb dip in the absorbing gas with the noncoincidence error varing from line to line, depending on the net laser power profile and cavity

configuration. The object of any power correction is to obtain a local flat power profile at the resonance dip such that any offset error due to power slope is minimized. This means that the laser gain profile must somehow be externally distorted such that a relatively flat local power point coincides with the resonance dip and the actual power slope must be monitored so that any + or - power slope error can be recorded as contributing to the measurement error.

The means of adjusting this power slope so that a local zero profile could be located among the + or - power slopes was fortuitously discovered when it was found that either red or blue pressure shifts could be arbitrarily and routinely obtained just by slightly tilting the diffraction grating within the oscillating range of that J line. Basically, for each J line there is a certain tuning range on the grating in which that line and that longitudinal mode dominates the laser gain. The laser gain profile is a function of the alignment and cavity arrangement and the position of the diffraction grating. It turns out,that by adjusting the grating,ie. slightly tilting the grating to create a different cavity configuration and consequently a different gain profile, the slope of the output laser power can be varied from + to - as the laser is 'pushed' across

the power peak while the laser is locked to the Lamb dip. Note that tuning the grating distorts the gain profile so that the maximum power point almost never coincides with the local zero slope.

Because each laser is different and because each J line has a different gain profile, the extent and magnitude of the tuning range varies from laser to laser and from line to line; some lines do not even reach the zero slope point before the gain for that line drops out and a different line or longitudinal mode competes for the laser gain. Due to construction differences from laser to laser, one laser had a predominantly + power slope while the other laser tend to oscillate on a - power slope. Thus, pressure shift data were obtained for lines that would fortuitously tune toward 'zero slope' within the range of the Lamb dip lock. Usually, less than half of the oscillating lines achieved zero power slope on resonance; these were usually midband lines.

POWER SLOPE ESTIMATES

To estimate the power slope error, let F(x) be the background associated with the fluorescence signal such

that

$$I(x)= F(x) +\gamma^2/(\gamma^2+x^2)$$

where $x = \omega-\omega_o$

Then the derivative $I'(x) = F'(x) + 2\gamma^2x/(x^2+\gamma^2)^2$

Setting $I'(x)=0$ and considering $x<<\gamma$,

$$2x/\gamma^2(1-2(x/\gamma)^2+ \ldots) +F'(x) = 0$$

or $x= -F'\gamma^2/2$ is the nonzero 'instrumental' error.

In all the powerscans, the power profile was almost an exact parabola so $F(x)$ can be approximated as

$$F(x) = -C(x)^2 + K \simeq A + Bx$$

such that the background $F(x)$ can be approximated as a straight line in the vicinity of the resonance dip. The net signal as seen by the detector is a convolution of the laser signal with the Doppler response; this Doppler response can be easily approximated as a parabola, $-ax^2+k$, plus a Lorentzian as was done in all the linescan fits. Thus the net fluorescence signal is

$$F(x)= (A+Bx)(-ax^2+k-D/L^2 \qquad (6.2)$$

where $x=\omega-\omega_o$ and $L^2=1+4(x/\gamma)^2$

Taking only the linear x terms and considering only the dominant terms, the derivative is of the form

$$A(-2ax+8Dx/\gamma^2) + B(k-D) = 0$$

Since $D/k = f$ is the fractional depth of the resonance dip, the actual zero crossing or offset error is

(6.3)

$$x=(B/A)\gamma^2(1-f)/(8f)$$

Thus the error is proportional to the laser power slope and varies quadratically with pressure. The factor $(1-f)/f$ includes the width, power and depth dependence since the error really depends on the steepness of the derivative at its zero crossing relative the flatness of the power slope at the zero crossing. Ideally, if the derivative and slope were exactly perpendicular there would be no error. But an additional power dependence in terms of the depth of the dip and the FWHM of the dip enters into the error signal because the steepness of the derivative at the zero crossing depends on the width and depth of the dip; the more power, the wider and deeper the dip becomes.

In the expression for the offset error, most of the factors can be estimated or obtained from previous linescan measurements. The FWHM is directly proportional to pressure and the fractional depth, as given in Chapter 4, can be approximated in two ways, either from the two level rate equations results or from the gaussian intensity averaged

lineshape. The depth in the first approximation is proportional to

$$\text{Depth} \propto S\{1/\sqrt{(1+S)} - 1/\sqrt{(1+2S)}\} \tag{4.6}$$

$$\text{so } \frac{1-f}{f} = \frac{\sqrt{(1+S)}}{\sqrt{(1+2S)} - \sqrt{(1+S)}} \tag{6.4}$$

On the other hand, for the gaussian intensity averaged profile the depth is proportional to

$$\text{Depth} \propto N\% \{2(\sqrt{(1+S)} - 1) - (\sqrt{(1+2S)} - 1)\} \tag{4.10}$$

so that the error for the gaussian intensity averaged profile is given by

$$\Delta = B\Gamma^2 \frac{\{\sqrt{(1+2S)} - 1\}}{8A\{2\sqrt{(1+S)} - \sqrt{(1+2S)} - 1\}} \tag{6.5}$$

where Γ is the FWHM as given in Chapter 4, Eq.(4.9) for the gaussian intensity averaged lineshape. Here, S is the maximum saturation parameter for the intensity profile

$$I = I_o \exp(-(r/r_o)^2)$$

A theoretical power error pressure shift can also be obtained directly from the expression for the the gaussian intensity averaged lineshape, (4.8 and 4.9). The net fluorescence signal can be considered as a convolution of a power slope (A + Bx) and the gaussian intensity average lineshape L . Then the derivative of the expression (A + Bx)L is taken , equated to zero while expanding the expression to first order in $x = \omega - \omega_o$. Thus the power error due to the slope is calculated as

$$\Delta \simeq \frac{B\{[\sqrt{2}\sqrt{(1+S+\sqrt{(1+2S)})}-2]\ [\sqrt{(1+S\sqrt{(1+2S)})}]\}\Gamma^2}{A\sqrt{2}\{-1+\sqrt{(1+2S)}-S/(\sqrt{(1+2S)}\}}$$

A plot of this theoretical error for various power levels is presented in Figure 40. Here the laser power slope is estimated for a typical 50 MHz laser gain profile with a 1 MHz power peak to resonance dip offset. An experimental estimate to the power error can also be obtained by measuring the slope B/A and by estimating the dip depth as a function of power from the linescans of the Lamb dip. This experimental estimate of the error, just like the theoretical estimate, looks almost exactly like an actual pressure shift, indicating that the power error is effectively masking out most of the shift.

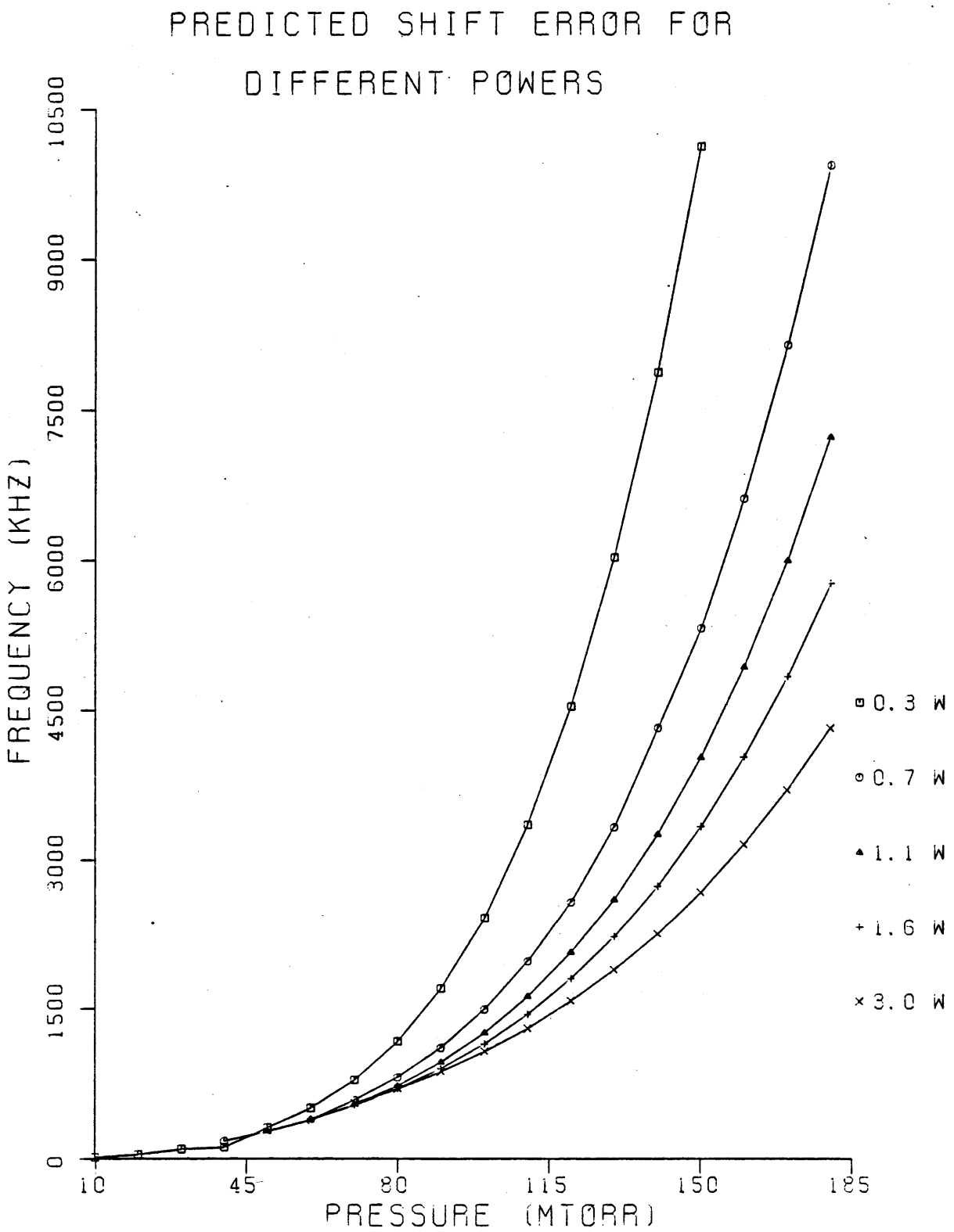

Figure 40 Predicted Power Slope Errors

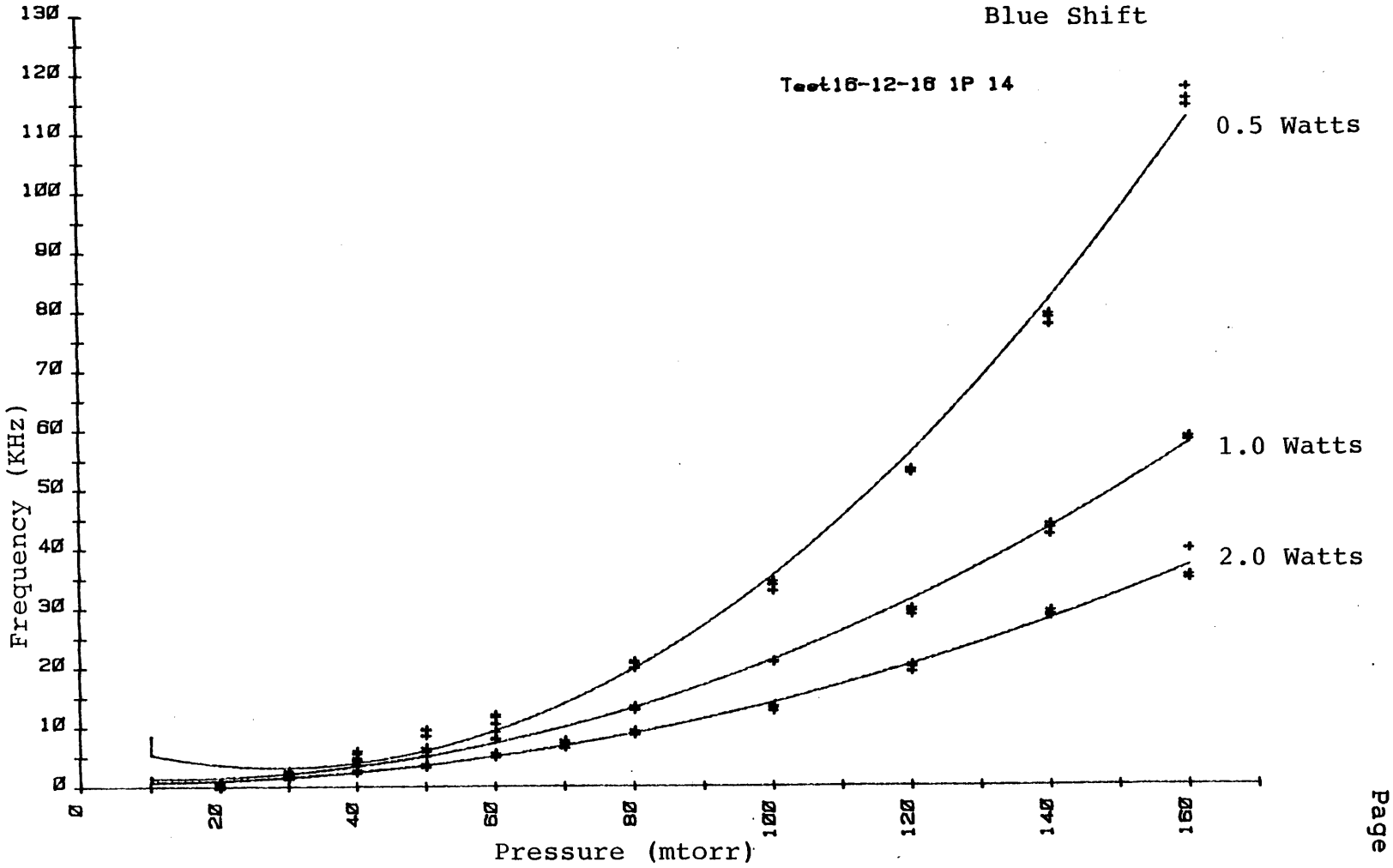

Figure 41 Pressure Shifts vs Power (p^2 Fit)

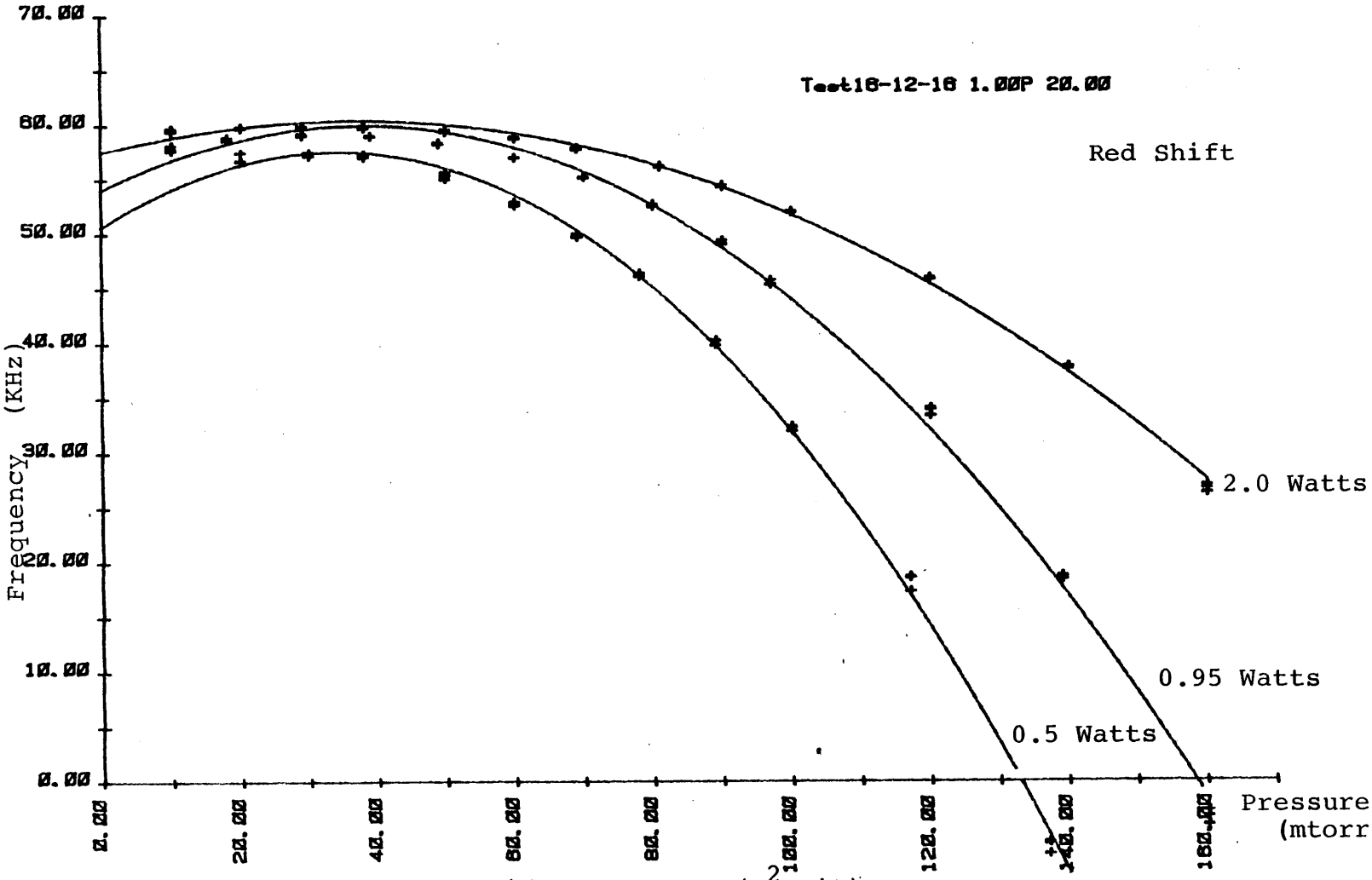

Figure 42 Pressure Shifts vs Power (p^2 Fit)

Experimentally, the proportionality factor related to the B/A power slope is the only term that needs to be measured to obtain a power error estimate; approximately

$$B/A = \nu_{offset}/\Delta\nu_{Dop}^2 \simeq 1/50^2 \simeq 2\times10^{-8}$$

All the other factors were known from previous measurements and estimates. The initial procedure used to estimate the pressure shift was to take several consecutive pressure shift runs while varying the power into the absorption cell with an external dimethyl ether absorption cell. Note that in these preliminary measurements, the grating position was fixed at peak output power since the correlation between slope and grating position had not been made as yet. Thus by measuring these pressure shifts at different power levels, the power proportionality factor could be obtained by fitting the pressure shift curves, $\delta(p)$ to a two parameter error equation

$$\delta(p) = A_1 p + A_2 \gamma^2(p)\ (1-f)/(8f)$$

where p is the pressure, A_2 is the power proportionality constant (slope) and A_1 is the residual 'pressure shift' after the power error has been subtracted out. Two power scans were used to obtain a fit and a third scan was used to correlate the previous A_1 and A_2 values. If nothing drastically changed or drifted during these successive runs,

any two power runs should give reasonably close estimates of A_1 and A_2. In these pressure power runs, the fitted values of A_2 were usually within 10% of each other for the 'good' data runs but the actual values of the residual pressure shift parameter A_1 were usually not that close.

Figures 41 and 42 show typical red and blue pressure shift runs at three different power levels; these data points are fitted to a pressure squared curve. Figures 43 and 44 show the power data runs with a theoretical fit (Eq. 6.3,6.5) of the pressure shift including the power error. The theoretical fit works quite well at the higher pressures but does not correlate with the data at the lower pressures. At the lower pressures (in Figure 43, red shift) there seemed to be an upturn in the pressure shift or else the shift was so small that it could not be distinguished from the noise in the measurements (Figure 44,blue shift has a linear slope). Accordingly the extracted least squares fitted pressure shift varied by about ±15 KHz/torr about a zero pressure shift for each power level.

Even though the power slope measurements demonstrated what was the major problem in the shift measurements, it did not yield a satisfactory or conclusive value of the pressure shift. In essence, the pressure shift was obtained by

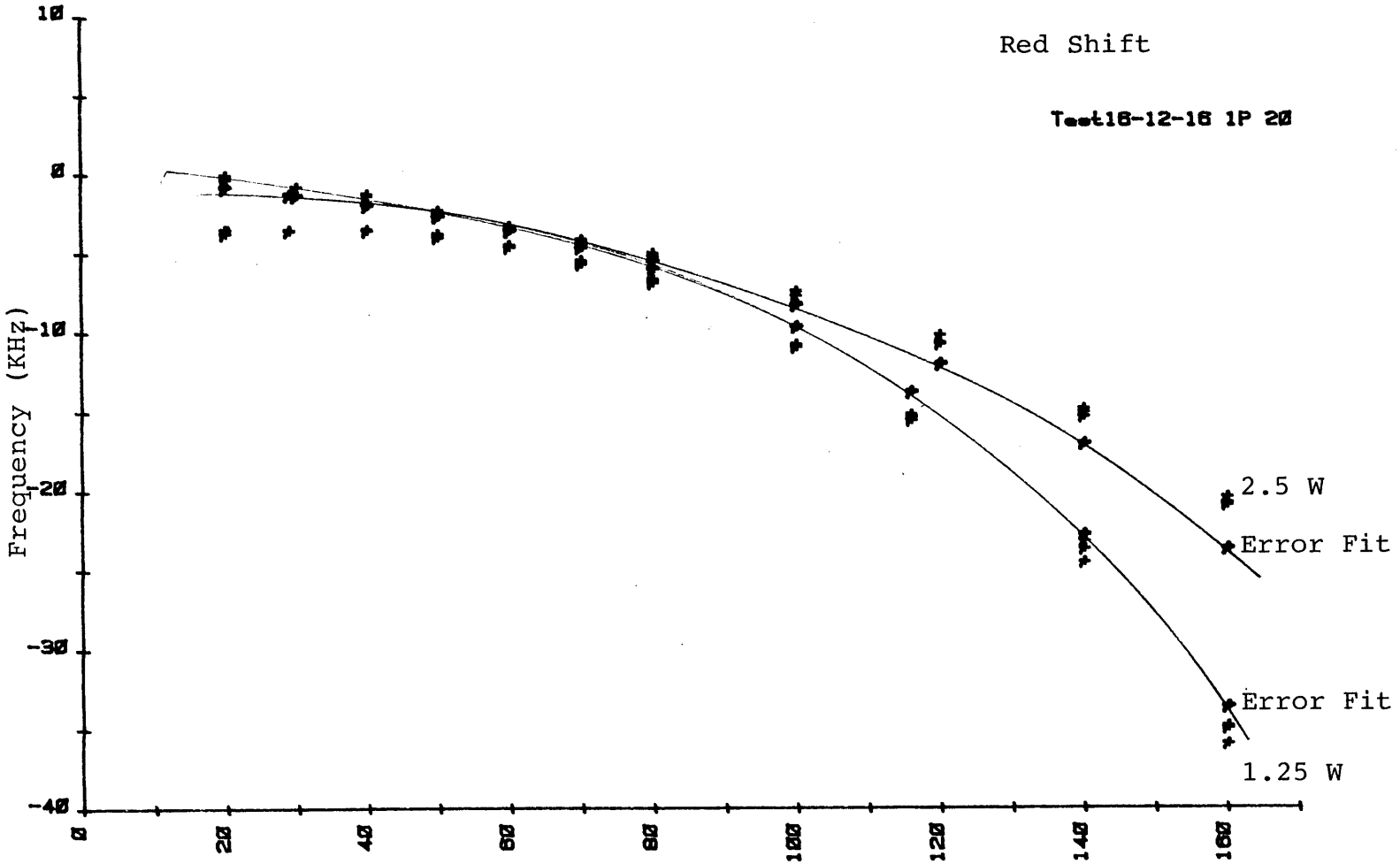

Figure 43 Error Fit to Power Shift

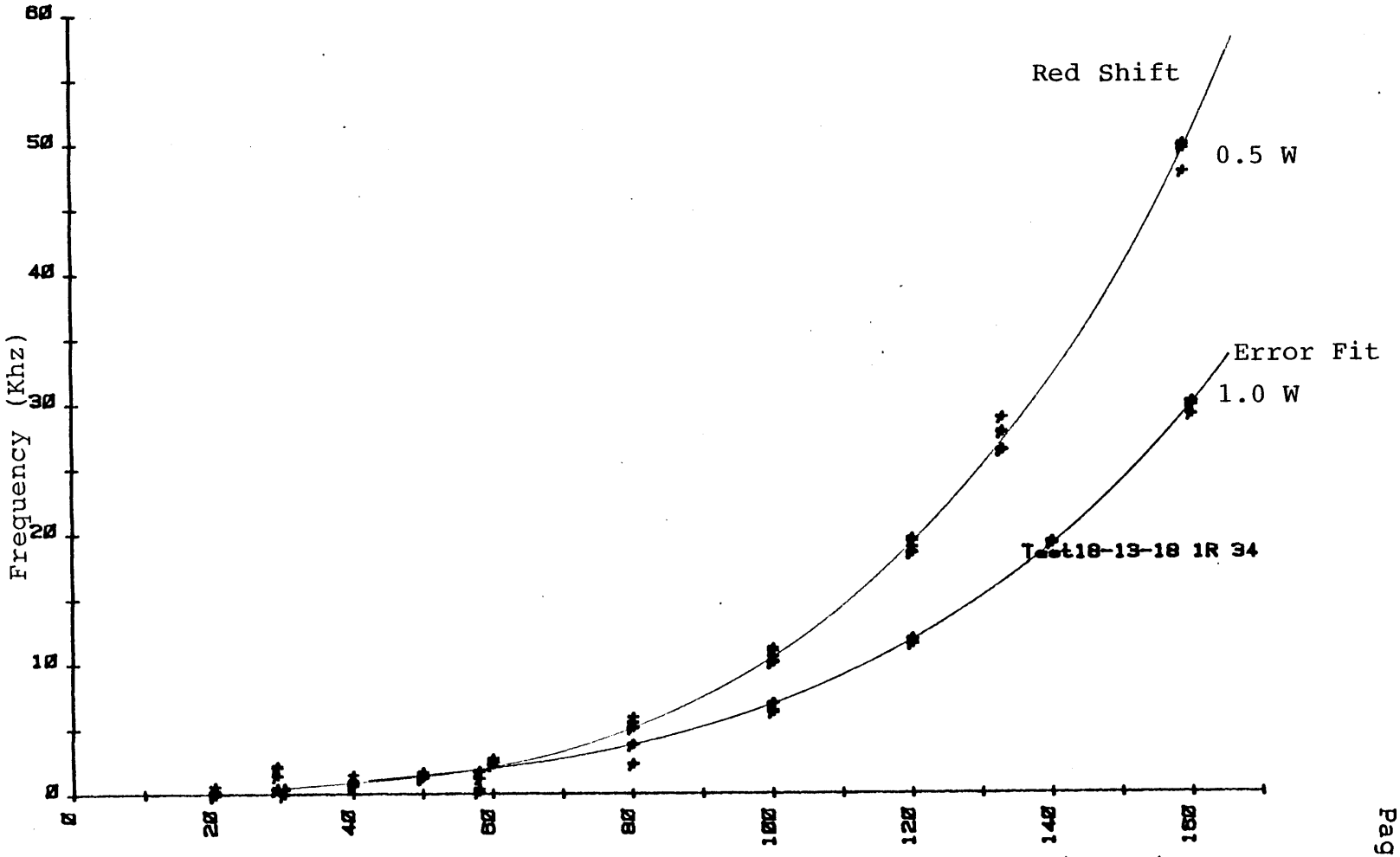

Figure 44 Error Fit to Power Shift

substracting off a very large (>60%) error to arrive at a very small number (10-20%). This method is prone to numerical error as indicated by the varied pressure shift fits A_1, for the various power levels. Even then, this method was very time consuming (approximately 3 hours) and again prone to drift and power variations since it required three consecutive data runs. The slope parameter fit gave a good fit to the shift error data but it sometimes depended too much on luck with everything going just right to obtain a reasonable result.

On the other hand, finding out that the direction of the shift, red or blue, depended on the grating position gave an independent adjustment to alter the background slope. As an example, Figure 45 is a data run taken just by tuning the grating to a different position such that the slope of the blue pressure shift was doubled. A different experiment, whose results are shown in Figure 46, gave a complete range of red to blue pressure shifts when the data runs were taken by just systematically tuning across the the grating while varying the pressure. This gave vivid evidence of the existence of the slope effect plus the dependence of the slope adjustability with the diffraction grating. To visually see this slope effect, several other linescans were

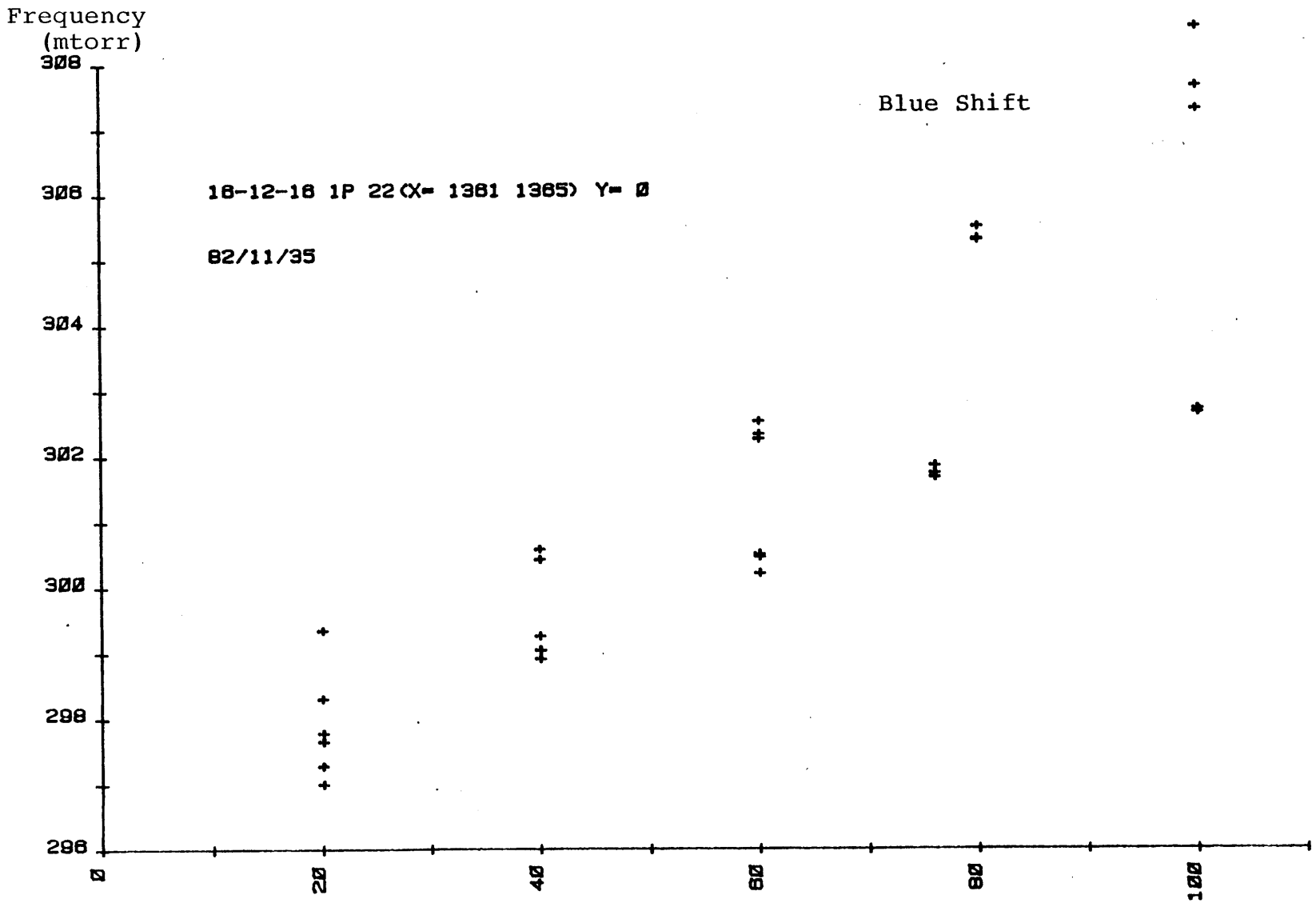

Figure 45 Pressure Shift as Grating Position is Changed

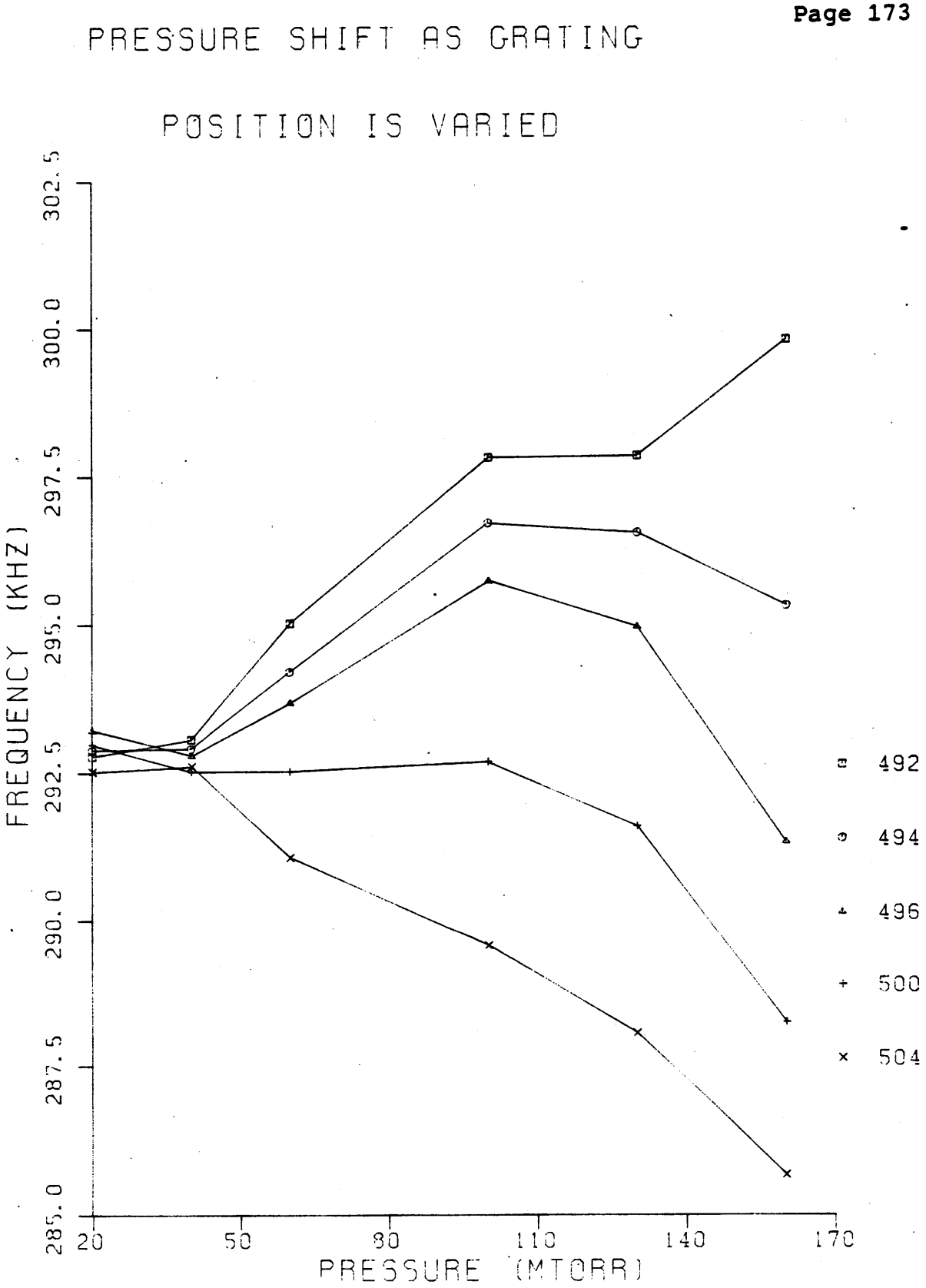

Figure 46 Pressure Shifts for Various Grating Positions

taken as a function of grating positon. Figure 47 shows a selected portion of a series of linescans and clearly indicates a definite change in the physical shape of the net fluorescence signal as the slope as a function of grating positon was varied from + to zero to - . On the other hand, Figures 48 and 49 show power measurements with their corresponding net fluorescence signal as a function of grating position. These graphs corroborate the power slope direction and the corresponding asymmetry in the net fluorescence signal as the power slope changes from positive to negative when the grating position is varied. All of these preliminary measurements provide graphic and analytic evidence that the power slope exists and has a definite effect on the frequency shift measurements.

POWER SLOPE MEAUREMENT

The power variation across the resonance dip as shown in Figure 32, is so small (1%) that it is almost impossible to do any quantitative division or subtraction of the power variation. Instead of measuring this absolute power variation, the power slope, or the first derivative of the laser power output is measured. This slope signal was already present because the 130 Hz modulation frequency was

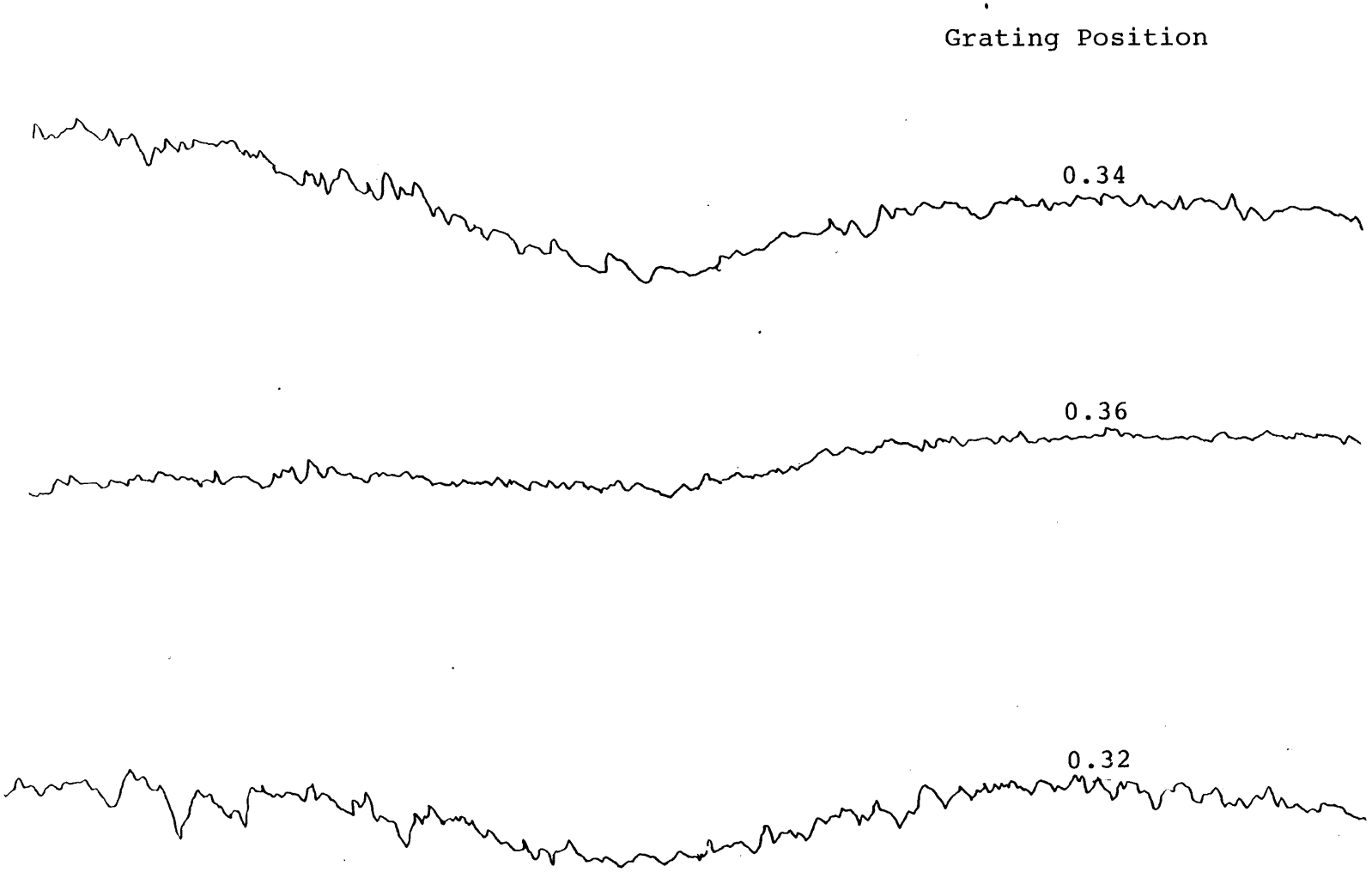

Figure 47 Lamb Dip vs Grating Position

16-12-16 I-P(20) Grating Position

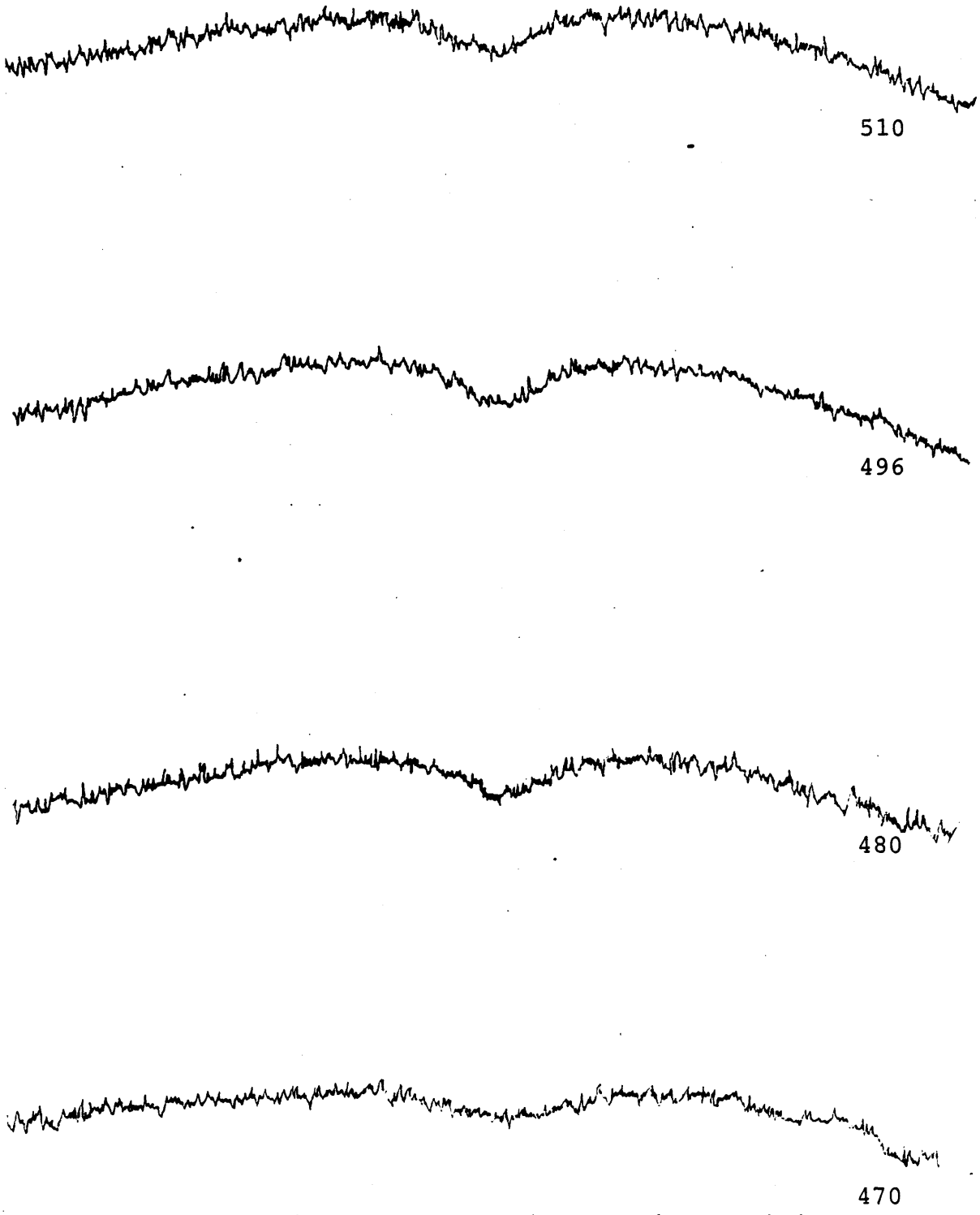

Figure 48 Lamb Dip Correlated with Grating Position

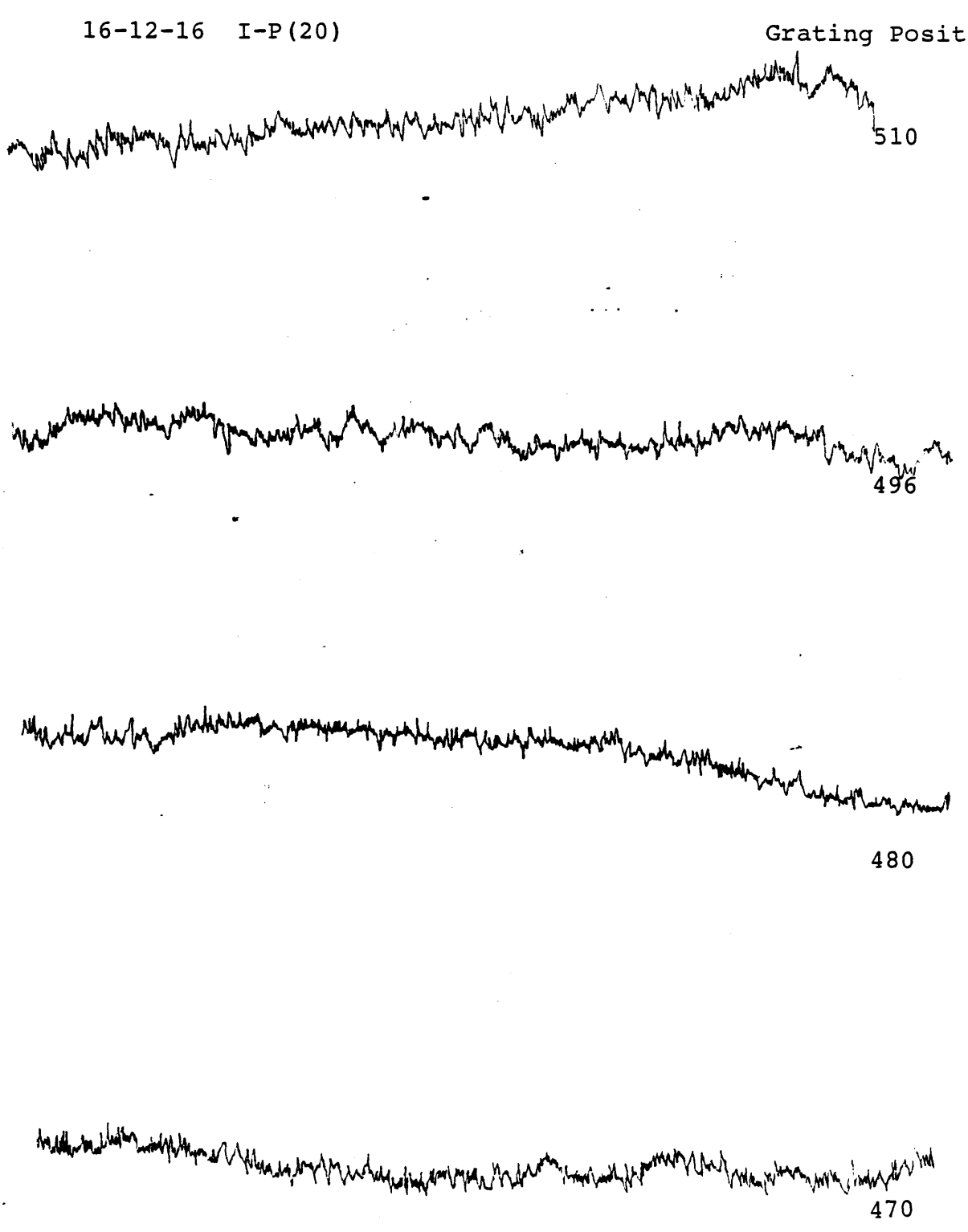

Figure 49 Power Slope Correlated with Grating Position

already applied to the laser to synchronously detect the fluorescence signal. By synchronously detecting the laser power output at the 9-10 μm radiation, with an additional 9 to 10 μm detector, the slope of the laser power can be measured with a large degree of reliability. More important, the transition from + to - slope can be easily seen on the lockin DC output and each + and - slope can be verified to give a corresponding blue or red shift respectively.

Figure 50 is a block diagram showing the slope measurement setup. The additional slope detector was placed behind the 50/50 beam splitter since both laser beams were already reflected in that direction. Figure 51 is a linescan showing the correlation between the + and - slope and the actual laser power profile. Note that the slope is actually 180 degrees out of phase with the normal direction associated with the + and - slope. These power scans were 40-50 MHz PZT scans of the laser output power at a fixed grating position while the laser is unlocked; this shows the wide variation of the slope and power profile along the tuning range of the PZT. The same slope scans were also correlated with the actual derivative scans and the actual chopped fluorescence signals so that the effect of slope and

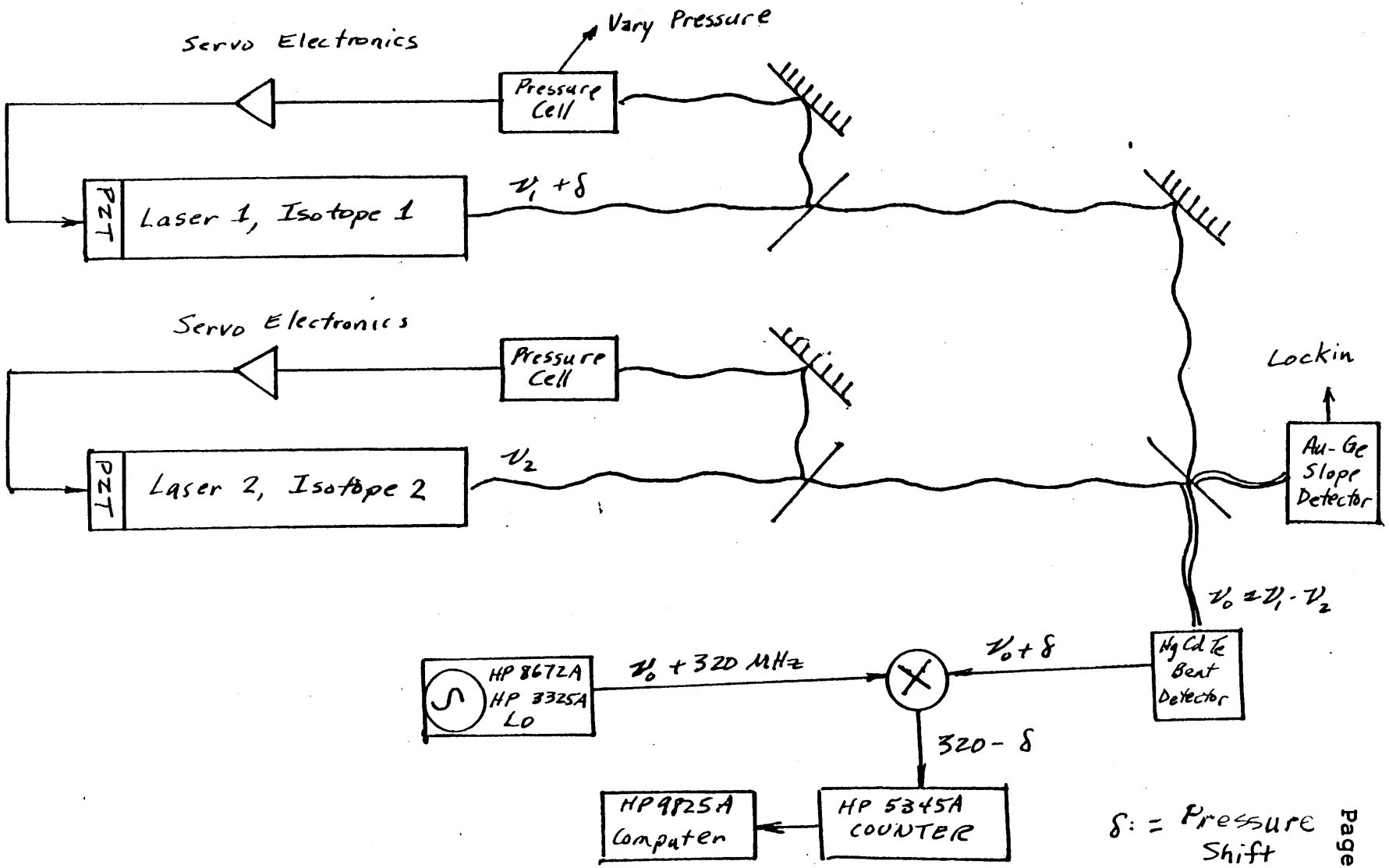

Figure 50 Block Diagram of Pressure Shift and Power Slope Measurements

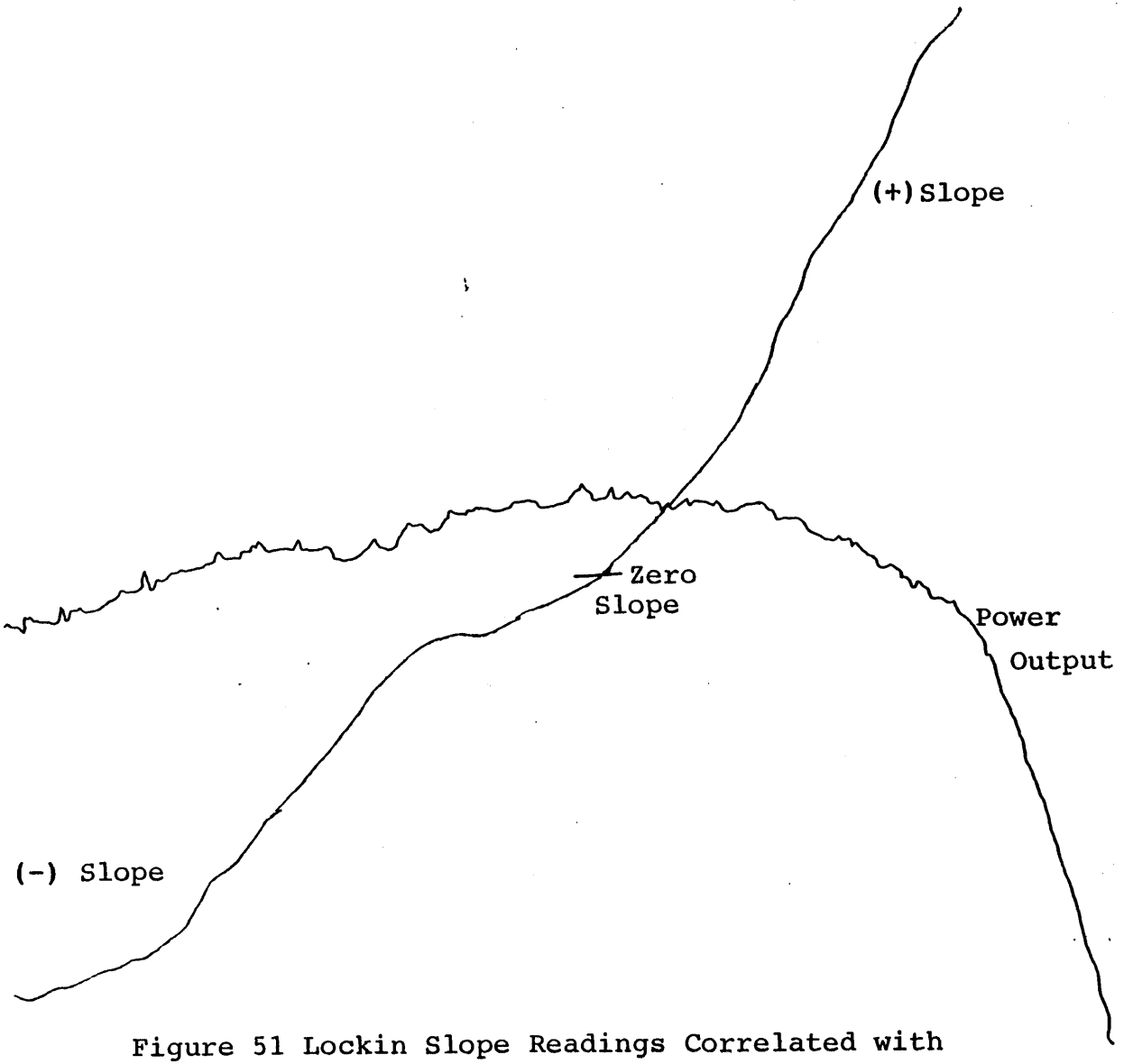

Figure 51 Lockin Slope Readings Correlated with

Power Output Slope

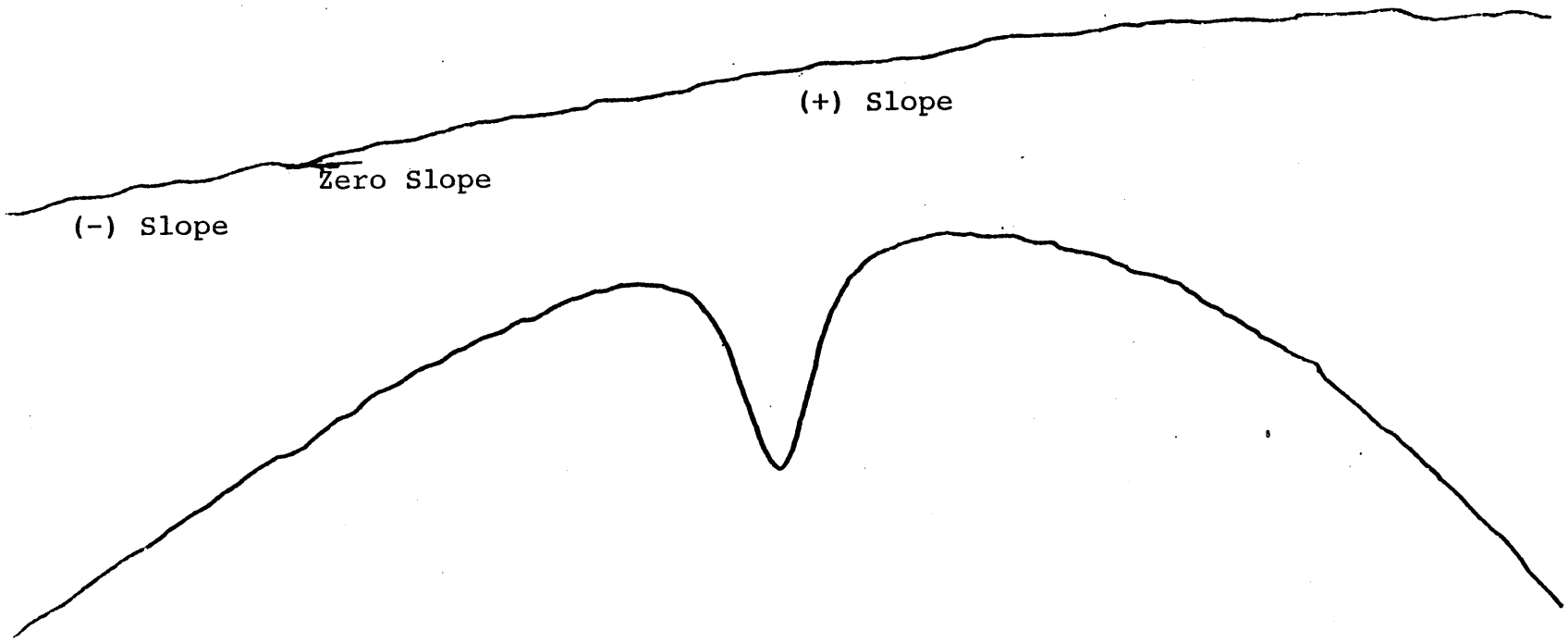

Figure 52 Fluorescence Signal vs Skewed Power Slope

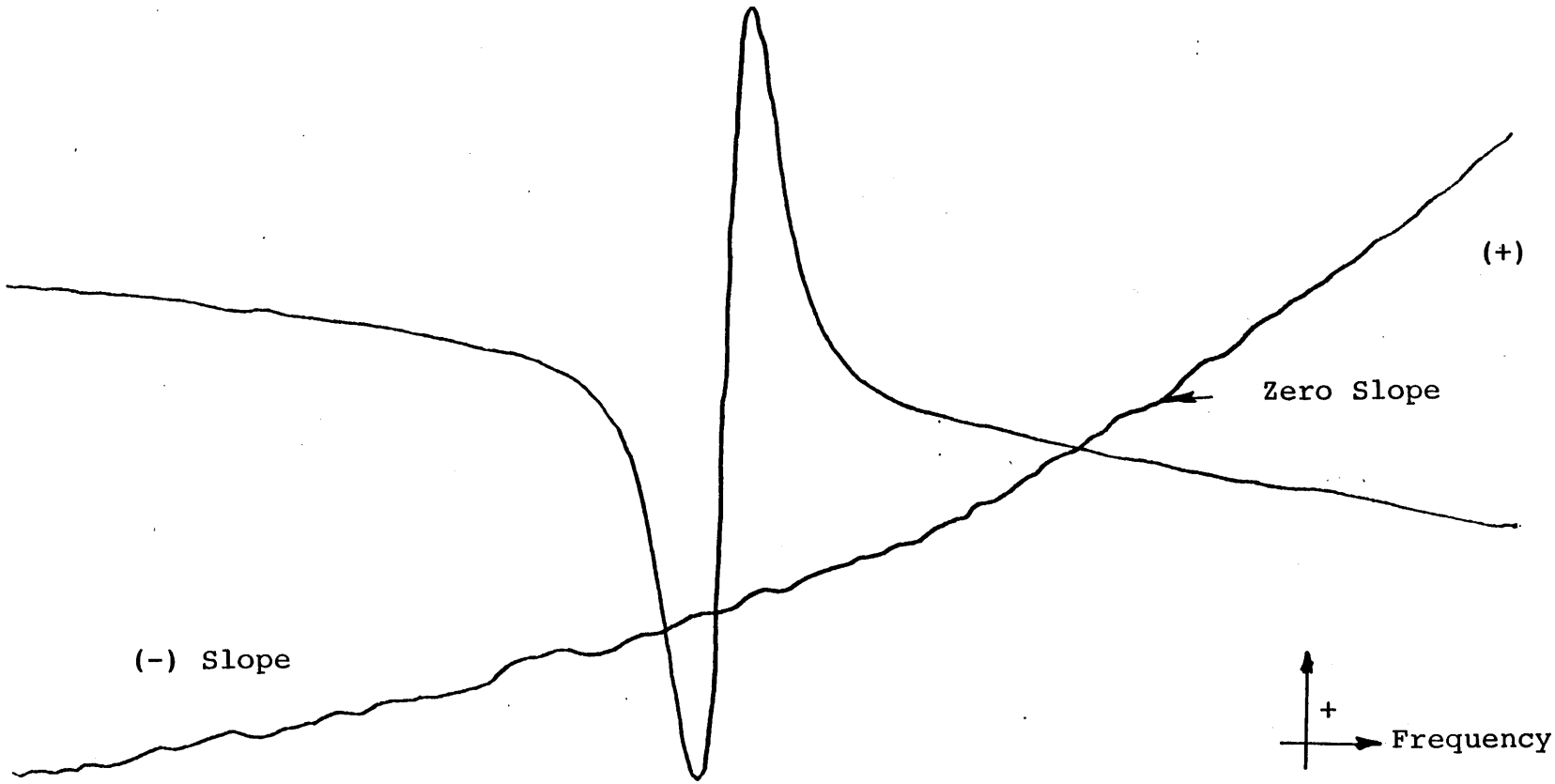

Figure 53 Derivative Signal vs Skewed Power Slope

power can be seen on the fluorescence signals as shown in Figures 52 and 53.

Picking the detector and eliminating most of the ground loops and excessive noise was a significant problem. The slope detector had to be sensitive enough to detect a very small (<1%) intensity modulation on top of a very large laser background signal over the entire 9 to 11 μm range **while the laser was locked.** When the laser is unlocked, the slope signal is over 20 to 50 times the slope signal that is obtained when the laser is locked. Thus a large area detector that has a large DC signal response (mV to V) at the 9 to 10 μm is needed since the derivative signal would be less than 1% of this full DC response(ie.100% amplitude modulation response).

The ideal detector is a large area Cu-Ge detector which gives volts of DC output; unfortunately, Cu-Ge or Zn-Ge detectors have to be liquid helium cooled in contrast with the other three detectors which are liquid nitrogen cooled. Another disadvantage is the short time between liquid helium refills as opposed to the experimental run times that can last more than 24 hours. Because of these reasons and because of availability, a Au-Ge, liquid nitrogen cooled,

relatively large area (3mm diameter) detector with an input resistance of 110K, operating in the photoconductive mode, was used as the slope detector. Besides having a lower response than a comparable Cu-Ge detector, the response of the Au-Ge detector is 10 to 100 times lower for the 16-12-16 10μm band than in the 9μ band. Noise and 60 cycle,and 120 cycle pickup was an extreme problem when using such low signal levels on this detector and great care was taken to eliminate as much of the noise as possible.

The slope detector as shown in Figure 50, was placed right behind the 50/50 beam splitter. Thus, by blocking one of the laser beams, the other laser beam, after passing through an 80% attenuator mirror and a CaFl attenuator, was focused upward onto the detector via a parabolic reflector. Care was taken not to saturate the detector and not to focus the beam right on the detector surface or contact wire but rather to maximize the signal without getting any 60 or 120 Hz pickup. The slope signal was synchronously detected by a separate lockin that was externally triggered directly from the oscillator box (directly from the reference 555 timer). One important question that arose during the run concerned the correct phasing, especially since the signal goes through zero and reverses sign as it passes from + to -

slope. Using a PAR 5301, which is a microprocessor based unit with automatic ranging and phase tracking, several plots were taken as shown in Figure 54, to see what kind of phase errors were involved in just using a single phase adjustment for the slope detection lockin as a function of tuning the grating. Another phased tracked plot was taken of the 4.3 and 10 μm signal as a function of pressure. The phase graph, shown in Figure 55, taken with the servo locked to the Lamb dip, indicates that there is actually very little change in phase as the pressure is changed as was shown in Figure 4 or else the change in phase has an imperceptible effect on the resulting signal.

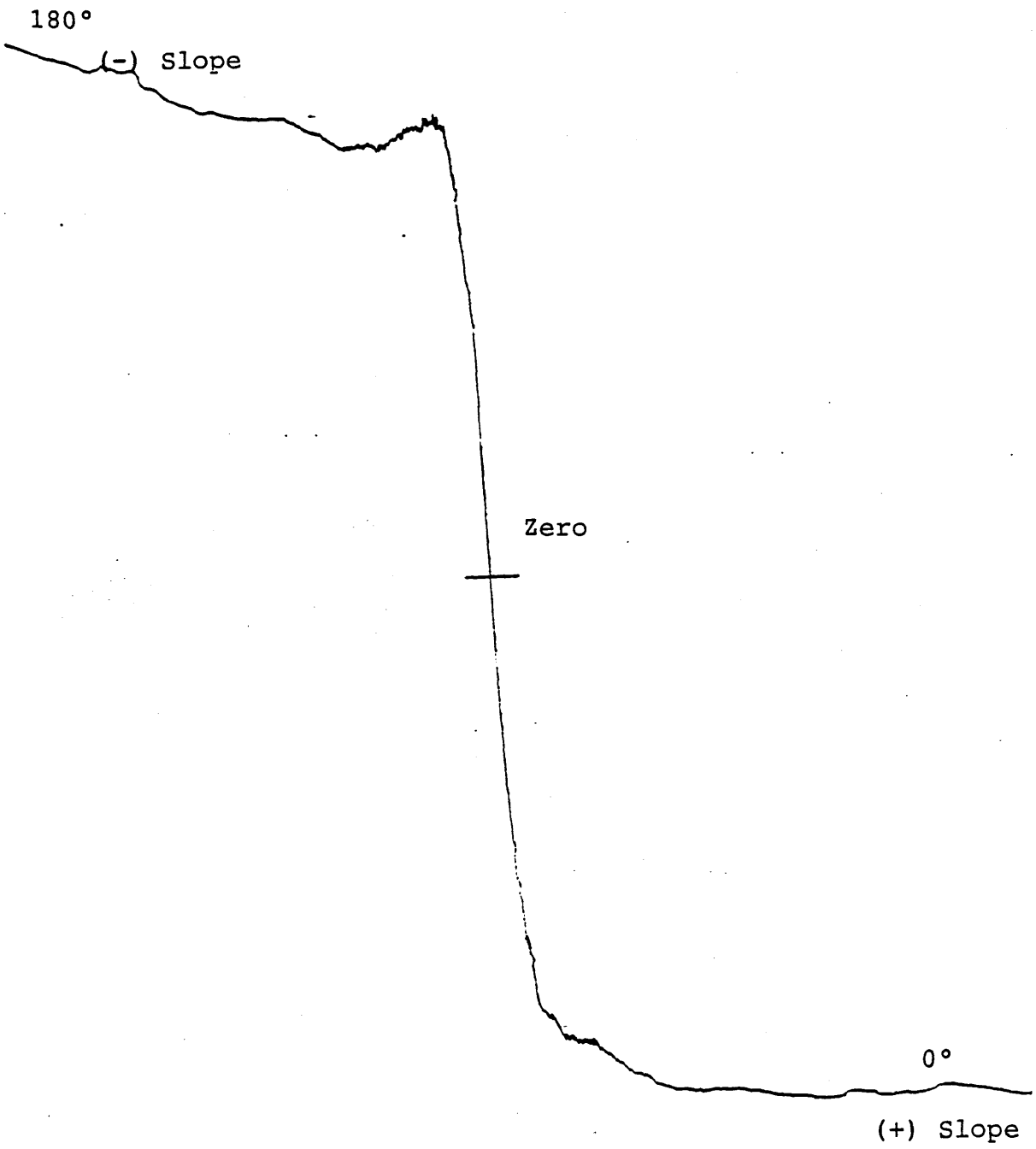

Figure 54 Phase Locked Lockin Slope Signal

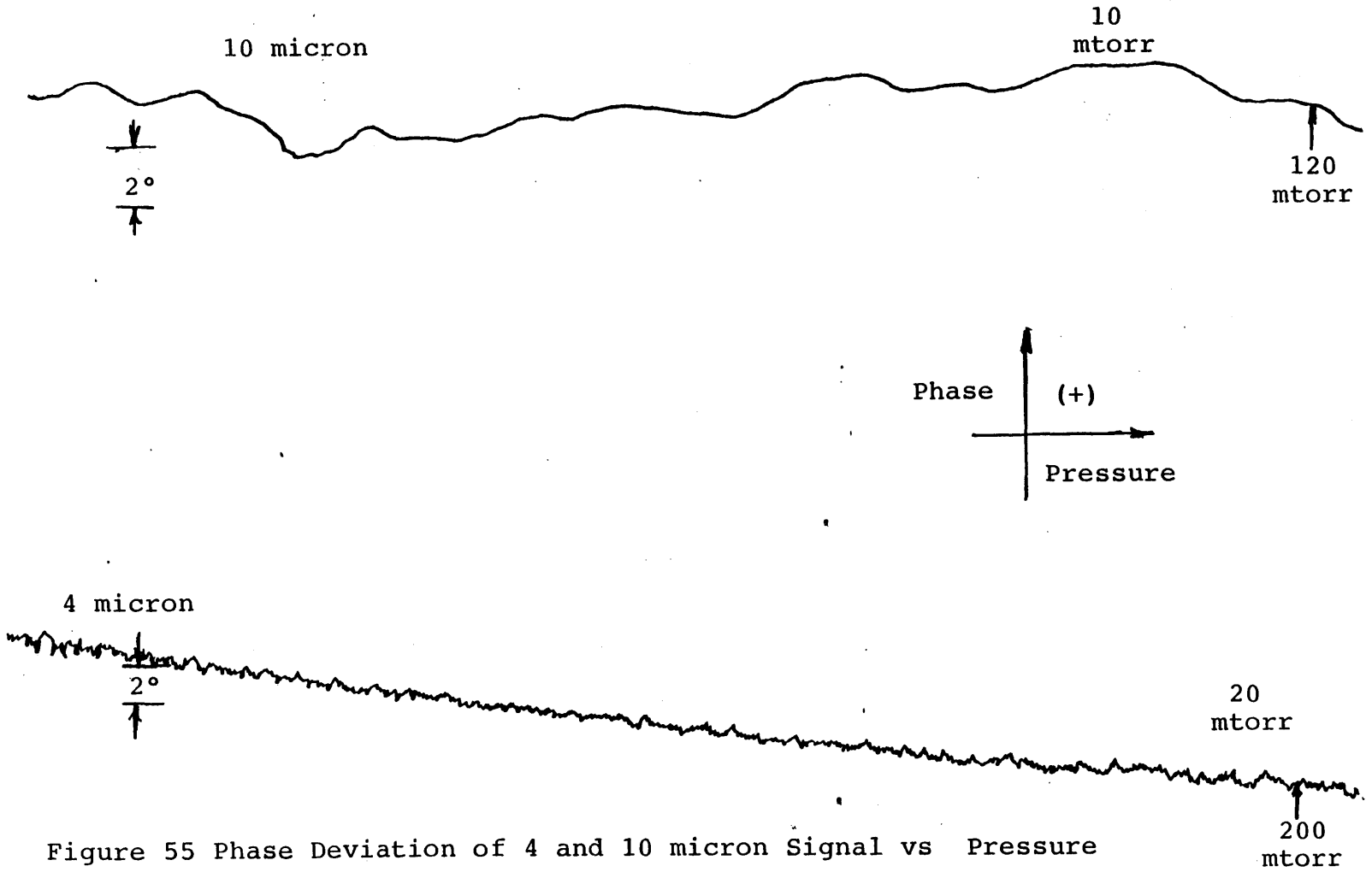

Figure 55 Phase Deviation of 4 and 10 micron Signal vs Pressure

CHAPTER 7 PRESSURE SHIFT MEASUREMENTS

DATA TAKING PROCEDURE

The following procedure was taken to ensure consistent data runs. Each laser was adjusted and locked to its individual molecular resonance. The grating was adjusted for peak power output with an absorption cell pressure of about 50 mtorr for an optimum signal in Laser 2. The pressure in Laser 1 is set as low as possible (near the starting pressure point) when the system is initially locked with the grating set near zero power slope. This point is known from a preliminary grating scan; the range of the slope variation from + to - (or vice versa) and the grating scan range in which that particular line will oscillate before the next J line will jump in is roughly known. Then by moving the micrometer drum (diffraction grating) forward so that the spring plunger moves downward without any slack, the grating is slowly rotated about its pivot and the power slope, as monitored on the slope detector, varies while the laser is servo locked to the resonance peak. With the laser output frequency locked on the Lamb dip resonance, the laser output essentially sweeps across a distorted gain profile as

the power slope is varied from + to - or vice versa. When the laser power slope is as close to zero as possible (within noise limitations,ie ±10 mV on a full scale of ±10V) the grating is set at zero slope and data can be taken. Subsequently, pressure is let into the absorption cell and the corresponding beat frequency at that pressure with all the other relevant information is recorded on disk. At each pressure, the data consist of the average of three separate trials; each trial consists of several (3 to 10) real time (no dead time between counts) 10 second counting intervals. At each pressure interval, the slope reading measured by the lockin is also recorded so that an estimate of the slope error correction can be made. By continuing this process up to the desired final pressure, a pressure shift run along with the corresponding slope drift error readings are taken. These pressure runs are usually repeated on the same J line at least one time with grating adjusted again if necessary. Sometime in between these pressure runs, a calibration run is taken in which the power slope is deliberately offset by a large + or - value and the corresponding 'error' pressure shift is recorded at this relatively constant offset slope. Using this calibration run and the corresponding value of the lockin reading, the slope proportionality constant can be determined by using the same nonlinear least squares fit

as in the previous power slope pressure shifts. Then, using this slope constant, the frequency error of each data point due to the power slope drift can be estimated from the corresponding slope readings and the expression (6.4,6.5) for the offset error. The calibration run (which probably differs in power from the zero slope power) is needed for each set of pressure shifts since the laser gain profile or cavity dispersion varies from line to line, laser to laser, and from day to day so that lockin readings measure the error for that particular laser configuration during that particular set of pressure shift data runs so that the frequency error due to the power drift can be estimated after fitting the proportionality slope constant from the calibration run.

To further corroborate the slope measurements on the detector, separate calibrations runs were taken with large (>±5V lockin) power slope readings for those lines that could tune large + or - power slopes with adequate power output. This was done to make sure that the slope effects actually dominated the error and that the slope error scaled linearly with the lockin readings. Figures 56 and 57 show such dual ± power slope calibration runs and accordingly verify the direction of the slope and shift. For all large

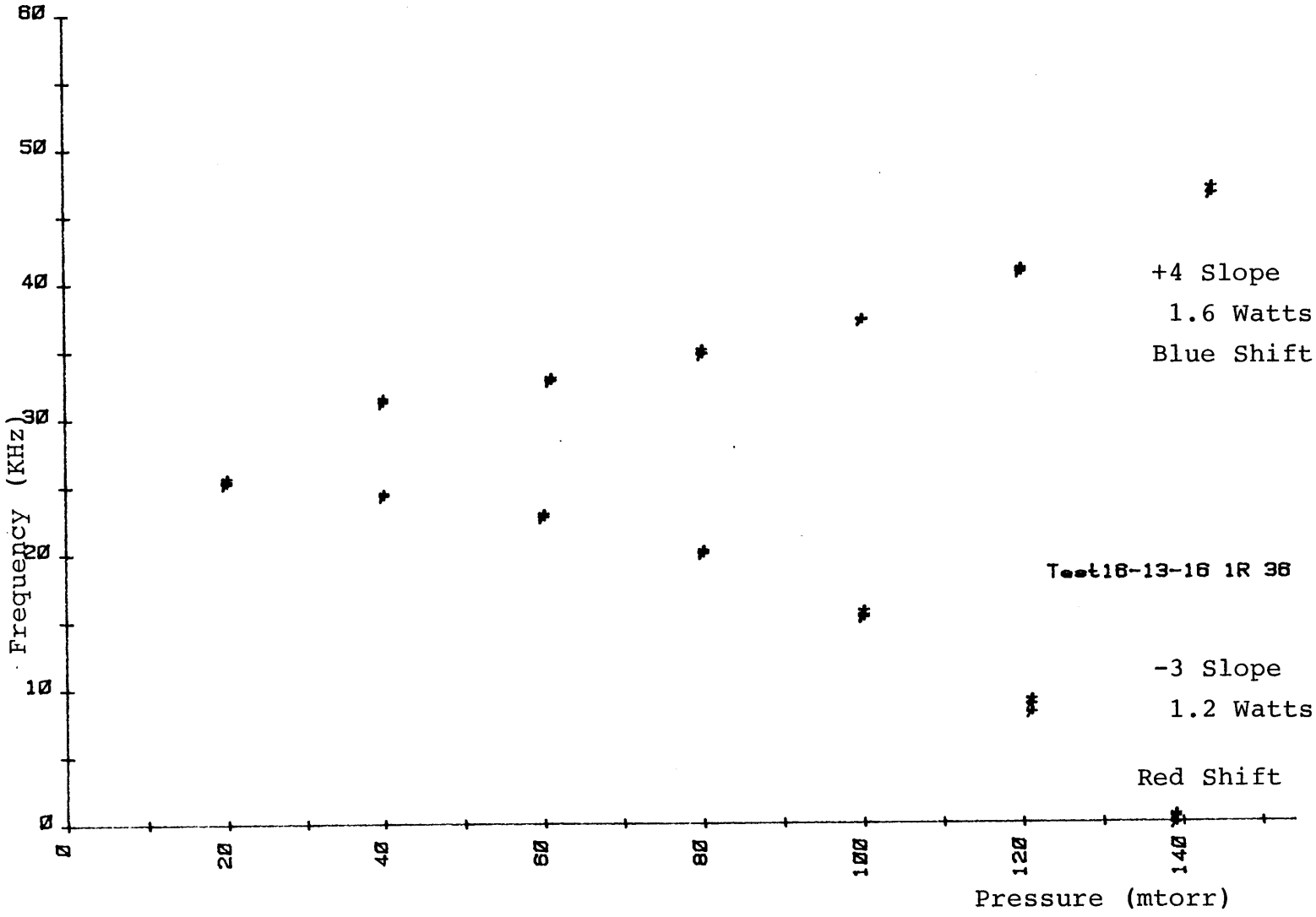

Figure 56 Blue and Red Shift vs + and - Slope

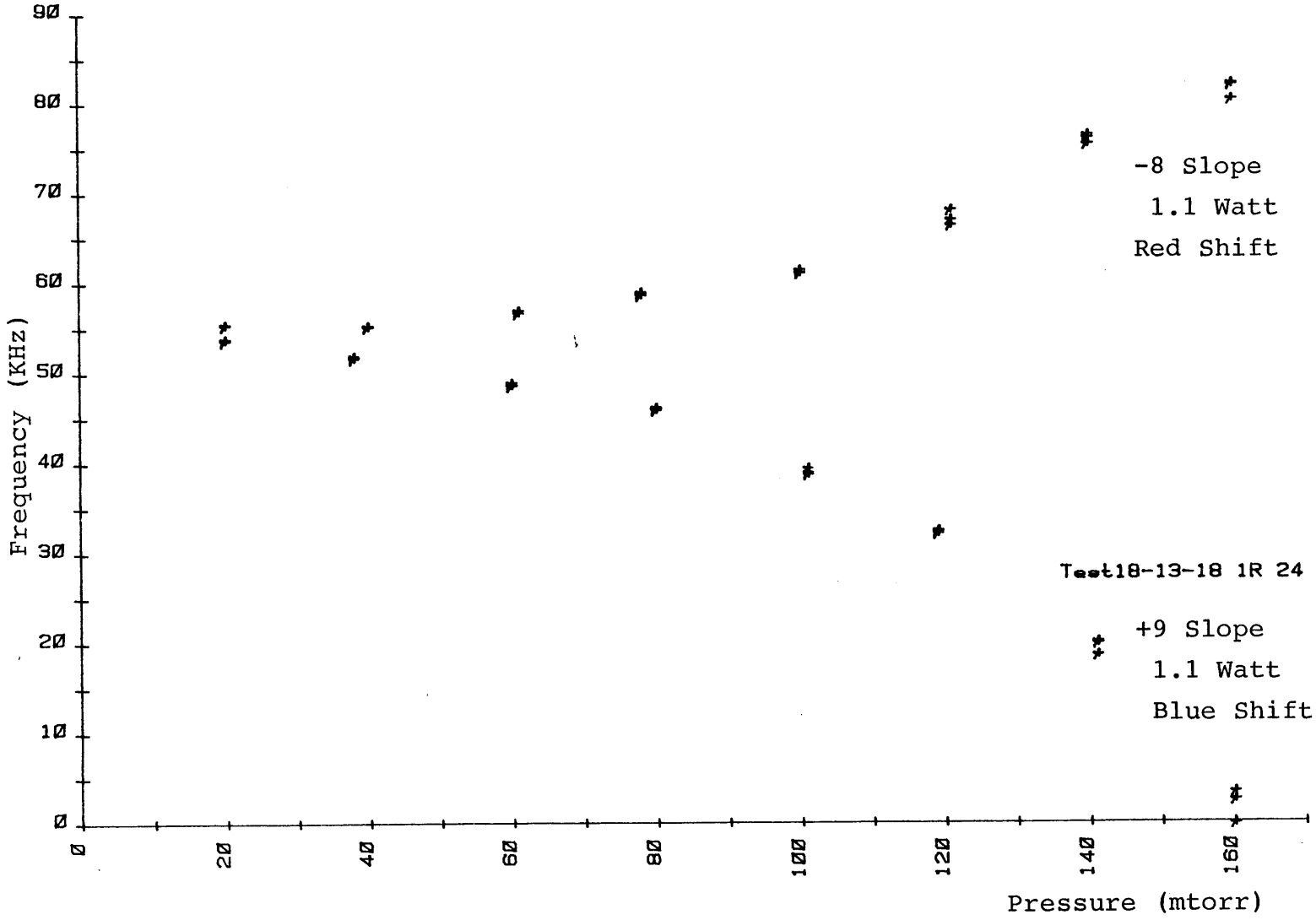

Figure 57 Blue and Red Shift vs + and - Slope

power slopes (>±4V on the lockin), the pressure shifts were always red (- slope) or blue (+ slope) for pressures greater than 80 mtorr when the power slope error pressure squared dependence becomes dominant; this was not always the case at the lower pressures since the true pressure shift could dominate and upturns or downturns were possible.

In the good data runs, it is assumed that the slope error is very small or else drifts about zero slope. One cause of this drift was the length of time for the grating and hence the laser cavity to relax after each adjustment. Ideally the grating adjustment should be as small as possible to minimize this relaxation with the final grating setting as near the power peak as possible. The entire laser cavity and absorption cell should have enough time to equilibrate at the final laser power levels; this is very important since the thermal drift due to a change in laser output power can easily change the cavity dispersion and alignment and consequently the power slope can easily drift with time after the 'final' slope adjustment. Essentially the grating has the slowest relaxation time and hence must be moved the least. There were numerous runs when the drift due to the relaxation and power thermalizations caused a steady or 'violent' change in the power slope during the pressure

runs; these runs were disregarded, especially if the power error correction or drifts were too large (On a ±10 V scale, large means >±0.6V where zero was achieved at least on the ±0.1V level; normally 'zero' slope was about ±.05V). Again, time and patience were the only solutions since the most desirable and optimum thing to do was to set the grating once at the start of the data run and never touch it again during the data run. Most of the data were taken under somewhat less than optimum condition.

It has been suggested that the best way to adjust the grating is to have an extremely slow feedback loop controlling a PZT attached to the diffraction grating. But servo stabilizing the power suffers from the problem of the extremely long relaxation times (probably greater than 30 minutes) associated with the grating mechanism; hence any small or steady correction translates into many, many finite responses until the final setting is reached. The final response unwittingly enough has the tendency to overshoot the desired result and any subsequent correction to the overshoot propagates the opposite overshoot, even if the adjustment is done electrically instead of manually.

DATA RESULTS

Using this procedure to systematically correct and account for the to power slope errors, pressure shift data were taken for as many lines that had a zero power slope and which had enough power to lock within a minimum standard deviation (≃ 200-400 Hz). Pressure shift measurements were taken for the P and R branches for both the I and II bands for four different CO_2 isotopes: 16-12-16, 16-13-16, 18-12-18, and 18-13-18. This wide spectrum of lines required constant juggling of the two different isotopes in the left and right lasers so that a 2 to 17 GHz beat could be generated from mixing the two different isotope lines together. A listing of such beat frequencies (2 to 18 GHz) between the various lines of the four isotopes is given in Appendix 5. From this beat frequency listing it can be seen that only certain P and R branches or I and II bands of certain isotopes overlap enough to generate adequate beat frequencies with sufficient power to lock. Normally, for a given branch or band, there is only one other isotope branch where small enough beat frequencies exist; if there is more than one isotope line that beats with the first isotope line, normally one of the second isotope lines will either have a higher power gain or else will be a midband J line

and accordingly will be chosen as the second lasing line. Very low gain lines from the low J or very high J lines are almost never used because there is not enough power to give a stable enough lock to yield accurate pressure shift data. Because of all the combinations possible and the juggling of the isotopes needed to cover the entire span of lines, the left and right lasers channels were continually switching roles as the reference Laser 2 or the pressure shift Laser 1. Thus, because of all the switching between lasers and different branches, each output of each laser was constantly being realigned so that the data is probably independent of the laser channel used and is independent of the alignment of each system.

The data taken with the power slope zeroed is stored on disk and then later plotted and corrected for any power slope drift. As was mentioned, each measurement consisted of three separate trials of several ten second counting intervals for each pressure point. In the power slope corrections, the estimates of the power error are obtained for each data point by combining the power slope reading (this is monitored for all pressures to determine the drift) with the calibration power curve to arrive at a power drift frequency error, derived in equation 6.3:

$$\Delta = B/A\gamma^2(1-f)/(8f)$$

Hopefully, this power error is small or the drift of the power slope during the pressure runs (lasting about 20 to 30 minutes) is not significant from pressure to pressure so that any 'correction' is very small. Data runs where there were large slope errors due to drift or which were very noisy because of a poor lock or weak beat signal were discarded in the final analysis. The ratio of good to 'bad' (drift) data was better than 3 to 2. Figure 58 emphasizes one of these power corrections where the correction actually helped to 'straighten' out the pressure shift. Some bands in certain isotopes (the II bands in the 16-13-16 and some 18-13-18 lines) were so weak that only questionable data were taken on these lines. Table 8 summarizes the pressure shift data after sorting out and discarding all the data dominated by drift.

The data is grouped according to the I and II bands for each isotope and the average is taken over all the different J lines in the I and II band data. Note, all the pressure shift values shown in the above table represents a **blue** shift, contrary to the previously reported red shift. This is very significant and will be explored in further detail

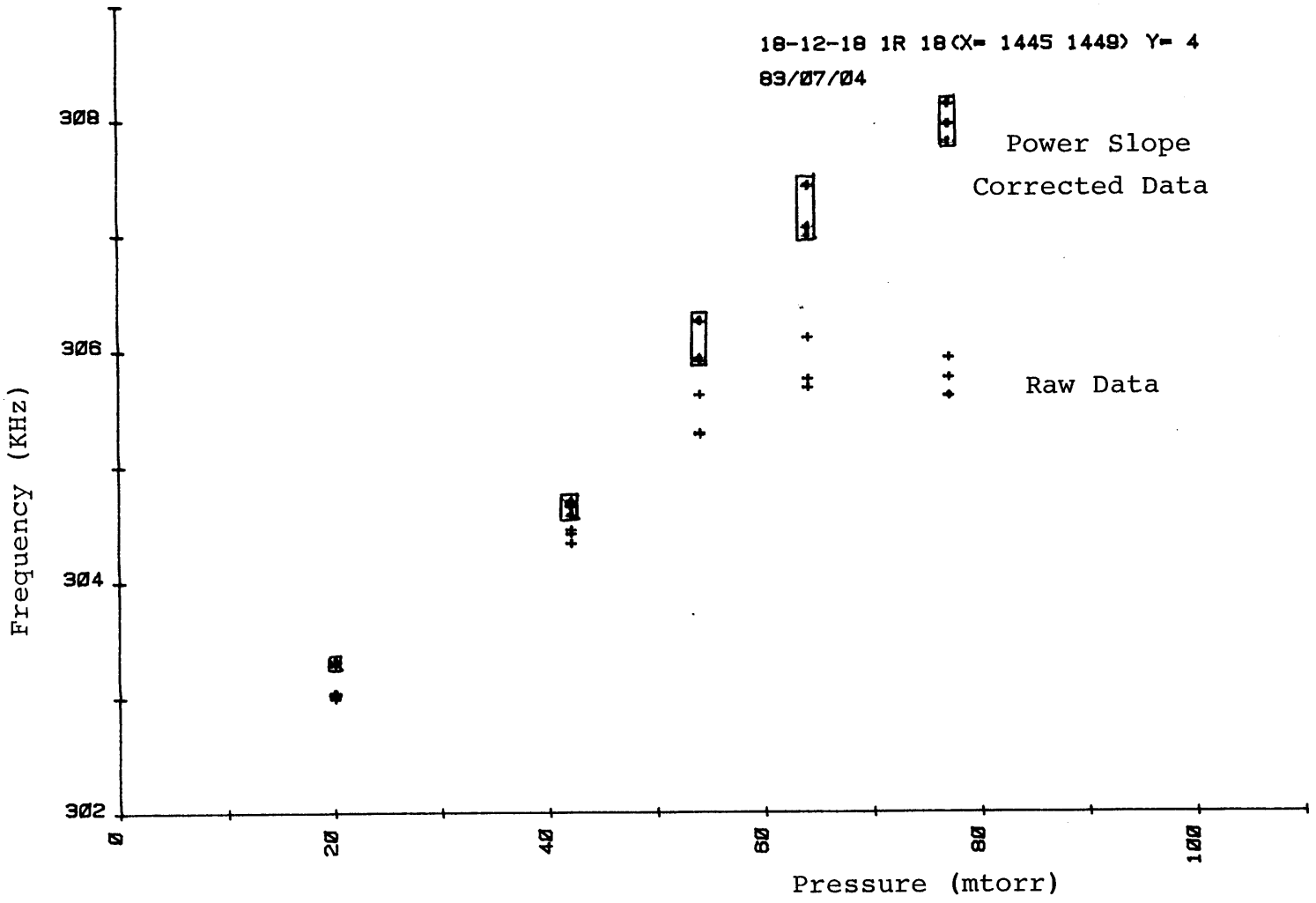

Figure 58 Power Slope Corrected Shift

Table 8

Pressure Shift Data

	I Band		II Band	
	Shift (KHz/torr)	σ	Shift (KHz/torr)	σ
16-12-16	62.1	18.1	63.2	18.1
16-13-16	50.3	16.8	87.2	37.8
18-12-18	81.1	28.6	72.3	29.8
18-13-18	51.9	21.2	43.8	22.3

in Chapter 8 where the theoretical fits are examined. Figures 59-65 show a wide range of blue pressure shifts for various I and II band, P and R branches for the four different isotopes. The power slope corrections were very small in these figures and hence are not included in the graphs for the sake of clarity. Though these figures show the values of the pressure shift 'increasing' or 'decreasing' with pressure, it must be remembered that the laser beat frequency $\nu_1-\nu_2$ is plotted; because this beat frequency is positive or negative, these graphs, which only

plot the last three digits of an eight digit number, can appear 'blue' or 'red' depending on whether the beat frequency is + or -.

It should be noted that not all pressure data taken were blue. In the earlier phase of the experiment, especially when we were not fully aware of the significance of the slope effect and were not aware of the grating slope adjustment, there were always a mixture of red and 'anomalous' blue shift, depending on what line was being measured. For instance, the 16-12-16 IP-20 line, always gave a red power error when locked on the power peak of the laser gain profile while the 18-13-18 IR-24 line always gave a blue power error on its power peak. Thus repeated measurements taken by locking on the power peak almost always gave a consistent linear red or blue shift with a nonlinear dependence at higher powers for these two lines. Only by fortuitously altering the grating did the magnitude and sign of the pressure shift change for these lines. Thus any of the earlier measurements, taken in ignorant bliss, gave erratic and quite different results, both in magnitude and sign, depending on just what the laser power slope was at the locking position.

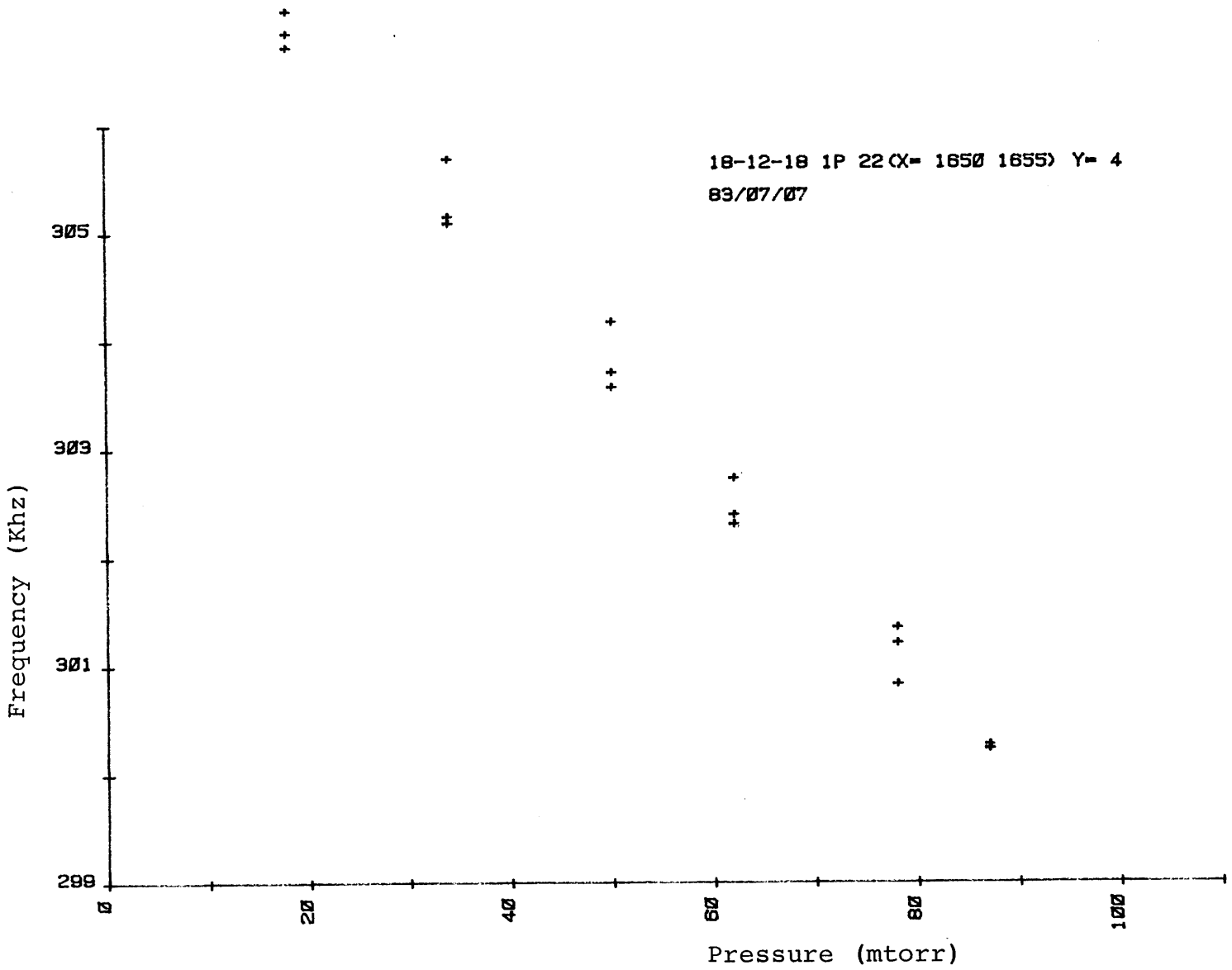

Figure 59 Pressure Shift

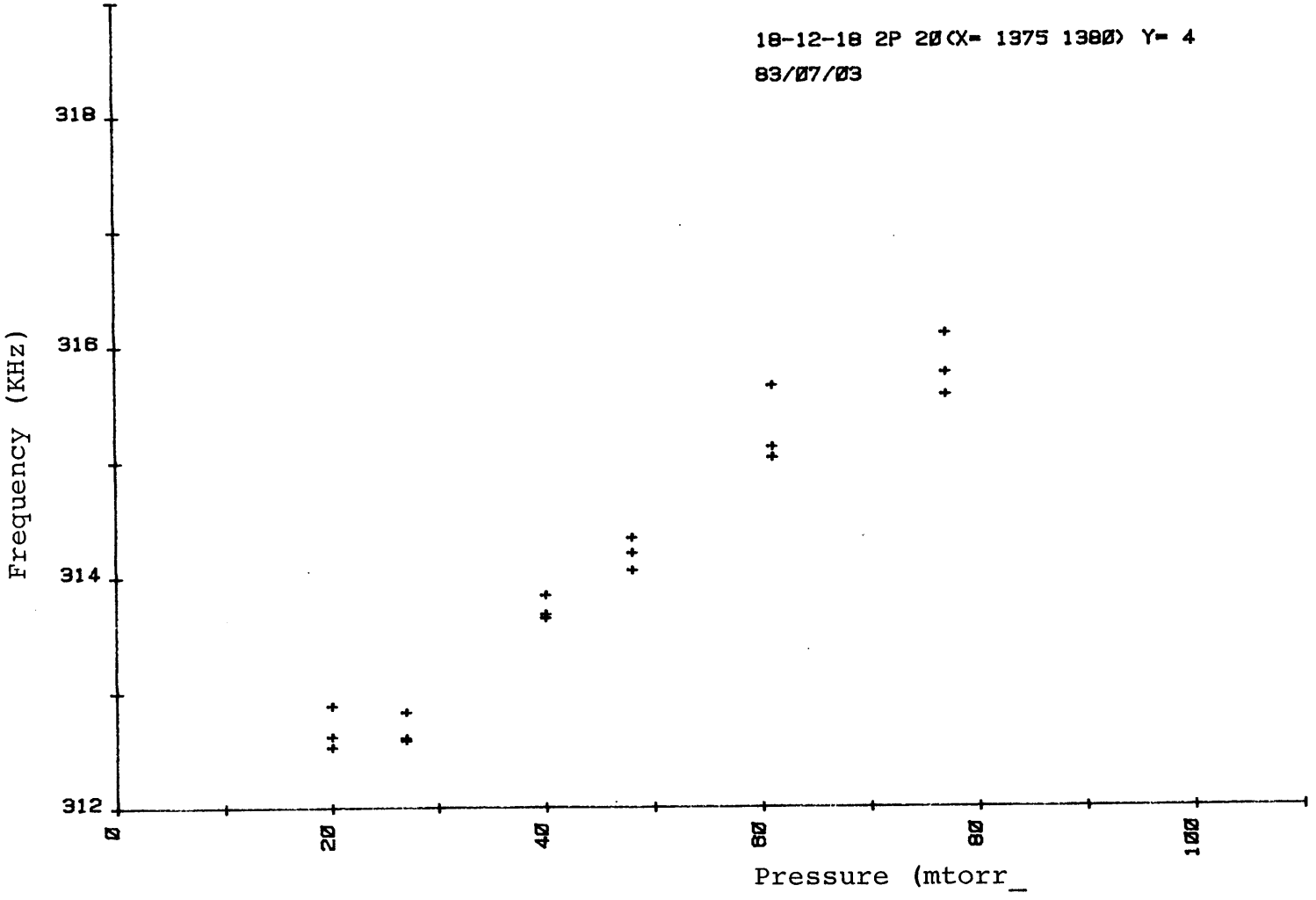

Figure 60 Pressure Shift

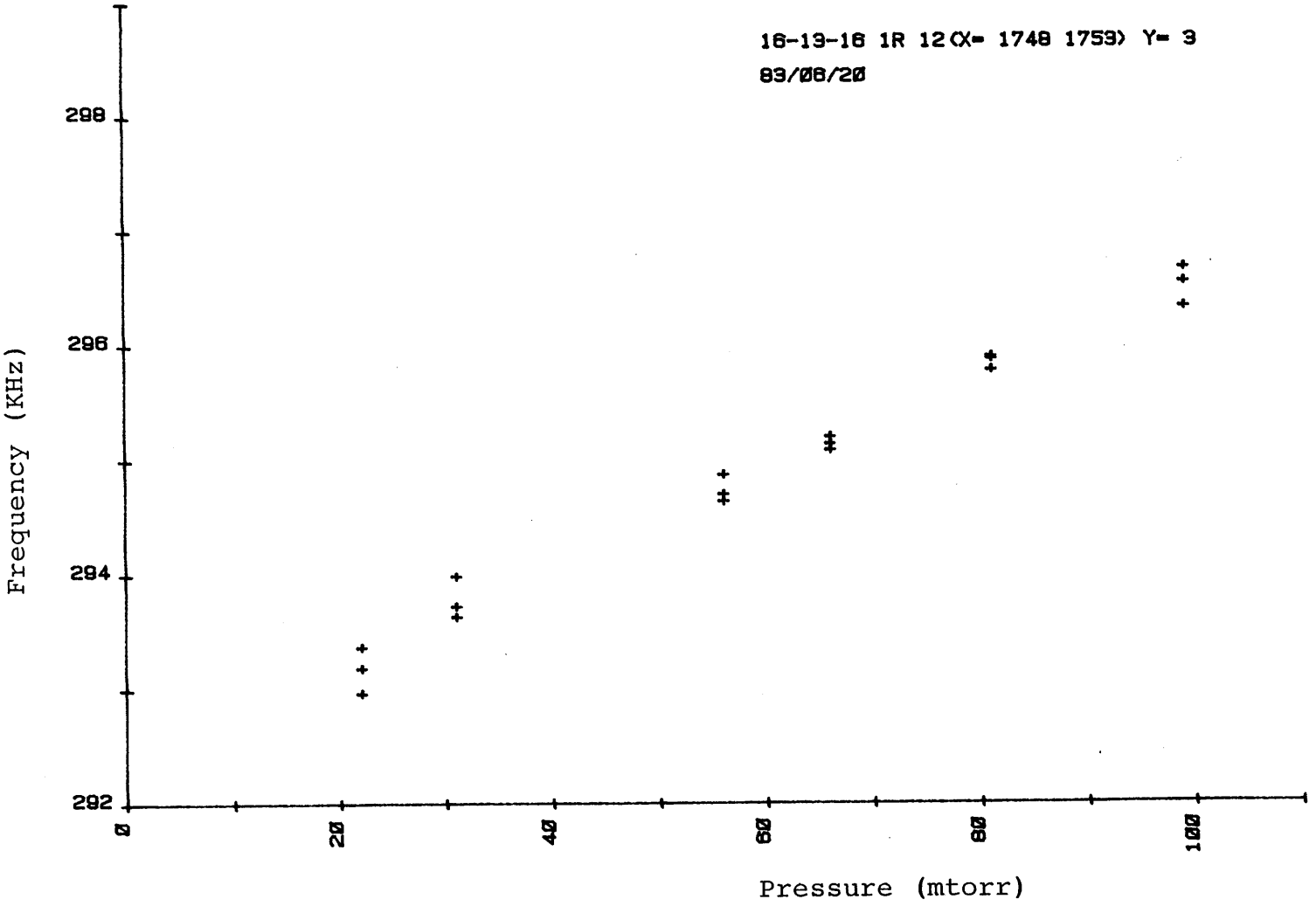

Figure 61 Pressure Shift

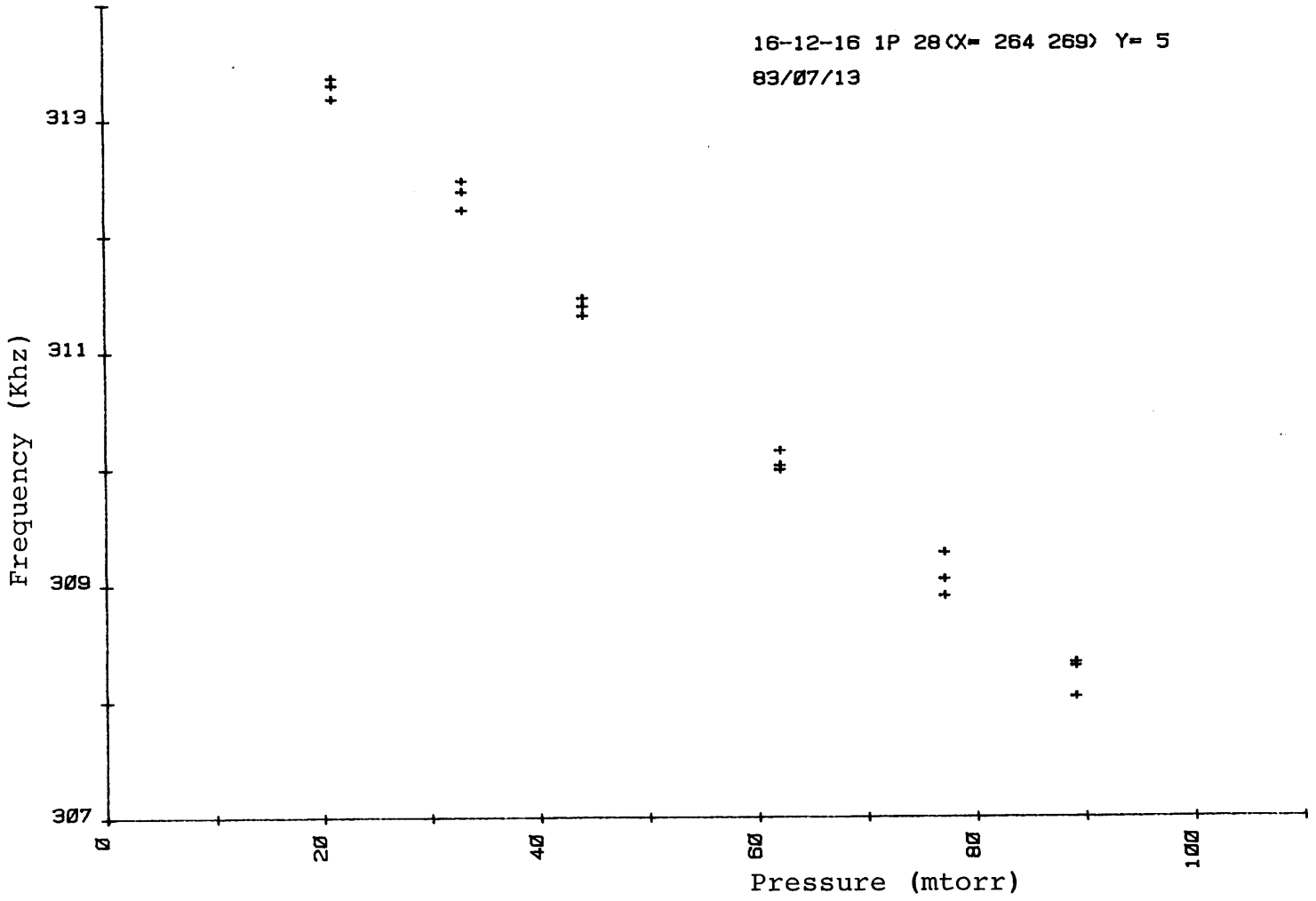

Figure 62 Pressure Shift

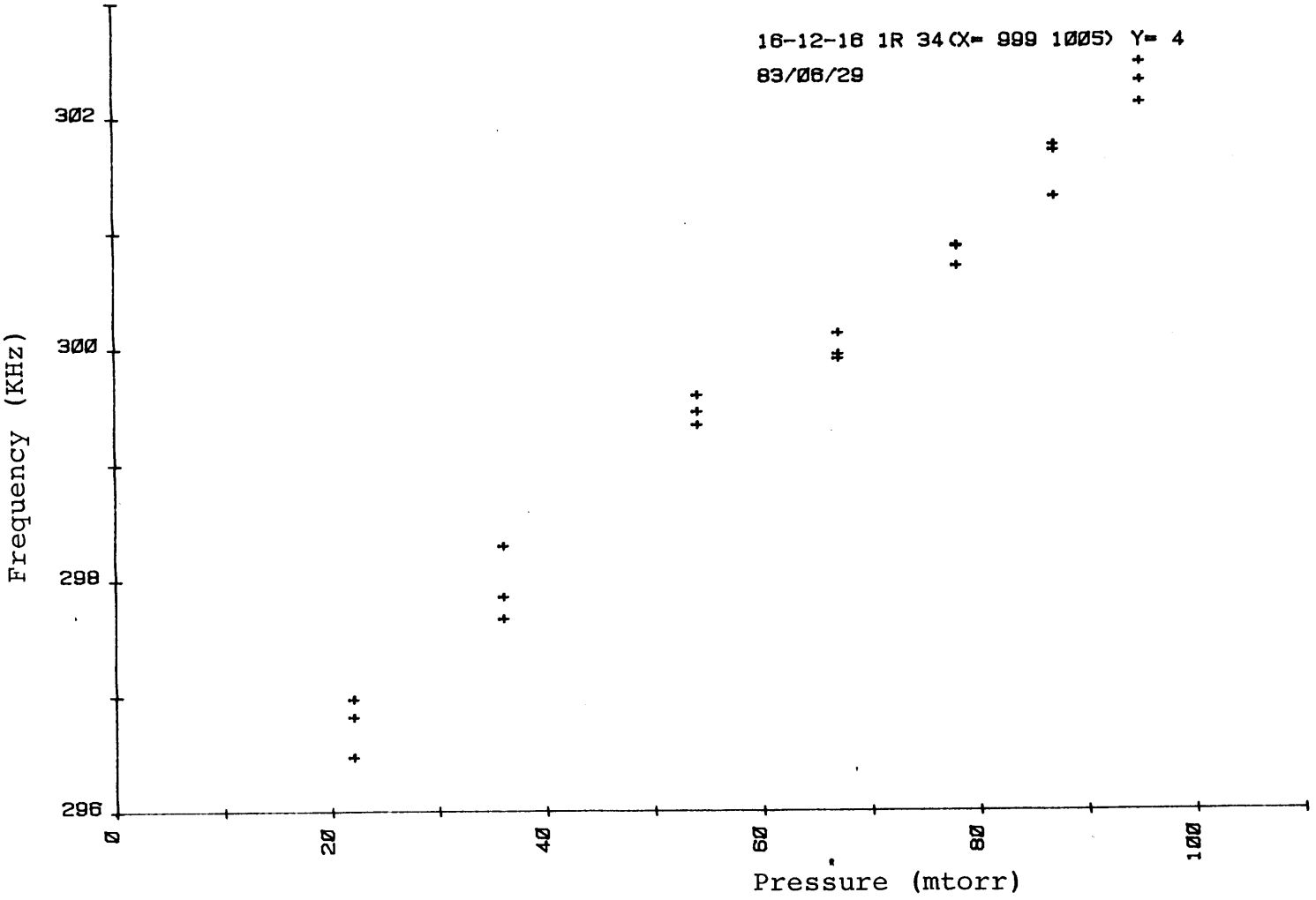

Figure 63 Pressure Shift

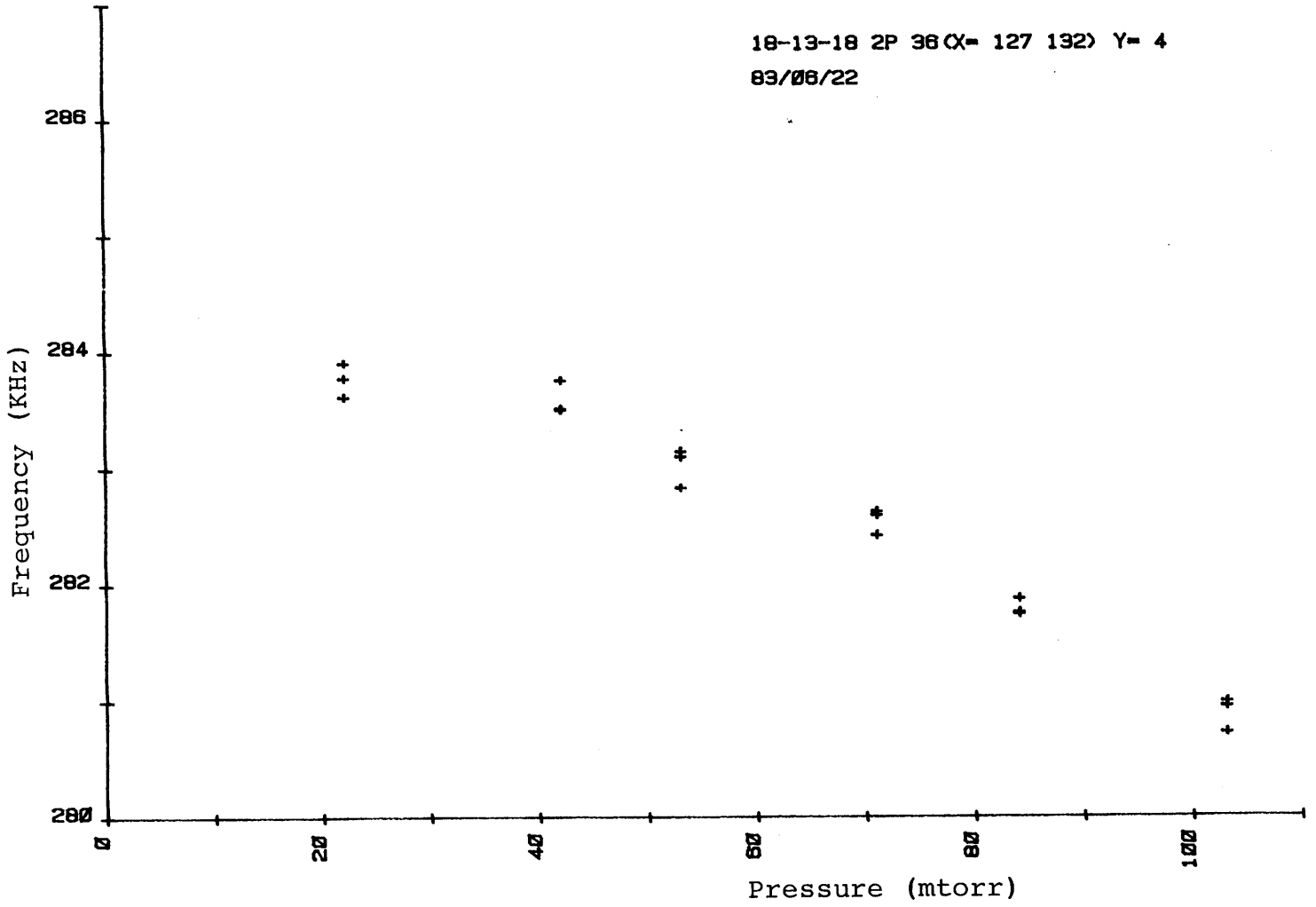

Figure 64 Pressure Shift

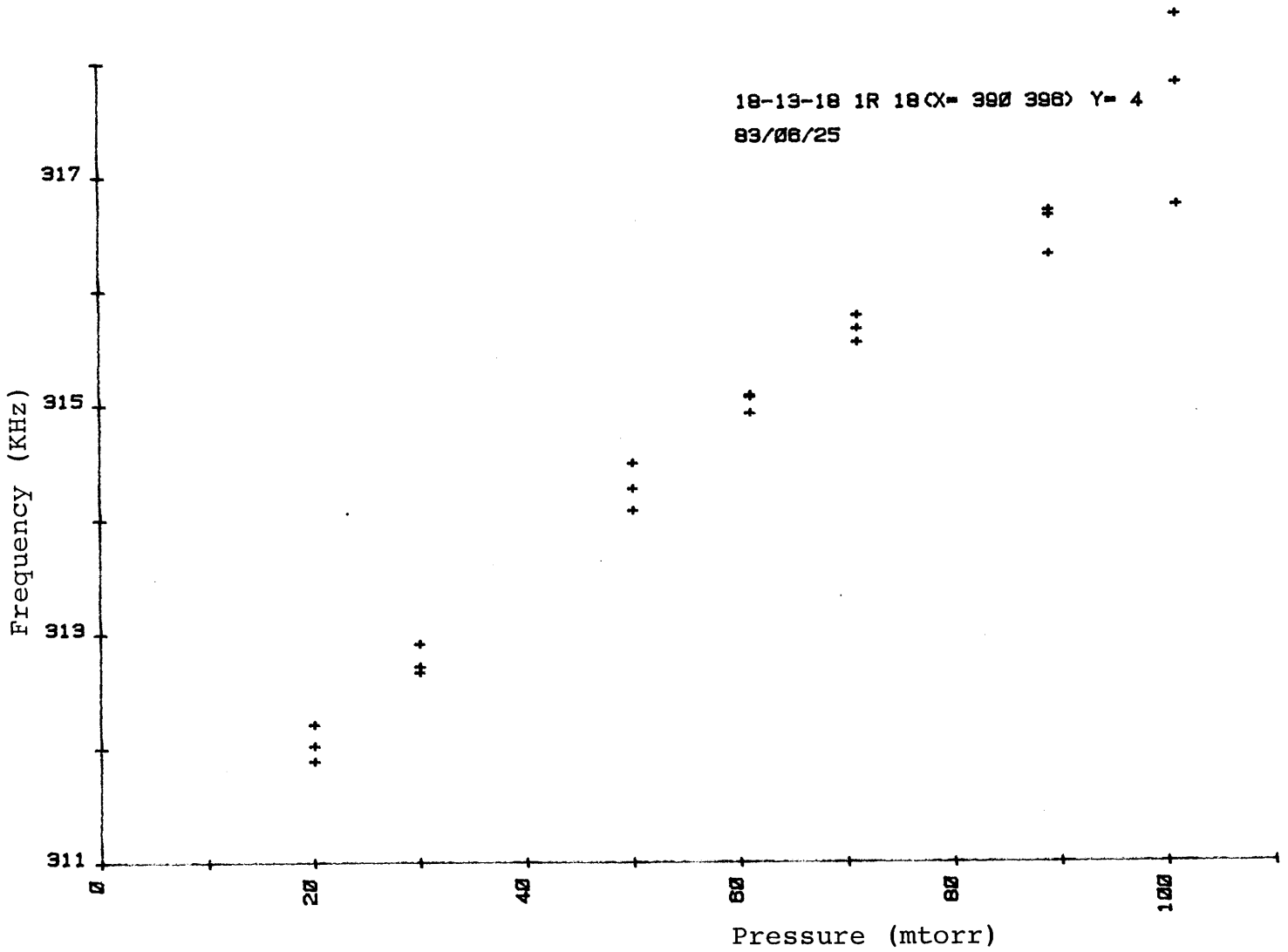

Figure 65 Pressure Shift

Another error that was made in the earlier data runs concerned the manner by which the pressure in the absorption cell was changed during the run. Initially, all data runs started at the highest pressure point and proceeded downward in pressure. This downward procedure was used because of the ease in changing pressures; the pressure was easily changed in a controlled manner by freezing the CO_2 out into a convenient cold finger immersed in liquid nitrogen. This was the wrong method to use since the power error and asymmetry is at its worst at higher pressures and any little offset or error would get magnified by the servo loop and PZT response; adjustment of the power slope is very poor at higher pressures since the servo correction is over a larger FWHM on a broader fluorescence background which accordingly taxes the servo loop even more. The correct procedure that was finally taken was to incrementally increase the pressure in the cell during the data run; this meant releasing the correct volume of CO_2gas from the reservoir of higher pressure CO_2 gas in the cold finger by means of a careful, manually controlled, dexterous flick of the wrist. Thus, all power slope adjustments were made at the lowest pressures where there is the greatest S/N (the smallest FWHM on the flattest background signal) and the least asymmetry so that correction by the servo loop is minimized.

Any other method would have a tendency to pull the servo loop more than necessary and would also suffer from the possibility of increased errors at the higher pressures.

It is for this very reason that pressure data runs did not go too high in pressure; the effect of the drift is magnified at the higher pressures since the error goes as the pressure squared. Any drift has a larger effect on the power error and correspondingly puts a greater strain on the servo loop at the higher pressures. Thus, all the pressure shift data runs stop after increasing the pressure to about 100 to 120 mtorr; by then the S/N deteriorates and the drift error dominates for all but the powerful lines.

In all the corrected pressure runs, no attempt was made to decrease the power into the absorption cell using an external attenuator (gas absorption cell). This was in part to allow as strong a lock as possible without adding an additional dispersion element whose effect could not be monitored by the slope detector.

A few pressure shift runs were taken for a few lines at various power levels; these measurements gave comparable pressure shifts at sufficient saturating power levels (>1 W)

while giving much larger 'pressure' shift (ranging from 2 to 3 times larger while being 'nonlinear' at higher pressures) results at lower powers (<1 W). The dimethyl ether absorption cell or the Brewster angle polarizer was used to attenuate the power; these were not the ideal power attenuators since they were wavelength dependent and the Brewster polarizer showed distinct mode behavior for different wavelengths.

In many of the calibration runs (red slope) taken with each set of corrected pressure shift data, a distinct upturn of the data points appeared, similar to the extremely small ± pressure shift seen in the earlier power runs used to estimate the power slope and the underlying pressure shift. In these earlier power runs, extremely small ± pressure shifts were obtained from the least squares fit after the power error was subtracted out. In those calibration or power runs, the pressure shift at very low pressures, < 50 mtorr appeared flat, nonexistent or reversed directions at the lower pressures. This reversal of the pressure shift, after a nonlinear red shift at higher pressures, was evident in many of the pressure shift runs, even in the power corrected slope runs (at higher pressures where drift dominates) as well as the final calibration runs (those with

a red slope power error). This reversal in direction can be interpreted as a small blue linear shift on top of a dominant red power error shift such that the reversal at lower pressure occurs when the linear shift becomes dominant. Calibration runs taken with a blue slope error normally reveals a blue shift at all pressure ranges but these runs reveal a significant linear blue shift at the lower pressures on top of the nonlinear blue error slope. Figures 66, 67 and 68 are calibration runs which vividly show this red or blue power error in conjunction with a linear shift.

There were several instances during the course of the experiment in which the sign of the pressure shift could be tested for the same isotope in either the left or the right laser; the sign of the pressure shift was unequivocally independent of which laser was used as the reference and which laser was pressure shifted in frequency. That is, after all the adjustments, realignments, and changes associated with switching from branch to branch and from laser to laser, the sign of the shift still remained the same.

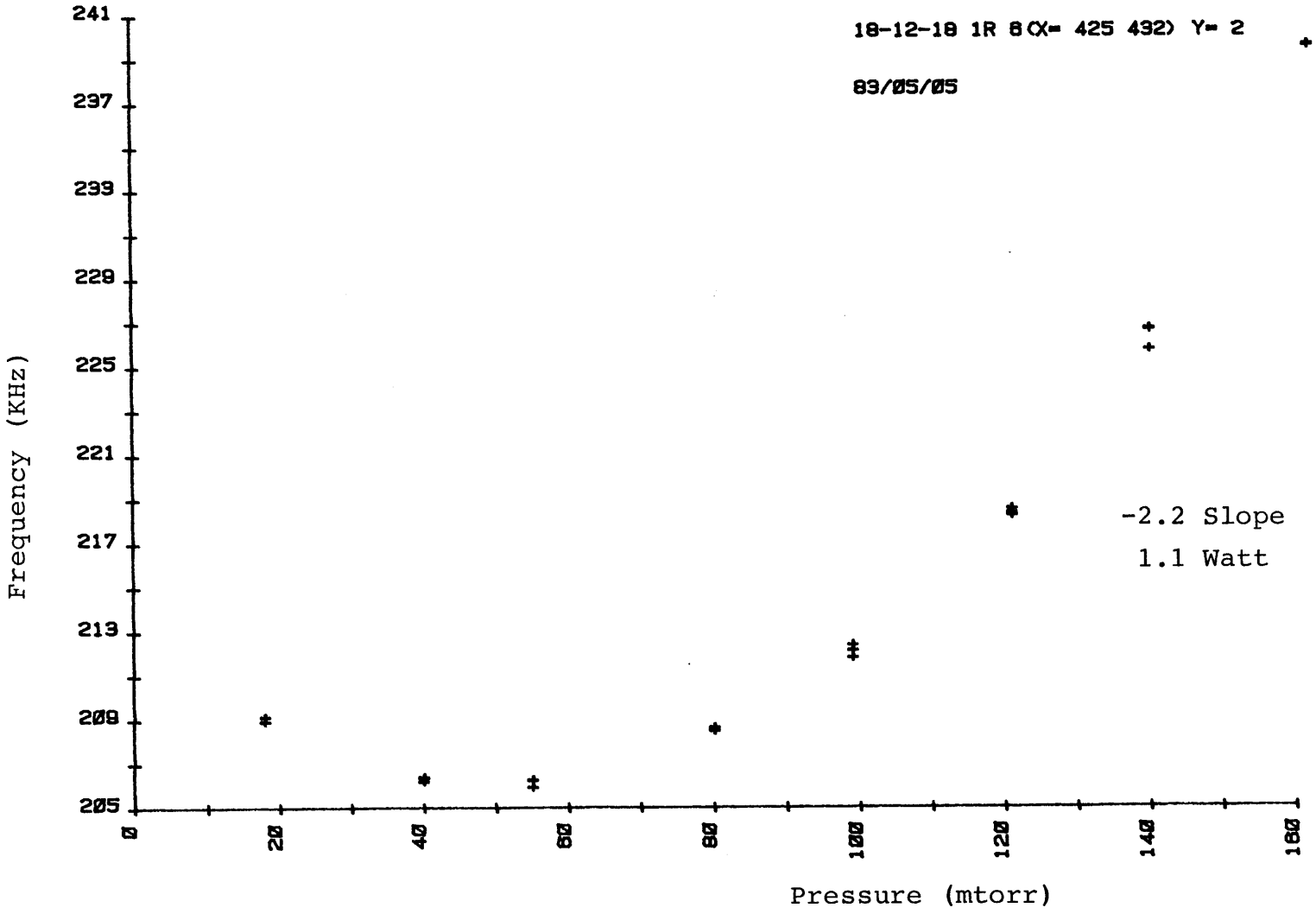

Figure 66 Calibration Run, Red Shift

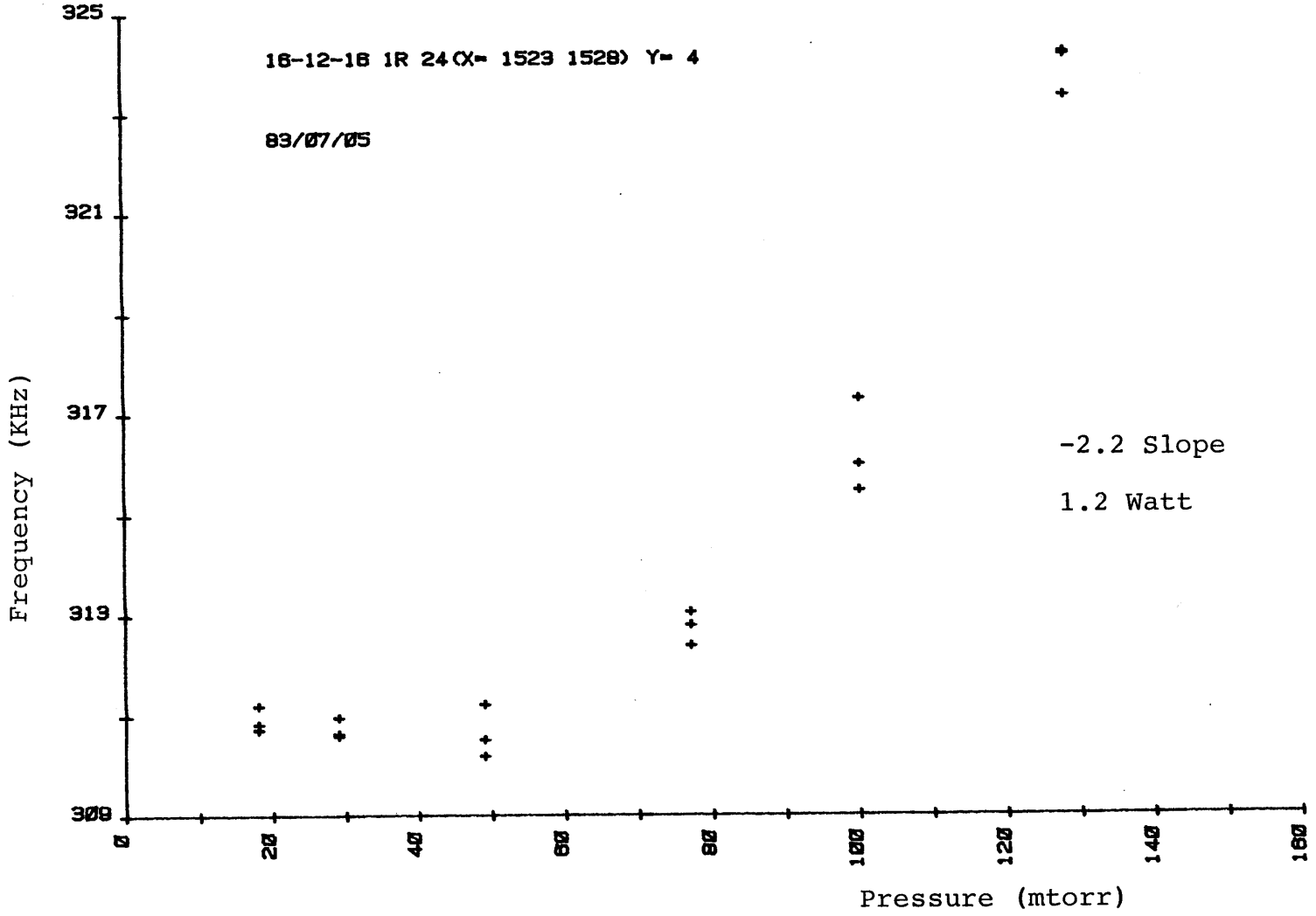

Figure 67 Calibration Run, Red Shift

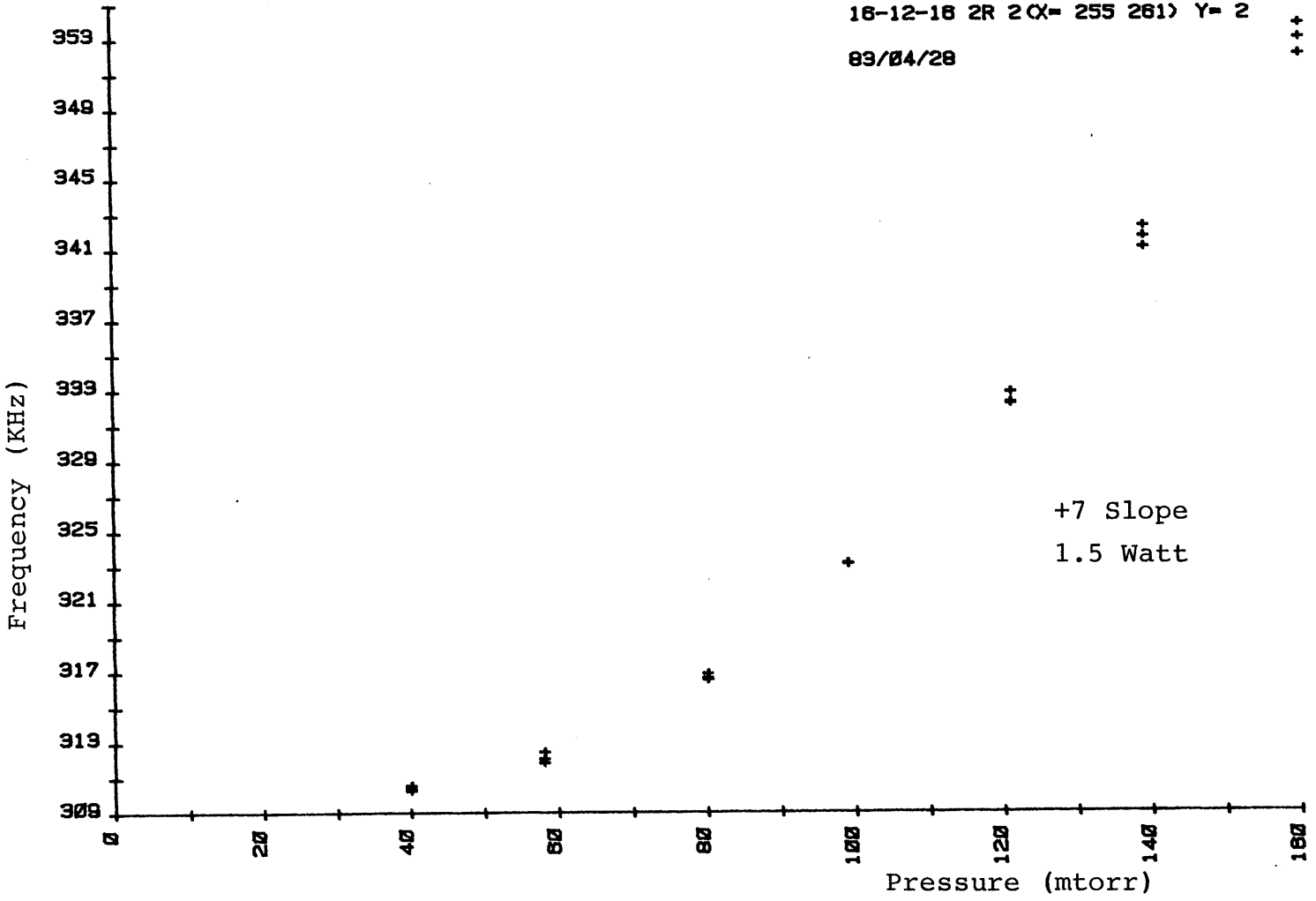

Figure 68 Calibration Run, Blue Shift

HIGH PRESSURE MEASUREMENTS

The basic question that is raised from these measurements concerns why the pressure shift is blue instead of being red [634-639] as other single measurements show. What is the real shift at higher pressures and is the effect seen at the lower pressures due to velocity changing collisions? Meyers and Rhodes[653,654] had measured velocity changing collisions in CO_2 for CO_2 and various other perturbers. Amazingly enough, the average change in velocity of each collision is not as small as initially thought from the typical classical or diffractive scattering angles; the change in velocity in CO_2 is of the order of one tenth the Doppler width[654]. There has also been indirect evidence of velocity changing collisions from the nonlinear behavior of the linewidth[280,647,651] at very low pressures in CO_2 but those results have not been as convincing as the actual velocity changing experiments. When the FWHM approaches 2 to 3 MHz, velocity changing collisions should become inconsequential since the average velocity change would not 'kick' the molecule out of the resonance hole in velocity space and therefore that molecule would not contribute any additional width or shift to the lineshape. Thus the question is whether the pressure shift reverses sign from

blue to red at high enough pressures due to the lack of the effect of velocity changing collisions and if so, at what pressure does this change occur? Several pressure shift measurements were taken at higher pressures (up to 200 mtorr) while trying to keep the power slope corrections and drift to a minimum. These pressure runs, for example in Figures 69 and 70, did not show a reversal in slope but appeared to indicate a gradual decrease in slope or a gradual flattening; unfortunately these conclusions were not entirely definitive since even a any tolerable drift or power error present at the lower pressures becomes magnified at the higher pressures and any slope adjustment grating movement 'inertia' is consequently enhanced enormously when operating at the higher pressures. The laser did not have sufficient output powers (1 to 2 W) to sufficiently saturate at much higher pressures and consequently the stability of the lock steadily decreased at the higher pressures.

It is evident that high pressure measurements of the pressure shift are not possible using the 4.3 μ fluorescence stabilization technique. A different technique must be used to measure the shift at higher pressures (>0.5 torr). Normally pressure shifts are measured by passing the laser radiation through two consecutive high pressure cells

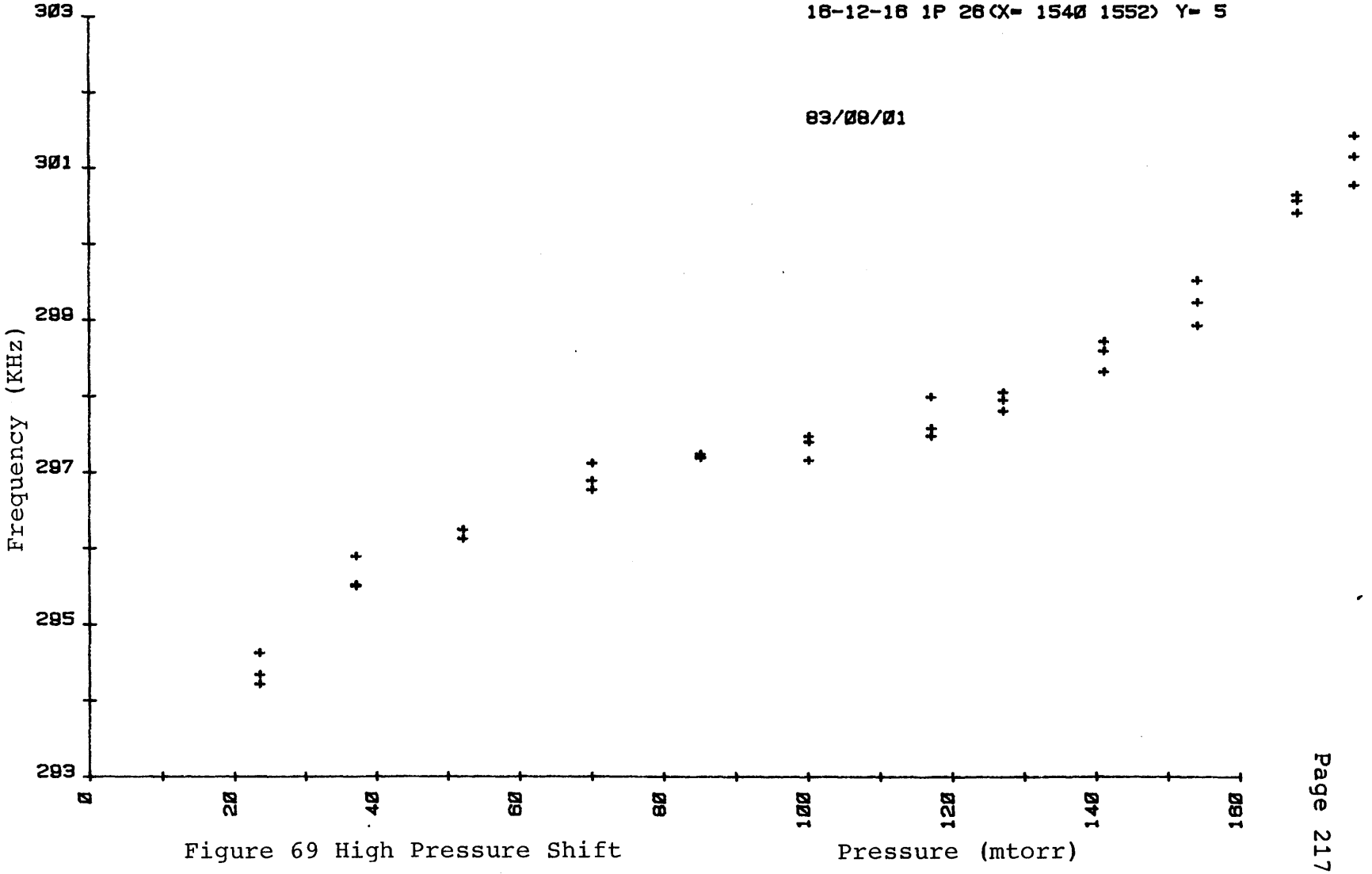

Figure 69 High Pressure Shift

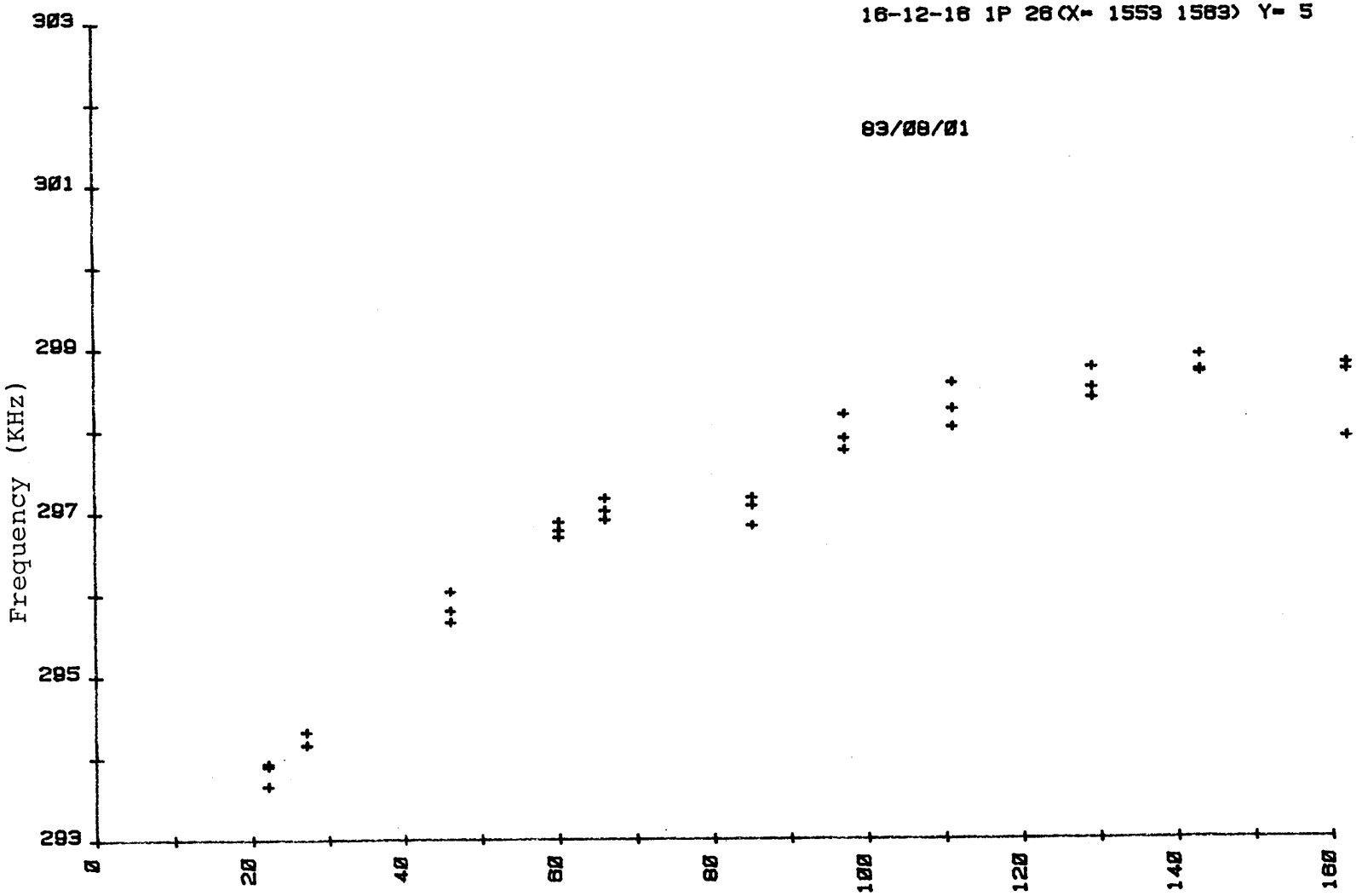

Figure 70 High Pressure Shift

filled at different pressures and then simultaneously measuring the linear absorption profile from the two cells on a spectrometer. If the pressure difference between the two cells is large enough and if the pressure shift is large enough, the frequency offset can be easily determined within the resolution of the spectrometer.

A similar two cell configuration was also set up to try to determine the direction of the shift at the higher pressures. The reference cell was the normal low pressure cell used in the 4.3 μm fluorescence stabilization loop. Part of the laser beam was split off and sent through a 1 meter long absorption cell with 1 inch diameter ZnSn windows. The 9 or 10 μm radiation, after passing through this cell, was directed onto an Au-Ge detector setup similar to that used in the power slope detection. Unfortunately, this method had two drawbacks. The absorption coefficient at the lasing transitions is very small (it is approximately 3×10^{-5} $cm^{-1}torr^{-1}$). Thus to see a 1% effect, one needs at least 10 torr of CO_2 gas. But at 10 torr, the FWHM is about 70 MHz which is on top of a significant power slope. The power error offset for the center of the absorption linewidth for pressures greater than 1 torr is tremendous and is of the order of the offset from the laser power peak.

Thus the results one would expect from this linear absorption experiment would be very crude since determining the center of the very small absorption amidst all these other errors is nearly impossible. The only way to get more signal is to work at higher pressures which results in a broader dip on top of a significant power slope.

The integrated or absorption dip measurements were taken by performing a laser line scan (5 MHz scan) across the Lamb dip while monitoring the low pressure 4.3 μm fluorescence derivative and the high pressure absorption dip at the same time. Both signals were simultaneously recorded on a two pen Houston chart recorder as a function of input ramp voltage (these linescans were not frequency locked but rough frequency intervals were marked according to the beat signal on the spectrum analyzer). The grating was adjusted so that zero power slope coincided with the peak of the Lamb dip as close as possible during these linescans. Hopefully, by measuring the absolute offset of the absorption dip center from the Lamb dip derivative center, the direction of the pressure shift could be determined. Because of the extremely small absorption coefficient and because the interaction of the power slope and the increasing FWHM gives rise to a large offset error, this linear absorption measurement also

gave ambiguous and inconclusive results as the pressure in the linear absorption cell was varied from 1 to 100 torr. Similar measurements were taken of the 9μ derivative slope signal using the same absorption cell and same procedure. Again, these results were ambiguous because of the large power slope and the small absorption coefficient.

Another alternative to the high pressure measurements was to use the zero of the 4.3 μm derivative signal as a monitor of the peak of the fluorescence response. This method gave very large S/N slopes up to 10 torr even though the Lamb dip was smeared out for pressures greater than 500 mtorr. In this measurement, the laser beam was split between two fluorescence cells so that a standing wave resonance could be created in both cells. Then, using the same two pen chart recorder and the same linescan and recording technique as described above, the derivative signals of the low pressure cell (normally used in the stablization loop) and a second high pressure cell were recorded as the pressure in the second cell was varied from 30 mtorr to 10 torr. In this case, the laser output was scanned over the dip linewidth and the zero crossing of both derivative signals were compared as the pressure was varied in the second cell. In these linescans (not phase or frequency locked),

resolution was very limited and was on the order of 10-20 KHz per division.

It was very important to adjust the grating so that the zero power slope coincided with the resonance dip center since any power slope could easily offset the zero of the second cell's derivative signal and create an erroneous shift signal This slope error was easily demonstrated by varying the sign of the power slope + or - at the derivative's zero crossing and then watching the huge power slope error shift the corresponding zero crossing blue or red respectively as the pressures were changed from 1 to 10 torr range. Correspondingly, as the sign of the power slope varied + or -, the + or - derivative maximum, instead of being equal in amplitude, showed a slight asymmetry by being slightly unequal (1 to 3%) in amplitude as a function of whether the net slope was + or -. This asymmetry was not an alignment problem but rather an almost imperceptible consequence of the slope effect. After adjusting the grating as close as possible to zero power slope at the dip minimum, 'correct' linescans showed that the pressure shift appeared blue or was nearly zero within the limited resolution (±10-15KHz) at the low pressures (<200 or <300 mtorr) but then definitely shifted red as the pressure was

varied from approximately 1 torr to 10 torr. Unfortunately, the derivative zero crossing was smeared out (as the Lamb dip disappeared) in the intermediate pressure (300 or 500 mtorr to 1 torr) regime so that the shift 'inflection' pressure point could not be determined.

These 4.3 μm derivative scans were repeated for several lines and the comparisions of the derivative zero crossings still showed a red shift at the higher pressures (crudely estimated as 80±50 KHz/torr). Figures 71 and 72 show how the zero crossing change compared with the reference derivative signal used as a relative marker as the pressure increases in the high pressure fluorescence cell. At pressures greater than 10 torr, the 4.3 μm derivative signal began to fall off in magnitude due to a relatively flat background and meaningful data could not be taken at the higher pressures. Nevertheless, this measurement indicated that the sign reversal of the shift could be a property of nonlinear spectroscopy and the velocity changing collisions versus linear spectroscopy and its normal phase changing collisions since each method and process is valid in different pressure regimes.

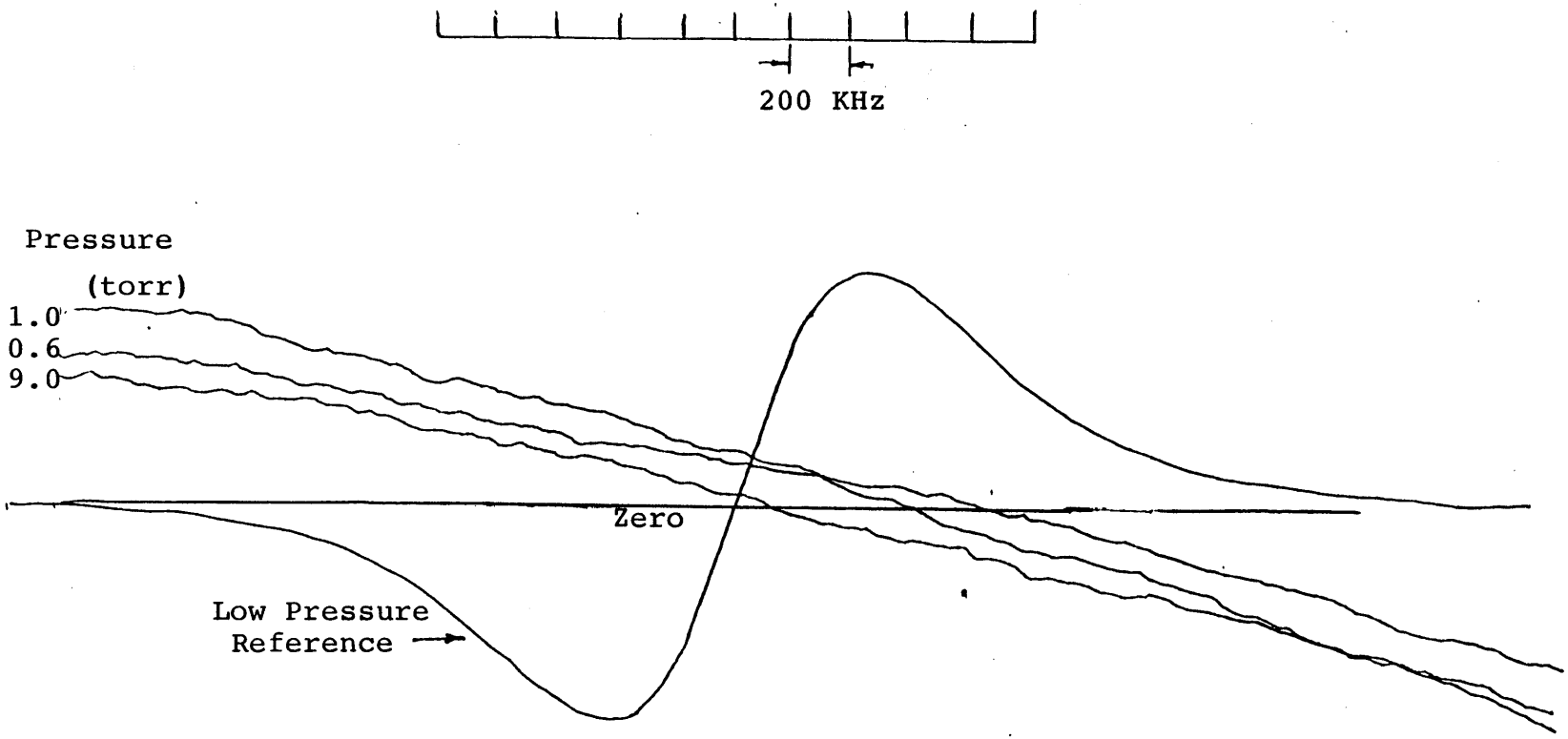

Figure 71 Zero Derivative Crossing vs Pressure

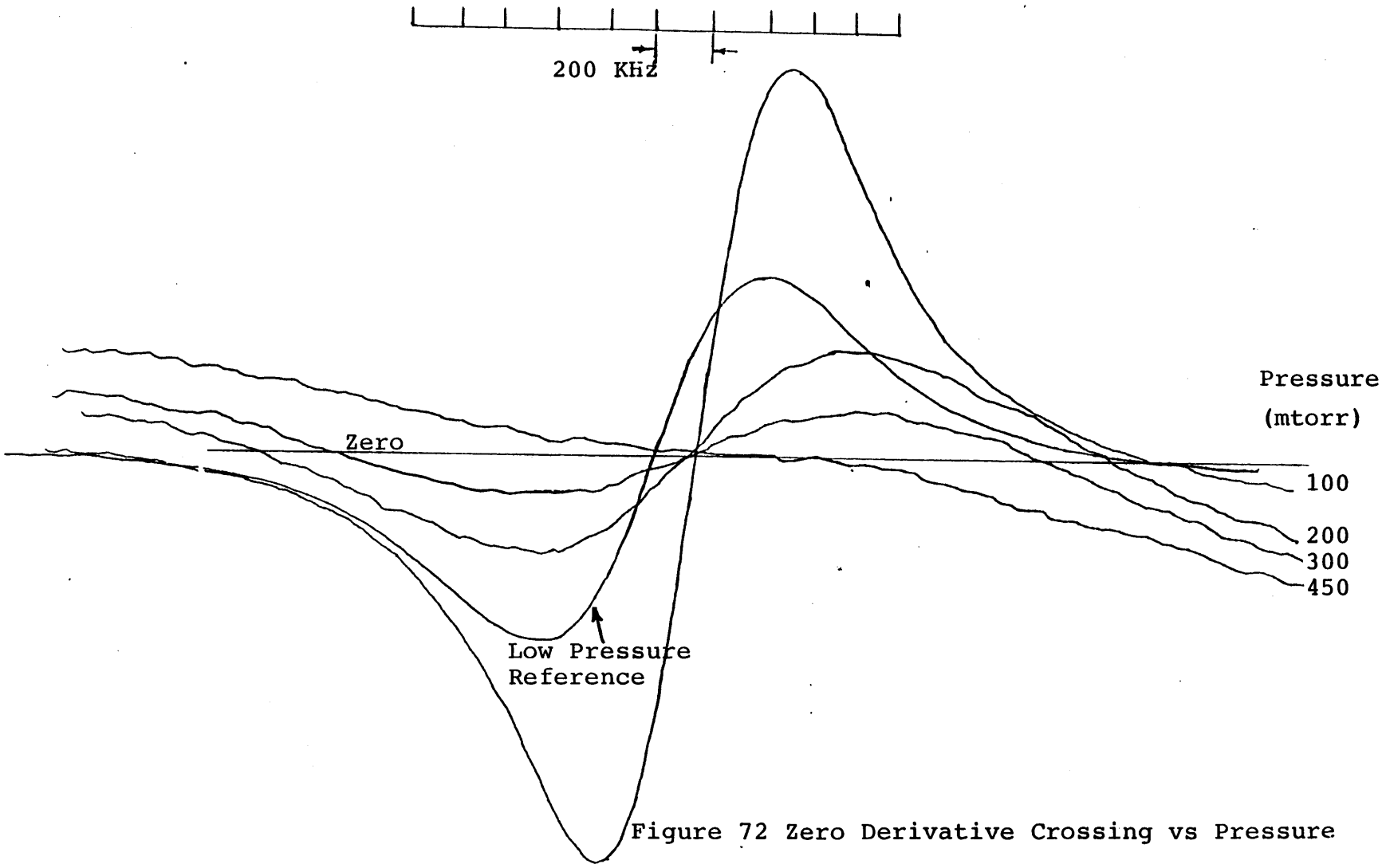

Figure 72 Zero Derivative Crossing vs Pressure

PERTURBER GASES

The effect of different perturber gases on the pressure shift of the lasing transitions of CO_2 were also studied using the two channel heterodyne system. The gases used in the measurements included Xe,Ar,N_2, He, H_2, CO, and CH_3Fl. In these measurements, the variable laser (Laser 1) was locked to a 20-30 mtorr resonance dip with the grating adjusted to give a zero power slope. Then the perturber gas was bled into the absorption cell from another pressure reservoir (filled at a higher pressure to prevent any backflow). The pressure run then proceeded like that of a normal CO_2 pressure shift measurement except only additional perturber gas was bled into the cell. During the data run, the power slope was continuously being monitored and somewhat corrected. These perturber pressure runs normally ranged up to 80-100 mtorr total pressure; there is only so much signal from the initial CO_2 gas and as more perturber gas is added in, the signal FWHM broadens without a great increase in the derivative amplitude. Correspondingly, the final pressures in these data runs were not as high (80 mtorr) as the pressures normally used with pure CO_2 and accordingly, the drift or slope errors had a larger effect on the stability of the lock at the higher pressures. Most

of the perturber gas shifts were linear up to a certain pressure at which the data points would 'scatter' apart. These perturber gas pressure shifts were taken over a period of time using both the right and the left lasers as the variable laser. Data were taken for select lines in three different isotopes for both the P and R branches in the I band. These different J lines were chosen to test the dependency of the perturber shifts on different isotopes, P or R branches, and especially, to see if the shift was laser dependent since each laser had to be realigned when changing from one branch of one isotope to another branch of another isotope.

The perturber shifts for all these different J lines are all consistent in sign and several data runs are summarized in Table 9. Here α are the perturber's polarizability and the C_6 constants are for CO_2 - Perturber potentials[54] The heavy perturbers, Xe, Ar, CO_2, N_2 pressure shift blue with Xe causing the largest shift and N_2 causing the smallest shift. On the other hand, He and H_2 pressure shift red while CH_3F shift blue. Figures 73, 74 and 75 show this red or blue shift for the various perturber gases.

Furthermore, to check out the idea of velocity changing collisions on the perturber gases, the 4.3 μm fluorescence

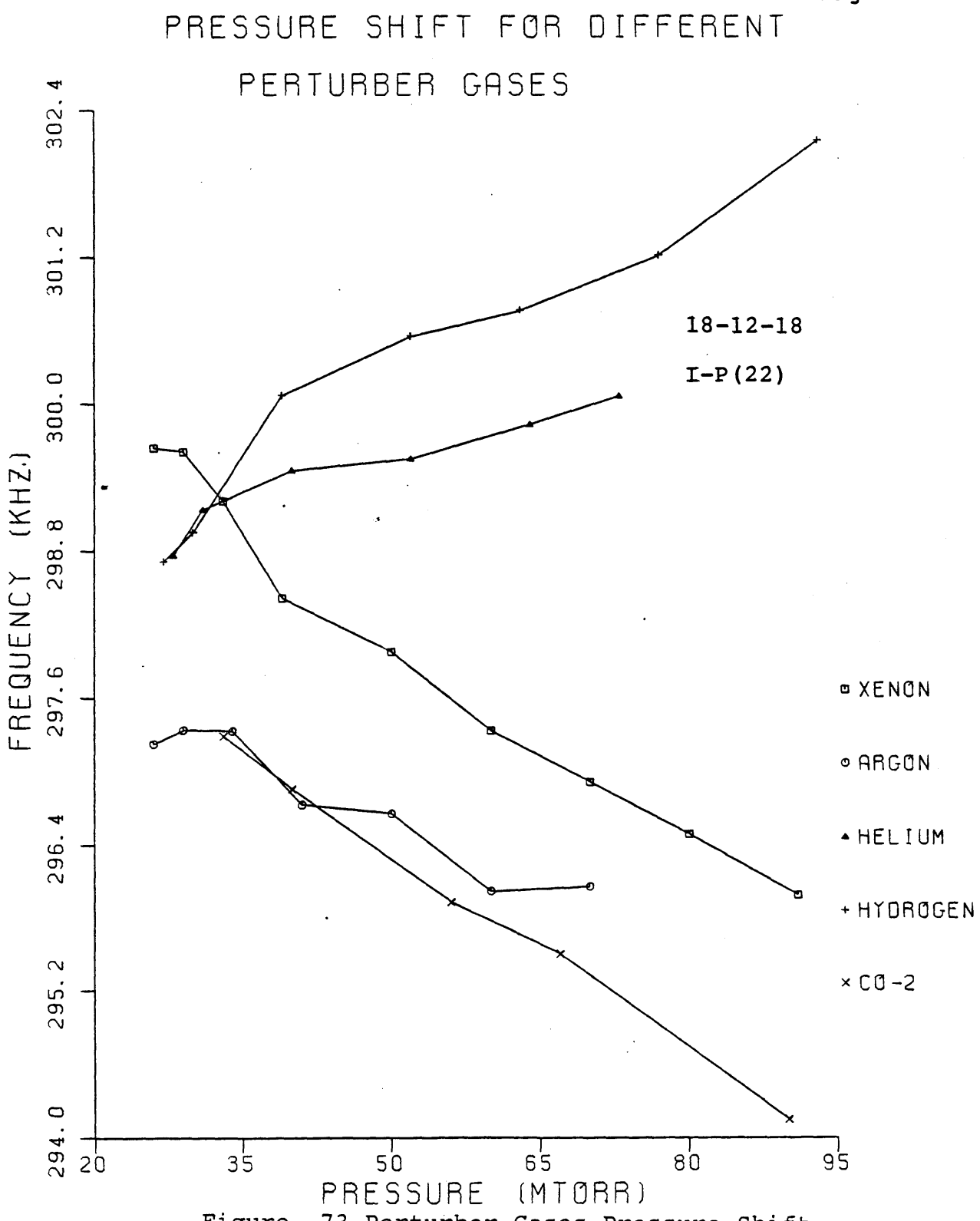

Figure 73 Perturber Gases Pressure Shift

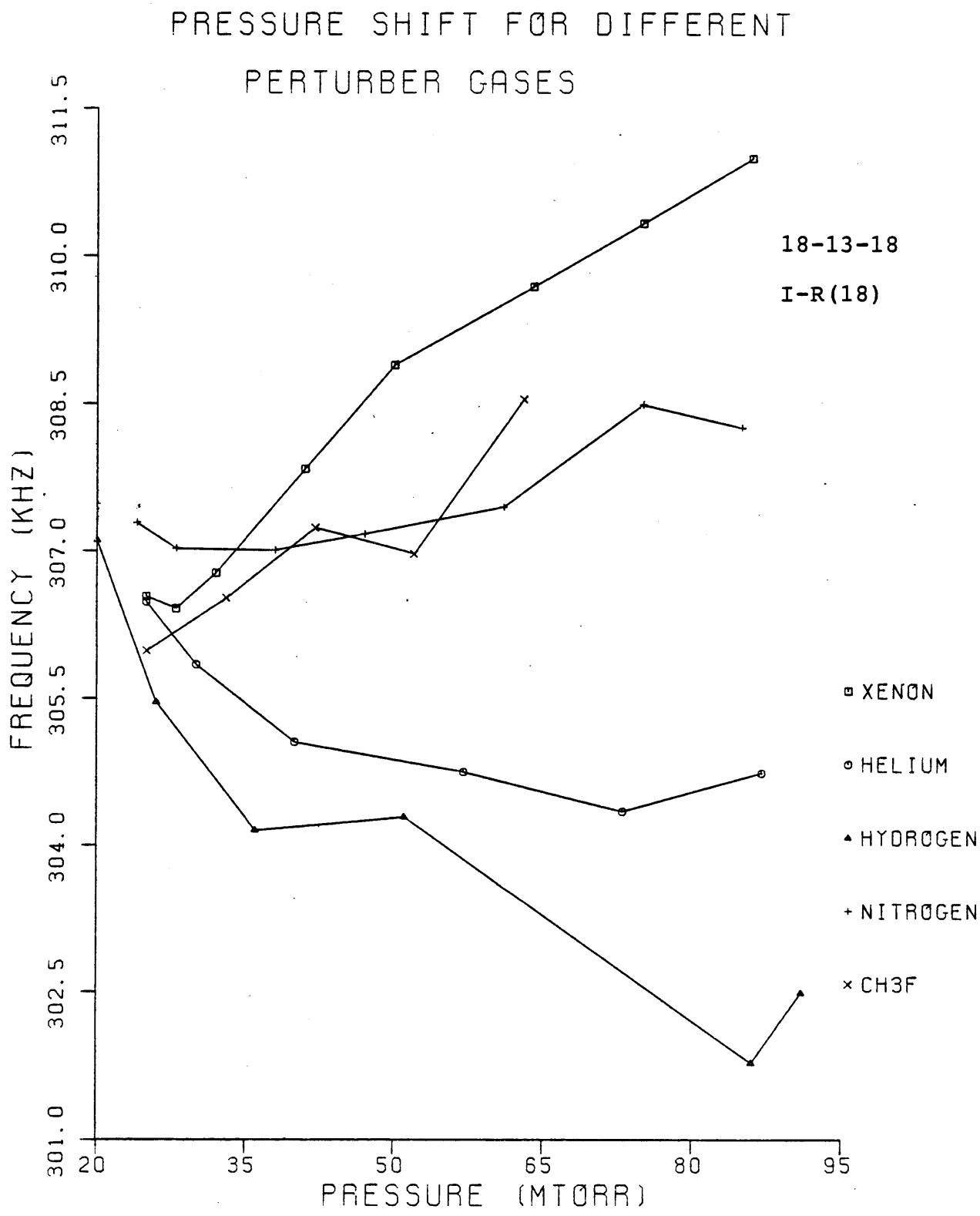

Figure 74 Perturber Gas Pressure Shift

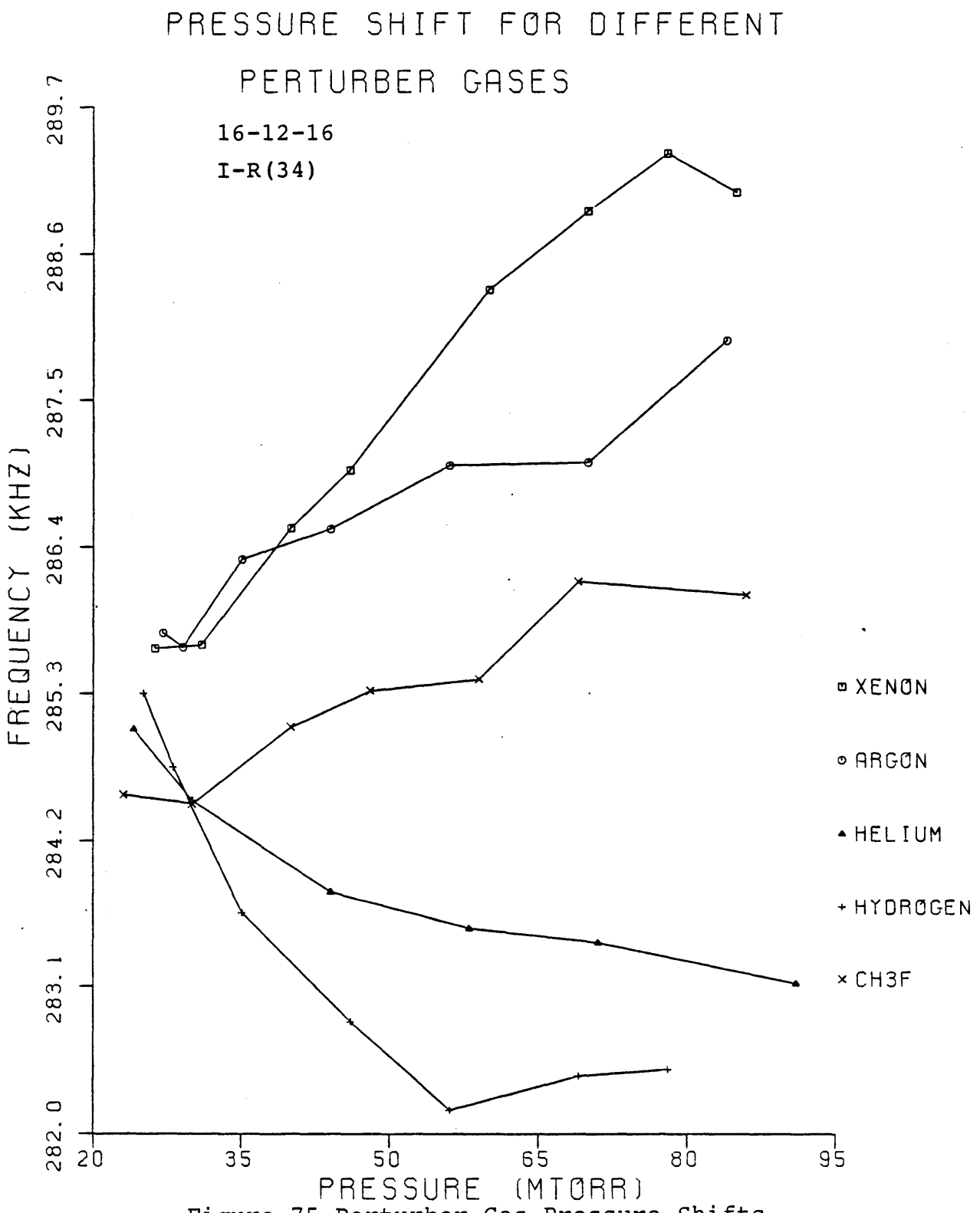

Figure 75 Perturber Gas Pressure Shifts

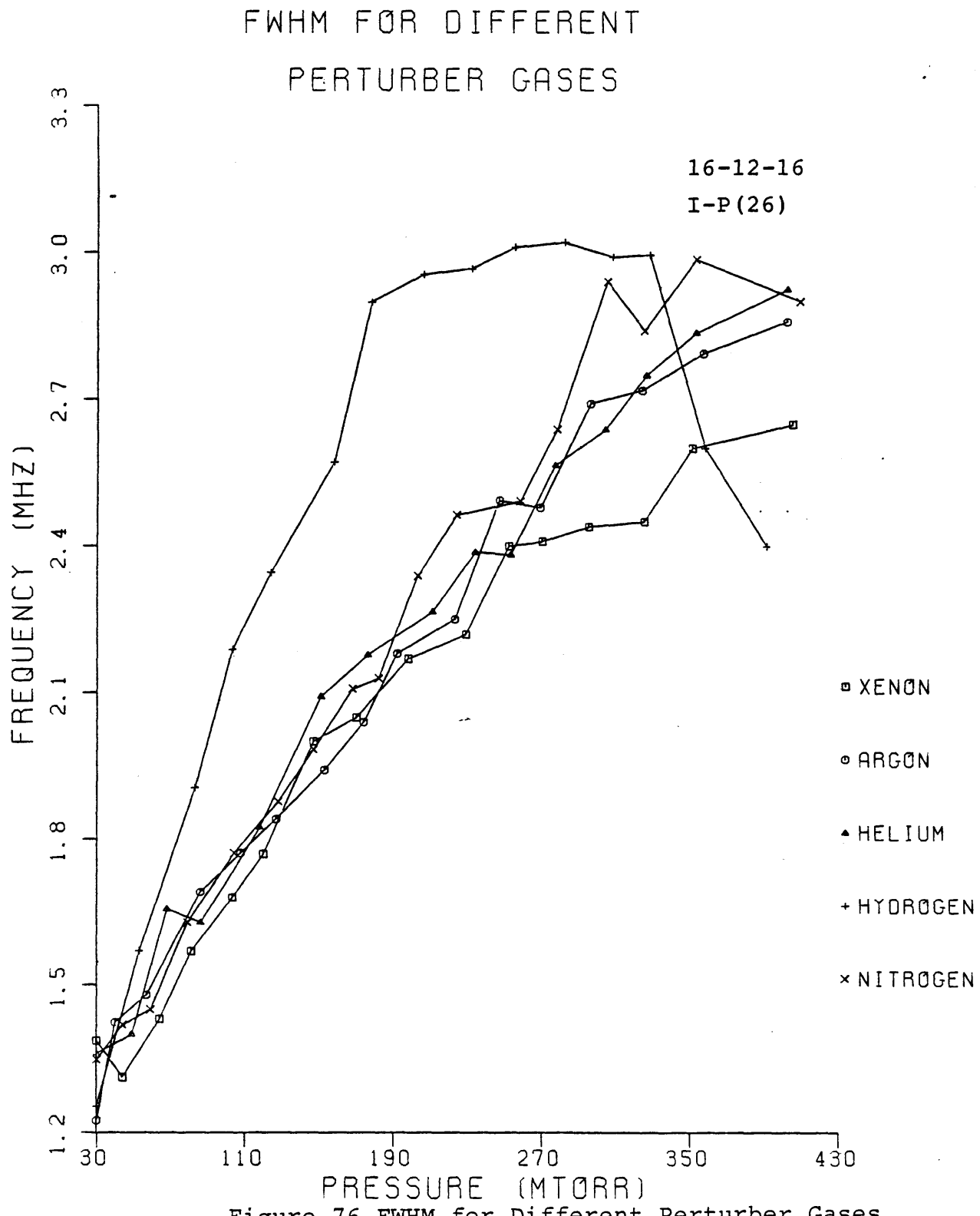

Figure 76 FWHM for Different Perturber Gases

Table 9

Perturber Gas Data

Gas Units	α a_o^3	C_6 $e^2a_o^3$	Run1	Run2 KHz/Torr	Run3
Xe	27.33	282	+52	+53	+51
Ar	11.09	114.5	+37	+22	+20
He	1.58	16.7	-20	-33	-20
H_2	5.43	46.	-36	-29	-98
N_2	11.75	118	+21	+23	+10
CO_2	19.3	192			

Run1 = 18-12-18 (IP-22)

Run2 = 16-12-16 (IP-24)

Run3 = 16-12-16 (IR-34)

lineshapes as a function of perturber gas pressures (initial pressure was 30 mtorr of CO_2 on 16-12-16 IP(26)) was recorded by scanning the laser output across the resonance dip. These linescans were not frequency or phase locked since a ramp voltage sweep was used while the frequency was estimated from the spectrum analyzer display of the beat frequency. Then, by roughly measuring the FWHM

from these linescans, a plot of FWHM vs pressure for the perturber gases is shown in Figure 76. The purpose of these linescans was to see if there was any upturn or downturn in the FWHM as a function of pressure and if so, to try to correlate this inflection pressure point (obtained from the linewidth scans) with the shift of the lineshape, in terms of the pressure at which velocity changing collsions become negligible. These measurements are very similar to what Meyer[651] did when he measured the FWHM for several perturbers using a high pressure, high intensity internal absorption cell (pressures up to 300 mtorr). Unfortunately the power levels in our lasers (1-2 Watts) were not sufficient to fully saturate the resonance at such high pressures (> 200 mtorr) and the resulting FWHM data obtained for the perturber gas at the larger pressures (>200 mtorr) are not completely reliable. These FWHM coefficients were similar to that obtained by Meyer with H_2 broadening CO_2 the most. Thus, the FWHM measurements are inconclusive in the sense that no apparent inflection pressure point was seen and there was not enough power to fully saturate the signal. It is still possible that such an inflection point does occur at the higher pressures but it is not apparent from the data taken under the present conditions in our experiment.

CHAPTER 8 THEORETICAL ANALYSIS

SEMICLASSICAL PERTURBATIVE THEORY

The most widely used formulation of the lineshape theory is the semiclassical perturbative techniques in terms of the different variations of Anderson[407] theory that has developed over the years. This semiclassical theory is based on standard time-dependent perturbation theory, treating the internal states of the radiator-perturber quantum mechanically while assuming that their individual trajectories followed a classical path. Thus the wavepacket and wavevector description is ignored since the particles are normally described using a rectilinear path

$$R^2(t) = b^2 + v_r^2 (t - t_c)^2$$

where b is the impact parameter and v_r is the relative velocity between the radiatior and perturber after the time t_c of the collision. Assuming binary collisions in the impact approximation, the radiators density matrix evolution equation is of the form

$$d\rho/dt = -i/\hbar[H_o + U, \rho] + (d\rho/dt)_{coll} \qquad (8.1)$$

The total Hamiltonian H is equal to H_o+U+V where H_o is the radiator's internal energy, U is the laser EM field and V=V(t) is the collision potential. In the impact approximation (time between collisions τ_c >> collision duration $\tau_d \simeq 10^{-12}$ sec) the laser field U cannot alter the radiators ρ during τ_d and is effectively zero during τ_d; between collisions assume V is short range enough not to alter ρ and is effectively zero while U slowly alters ρ. Thus the effects of U and V are essentially independent in their individual time regimes and can be added together as in equation (8.1).

The change in ρ due to the collisions is equal to the average change in ρ averaged over the perturber interaction rate

$$(d\rho/dt)^{coll}=\int P(v)dv\ (\Delta\rho)^{coll} \qquad (8.2)$$

where $(\Delta\rho)^{coll}=\rho_{final}-\rho_{initial}$= the change in ρ due to a collision at time $t=t_c$.

Here $P(v)dv$ is the classical rate of interacting with the perturber

=(interaction area in COM)(Flux)

$= (b\ db\ d\psi)(v_r N_p W(v_r)dv_r\ v_r^2 d\Omega)$

where ψ is the azimuthal angle along z' (relative velocity) in the COM and $d\Omega$ is the differential solid angle $\sin\theta d\theta d\phi$ where (θ,ϕ) are the Euler angles of the z' axis with respect to the lab's z axis. Here

$$W(v_r)=1/(u\sqrt{\pi})^3 \exp-(v_r/u)^2 \qquad \text{and } u^2=2kT/\mu$$

where μ is the reduced mass. Here it is assumed the active or radiator's velocity, $v_a << v_p$, the perturber's velocity or else the relative velocity, v_r is isotropically distributed.

The density matrix ρ is a two particle (radiator-perturber) density matrix. The perturber states are normally taken into account by summing (tracing) over final states and averaging over initial states; for simplicity it will be assumed that the perturber is a structureless particle that has the same initial and final staes, ie. ground state, so that only the radiator's structure will be considered in the ρ equation.

The calculation of $(\Delta\rho)^{coll}$ follows from the general solution of the equation of motion for a time dependent Hamiltonian:

$$\Psi=\Sigma_m c_m(t) \exp(-i\omega_m t) \psi_m$$

where ψ_m's are the eigenfunctions of the time independent equation. In this formulation the evolution equation during a collision is

$$c_m(t) = -i/\hbar \Sigma_n V_{mn}'(t) c_n(t)$$

where $V_{mn}'(t)=V_{mn}(t)\exp(i\omega_{mn}t)$ in the interaction representation and c_n is slowly varying except during a collision. Referring to the collision time $t=t_c$

$$V_{mn}(t) \equiv V_{mn}(t-t_c)$$

so that the equation

$$c_m(t)=-i/\hbar \Sigma_{n'} \exp(i\omega_{mn'}t_c)\ V_{mn'}'(t-t_c)c_{n'}(t) \tag{8.3}$$

By defining an evolution operator S_{mn}^c such that

$$c_m(t)=\Sigma_n S_{mn}^c\ (t-t_c, t_o-t_c)c_n(t_o)$$

and plugging into Eq. (8.3),

$$S_{mn}^c(t-t_c,t_o-t_c)= -i/\hbar \Sigma_{n'} \exp(i\omega_{nn'}t_c) \times V_{mn'}'(t-t_c)S_{n'n}^c(t-t_c,\ t_o-t_c) \tag{8.4}$$

with the initial conditions $S_{mn}^c(t-t_c,t_o-t_c)= \delta_{mn}$ for an arbritrary $c_n(t_o)$.

By defining

$$S_{mn}^c(t-t_c,t_o-t_c)= \exp(i\omega_{mn}t_c)\ S_{mn}(t-t_c-t_o)$$

and letting $\tau=t-t_c$, $\tau'=t'-t_c$ and $\tau_o=t_o-t_c$, the integral equation for the S matrix becomes

$$S_{mn}(\tau,\tau_o)=\delta_{mn} -i/\hbar\Sigma_{n'}\int_{\tau_o}^{\tau} d\tau' V_{mn'}(\tau')S_{n'n}(\tau',\tau_o) \tag{8.5}$$

for collisions at $\tau'=0$. In the impact approximation, $t_d<<t_c$ so that S can be considered $S(\infty,-\infty)$. Since the slowly varying part of the density matrix is

$\sigma_{mn}=c_m c_n^*$ and $\rho_{ab}=\sigma_{ab}\exp(-i\omega_{ab}t)$ then

$$\sigma_{mn}(t_c^+) =\Sigma_{ss'} S_{ms}S_{ns'}^* \exp[i(\omega_{ms}-\omega_{ns'})t_c]\ \sigma_{ss'}(t_c^-) \tag{8.6}$$

or $\rho_{mn}(t_c)= \Sigma_{ss'}S_{ms}S_{ns'}^*\rho_{ss'}(t_c)$

Then

$$\begin{aligned}(\Delta\rho)_{coll} &= \rho_{final}-\rho_{initial}\\ &=\Sigma_{ss'}(S_{ms}S_{ns'}^*- \delta_{ms}\delta_{ns'})\rho_{mn}(t_c)\end{aligned} \tag{8.7}$$

In general this equation is a two particle equation where the perturbers are averaged over initial states and summed over the final states.

Thus plugging (8.7) into equation (8.2)

$$(d\rho_{aa'}/dt)^{col} =-\int P(v)dv\ \Sigma_{bb'}\{\delta_{ab}\delta_{a'b'} -S_{ab}S_{a'b'}^*)\rho_{bb'}(t) \tag{8.8}$$

which is the starting point for all subsequent calculations.

Instead of calculating S, which is referred to a fixed lab axis, for every different molecular orientation (θ,ϕ,ψ), the frame of reference can be transformed to the collision

frame with z' along v_r such that the average over all molecular orientations would give an orientation independent result. Consider the radiator to have a total angular momentum J with the z' projection m_J. Then the collision form of the equation, after the angular averaging, becomes the often quoted starting point of all calculations[401]

$$(d\rho/dt)_{JaJb}=-\gamma\rho_{JaJb}$$

by letting $f(v_r)v_r dv_r = 4\pi v_r^3 W(v_r)dv_r$

$$\gamma=n_p\int dv_r\ v_r f(v_r)\int 2\pi b db \times\left[1-\sum_{\text{all M,q}}(-1)^{Mb-Mb'}\begin{pmatrix} Jb & 1 & Ja\\ -Mb & q & Ma\end{pmatrix}\begin{pmatrix} Jb & 1 & Ja\\ -Mb' & q & Ma'\end{pmatrix}\right] \times\langle JaMa|S|JaMa'\rangle^*\langle JbMb|S|JbMb'\rangle \qquad (8.9)$$

or

$$\gamma=N_p\int f(v_r)v_r dv_r \int 2\pi b db\ S$$

This S is the same S in Anderson's theory but should not be confused with the scattering matrix S commonly used in scattering theory.

A solution of (8.9) is obtained by perturbatively expanding the matrix integral (8.5)

$$S_{ab}=\delta_{ab}-i/\hbar\Sigma_n\int dt'\ V_{an}'S_{nb} \text{ in the form}$$

$$= T_0 + T_1 + T_2 + \ldots = \mathcal{T}\exp(-i/\hbar\int_{\infty}^{t}V'\,dt')$$

When assuming noncommutativity of the potentials, V(t') and V(t"), a time ordered operator T is the usual result. Then by plugging this expansion for S into (8.9), the probability function S will be composed of terms

$$S = S_0+S_1+S_2 + \ . \ .$$

The S_0 term consists of contributions from the $T_0^*T_0$ term; this results in $\delta_{MaMa}, \delta_{MbMb}$, and since

$$\Sigma(Jb\ 1\ Ja)^2 = 1$$
$$q,Ma,Mb\ (-Mb\ q\ Ma)$$

$S_0 = 1-1=0$

The S_1 term consists of contributions from either $T_0^*T_1$ or $T_0T_1^*$. Each T_0 term gives either δ_{MaMa}, or δ_{MbMb}, which, when combined with the 3J symbols, results in the exact same sum of the square of a 3J symbol as in the S_0 case.
Thus S_1 is pure imaginary and is of the form

$$S_1=i/\hbar\int dt[\Sigma_{Ma} \langle JaMa|V_{aa}^*|JaMa\rangle - \Sigma_{Mb} \langle JbMb|V_{bb}|JbMb\rangle] \qquad (8.10)$$

The sum over M_b or M_a serves to project out the isotropic part of the potential. This term is just the normal scalar phase shift composed of the difference of the diagonal matrix elements. Likewise the S_2 term is composed of the terms

$$T_0^*T_2,\ T_0T_2^*,\ \text{and}\ T_1^*T_1$$

so that

$$S_2=(i/\hbar)^2\Sigma_{Ma'}\int dt\int dt'\langle JaMa|V_{aa'}|Ja'Ma'\rangle \times \langle Ja'Ma'|V_{a'a}|JaMa\rangle \exp(-i(\omega_{aa'}(t-t'))$$

and similarly for the $T_0T_2^*$ and $T_1^*T_1$ expansions.

S_1 and S_2 are the basic results of the semiclassical perturbative theory based on Anderson's initial work. A survey of Anderson theory is given in the next section where the S_1 and S_2 and V terms are given in their original context (and henceforth labeled S_1 and S_2). The perturber states and their averages will also be taken into account in these expressions for S(b). It should be noted, that the actual expressions for S_2 and S_1 will be exponentiated to take care of several deficiencies in the theory.

ATC THEORY

The semiclassical perturbative analysis given in the last section summarizes the important concepts leading to main results of Anderson's theory. This section discusses and presents (Anderson's theory as modified by Tsao and Curnutte [408] and Frost[493] in the ATCF theory) the ATC theory, as it appears in the literature while including the averaging over the initial states and the summing of the final states of the perturbers.

In Anderson's theory, the lineshape is of the form

$$\frac{nv\sigma_r}{(\omega-\omega_o-nv\sigma_i)^2+(nv\sigma_r)^2}$$

where the FWHM and the lineshift is given by the real and imaginary part of the cross section σ

$\gamma = n\langle v\sigma_r\rangle$ and $\omega = n\langle v\sigma_i\rangle$

Here n is the density of the perturbing molecules and the <> indicates an average over the Maxwellian distribution of the relative velocities. In practice,the velocity average is usually replaced by an average v_o . The collision cross section is actually a sum over final states and an average over all the optical cross sections for the perturbing molecules in the initial state 2

$$\sigma = \sigma_r + i\sigma_i = \Sigma_2\ \rho_2\sigma_2$$

where ρ_2 is the Boltzmann factor for the perturbing molecule in state 2; normally this will refer to a particular J transition so

$$\rho_2 = \frac{(2J_2+1)\exp(-E_{J2}/kT)}{\Sigma_n\ (2J_n+1)\exp(-E_{Jn}/kT)}$$

where $\Sigma_2\ \rho_2 = 1$ and then $\sigma_2 = 2\pi\int S(b)bdb$ as in Equation (8.9).

S(b) can be regarded as a probability weighting factor which indicates whether or not a collision is effective in disturbing the molecular radiation. As mentioned in the last section

$$S = S_0(b) + S_1(b) + S_2(b) \text{ where } S_0(b) = 0$$

and after summing over all final states, the S(b) in the context of Anderson theory for a given perturber J_2 is

$$S(b) = 1 - \sum_{\substack{2' \\ \text{all } M}} \frac{\langle J_f M_f 1M | J_i M_i \rangle \langle J_f M_f' 1M | J_i M_i \rangle}{(2J_i+1)(2J_2+1)} \times \langle f2|U^{-1}(b)|f'2'\rangle \langle i2'|U(b)|i2\rangle \qquad (8.11)$$

$$ih(d/dt)U = V'U \quad \text{and} \quad U(t) = \mathcal{T}\left[\exp(i/\hbar \int_0^t V'(t')dt')\right]$$

$$V'(t) = \exp(iH_0t)\ V \exp(-iH_0t)$$

where $\mathcal{T}$ is the time ordering operator and $H_0 = H_1 + H_2$ is the unperturbed Hamiltonian. V is the interaction potential between the two molecules which can be expanded as a power law potential C_nR^{-n} in terms of spherical harmonics Y_{lk}

$$V = \sum_{\text{all } l,k} C_{lk}C_{l'k'}R^{-n}\ Y_{lk}(1)Y_{l'k'}(2)$$

The definition of U in this context is the same as S_{nm} in (8.5) Normally, all the contributions to V from all the various interactions are scalarly summed to arrive at a final potential since it is assumed there are no interference terms among the various orders of the spherical

harmonics for the same molecule. Actual values for S_2 have been computed for many of the common electrostatic interactions and are referenced throughout the literature (408,416,493).

In the ATC theory, as with all lineshape theories, there are several 'inherent' faults associated with the theory. Since U is unitary, it follows that the maximum value for S(b) is one; due to the nature of the expansion, there is a limiting bound on the impact parameter for the distance of closest approach b_o since the function would blow up as b approaches zero. This distance was artificially picked by finding b_o such that $S_2(b_o) = 1$. Then the collisional cross section could be divided into hard collisions and weak collisions by

$$\sigma_R = \pi b_o^2 + 2\pi \int_{b_o}^{\infty} S_2(b)\, b\, db$$

$S_2(b) = S_{2,i}^{outer}(b) + S_{2,f}^{outer}(b) + S_2^{middle}(b)$ where the terms S_2^{outer} and S_2^{middle} refer to the matrix elements of the U operator between two identical states (both initial or both final states) or the matrix element between different states (final and initial states) respectively.

S_1, (eq. 8.10) which just projects out the isotropic form of the potential and is the first order contribution to the

lineshift, was initially assumed to be zero since only rotational transitions were considered. It came as a surprise when the microwave lineshifts were finally satisfactorily measured[461-463] (after eliminating all the various sundry power slope errors and asymmetries) since ATC theory predicted zero lineshift in S_1 and S_2. Theoretically S_2 was purely real because the interaction V was considered commutative in the time dependent perturbative expansion [408]. Then, by removing this 'artificial' simplification, Frost[493] and Herman[442] showed that S_2 has an imaginary component and accordingly, microwave lineshifts could possibly originate from the S_2 term in ATCF theory. Another way to obtain this lineshift was to relate the imaginary part of S_2 to the real part of S_2 by the Kramers-Kronig[475] dispersion relations or equivalently by the Hilbert transform[453] of the real S_2 terms (See Appendix 7). Even after these corrections, the 'appropriate' cutoff procedure for small b was further complicated since S_2 was now both real and imaginary and setting $S_2(b_o) = 1$ was not entirely correct[442]. The final solution to the cutoff procedure, as realized by Leavitt [603-605], Bonamy[602], and others[589-601], was to exponentiate the interruption function such that

$$\sigma = \int 2\pi b db \exp(-S(b))$$

This not only alleviated the cutoff problem but also allowed for inelastic collisions since the maximum value of S(b) was not restricted to unity. This was taken a step further and generalized on theoretical grounds by Leavitt and Bonamy. They both treated the expansion of the S interruption function to all orders and combined terms using a linked cluster expansion[602,604] to arrive at the exact infinite order expansion of the S function. This generalization overcame all the previous faults with the ATC theory while providing the correct real and imaginary components to all orders. This theory is especially well summarized by Leavitt[605] who used a tensor approach to derive all the dispersion, induction and electrostatic interactions for a linear-linear molecular collision. Elastic, inelastic, phase changing and reorientating collisions (the internal energies do not change but the direction of the angular momentum of the molecules do change) are included in the final theory. Leavitt showed the previous lineshape theories by ATC[408], Murphy-Boggs[501], Gordon[399], Cattani[589], Bonamy[602], and Salesky and Korff[600] were just specialized cases of his theory. Bonamy differed from Leavitt by considering a more realistic parabolic trajectory model to approximate the perturber's path in contrast to the usual rectilinear paths. This trajectory

correction is only important if close collisions are important in determining the total cross section; then the trajectories will be modified by the isotropic part of the intermolecular potential. Before going on, normal coordinate transformations will be given since they are important in the calculating the expected shifts.

NORMAL COORDINATE ANALYSIS

CO_2 is a linear triatomic (N=3) molecule possessing four normal modes of vibration (3N-5) with a pair of degenerate perpendicular modes. It is instructive and necessary in the pressure shift calculations to express these normal mode coordinates in terms of the original Cartesian coordinates.

The most widely used method to obtain the normal coordinates is based on a **FG** matrix analysis. In this method the obvious internal coordinates (the two CO bond extensions and the two OCO bends) are combined judiciously via symmetry arguments to formulate an alternate vibrational eigenvalue problem.

Let **B** be the matrix relating the (3N-5) symmetry coordinates **S** to the 3N Cartesian **R** coordinates: **S=BR** Then

define a square matrix G where $G_{ij}=\Sigma_k (B_{ik}B_{jk}/m_k)$ and m_k are the masses. The potential and kinetic energies are respectively $2V=S^TFS$, and $2T=\dot{S}^TG^{-1}\dot{S}$. Then define L such that $S=LQ$ where Q are the normal coordinates. These substitutions result in a matrix eigenvalue problem

$$L^{-1}GFL=\Lambda G$$

or $|GF-\lambda I|=0$ where the λ are the eigenvalues.

For the $D_{\infty h}$ group the irreducible representations of the vibrational levels are of Σ^+_g, Σ^+_u,and Π_u symmetry;therefore the internal coordinates are defined as in Figure 1 :

$$S_1=z_1-z_2$$

$$S_2=z_2-z_3$$

$$S_3=\theta_{xz}=\rho(x_1-2x_2+x_3)$$

$$S_4=\theta_{yz}=\rho(y_1-2y_2+y_3)$$

where $R_{CO}=1/\rho$= bond length. Using the internal coordinates S, the symmetric coordinates S are

$S_1=(S_1+S_2)/\sqrt{2}=(z_1-z_3)/\sqrt{2}$ has Σ^+_g symmetry

$S_3=(S_1-S_2)/\sqrt{2}=(z_1-2z_2+z_3)/\sqrt{2}$ has Σ^+_u symmetry while

$S_2=\rho(x_1-2x_2+x_3)$ and

$S_4=\rho(y_1-2y_2+y_3)$ are the degenerate modes.

Then the **G** matrix becomes diagonal and the **F** matrix follows from the potential function of the internal coordinates where k_r and k_θ are the force constants associated with the internal (natural) stretches and k_{12} is the force constant to account for any anharmonic cross coupling between the two natural stretches.

$$2V=k_r(S_1^2+S_2^2)+2k_{12}\ S_2S_1+k_\theta\ (S_3^2+S_4^2)$$

$$2V=(k_r+k_{12})S_1^2\ +(k_r-k_{12})S_3^2\ +2k_\theta(S_2^2+S_4^2)$$

Then

$$2V=F_{11}S_1^2\ +F_{33}S_2^2+\ (F_{22}+F_{44})S_3^2$$

Thus the secular equation becomes

$$\begin{vmatrix} \mu_o(k_r+k_{12})-\lambda & 0 & 0 \\ 0 & 2\rho^2(\mu_o+2\mu_c)\ k_\theta-\lambda & 0 \\ 0 & 0 & (\mu_o+2\mu_c)\ (k_r-k_{12})-\lambda \end{vmatrix} =0$$

where λ are the vibrational eigenfrequencies. The normal coordinates follow from the definition of the potential:

$$\lambda_1Q_1^2\ +\lambda_2Q_2^2\ +\lambda_3Q_3^2\ =(k_r+k_{12})\ S_1^2+(k_r-k_{12}\ )S_3^2+k_\theta\ S_2^2$$

Plugging in the eigenfrequencies and matching coefficients for each Q_i and S_i (since the symmetry coordinates were picked to diagonalize the eigenvalue problem), the definitions of the normal coordinates are:

$$Q_1=(z_1-z_3)/\sqrt{(2\mu_o)}$$

$$Q_2=(z_1-2z_2+z_3)/\sqrt{(2(\mu_o+2\mu_c))}$$

$$Q_3=(y_1-2y_2+y_3)/\sqrt{(2(\mu_o+2\mu_c))}$$

(8.12)

A more convenient form of the normal coordinate transformations is obtained by defining the equilibrium coordinates (x,y,z) shown in Figure 1 as

$1=(0,0,-R_e)$ $2=(0,0,0)$ $3=(0,0,R_e)$

and defining $\Delta r=r-r_o$ where r_o is the equilibrium value. Then the coordinate transformations are

$$Q_1=\sqrt{(m_o/2)}(\Delta z_3-\Delta z_1)$$

$$Q_{2x}=\sqrt{(2m_om_c/m_t)}(\Delta x_2-1/2(\Delta x_1+\Delta x_3))$$

$$Q_{2y}=\sqrt{(2m_om_c/m_t)}(\Delta y_2-1/2(\Delta y_1+\Delta y_3))$$

$$Q_3=\sqrt{(2m_om_c/m_t)}(\Delta z_2-1/2(\Delta z_1+\Delta z_3))$$

(8.13)

and where $m_t=m_c+2m_o$

The inverse transformations become:

$$x_1=x_3=-\sqrt{(m_c/(2m_om_t))}\ Q_{2x}$$

$$x_2=\sqrt{(2m_o/(m_{cm}))}Q_{2x}$$

$$y_1=y_3=-\sqrt{(m_c/(2m_om_t))}\ Q_{2y}$$

$$y_2=\sqrt{(2m_o/(m_cm_t))}Q_{2y}$$

$$z_1=-\sqrt{(m_c/(2m_om_t))}Q_3-\ 1/\sqrt{(2m_o)}Q_1-R_e$$

$$z_2=\sqrt{(2m_o/m_cm_t)}Q_3$$

$$z_3=-\sqrt{(m_c/(2m_om_t))}Q_3+\ 1/\sqrt{(2m_o)}Q_1+R_e$$

(8.14)

APPLICATION TO CARBON DIOXIDE

After considering all the possible lineshape theories and their range of applicabilities, it appears that a variant of the semiclassical perturbative ATCF theory in the form given by Bonamy[602] or Leavitt[605] is the most appropriate theory to use in evaluating the pressure shifts[638] of the lasing transition in CO_2. Since CO_2 is a linear, symmetric triatomic with no permanent dipole moment (with zero hyperpolarizability tensors as defined by Leavitt), the dominant interaction between the active, excited state CO_2 molecule and a ground state CO_2 structureless perturber would be the electrostatic quadrupole-quadrupole (Q-Q) interaction plus an isotropic $1/R^6$ dispersion and induction

term[55-62]. Any induced dipole-quadrupole and any higher order terms (octopole-octopole) would be much smaller than the Q-Q term and can effectively be ignored. Likewise only the isotropic $1/R^6$ terms can contribute to the $S_1(b)$ component. Then, the simplified cross section follows from Equation (8.9).

$$nv\sigma = n\Sigma_{J2}\ \rho_{J2}/(2\pi)\int vf(v)dv \times \int 2\pi bdb\ \exp\{-(S_{2f}+S_{2i}+S_{2m})\ -i(S_{1f}-S_{1i})\}$$

where i and f designate the initial ν_1 or $2\nu_2$ levels and the final ν_3 levels in this absorption process. Here n is the density of the perturbers and v refers to the relative velocity. The shift δ can be given in terms of the real and imaginary parts of the S function (8.11)

$$\delta = n/(2\pi)\int vf(v)dv\int 2\pi bdb \times \exp[-(ReS_{2f}+ ReS_{2i}+ReS_{2m})]\times \sin(S_{1f}-S_{1i}\ +Im\ S_{2f}-Im\ S_{2i}) \qquad (8.15)$$

where the subscript m stands for the middle S_2 term and represents the interference or correlation between the i and f states since the total elastic and inelastic contributions from each i and f states do not contribute independently to the resulting shift of broadening of the radiator. Here the imaginary part of S_2 is just taken to be the Hilbert transform of the real part of S_2 and can be easily computed

for all the normal resonance functions, as shown in Appendix 7.

Normally, the isotropic S_1 component, which is the first order contribution to the lineshift is zero unless, as emphasized by many other theories, including the IOSA[360] and ECS[368] theories, there is a small vibrational dependence between the two states which will give rise to a small vibrational dephasing between the two levels. In CO_2, because of the mixing between the harmonic eigenfunctions of the three fundamental normal modes and because of the strong Fermi-like resonances present throughout many of the vibrational levels, there is the possibility of a significant nonzero diagonal oscillator matrix element in both the final and initial states. Quantitatively, as was pointed out in the $3\nu_3$ work done by Arcas[638], the vibrational mixing can be represented by expanding the isotropic potential in terms of the three normal coordinates q_1, q_2, and q_3 :

$$V_{iso}=V_{iso}(eq) + \frac{\partial V_{iso}}{\partial q_1}\Big|q_1 + \frac{1}{2}\frac{\partial^2 V_{iso}}{\partial q_1^2}\Big|q_1^2 + \ldots \qquad (8.16)$$

Since the first order scalar phase shift η is (8.10)

$$S_1 \simeq \Delta\eta = 1/\hbar \int \Delta V \, dt$$

$$S_1 = 1/\hbar \int dt \, [\langle v_f | V_{iso} | v_f \rangle - \langle v_i | V_{iso} | v_i \rangle]$$

(8.17)

where V_{iso} is given by the normal coordinate expansions

If the Van der Waals forces are considered the dominant $1/R^6$ isotropic forces

$$V \simeq 3U\alpha_1\alpha_2/(4R^6) \simeq 4\epsilon(\sigma/R)^6$$

(8.18)

where U is the effective ionization potential and α are the isotropic polarizabilities of the individual molecules. For CO_2 the Van der Waals constant is about 192 a.u.(atomic units) or 183.7×10^{-60} erg-cm^6 and $\epsilon \simeq 248\times10^{-16}$ erg or $\epsilon/k = 180°K$ and $\sigma \simeq 3.48°A$ while $\Theta \simeq 3.6\times10^{-26}$ esu-cm^2 = 2.67 au. An equivalent representation for the Lennard Jones potential (6,12) is

$$V(R) = 4\epsilon\sigma^6(\sigma^6/R^{12} - 1/R^6)$$

(8.19)

where the R^{12} term is much smaller relative to the R^6 term. The Van der Waals coefficients C_6 have been calculated for CO_2 interacting with CO_2 and several other perturbers by R.T. Pack[54] The polarizability, dipole moment, and the quadrupole moment and the corresponding first and second derivatives as a function of the normal coordinates $q_1, q_2,$

and q_3 have also been calculated by Morrison and Hay[46]. By considering the only nonzero derivatives of the isotropic potential (8.16) to come from the polarizability derivatives:

$$\partial V/\partial q = V(\alpha'/\alpha) \qquad (\partial^2 V/\partial q^2) = V(\alpha''/\alpha)$$

where $\alpha' = \partial\alpha/\partial q$ and $\alpha'' = \partial^2\alpha/\mu q^2$

Note that only the first derivative of α with respect to q_1 and the second derivative of α with respect to q_2 and q_3 are nonzero, as was pointed out in Chapter 2.

Then the scalar phase shift (8.17) will be proportional to

$$S_1 = 1/\hbar \int dt \langle v_f|\partial V/\partial q\ q|v_f\rangle - \langle v_i|\partial V/\partial q\ q|v_i\rangle \tag{8.20}$$

$$= 1/\hbar \int dt(\alpha'/\alpha)\Delta M\ (-C_6/R^6 + C_{12}/R^{12})$$

$$= 1/\hbar(\alpha'/\alpha)\Delta M\ \eta(R)$$

where the usual elastic phase shift[297,304]

$$\eta(R) = \int dt(-C_6/R^6 + C_{12}/R^{12})$$

$$= \frac{63\pi C_{12}}{256\hbar v b^{11}} - \frac{3\pi\ C_6}{8\hbar v b^5} \tag{8.21}$$

Here $\langle\Delta M\rangle = \langle f|q|f\rangle - \langle i|q|i\rangle$ is difference of the final and initial states matrix elements. The harmonic oscillator matrix element is defined to be

$$\langle v|q|v-1\rangle = \sqrt{[\hbar/(2\sqrt{(km)})]}\ \sqrt{(v+1)} \simeq 5.3\times 10^{-2}\sqrt{(v+1)}\ a_o = M$$

For CO_2, $k = 16.8\times 10^5$ dyne/cm and m=16 amu

and $(\alpha'/\alpha)=11.19/15.76 = 0.71$ for the q_1 mode[46]. Define

$$\Delta M = 5.3\times 10^{-2}\Delta N$$

where $\Delta N= N_f-N_i$ is the dimensionless harmonic oscillator matrix element. Then

$$\langle v|\partial V/\partial q\ q\rangle \simeq 5.3\times 10^{-2}\sqrt{(v+1)}(\partial V/\partial q)$$

$$\simeq 3.7\times 10^{-2}\sqrt{(v+1)}\ (-C_6/R^6+C^{12}/R^{12})$$

Plugging in $C_6=4\epsilon\sigma^6$ and $C_{12}=4\epsilon\sigma^{12}$, the Lennard-Jones contribution to the first order term is

$$S_1=\frac{3\pi\epsilon\sigma\ \alpha'(\sigma/R)^5\ [21(\sigma/R)^6-1]\Delta M}{2\hbar\nu\ \alpha} \qquad (8.22)$$

In reality the total dispersive and inductive contributions to the effective isotropic C_6 potential term must be used in calculating the S_1 contribution to the shift; then the total potential is comprised of the dispersion and inductive terms

$$-(\alpha_1\mu^2_2+\alpha_2\mu^2_1+3/2U\alpha_1\alpha_2)/R_6 = -C_{6eff}/R^6$$

The only nonzero contribution to S_1 from the dispersive term comes from $\partial\alpha/\partial q_1$ as was previously mentioned. The only nonzero inductive contribution to S_1 comes from

$$\partial^2V/\partial q^2 = 2\alpha_2\mu'_1\mu'_1$$

since only $\partial\mu/\partial q_2$ and $\partial\mu/\partial q_3$ are nonzero[46].

The nonzero inductive contribution to the total S_1 term, using the q_2, q_3 dipole derivative values and using the normal coordinate transformations (8.13) presented in the previous section, turned out to be at most only 10% of the dispersive contribution and can be neglected in further calculations. Thus the S_1 term and essentially the lineshift calculation is determined predominantly by the Van der Waals forces.

The anisotropic S_2 term is composed mainly of the familiar Q-Q interaction; it is given in the literature[408] as

$$S_2(b) = (16/25)(\theta_1\theta_2/\hbar v)^2\ 1/b^8 \times$$
$$\times [\Sigma_{J2,}\Sigma_{Ji,}\ \{C_{J2,}{}^2 C_{Ji,}{}^2\ (\mathrm{Re}\ f_3(k) + \mathrm{Im}\ F_3(k))\}$$
$$+ \Sigma_{J2,}\Sigma_{Jf,}\ \{C_{J2,}{}^2 C_{Jf,}{}^2\ (\mathrm{Re}\ f_3(k) + \mathrm{Im}\ F_3(k))\}$$
$$D\Sigma_{j2,}\{C_{J2}\ \mathrm{Re}(f_3(k))\}] \qquad (8.23)$$

Here $f_3(k)$ is a resonance function whose real and imaginary components consist of the modified Bessel functions of the first kind K_0, K_1, I_0, and I_1

$$f_3(k)=k^2/144\{\ (144+80k^2+19k^4+4k^6)K_1^2$$
$$+2k(72+31k^2+6k^4)K_1K_0\ +k^2(36+11k^2+4k^4)K_0^2\}+$$
$$+i\pi k^2/144\{\ -(144+80k^2+19k^4+4k^6)K_1I_1$$
$$+2k(72+31k^2+6k^4)K_1I_0\ +k^2(36+11k^2+4k^4)K_0I_0$$
$$-(72+31k^2+6k^4)\}$$

The argument of the resonance function f_3 is defined in terms of the initial state ii' or the final ff' state as

$$k=b/v(\omega_{ii'}+\omega_{22'})$$
$$\simeq 2\pi b/v\{B_i\ [J_i(J_i+1)-J_i'(J_i'+1)]$$
$$+\ B_2[J_2(J_2+1)\ -J_2'(J_2'+1)]\}$$

Here $\omega_{ii'}$ and $\omega_{22'}$ represent the change in energy between the perturber state 2→2' and and initial radiator state J→J' during the collision, as allowed by the Q-Q interaction. The sum $\Sigma_{J'}$ is over all possible J' allowed by the Clebsch Gordon coefficients C in a Q-Q interaction: J'=J,J ± 1. Here

$$C_{Ji'}^2 = \langle J_i 210|J_i'1\rangle^2$$
$$C_{J2'}^2 = \langle J_2 210|J_2'1\rangle^2$$
$$D= 2(-1)^{(JI+JF)}\sqrt{(2J_i+1)}\sqrt{\ (2J_f+1)}C_{JI}C_{JF}\times$$
$$\times W(J_iJ_fJ_iJ_f,12)$$

where W is a Racah coefficient.

Specifically the only possible values for C are

$$C_{J-1}^2 = \frac{3J(J-1)}{2(2J+1)(2J-1)}$$

$$C_J^2 = \frac{J(J+1)}{(2J+3)(2J+1)}$$

$$C_{J+1}^2 = \frac{3(J+1)(J+2)}{2(2J+3)(2J+1)} \qquad (8.24)$$

and

$$W = \frac{2[3X(X-1)-4J_i(J_i+1)J_f(J_f+1)]}{\sqrt{[(2J_i-1)2J_i(2J_i+1)(2J_i+2)(2J_i+3) \times (2J_f-1)2J_f(2J_f+1)(2J_f+2)(2J_f+3)]}}$$

where $X=J_i(J_i+1)+J_f(J_i+1)-(1)(2)$

The $f_3(k)$ resonance function was evaluated using a polynomial approximation which has been tabulated[484] for several of the common resonance functions. Appendix 7 tabulates several of these resonance functions along with the corresponding Hilbert transforms(imaginary component); many of these functions have not been tabulated previously in the literature.

Using all of these results, the integral over b was numerically evalucated using several different integration routines (Gaussian quadrature, DCADRE,and adaptive Gaussian methods from the NAG and IMSL libraries) while just using an

average velocity in the $\delta = nv\sigma$ evaluation. It turned out, using this semiclassical calculation, that the sign and magnitude of the lineshift essentially depended on the difference of the harmonic oscillator matrix elements in the initial and the final states (ΔM or ΔN). There was almost no Q-Q dependence since the $S_{2i} \simeq S_{2f}$ and hence cancelled out when compared with the S_1 term in the sine expression. Because there is very little Q-Q dependence, this calculation predicts very little J dependence and no difference in the lineshift between the P and R branches. The sign and magnitude of the pressure shift depends on how large and how much the initial and final vibrational levels are mixed.

The $|f\rangle$ and $|i\rangle$ vibrational states are not perfect oscillator states but are composed of linear combinations of the basis harmonic states and their overtones:

$$|\nu_1\rangle = \alpha|000\rangle + \beta|001\rangle + \gamma|020\rangle + \delta|200\rangle + \ldots$$

Thus a harmonic bases decomposition for each level and for each CO_2 isotope considered is needed to compute this matrix element. Following the procedure outlined in Chapter 2 on the energy matrix diagonalization by Suzuki and using

the potential constants obtained by Chedin, the eigenvalue problem and its solutions are outlined and given in Appendix 1. From this, the matrix element for each Fermi level for each isotope is obtained and shown in Table 10 where $M = 5.3 \times 10^{-2} N$.

Table 10

Matrix Elements $\langle v|q_1|v\rangle = N$

Isotope	N_{II}	N_I	ΔN_{II}	ΔN_I
16-12-16	.0968	.0532	.1281	.1717
16-13-16	.0619	.0879	.1575	.1314
18-12-18	.1220	.0244	.1041	.2019
18-13-18	.1058	.0403	.1147	.1803

This table lists (note the 'correct' labelling of the energy levels as mentioned in Chapter 2 in Table 3) the expected difference ΔN for the upper (10μm) or lower (9μm) levels of the Fermi doublet. Since the dominant term for the lineshift in the S(b) expansion comes from $\sin(S_{1f}-S_{1i}) \simeq (S_{1f} - S_{1i}) \propto \Delta N$, the predicted pressure shift will be red shifted in proportion to the Fermi level matrix elements

given in Table 10. In 16-12-16 and 16-13-16 the predicted pressure shifts are roughly equal for both the 9 and 10 μm band transitions while the predicted shifts are roughly in a 1 to 2 ratio for the 9 and 10 μm band in 18-12-18 and 18-13-18. But the measured shifts, using the nonlinear absorption techniques at the low pressures, were blue shifted.

An analytical expression for the $\int db$ integral could be obtained by making a few approximations. Physically, the cutoff parameter so prevalent in the early Anderson can be viewed as the radius of a hard sphere potential; any coherence will be automatically destroyed for collisions closer that this hard sphere radius. Thus the broadening cross section can be taken as πb_o^2 where b_o represents the impact radius in which the dominant dipole destructive mechanism is effective. In atoms, the coherence is destroyed primarily by elastic collisions since the energy levels and scattering amplitudes are easily altered in any collision within the electronic transitions. In the case of molecules, the dominant coherence destruction mechanism is inelastic collisions; elastic collisions have very little effect on the molecular transitions since the participating potentials in the vibrational or rotational transitions are

very nearly identical (same electronic state) such that it could easily survive the usual elastic collisions. Then the broadening cross section is

$$\sigma \simeq \int 2\pi b db \exp[-(b_o/b)^n] \simeq \pi b_o^2$$

where b_o is the effective elastic or inelastic cutoff parameter for the atomic or molecular transitions respectively.

In the case of CO_2, the inelastic contribution comes from the Q-Q interaction; the broadening cross section then gives an effective inelastic radius $b_i \simeq 11.5\ a_o$; note that the inelastic radius b_i has a slight J dependence just as does the linewidth. Using this concept with the elastic contribution to the cross section coming from the Van der Waals term, the shift in terms of the inelastic and elastic radii is

$$\delta \propto \int 2\pi b db \exp[-(b_i/b)^8] \sin[(b_e/b)^5 + (b_i/b)^8]$$

Analytic expressions for the shift can be obtained in terms of the Gamma function $\Gamma(x)$ by replacing $\sin(\eta) \simeq \eta$. In this case the integral was proportional to

$$\sigma_{broad} \simeq \sigma_{inelast} = \int 2\pi b db \{1-\exp[-(a/b)^8]\}$$

$$= \pi a^2 \Gamma(3/4)$$

where the inelastic radius $b_i = a = 11.6\ a_o = 5.74$ A° in the case of

CO_2.

Likewise the shift calculation becomes, for the elastic radius $b_e = \beta$

$$\int 2\pi b\, db \exp[-(\alpha/b)^8] \{(\beta/b)^5[(\gamma/b)^6-1]\} =$$
$$= \pi\beta^5/(4\alpha^3)\ \Gamma(3/8) + \pi\beta^5\gamma^6/(4\alpha^9)\ \Gamma(9/8)$$

Arcas and Boulet [638] have measured the pressure shift for several ground state transitions (including $3\nu_3$) using straight linear absorption. In this experiment the CO_2 radiation is sent through two consecutive absorption cells filled with 4 and 760 torr of pressure; since the pressure differential was so large and a ground state absorber was used, the actual absorption profiles and the corresponding shift could be compared directly on a spectrometer and evaluated after the proper deconvolutions. This linear absorption technique gave 400 to 600 KHz/torr red shifts with error bars of ±160 KHz/torr. Their experimental values agreed with comparable S_1 and S_2 pressure shift calculations using the corresponding $3\nu_3$ vibrational harmonic functions. Further work in other bands showed a similar agreement between theory and experiment[638].

In summary, the major discrepancy betwen the experimental results for the lasing 9 or 10 μm pressure

Table 11

Perturber Gas Data

Gas	Rate	C_6	Run1	Run2	Run3
Units	au	$e^2a_o^3$		KHz/Torr	
Xe	1580.63	282	+52	+53	+51
Ar	961.99	114.5	+37	+22	+20
He	264.18	16.7	-20	-33	-20
H_2	325.88	46.	-36	-29	-98
N_2	916.91	118	+21	+23	+10
CO_2	1200.59	192			

Run1 = 18-12-18 (IP-22)

Run2 = 16-12-16 (IP-24)

Run3 = 16-12-16 (IR-34)

shifts versus the $3\nu_3$ measurements and theoretical predictions is that the nonlinear saturated absorption technique gave blue shifts while the linear absorption experiment and the traditional presure broadening results gave red shifts. The perturber gas data show in Table 11 also gave the same blue shift trend with Xe,Ar,N_2, and CO_2 while being red shift for He and H_2 The perturber results

suggest that the dominant contribution to the shift comes from the dispersion term in the S_1 factor just as it was for the CO_2-CO_2 collisions. Table 11 also shows the corresponding C_6 coefficients[54] for CO_2-X perturber Van der Waal contributions. This table also calculates the simple collision rate[297] obtained from simple impact phase shift theory

$$\gamma \simeq \text{rate} \propto nv\sigma \propto v(C_6/v)^{2/5}$$

$$= (C_6)^{2/5} v^{-3/5}$$

The perturber shifts appear to scale roughly (30%) with this rate even though the sign is different. On the other hand, since the shifts are proportional to ΔM,

$$S_1 \propto C_6(a'/a)\Delta M$$

The perturber shifts seem to scale with C_6 within 30% but there is still a difference in sign between the theory and the measurements.

One possible cause of this anomalous shift could be the influence of velocity changing collisions on the active molecules. One extreme limit would be the situation of pure velocity changing collisions (VCC) which would always kick the active particle out of the interaction 'hole' (see the VCC section in Chapter 10). In this case, the total cross

section must be used to calculate the shifts. This translates, in terms of the phase shift term, $\sin(\eta(b))$

$$\sin(S_f - S_i) \rightarrow \sin(S_f) - \sin(S_i)$$

Or including all the terms, the phase term becomes in VCC

$$\sin(S_{1f} + \mathrm{Im}\ S_{2f}) - \sin(S_{1i} + \mathrm{Im}\ S_{2i})$$

In (8.20) S_1 is proportional to the regular phase shift and depends on the difference of the initial and final potentials. Thus the regular phase shift

$$\sin(S_f - S_i) \propto \sin(\Delta V) \simeq \Delta V$$

In the case of pure velocity changing collisions, the dephasing rate is proportional to the total cross section

$(\sigma_1 + \sigma_2)/2$ for levels 1 and 2.

Then the phase is equivalent to

$$\sin(S_f - S_i) \propto \sin(V_{of} + \Delta V_f)/2 - \sin(V_{oi} + \Delta V_i)/2$$

where the total potential V_o must now be taken into account. Usually $V_{oi} \simeq V_{of}$ which cancelled out in the classical phase shift terms but does not in the pure velocity changing collisions (VCC) regime. Instead, the V_o term adds an extremely rapidly oscillating phase contribution to the sine function; this phase contribution averages to zero except for the final oscillation right before the inelastic exponential term cuts off the effective contribution at the minimum impact parameter. Even after substituting all the

terms in the VCC phase shift and varying the parameters to determine if there could be a change in of the shift, the calculated VCC shifts were much smaller (about -10KHz/torr) than that calculated for the traditional pressure regime but the shifts were still red. In essence, the VCC phase shift is proportional to

$$\sin(1+M_f)V_f - \sin(1+M_i)V_i$$
$$\simeq 2\cos[(V_f+V_i)/2]\sin(\Delta M)$$
$$\simeq 2(\Delta M)\cos[(V_f+V_i)/2]$$

where M is very small compared to 1 and V.

In pure VCC, the shift is still proportional to

$$\sin(\Delta V)\simeq \Delta v$$

which still gives a red shift (but of much smaller magnitude), in contrast to the experimental results. Again the S_2 Q-Q contributions were neglible compared to the S_1 terms in the VCC calculations. In addition, other inductive, dispersive contributions for a pure linear-linear molecular collision, as given by Leavitt[605] was taken into account but these effects did not alter the original VCC result; the isotropic dispersive terms was still the dominant term in all the calculations.

In addition, using the elastic and inelastic radii to approximate the VCC integral when $\sin\vartheta \simeq \vartheta$, the change of variables give

$$\int 2\pi b\,db\, \exp[-(\alpha/b)^8/2]\ (\beta/b)^5\Delta\ \cos\{(\beta/b)^5(1+\Sigma/2)\}$$

$$=\pi\beta^5/(4\alpha^3)\Delta \int dx\ [\exp(-x/2)]/x^{(5/8)}$$

$$\times\ \cos\{(\beta/\alpha)^5 x^{(5/8)}[1+\Sigma/2]\}$$

where Δ and Σ are the difference and the sum of the oscillator matrix elements in the final and initial states as it is usually defined. One can see from this analytic form of the integral that it does not change sign; the sign of the shift is still dependent on Δ as before but due the rapid oscillations of the phase terms, the pure VCC shift is much smaller than the shift using standard pressure broadening theory.

CHAPTER 9 CONCLUSIONS

The purpose of the experiment was to measure the pressure shift in the 9 and 10 μm lasing transition in CO_2 using the 4.3 μm saturated fluorescence stabilization technique to obtain Doppler free homogeneous linewidth resolution. Preliminary and previous shift measurements revealed a small 100 to 300 KHz/torr red shift[634,637] (small compared to the 7-8 MHz/torr FWHM line broadening[606-633]) and also revealed a 'nonlinearity' at the higher pressure besides being somewhat nonreproducible from measurement to measurement. By using these nonlinear techniques to probe within the Doppler background and by using a heterodyne technique to measure the pressure shifts, our measurements, in contrast to the 160 to 200 KHz/torr red shift predicted from traditional pressure broadening theories[602,605,638], revealed a 50 to 80 KHz/torr blue shift in the 20 to 120 mtorr pressure regime. Subsequent higher pressure measurements (1-10 torr) taken to estimate the sign of the pressure shift revealed that the shift of the Doppler profile was red (-80%50 KHz/torr) at these higher pressures. Even more intriguing, the perturber gas data revealed a blue shift for Xe, Ar, N_2 and CH_3F while He and H_2 were red

shifted with the relative magnitudes of the shifts corresponding roughly to their respective polarizabilities. Thus, using nonlinear spectroscopic techniques, the shift of the Lamb dip measured at the low pressure regime gave an anomalous shift opposite to that predicted by traditional pressure broadening theory and to that measured by linear spectroscopic techniques. As it turned out, this was not the first instance of such a reversal of the pressure shift at low and high pressures since the HeNe system stabilized on the molecular vibrational-rotation P(7) transition of CH_4 revealed the same blue[189] to red[190] transition (though in this case, this behavior appears to have gone unnoticed by the experimenters) as pressures were varied from low (where saturated absorption was used) to high (where linear absorption was used) pressures. This is in contrast to the red shifts measured in the HeNe system stabilized on the electronic transitions of I_2[195-200].

As was stated earlier, pressure shifts result from the difference in the scattering amplitudes or in the difference in the interaction potential of the upper and lower states; in the case of vibrational-rotation transitions, this difference is very small so that the shift is much smaller

than the broadening coefficients. Considering the broadening and shift expressions:

$$\gamma \propto \int 2\pi b \, db[1-\exp(-\mathrm{Re}\ S_2)\cos(S_1+\mathrm{Im}\ S_2)]$$

$$\delta \propto \int 2\pi b \, db[\exp(-\mathrm{Re}\ S_2)\sin(S_1+\mathrm{Im}\ S_2)] \quad .$$

The difference in the potentials can be regarded as a difference of the isotropic and the anisotropic (J dependent) parts of the potentials in terms of S_1 and S_2 terms. Here S_1 represents the slight isotropic (dispersion Van der Waals R^{-6} force) dependence arising from the vibrational dephasing due to the slight anharmonicities in the vibrational levels. For CO_2, the S_2 term predominantly consists of the quadrupole-quadrupole interaction that leads to the rotational dephasing. Likewise, in CO_2 the dominant contribution to the linebroadening parameter[606-618] is the real part of S_2 (or inelastic scattering due to the quadrupole-quadrupole terms). Thus the linebroadening term hardly depends on the $\cos(S_1+\mathrm{Im}\ S_2)$ term which is usually unity in the region of importance. This vividly demonstrates the latitude in which line broadening theories can apply and perhaps err since the line broadening calculation is relatively insensitive to the exact potentials and values. This also demonstrates why there is almost no vibrational dependence in the line broadening

coefficient for CO_2 since the vibrational term, S_1, is unimportant. All vibrational bands show a similar J dependence in the line broadening coefficient due to the exp(-Re S_2) term.

On the other hand, our shift measurements show that there is practically no P or R dependence for either CO_2 or the perturber gas data; thus the Im S_2 term is insignificant compared to the S_1 term in the region of importance. In contrast to the line broadening problem, the details of the theory are very important in calculating the lineshift and in the case of CO_2, the S_1 term through its vibrational dependence of the isotropic potential, is the most important factor in determining the lineshifts. This follows experimentally since there is practically no P or R dependence in either the I or II bands; likewise the perturber shift data did not show any P or R dependence while scaling roughly (excluding He and H_2) within 30% of their Van der Waals C_6 constants.

But the pressure shifts, instead of scaling along with the Fermi resonance in the vibrational terms, is blue, in contrast to the red shift predicted by the standard phase changing collision theory. Only at higher pressures (>1,10

torr) does this shift turn red as expected by the traditional theory. One possible explanation to this lies in the pressure regime within which CO_2 is being investigated. Velocity changing collisions can play a major role in saturation spectroscopy at the very low pressure regimes where the change in velocity per collision can kick the particle out of the interaction 'hole'. In many saturated absorption experiments[266-280], a nonlinear dependence of the line broadening coefficient was seen depending on whether the Doppler shift due to average velocity change $ku\theta$, where k is the wave vector and θ is the average scattering angle, was greater or less than the homogenous resonance width Γ. If $ku\theta$ is greater than Γ, the particle would get 'kicked' out of the resonance hole with each velocity changing collision and consequently contribute to an additional width or shift. If $ku\theta$ is less than Γ, then the particle will still interact with the field after each collision and will not contribute to any additional width or shift. In CO_2, this nonlinear dependence of the line broadening coefficient[280,647,651] has been observed at low pressures (<30,50 mtorr), indicating a regime where diffractive scattering due to velocity changing collisions has occurred. In this case, the diffractive angle $\theta \simeq 1.6 \times 10^{-2}$ and the velocity change[647]

$\Delta v = u\theta \simeq 2.4$ m/s

On the other hand, momentum transfer studies[653,654] where $\Delta J = 0, \pm 1, \pm 2$ indicate a much larger velocity change

$\Delta v \simeq 2.8 \times 10^3$ cm/s or $k\Delta v \simeq 1.76 \times 10^7$ s^{-1}

or $\gamma = 2.7$ MHz $= k\Delta v$

which means that our pressure shifts were measured entirely in the regime of velocity changing collisions (the transition point is 200-300 mtorr). In pure velocity changing collisions, the lineshift turns out to depend on

$\sin(S_{1f}) - \sin(S_{1i})$ instead of $\sin(S_{1f}-S_{1i})$

Even so, the predicted velocity changing lineshift was very small (-10 KHz/torr).

The most intriguing part of the velocity changing conjecture is that a nonlinear pressure shift[189,194] has been seen on the HeNe laser stabilized on the CH_4 resonance. In this case, using the very high resolution available with the CH_4 resonance dip, a nonlinear change in the slope of the shift when was observed when $ku\theta \simeq \gamma$ (1 to 10 mtorr). But this nonlinear pressure shift was also blue which is in direct contrast with an earlier measured red shift[190] using a linear absorption technique on the same transition but operating at pressures between 10 to 200 torr. Thus there appears to be a real difference between the high and

low pressures when linear versus nonlinear spectroscopic methods are utilized.

During the past few years there have been several other anomalous pressure shifts[641-645] involving atomic (electronic) transitions where linear and saturated spectroscopic techniques gave opposite results But in these cases, it is entirely possible for the shift to change sign since the potential depends on the expectation values of powers of the **r** coordinates for each individual state and these values can easily change sign for different electronic states. The pressure shifts obtained for the vibrational-rotation molecular (not electronic) transitions suggests that there could be something fundamentally different between the ultrahigh resolution experiments using saturated absorption versus the ordinary linear spectroscopic techniques. The question is whether the shift of the Lamb dip resonance, which this experiment measures, is the same as the true shift of the ensemble Doppler response of the system which turned out to be red shifted.

The Lamb dip experiment is a velocity selective technique that tests the response of the $v_z = 0$ molecules, which also have approximately 1/3 less energy than the rest of the

molecules. There is the possibility that this group of molecules will have a different response, temperature dependence and effective potential due to the lower kinetic energy, with the other perturbers, especially since these molecules exhibit a nonlinear response to a saturating laser field. Each resonant molecule has to interact twice with the laser field in the saturated absorption experiment. It is possible that the Lamb dip could shift and respond differently from the inhomogenous Doppler profile as a function of collisions, especially for similar potential functions in the initial and final states. In a molecule, the dipole coherence is not destroyed for small angle collisions but is destroyed due to inelastic collisions; the relative velocity between the dipole and the perturber can matter in the vibrational-rotation transitons unlike in electronic state coherences where any elastic collision can destroy the dipole coherence. In this respect, further experiments that attempt to measure the pressure shift should attempt to utilize some other Doppler free technique such as a two photon experiment to avoid using the saturated absorption techniques.

CHAPTER 10 LINESHAPE THEORY

SURVEY OF LINESHAPE THEORY

Over the years there have been several different approaches for computing the pressure broadening of spectral lines and accordingly there have also been several reviews[281-307] summarizing the different aspects of current experimental and theoretical treatments of the theory. These reviews include those of Chen and Takeo[289], Rabitz[296], Sobelman[297], Breene[289], Hindmarsh and Farr [304], Lewis[301], and Schuller and Behemenberg[300]. The objective of this section is not to emulate these reviews but rather to present some overall view of the different theories that are available and how they relate and are similar to each other. Resonance broadening and Stark broadening will not be considered in this survey.

Figure 77 gives a brief summary showing the differences, approximations and relationships between the various lineshape theories. As can be seen, almost everything can be traced back to the evaluation of the Fourier transform of the correlation function. Besides the unified branch, the

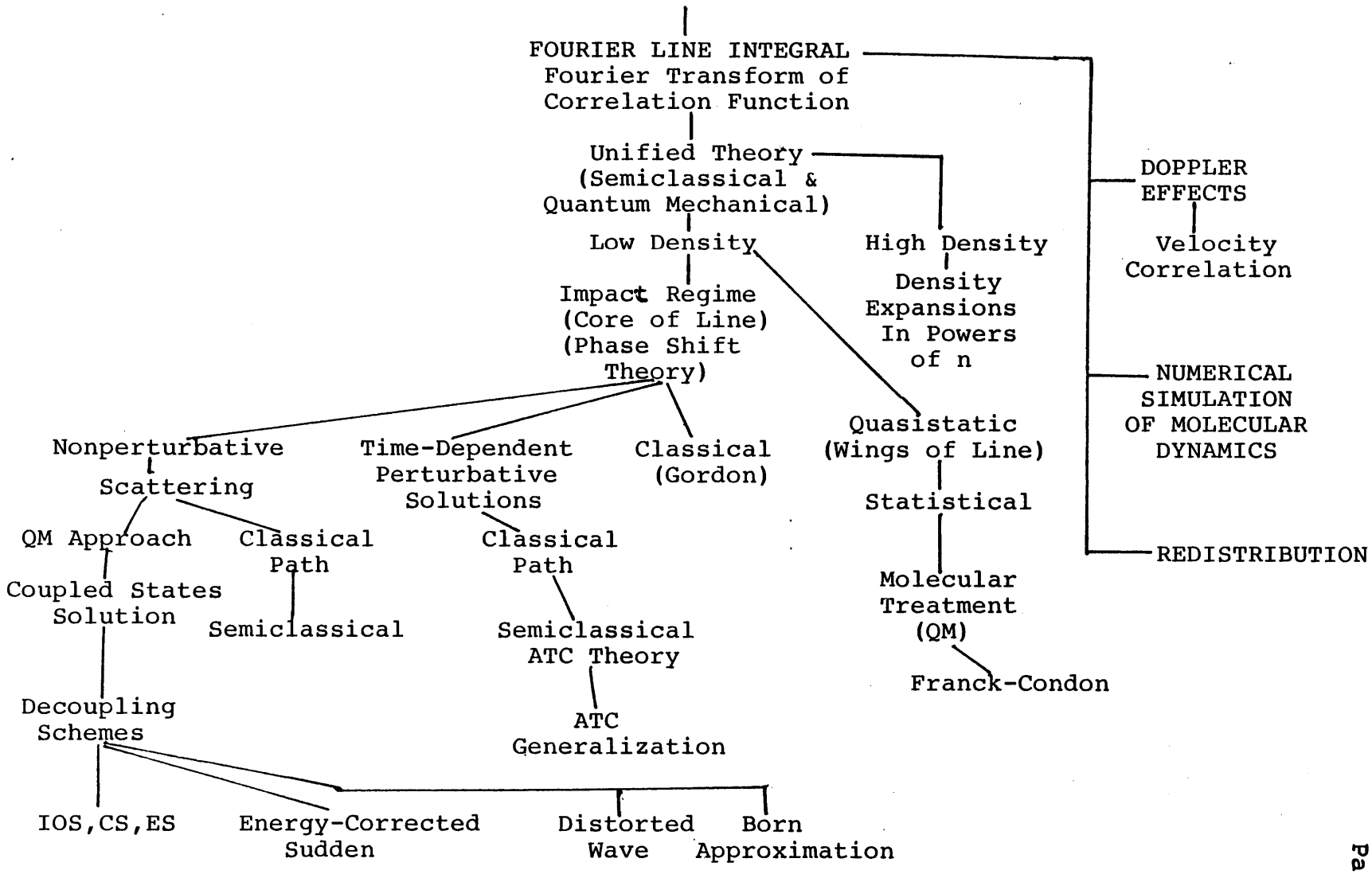

Figure 77 Overview of Lineshape Theory

redistribution and Doppler effects are treated separately. There have also been lineshapes obtained from numerical simulation of the molecular dynamics. Most theories deal in the low density (binary collision approximation) but there have been lineshape theories based on density expansions to account for the high density regime.

In almost all theories of line broadening, the line profile that had been calculated gave the frequency dependence for the emission or absorption without any regard to the history of previous radiation, probability of emission or the polarization of the resulting radiation. The radiation redistribution function which includes the 'past' history, $F(\omega_1,\omega_2)$ describes the probability and profile of the ω_2 radiation given ω_1 was absorbed or emitted. This radiation redistribution problem[329-340] has recently been considered by Burnett and Cooper[330] but in all the subsequent discussions of the existing theories, it will be disregarded.

The theory of the spectral lineshape had its initial beginnings from the hard sphere collision and complete quenching of the radiation picture proposed by Michelson in 1895 to the simple charge oscillator model proposed by

Lorentz in 1906[281]. Lorentz used a probability distribution for the times between quenching collisions which gave rise to the familiar Lorentzian intensity distribution. Instead of considering complete interruption of the radiation, Lenz and Weisskopf[282] considered the gradual frequency shifts and the line broadening being due to changing phase shifts as the perturber approached the radiating atom. If these phase shifts are large enough, then the radiation is interrupted by the phase changing collisions and the lineshape is subsequently broadened. In all the above pictures, the radiation and the subsequent intensity profiles were obtained using a "Classical Fourier Analysis (CFA) technique where the intensity profile of the light emitted from an oscillator is given as the squared modulus of the complex Fourier transform of the emission or absorption frequency function f(t) where

$$f(t) = \mathrm{Re}\ \{\exp\int[i\omega_o t + i\eta(t)]\} \quad t>0$$

and the frequency is $\omega(t) = \omega_o + d\eta(t)/dt$ and $\eta(t)$ is the phase change or shift at time t. Then the intensity spectrum

$$I(\omega)=1/2\pi\int\exp(-i\omega t)\ \Phi(\tau)d\tau$$

where the correlation function is defined to be

$$\Phi(\tau)=\lim(T\to\infty)1/T \int f^*(t)f(t+\tau)dt = \langle \exp(i\Delta\eta(\tau)\rangle$$

This is the standard result of CFA. The intensity spectrum is actually the Fourier transform of the correlation function. Physically, since the phase shifts are considered to give rise to the frequency spread, the mean phase shifts will be proportional to the correlation of the oscillation before and after the collision; thus the interaction must be known for a correlation time τ.

In simple phase shift theory, in the impact approximation, the correlation function becomes

$$\Phi = \exp(n V \tau(\sigma' - i\sigma'') \text{ where}$$

$$\sigma' = 2\pi \int [1-\cos\eta(b)]b\, db$$

$$\sigma'' = 2\pi \int [\sin\eta(b)]b\, db$$

and the intensity spectrum becomes the familiar

$$I(\omega) = I_o \frac{n V \sigma'}{(\omega-\omega_o - n V \sigma'')^2 + (n V \sigma')^2}$$

Note that V represents the average relative velocity. In reality the cross section should be averaged over the relative velocity distribution.

Several assumptions are made in these phase shift theories and are listed as follows.

1. Impact Assumption. The collision duration is very short compared to the time between collisions so that radiation is ignored during the collision duration.
2. Binary Collisions. The pressures are low enough and the particles fast enough so that only two particle collisions are considered and there are no three body or many body correlations.
3. Classical Path Assumption. The perturber trajectories can be described classically; this trajectory is most commonly viewed as rectilinear up to a minimum impact parameter.

In the semiclassical theory, the interaction of the radiation fields are treated classically and the radiator's state are treated quantum mechanically. Initially, only elastic or adiabatic collisions are considered in the classical treatments.

In the interruption or impact approach (phase shift) to line broadening which is valid in the line core corresponding to the period between collisions ($\Delta\omega \rightarrow 0$), the radiation emitted during the duration of the collision is ignored. On the other hand a different approach was initiated by Holtsmark (for Stark broadening), Kuhn, and Margeneau[287] where the total environment influences the

frequency emitted by the radiator. Here the frequency is not determined by the phase interrupting collisions but rather by the total potential difference in the initial and final states due to the surrounding perturbers and hence the line profile will be a function of the probability over all times (including the collision time) of the occurrence of the particular configuration of perturbers which give rise to the ΔV. Hence the frequency becomes

$$\omega_o+\Delta\omega=\omega_o+\Delta V/\hbar$$

This is the quasi-static or statistical approach to the line broadening problem as advocated by Margeneau and Kuhn[287]. The quasistatic theory, where the relative motions of the perturber and active atoms is very small during the time scale $1/\Delta\omega$, is best applied at the line wings which corresponds to the duration of the collision. Assuming just a one perturber model, the intensity at large $\Delta\omega$ will be proportional to the probability of finding a perturber between the intermolecular distances R and R+dR:

$$I(\Delta\omega)\, d\omega = 4\pi nR^2|dR|$$

where n is the number density of the perturber. Thus, assuming binary collisions and nearest neighbor interactions,

$$I(\Delta\omega) = 4\pi nR_2\, |d\Delta V/dR|^{-1}\hbar$$

By substituting in the appropriate power law potentials, the frequency dependence of the intensity profile is easily obtained.

An intensity profile very similar to that obtained from the quasistatic approach was derived by Jablonski[293] using a quantum mechanical treatment. Here, Jablonski treated the radiator and perturbers as one big quasimolecule where the change in energy $\Delta\omega$ is considered to manifest itself in the change of the the translational energy of the perturber. The intensity distribution is proportional to the probability distribution function for the required change in the perturber's translational energy. By using a total wave function composed of the product of the perturber and radiators wave functions, the intensity spectrum is proportional to the perturber's Franck-Condon factors and the radiator's dipole matrix elements; the corresponding wave functions are evaluated using JWKB approximations to the solution of the Schroedinger equation.

Thus, the early line broadening theories were characterized by the two different approaches, the phase shift Fourier analysis theory versus the quasistatic calculations based on the molecular models; each method was

valid in different regions of the line profile and also gave apparently irreconciliable results. Eventually Foley[284] and finally Lindholm[283] and Holstein showed how the results of the static theory followed from the Fourier analysis and vice versa. Then a general or unified theory, based on the Fourier analysis approach, was developed by Anderson and Talman[286] as well as Lindholm and Foley; this theory gave a general expression for the lineshape which reduced to the different theories in the appropriate limits. In this unified theory, the phase shifts are evaluated in terms of the N binary potentials between the N perturbers and the radiator; these N potentials were treated as isolated spherical, adiabatic interactions in the correlation time τ. Anderson's unified theory predicted the Lorentzian core in the impact limit ($\tau \to \infty$), and the line wing profile as $v \to 0$ in the static limit, as well as an asymmetry of the core profile. This unified theory did not include inelastic effects or the possibility of an anisotropic interaction potential; this is remedied in the quantum mechanical approach to the problem[341-352].

The most widely used method of computing the line profile for molecular rotation or rotation-vibrational spectrum is based on the work of Anderson[407]. In relation to the

previous theories, Anderson was the first to apply the impact theory to a quantum mechanical treatment (of the internal states) of the spectral profile relating the experimental molecular rotational or vibrational-rotation transitions (microwave or infrared) to a theoretical prediction based on the actural electrostatic and dispersion forces between the radiator and perturber system and gives a theoretical prediction of the linewidth and lineshift as a function of the initial and final radiator's states. The Anderson theory is essentially a dipolar transition, perturbative impact theory based on the impact, binary collision, classical path approximations while treating the internal coordinates of the molecules quantum mechanically. As in all the quantum mechanical theories, a time evolution operator that describes the collision dynamics is expanded in the standard time-dependent perturbation theory.

In the impact limit, the correlation time $s \to \infty$ as all collisions are completed and the time evolution U operator is replaced by the S operator $S=U(\infty,-\infty)$. Thus, the quantum mechanical result, which includes inelastic collisions and interaction anisotropy, has the FWHM and shift given as

$$\gamma = n \int f(v) v dv \int 2\pi [1 - \exp(-(\mu_i + \mu_f)) \cos(\eta_f - \eta_i)] b db$$

$$\delta = n \int f(v) v dv \int 2\pi [\exp(-(\mu_i + \mu_f)) \sin(\eta_f - \eta_i)] b db$$

where $S^{+}_{ff}S_{ii} = \exp(-\mu - i\eta)$ and μ represents the inelastic and η represents the elastic (phase changing collisions) interactions.

Anderson's theory, as modified and expanded by Tsao and Curnutte[408] and later by Frost[493], provides the basis for the ATC or ATCF variations of the semiclassical (classical path) perturbative approaches[399-406] to the lineshape theory. There have also been other semiclassical approaches to the problem which do not use perturbation theory[399-406]. In essence, ATCF theory and its variants [407-418] have been extensively developed and modified over the years (generalized by Leavitt[603-605] and Bonamy[602]) such that it is the basis for almost all microwave and infrared analysis was treated in detail in Chapter 8. Other quantum mechanical approaches to the collision problems have been based on the formulation of Baranger[292] and Fano.

There has also been a great deal of work over the last few years dealing with atom-molecule collision dynamics and the 'sudden' decoupling schemes[353-375] needed in these inelastic and elastic collisions. These decoupling methods are needed since an infinite set of coupled equations, based on expanding the wavefunction over a complete set of

eigenstates, result from the scattering dynamics involved in solving the Schrodinger equation. Here, the problem of calculating the relevant cross sections and scattering amplitudes for a given intermolecular potential V has been reduced to evaluating the scattering S matrix for the potential functions. To evaluate this S matrix, the scattering amplitudes and partial wave expansions are needed from the solution of Schrodinger's equation. The exact solution for the total wavefunction comes from a set of coupled differential equations where each eigenstate of the isolated active molecules is coupled to all the other eigenstates of the perturber through their partial wave expansion. Thus, the quantal formulation results in an infinite coupled set of partial wave differential equations. This set is reduced to a large close-coupled set of equations by judiciously choosing wavefunctions used in the eigenstate expansion. Still the major problem lies in the 2J+1 degeneracy associated with the energy levels of the rotating molecule which sets an upper ceiling on the maximum value of J, especially since the computer time required to solve the coupled equations depends on the cube of the number of equations in the set. There have been several 'sudden' attempts to decouple these equations. These sudden decoupling schemes are based on the same principle that is

employed in the Born-Oppenheimer approximations; some motions are much slower than others so that the slower motions can be considered fixed relative to the other motions. The equations for the rapidly varying degrees of freedom can be solved as a function of the slower degrees of freedom and the resulting scattering amplitudes are averaged over the slower degrees of freedom to obtain the final scattering amplitudes. The 'slow' nuclear motions (compared to the relative radial motions) that are used in this decoupling schemes include:

1. The Centrifugal Sudden (CS) or j_z conserving coupled states approximation where the orbital angular momentum or the centrifugal potential is approximated as an average value $l_o(l'_o+1)\hbar^2/2\mu r_2$; l_o is the average or initial value of l.

2. The Energy Sudden (ES) approximation where the molecular rotation or the rotational energy is approximated as an effective $j^2 \simeq j_o\ (j_o+1)\hbar^2$. Thus all wave numbers are replaced by an effective k_o .

3. The Infinite Order Sudden Approximation (IOSA) where both the ES and CS approximation are taken. Then all effects of the potential are included to all orders and the orientation of the interaction only enters as a parameter without any energy dependence. Other approximate methods[368-375]

include just the Enery Corrected Sudden (ECS) approach, distorted wave approximation, and the exponential distorted wave methods.

The quantum close-coupled calculations and the subsequent 'sudden' decoupling methods have received a great deal of interest recently but they still have not approached the widespread usage that the semiclassical ATC theories have, except in the simplest rare gas-diatom collisions. There are several other different isolated approaches or varieties to the theory of line broadening including the Liouville and Green functions formulations, and the use of Feynman diagrams;however these will not be considered here (288).

In all these theories, Doppler broadening was not taken into account. Normally, Doppler broadening occurs if one can consider the oscillator to have only one frequency

$$\omega_o(1+k.v)$$

at a constant velocity or else, the radiator's velocity is constant about ω_o for a time τ . This means, that for normal Doppler broadening to be valid, the width of the spread, $\Delta\omega = 1/\tau$, must be small compared to the Doppler spread, $\Delta\omega < k.v$ or by considering the mean path length as $l=v\tau$, the mean free path of the radiator must be large

compared to the wavelength of the radiation, $l >> \lambda$. This is valid except at very high pressures and for very long wavelength radiation.

One important point to make is the correlation or synthesis of Doppler and pressure broadening in the spectral profile. These effects arise because there are two types of frequency shifts that are important to a radiator: translational motion of the radiator leading to Doppler frequency shifts and the usual phase interrupting collisions leading to the phase and frequency shifts. Normally the two effects are considered statistically independent such that the collisions do not alter the radiator's trajectory and the resulting Doppler profile is Gaussian; the combined uncorrelated effects are represented by convolving the Gaussian and Lorentzian profile into what is referred to as the Voight profile.

There can be a correlation between Doppler broadening and pressure broadening since the distribution of the perturber velocities depends on the radiator's velocity. The collision frequency and the size of the phase shifts depends on the radiator's speed since the duration and the time

between collisions depend on the relative velocity of the perturber and radiator.

There have been a few attempts by Galatry[376], Gerstein and Foley[377], Rautian and Sobelman[378], and Ward and Cooper[397] to combine both Doppler and pressure broadening into a general theory[376-398] The correlation between the Doppler effect (quantum mechanically, the Doppler shift is just the recoil momentum given by the photon to the radiating system) and pressure broadening is most evident in Dicke narrowing[396] where the recoil momentum is shared with the other surrounding collision partners and this results in a decrease in the effective Doppler shift below that which would have been obtained if all the recoil momentum had been absorbed by the radiating atom. The Doppler profile is narrower than it would have been without the pressure effects since the effect of collisions reduces the effective radiator velocities in Dicke narrowing.

VCC VERSUS TRADITIONAL BROADENING THEORIES

An another very important effect, entirely ignored by all previous pressure broadening theories until recently, is the effect of velocity changing collisions (VCC) on the line

profile. VCC has been a very recent topic that has been studied and observed in transient phenomena and in saturated absorption experiments[684-713]. The concept of VCC requires an entirely different viewpoint in the sense that classical trajectories generally do not have a meaning for the coherences between the initial and final states. Thus one complete description of the VCC is obtained by using a quantum mechanical kinetic density matrix analysis[658-683] as formulated and summarized by Berman[677-683]. This framework yields the classical pressure broadening theories provided certain velocity changing coherence kernels are very narrow compared to the normal dipole coherence velocity distributions. The range of validity and the limits of classical theory which ignores the trajectory effect versus the quantum mechanical picture of VCC will now be considered.

Consider a two level system, levels 1 and 2, where $\omega_1 > \omega_2$, whose interaction potentials are U_1 and U_2 with the corresponding scattering amplitudes f_1 and f_2. Physically, VCC interactions are allowed in the classical picture of broadening for state (level) independent interactions (these are usually the same electronic states, especially for vibrational or rotational transitions in molecules). Then

the wave functions and scattering amplitudes for both levels are approximately equal so that there is little or no pressure shift in these interactions. There would be no discrimination between the upper or lower states since the scattering in levels 1 and 2 would lead to the same scattering angle and trajectory. In this case, the coherence ρ_{12} would be preserved for the elastic scattering and its decay would depend on other quenching, inelastic or phase changing collisions. Thus VCC can reduce the Doppler phase factor **k.v** and result in Dicke narrowing when the mean free path is smaller than the wavelength of the radiation.

Another entirely different example where standard pressure broadening applies is in the case of the single interacting level, where only one level moves, or interacts (ground state with an excited state or metastable state); then the quantum mechanical interference $f_1 f_2^*$ destroys all the contributions to ρ_{12} except in the forward direction and there is no VCC and no Dicke narrowing.

On the other hand, for state dependent collisions ($U_1 \neq U_2$ and $f_1 \neq f_2$ in electronic transitions), traditional pressure broadening would hold if the quantum mechanical interference effects would destructively interfere and 'wash' out any VCC

effects (valid in the limit of many partial waves). In this case (usually in atomic electronic transitions) the coherence ρ_{12} decays right after the collision unless for cases in which $f_1 f_2^*$ has a point of stationary phase. Thus any state selective collision decreases the effect of Dicke narrowing and increases the effect of collisional broadening (elastic collisions have the same broadening or dephasing effect for atoms as inelastic collisions do for molecules).

Traditional pressure broadening theory is valid and VCC does not have to be taken into consideration when the population and coherence kernels, $W_{11}(v' \rightarrow v)$ and $W_{12}(v' \rightarrow v)$, as introduced in the standing wave saturated resonance theory in Chapter 4, can be ignored[683].

For the classical picture (distinct trajectories) to be valid, the uncertainties in the impact parameter b and the scattering angle θ should be

$$\Delta b < b \text{ and } \Delta\theta < \theta$$

From the uncertainty principle

$$\Delta p_t \Delta b \geq \hbar \quad \text{with } \Delta p = \Delta v_t \simeq mv\Delta\theta = \hbar k \Delta\theta$$

so that

$$\theta >> \theta^d = 1/(kb_i) \text{ for the population kernel}$$

$$\theta_2 - \theta_1 >> 1/(kb_w) \text{ for the coherence kernel}$$

where b_i is the characteristic interaction length and b_w is the Weisskopf radius (the impact parameter in which the phase change is unity) and θ^d is the diffractive scattering angle. Thus the distinction between the classical and quantum mechanical descriptions in terms of scattering angles and impact parameters is

$\theta << \theta^d$ and $b > b_i, b_w$ Quantum Mechanical

$\theta >> \theta^d$ and $b < b_i, b_w$ Classical

For distinct trajectories ρ_{12} is destroyed and for diffractive scattering ρ_{12} is not destroyed by velocity changing collisions. From this, both diffractive scattering angles $\simeq$ (deBroglie wavelength/ Weisskopf radius) and classical scattering angles$\simeq$ (Potential/Thermal Energy) exist. In the case of CO_2 these angles are

$\theta^{diff} \simeq \lambda_D / b_w = 5 \times 10^{-3}$ and

$\theta^{class} \simeq V_{QQ}/kT = 1 \times 10^{-2}$

The regime where classical versus quantum mechanical descriptions are necessary can also be seen in terms of how long the dipole coherence lasts after a collision. For quasiclassical scattering, assume the coherence is lost if the individual state wavefunctions are separated by more than the deBroglie wavelength λ. Then since the atom

travels $l=ut$ after a collision, the separation between the two levels is $R=l\theta$; thus, in this semiclassical picture, the dipole will last a time τ after the collision

$$\tau=\lambda/(u\theta) \simeq 10^{-12}/\theta \quad (u\simeq 10^{4}\text{cm/s},\ \lambda\simeq 10^{-8}\text{cm})$$

In the quantum mechanical description, $\theta=\lambda/b_w$ so that

$$\tau=b_w/u\theta=\lambda/u\theta^2= 10^{-12}/\theta^2$$

As it turns out, VCC can have a significant role in the standing wave saturated resonances. VCC can be ignored as long as the 'coherence envelope' λ_{12} is slowly varying compared with the coherence kernel $W_{12}(v'\rightarrow v)$, provided $k\Delta u \ll 1/\tau$, where k is the radiation wave number and τ is the dipole coherence time. Normally $1/\tau\simeq \gamma+\Gamma_{12}$ where γ is the natural linewidth and Γ_{12} is the coherence width due to phase changing collisions. As the pressure increases, the effective time interval in which VCC can influence the dipole transition decreases and the importance of VCC diminishes since any change that will affect the coherence in the shorter time intervals will be more likely to come from inelastic or phase interrupting collisions instead of the small angle velocity changing collisions. Effectively the ratio is

$$\lambda_{12}/W_{12}\simeq (\gamma+\Gamma_{12})/ku\theta$$

The pressure regimes in which VCC can or cannot be ignored will depend on whether this ratio is greater or less than unity. Accordingly, in saturated absorption resonances, where the resonance is due to velocity selection within a homogenous linewidth Γ, there will be two regimes in which VCC can manifest itself[220,660].

Let Γ be the width of the resonance 'hole', and let $\Delta v = u\theta$ be the average velocity jump. If the Doppler shift $ku\theta >> \Gamma$, each velocity jump, on the average, will 'kick' the particle out of the hole and out from interacting with the radiation field. Hence this effect will contribute to the broadening and not to the shift. As the pressure increases such that $ku\theta << \Gamma$, each particle, on the average, will stay in the hole after each velocity change and VCC will have no effect on the broadening or the shift. Thus the broadening γ and shift δ in these two regimes can be represented as follows

$$\gamma = nv\sigma_i$$
$$= \Gamma \qquad ku\theta << \gamma$$
$$\delta = \Delta$$

for the traditional pressure regime and

$$\gamma = nv(\sigma_e+\sigma_i)$$
$$= \Gamma + \nu_R \qquad ku\theta >> \gamma$$
$$\delta = \Delta + \nu_I$$

where Γ and Δ are the traditional pressure broadened width and shift and σ represents the elastic and inelastic broadening cross sections and ν represents the real and imaginary part of the integrated VCC coherence kernels. Note this is the same as the Berman treatment wher the total cross section minus the velocity changing collisions cross section results in the regular phase shift cross section in traditional pressure broadening theory.

This nonlinear dependence of the broadening as a function of pressure has been seen in several saturated resonance experiments including in NH_3[269], CO_2[267,280,647], CH_4[266], I_2[270-272, 275], Xe[268], and He[274]. The nonlinear dependence on the shift, has been seen in CH_4[189,194] where the resolution necessary to see such an effect was available. Other nonlinear shifts have been seen in I_2[200,275] but have not been measured as demonstrably.

PRESSURE SHIFTS

Pressure broadening of emission and absorption lines have

been measured ever since optical spectroscopy became a science. Accordingly, all early lineshape theories concentrated on explaining the pressure dependence of the linewidth. In comparison, there were initially very few pressure shifts measurements and it was only recently that pressure shifts measurements became more common. This is due in part to the fact that any shift measurement had to deal with both the resolution and/or deconvolution associated with the spectrometer or interferometer and the limit in resolution caused by the Doppler response. Even with the advent of the laser, which effectively eliminated the need for any instrumental or apparatus deconvolution, and with the emergence of several Doppler free techniques, the number of pressure shift measurements, in contrast to the numerous linebroadening measurements, are still finite in number (see bibliography[508-551]) and range from the infrared[419-460], microwave[461-495], or Raman[576-590], to the atomic, hyperfine[560-575], or Rydberg shifts[552-559]. In the case of atomic or hyperfine shifts, the power law potential constant $C_6 \simeq -\alpha e^2 \langle r^2 \rangle$ is proportional to the polarizability α and the expectation value $\langle r^2 \rangle$ (mean squared radius of the orbit of the optical electron in that state) of the excited electron. For Rydberg atoms, the 'Fermi' shift is $\omega \simeq n A \hbar / m$ where A is the scattering length

for the valence electron on a perturber atom. Simple classical adiabatic phase shift theory as given by Sobelman [297], gives a simple relation between the (HWHM) broadening γ and the shift δ parameters:

$$\delta/\gamma = \tan(\pi/p-1) = \tan(\pi/5) = 0.726$$

for a normal power law potential $V = \pm C_p R^{-p}$ where p = 6 for the normal Van derWaals dispersion force. Likewise, Hindmarsh[517] developed a more complicated expression for this ratio for the Lennard-Jones (6,12) potential in terms of parameterized functions $B(a)$ and $S(a)$. Correspondingly, there has been quite a bit of work in atomic spectroscopy with the alkali metal and alkali earth versus noble gas perturbers using this simple phase shift theory.

The major impetus of the initial pressure shift measurements revolved around the HCl and HF and/or diatom/atom perturber shifts[419-460] because of several ambiguities and the J dependent oscillatory shifts seen in these interactions. These experimental results were the first real test of ATC theory since lineshifts were highly dependent on the exact phase shifts, potentials, and cutoff parameters used. Basically, any infrared pressure

broadening theory had to explain the following pressure shift features observed in the HCl or HF lineshifts:

1. There exist a dependence of the shift on the vibrational quantum number which appeared to scale with v.
2. There is a definite P and R branch and J dependency of the shift for a given vibrational band.
3. The shift depends on the temperature and the corresponding relative velocity.
4. The shift depends on the nature of the perturber (light, heavy, dipole, etc.) and is related to the polarizability, especially for the noble gas perturbers.

Because of all these observations, the lineshift data pointed out several of the deficiencies inherent in ATC theory. ATC theory is basically a long range, dipolar, perturbative theory using an artificial cutoff impact parameter and a sometimes questionable straight line trajectory model. Because of the ease of its usage and because this theory was the first to have actually used known dispersive or electrostatic forces to compute the lineshape parameters, ATC theory was used and 'altered' (with modified cutoff parameters or with additional anisotropic potential terms including higher ordered terms

in the multipole expansions) to fit the experiment or to obtain 'new' measurements of the dipole or quadrupole moments. As in all linebroadening theories, considering the accuracy of the measurement and the nature of the line broadening calculation, (slowly varying cosine term of the order of unity in the region of closest approach) most calculated line broadening values 'agreed' sufficiently with the experiments, irregardless of the cosine term, to be considered a success. On the other hand, the nature of the shift calculations (rapidly oscillating sine function whose value usually depended on the final few oscillations near the cutoff impact parameter) pointed out the severe faults associated with the older ATC theory. These deficiencies included the noncommutativity of the interaction potential (first realized by Herman[436,442]) which gave rise a contribution to the shift from the imaginary component of the S_2 term and an infinite order treatment of the vibrational dephasing contribution in the S_1 term.

Thus, the contribution to the pressure shift comes from the vibrational dephasing due to the anharmonicities of the active levels which are present in the isotopic potential in the S_1 term, and in the rotational dephasing due to the anisotropic potentials in the S_2 terms. This assumes that

there is no vibrational-rotation coupling and accordingly, explains all 4 observations. On the other hand, the anomalous oscillatory shifts seen in the (Perturber→Active) HF→HCl, HCl→DCl, HF→DF (but not vice versa) arise since the two transitions in resonance differ in energy by an integral of the inerial constant B, ($B_{Perturber} \simeq 2B_{Active}$) such that each successive J gives a different shift contribution[452,543]. In physical terms, shifts result either if there is a net averaged difference between the scalar potentials of the two interacting levels during a collision or if the anisotropic vector potential gives rise to differences in the scattering amplitudes between the two levels.

BIBLIOGRAPHY

Carbon Dioxide

1. A.J.Chedin,J. Mol. Spect. 76 430 (1979)

2. L.S.Rotman,L.D.G.Young, JQSRT 25 505 (1981)

3. D.C.Tyte,Carbon Dioxide Laser, Adv. in Quantum Electronics Vol. 1,pg. 129,Academic Press, 1970

4. F.R.Petersen,E.C.Beaty,C.R.Pollack, J.Mol.Spect. 102 112 (1983)

5. P.K.L.Yin, App. Optics 8 997 (1969)

Anharmonic Force Constant of Carbon Dioxide

6. M.H.Andrade,Silva,G.Amat, J.Mol.Spect. 29 384 (1969)

7. I.Jobard,A.Chedin,J.Mol.Spect. 57 464 (1975)

8. Z.Cihla,A.Chedin,J.Mol.Spect. 40 337 (1971)

9. A.Chedin,Z.Cihla,J.Mol.Spect. 47 542 (1973)

10. M.A.Pariseau,I.Suzuki,J.Overend, JCP 42 2335 (1965)

11. I.Suzuki,J.Mol.Spect. 25 479 (1968)

12. I.Suzuki, Bull. Chem.Soc.Jap. 44 3277 (1971),48 3565 (1975),48 1685 (1975),52 1606 (1979)

13. I.Suzuki,J.Mol.Spect. 80 12 (1980)

14. C.R.Quade, JCP 64 2783 (1976)

15. K.A.Davies,J.Overend, Spectrochem.Acta 32A 1571 (1976)

16. M.L.Grenier-Besson,A.Mahmoudi,J.Phys.(Fr.) 44 923 (1983)

17. K.G.Brown,W.P.Person, JCP 65 2367 (1976)

18. T.V.Gosteminskaya,L.V.Belyavskaya,V.P.Morozov, Ivest. VUZ 7 605 (1980)

19. O.S.VanRoosmalen,A.E.L.Dieperink,F.Iachello,Chem.Phy.Lett. 85 32 (1982)

20. M.Lacy, Mol.Phy. 45 253 (1982)

Fermi Resonance,Early Work

21. H.Nielsen, Rev. Mod. Phy. 23 90 (1951)

22. D.M.Dennison,Rev.Mod.Phy. 12 175 (1940)

23. H.Nielsen,G.Amat,M.Goldsmit, JCP 26 1060 (1957),24 44,838 (1956)

24. S.Maes, J.Mol.Spect. 9 204(1962), Cahiers Phys.14 125 (1960)

25. W.Low, Phy.Rev. 97 1664 (1955)

26. G.Amat,M.Pimbert,J.Mol.Spect. 16 278 (1965)

27. G.Amat,J.Chim.Phy. 64 91 (1967)

28. C.P.Courtoy, Can.J.Phy. 35 608 (1957)

29. C.Chackerian,D.F.Eggers, J.Mol.Spect. 27 59 (1968)

30. H.R.Gordon,T.K.McCubbin, J.Mol.Spect. 19 137 (1966)

Measurements of Fermi Resonances in Different Phases

31. J.F.Bertran, Spectrochem.Acta 39A 119 (1983)

32. Y.Garrabos,R.Tufeu,B.L.Neindre,G.Zalczer,D.Beysens, JCP 72 4637 (1980)

33. C.H.Wang,R.B.Wright,Chem.Phy.Lett. 23 241 (1973), JCP 58 2893 (1973)

34. R.C.Hanson,K.Bachman,Chem.Phy.Lett. 73 338 (1980)

35. H.E.Howard Lock,B.F.Stoicheff,J.Mol.Spect. 37 321 (1971)

Effects of Fermi Resonance

36. S.Montero, JCP 79 4091 (1983)

37. E.L.Sibert,J.T.Hynes,W.R.Reinhart, J.Phy.Chem. 87 2032 (1983)

38. I.Weider,G.B.McCurdy, Phy.Rev.Lett. 16 565 (1966)

39. L.A.Zhigula,T.D.Kolomiitsova,I.V.Pavlushkov,D.N.Shchepkin, Opt.Spect.46 492 (1979)

40. A.P.Galtsev,V.M.Osipov, Opt.Spect. 30 365 (1971)

41. A.A.Likalter, High Temp.Jour.(Russ.) 20 506 (1982)

42. D.Bailly, C.Rossetti, Opt. Comm. 42 323 (1982), J.Mol.Spect. 102 384, 392 (1983)

43. D.C.Clary, Chem.Phy.Lett. 74 454 (1980)

44. V.M.Osipov, Opt. Spect. 46 24 (1979)

45. H.W.Klockner,K.Srinivasan,H.Finsterholzn, H.W.Schrotter, App. Spec.32 401 (1978)

Molecular Properties of CO-2

46. M.Morrison,P.J. Hay, JCP 70 4034 (1979), J.Phy.B 10 L647 (1977)

47. T.E.Gough,B.J.Orr,G.Scoles, J.Mol.Spect. 99 143 (1983)

48. H.Statz,C.L.Tang,G.F.Koster, J. App.Phy. 37 4278 (1966)

49. B.V.Telegin,V.V.Fomin,Opt.Spect. 49 364 (1980)

50. V.F.Brattsev,L.I.Semenova, Opt.Spect. 49 22 (1980)

51. H.Finsterholzl,B.Bunsenges, Phy.Chem. 86 797 (1982)

52. T.D.Kolomiitsova,D.N.Schchepkin, Opt.Spect. 47 167 (1979)

53. I.F.Golovnev,V.G.Sevastyanenko,R.I.Soloukhin, Inzh.Fiz.Journ.36 197 (1979)

Potential Constants of Carbon Dioxide

54. R.T.Pack, JCP 61 2091 (1974),64 1659 (1976)

55. B.J. Jhanevar,W.J.Meath, Chem.Phy. 67 185 (1982)

Intermolecular Potential for Carbon Dioxide

56. T.B.MacRuby,W.A.Steele,B.Berne, JCP 64 1285 (1976)

57. C.S.Murthy,K.Singer,I.R.McDonald, Mol.Phy. 44 135 (1981)

58. R.O.Jones, JCP 79 1885 (1983)

59. J.E.Miller,R.O.Jones,J.Harvey, JCP 79 1874 (1983)

60. S.Cabus,H.Gollisch, J.Phy.B. 15 L265 (1982)

61. A.Hasanein,M.Ferrario,M.Evans, Advs. in Mol.Relax.Interact.Proc. 20 215 (1981)

62. R.M.Roth,R.B.Gerber,M.A.Ratner,J.Phy.Chem. 87 2376 (1983)

Carbon Dioxide + X Collision Models

63. P.M.Agrawal,L.M.Raff, JCP 75 2163 (1981)

64. G.Jolicard,G.Durand,X.Chapuisat, JCP 74 2206 (1981)

65. H.Suzukawa,M.Wolfsberg,D.Thompson, JCP 68 455 (1978)

66. D.Clary, JCP 75 209 (1981), 78 4915 (1983)

67. D.C.Clary,A.D.Depristo, JCP 79 2206 (1983)

68. N.Sathyamurthy,L.M.Raff, JCP 66 2191 (1977)

69. G.Rotzoll,A Lubbert, JCP 71 2275 (1979)

70. C.L.Stroud,L.M.Raff, JCP 72 5479 (1980)

71. H.J.Loesch, Chem.Phy. 18 431 (1976)

72. S.Odiot,J.L.Cantara,S.Fliszar,Chem.Phy.Lett. 71 307 (1980)

73. M.Keil,G.Parker,A.Kupperman,Chem.Phy.Lett. 59 443 (1978)

74. R.Preston,R.T.Pack, JCP 69 2823 (1978), 66 2480 (1977)

75. G. Parker,R.Snow,R.T.Pack, JCP 64 1668 (1976)

Radiation Trapping

76. M.A.Kovacs,A.Javan, JCP 50 4111 (1969)

77. C.K.Rhodes,M.J.Kelly,A.Javan, JCP 48 5730 (1968)

78. R.K.Huddleston,G.T.Fujimoto,E.Weitz, JCP 76 3839 (1982)

79. T. Holstein, Phy.Rev. 72 1212 (1947), 83 1159 (1951)

80. I.M.Beterov,Y.A.Matyugin,S.G.Rautian,V.P.Chebotayev, JETP 31 668 (1970), Opt.Spect.28 191 (1969)

81. M.I.Dyakonov,V.I.Perel, JETP 21 227 (1965), 20 997 (1965), 31 585 (1970)

82. V.I.Perel,I.V.Rogova, JETP 34 965 (1972)

Rotational,Vibrational Relaxation in CO-2

83. R.R.Jacobs,S.J.Thomas,K,Pettipiece, IEEE JQE 10 480 (1974)

84. R.R.Jacob,K.J.Pettipiece,S.J.Thomas, Phy.Rev. 11 54 (1975)

85. I.Burak,L.A.Gamss, JCP 65 5335 (1976)

86. I.Burak,Y.Noter,A.Szoke, IEEE JQE 9 541 (1973)

87. K.Bulthius,B.P.Ponsen, Chem.Phy.Lett. 21 415 (1973)

88. J.Stephenson,C.B.Moore, JCP 56 1295 (1972)

89. R.Jacobs,K.Pettipiece,S.J.Thomas, App.Phy.Lett. 24 375 (1974)

90. G.Jolicard,L.Galatry, JCP 63 2787 (1975)

91. D.C.Dumitras,St.Cerc.Fiz. 28 369 (1976) ,Bucharest

92. V.V.Tuchin,B.A.Kuzyakov,Sov.JQE 11 791 (1981)

93. R.K.Huddleston,E.Weitz, Chem.Phy.Lett. 83 174 (1981)

94. A.A.Vostrikov,S.G.Mironov,A.K.Rebrov,B.E.Semyachkin, Sov.JQE 11 817 (1981)

95. K.Herzfeld, JCP 47 743 (1967)

96. R.C.Sepucha, Chem.Phys.Lett. 31 75 (1975)

97. A.S.Biryukov,V.K.Konyukhov,A.I.Lukovnikov,RI.Serikov, JETP 39 610 (1974)

98. V.P.Kabashnikov,J.App.Spect. 17 51 (1972)

99. S.M.Gladkov,M.G.Karimov,N.I.Koroteev, JETP Lett. 35 470 (1982)

100. I.M.Bertel,V.O.Pertukhov,A.S.Solodukhin,S.A.Trushin, V.V.Churakov, Sov.Phy.Tech.Phy.27 1429 (1982)

101. L.O.Hocker,M.A.Kovacs,C.Rhodes,G.W.Flynn,A.Javan, Phy.Rev.Lett.17 233 (1966)

102. C.K.Rhodes,M.J.Kelly,A.Javan, JCP 48 5730 (1968)

103. C.Dang,J.Reid,B.K.Garside, App. Phys. B 31 163 (1983)

104. S.M.Gladkov,M.B.Karimov,N.Koroteev, JETP Lett. 35 470 (1982)

105. R.J.Mawhorter,M.Fink,B.T.Archer, JCP 79 170 (1983)

Cross Relaxation Effects

106. V.S.Letokhov,B.D.Pavlik, JETP 37 408 (1973)

107. T.Kan,G.Wolga, IEEE JQE 7 141 (1971)

108. P.Smith, IEEE JQE 8 704 (1972)

109. H.Granek, IEEE JQE 10 320 (1974)

110. J.S.Goela,T.F.Morse, IEEE JQE 12 281 (1976)

111. Y.U.Brzhazovsky,V.P.Chebotayev,L.S.Vasilenko, IEEE JQE 5 146 (1969), JETP 28 1108 (1969)

112. P.W.Smith,T.Hansch, Phy.Rev.Lett. 26 740 (1971)

113. A.V.Otieno, Opt.Comm. 26 207 (1978)

114. H.Granek,C.Freed,H.Haus, IEEE JQE 8 404 (1972)

115. C.P.Christiansen,C.Freed,H.Haus, IEEE JQE 5 276 (1969)

Laser Design and Frequency Measurements

116. C. Freed, IEEE JQE 4 404 (1968)

117. C.Freed, Designs and Experiments Relating to Stable Gas Lasers, Lincoln Lab Tech. Note 1973-14 (1973)

118. C.Freed,'Design and Experiments relating to Stable Lasers', in Proc.Frequency Standards and Metrology Seminar, Univ.Lavel, Quebec P.Q.Canada, Sept.1, 1971, pg.226-261

119. C.Freed,A.Javan, App.Phy.Lett. 17 53 (1970)

120. C.Freed,R.G.O'Donnell,A.H.Ross,J.Mol.Spect. 49 439 (1974), IEEE Inst.Meas.IM-25 431 (1976)

121. C.Freed,R.G.O'Donnell, Metrologia 13 151 (1977)

122. C.Freed,L.C.Bradley,R.G.O'Donnell,IEEE JQE 16 1195 (1980) 276 (1969)

123. C.Borde,L.Henry,IEEE JQE 4 874 (1968)

CO-2 Lasers Stabilized by SF-6 and OsO-4

124. O.N.Kompanets,A.R.Kukudzhanov,V.S.Letokhov,E.L.Mikhailov, JETP35 687 (1973), Sov. JQE 3 293 (1974)

125. N.G.Basov,O.Kompanets,V.S.Letokhov,V.Nitkitin, JETP 32 214 (1971), JETP Lett.9 345 (1969)

126. E.N.Bazarov,G.A.Gerasimov,V.P.Gubin,A.I.Sazonov, N.I.Starostin,V.V.Fomin, Sov. JQE 10 1550 (1980), Radioelectronics and QE 24 79 (1981)

127. E.N.Bazarov.G.Gerasimov,V.P.Gubin,Posudin, Radioelectronics 20 32 (1977), 24 63 (1981)

128. O.N.Kompanets,A.R.Kukudzhanov,E.Mikhailov, Sov. JQE 7 1150 (1977), JETP 42 15 (1975)

129. V.M.Gusev,O.N.Kompanets,A.R.Kukudzhanov,V.S.Letokhov, E.L.Mikhailov, Sov. JQE 4 1370 (1975)

130. D.Souihac,A.Gundjian, App.Opt. 21 1478 (1982)

131. A.Clairon,L.Henry, C.R.Acad.Sc.Part. B 279B 419 (1974)

Speed of Light,Laser Frequency Synthesis

132. T.Blaney, C.C.Bradley.G.J.Edwards,B.W.Jolliffe, D.J.E.Knight, W.R.Rowley,K.C.Shotton,P.T.Woods, Proc. Roy.Soc.Lond.A 355 61-88,89-114 (1977)

133. J.J.Jimenez,F.R.Petersen, Infrared Phys. 17 541 (1977)

134. D.J.Knight, J.Phys.(Fr.) C8, 42 C8-495 (1981)

Absolute Measurements

135. K.M.Evanson,J.S.Wells,F.R.Petersen,B.L.Danielson,G.W.Gay, App.Phy.Lett.22 192 (1973)

136. T.G.Blaney,C.C.Bradley,G.J.JEdwards,D.J.Knight, Phys.Lett.A 43A 471 (1973)

137. D.A.Jennings,F.R.Petersen,K.M.Evenson, App.Phy.Lett. 26 510 (1975)

138. T.G.Blaney,G.J.Edwards,B.W.Jolliffe,D.J.Knight,P.T.Woods, J.Phy.D9 1323 (1976), Nature 254 584 (1975)

139. B.G.Whitford,D.S.Smith,Opt.Comm. 20 280 (1977)

140. B.G.Whitford, Opt. Comm. 31 363 (1979), IEEE Inst.Meas.29 168 (1980)

141. D.A.Jennings,F.R.Petersen,K.M.Evenson,Opt.Lett. 4 129 (1979)

142. H.P.Layer,W.R.C.Rowley,B.R.Marx, Opt.Lett. 6 188 (1981)

143. F.R.Petersen,K.M.Evenson,D.A.Jennings,A.Scalabrin,IEEE JQE 16 319 (1980)

144. D.J.Knight,G.J.Edwards,P.R.Pearce,N.R.Cross, IEEE Inst.Meas. 29 257 (1980)

145. Y.S.Domnin,N.B.Kosheljaevsky,V.M.Tatarenkov,P.S.Skunjatsky, IEEE Inst.Meas.29 264 (1980)

146. A.Clairon,B.Dahmani,J.Rutman, IEEE Inst.Meas. 29 268 (1980)

147. A.Clairon,A.VanLerberghe,C.Salomon,M.Ouhayoun,C.Borde, Opt.Comm. 35 368 (1980), J.Phys.(Fr.) C8 42 C8-127 (1981)

148. V.P.Chebotayev,V.G.Goldort,V.M.Klementyev,M.V.Nikitin, B.Timchenko,V.F.Zakharyash, App.Phys.B29 63 (1982)

149. Y.S.Domnin,N.B.Kosheljaevsky,O.N.Kompanets,A.R.Kukudzhanov, JETP Lett.30 249 (1979)

150. Y.S.Domnin,N.B.Kosheljaevsky,V.M.Tatrenko, JETP Lett. 30 253 (1979)

151. C.R.Pollack,F.R.Petersen,D.A.Jenning,J.S.Wells,A.G.Maki, J.Mol.Spect.99 357 (1983)

152. Y.S.Domnin,N.B.Kosheljaevsky,V.M.Tatrenko,P.S.Skunjatsky, JETP Lett. 34 167 (1981), Sov.JQE 10 116 (1980)

153. K.M.Baird, Phy.Today, January, 1983,pg. 52

154. C.R.Pollack,D.A.Jenning,F.R.Petersen,J.S.Wells, R.E.Drullinger,E.L.Beaty,K.M.Evenson, Opt.Lett.8 133 (1983)

155. D.A.Jenning,C.R.Pollack,F.R.Petersen,R.E.Drullinger, K.M.Evensen,J.S.Wells,J.L.Hall, Opt.Lett.8 136 (1983)

156. F.R.Petersen,E.C.Beaty,C.R.Pollack, J.Mol.Spect. 102 112 (1983)

Reviews and Comparisons of Stabilized Lasers

157. A.Brillet,P.Cerez,J.Phys.(Fr.) C8 42 C8-73 (1981)

158. B.W.Jolliffe,G.Kramer,J.M.Chartier, IEEE Inst.Meas. 25 447 (1976)

159. H.P.Layer,W.R.Rowley,B.Marx, Opt.Lett. 6 188 (1981)

160. K. Shimoda, Jap.J.App.Phys. 12 1222 (1973)

161. N.B.Koshelyaeviskii,A.Oboukhov,V.M.Tatarenkov,A.N.Titov, J.Chartier,R.Felder,Metrol.17 3 (1981)

162. Y.Zacharenko,A.Kotkov,N.Melnikov,J-M.Chartier,R.Felder, Metrolog. 17 81 (1981)

163. J.Blaba,J.Smydke,J.M.Chartier,M.Glaser,Metrolog. 19 73 (1983)

164. I.M.Chartier, IEEE Inst.Meas. 32 81 (1983)

165. V.P.Chebotayev, Sov. JQE 8 1130 (1978)

166. V.P.Kaprolov,G.M.Malyshev,P.A.Pavlov,V.E.Privalov, Y.Fofanov, Opt.Spect. 50 34 (1981)

Ultra-Stable and Reproducibility

167. S.N.Bagaev,E.V.Baklanov,A.Titov,V.P.Chebotayev, JETP Lett. 20 130 (1974), App.Phys.7 71 (1975)

168. M.V.Danilieko,A.M.Fal,V.P.Fedin,M.T.Shpak,L.P.Yatsenko, Sov. JQE 12 1307 (1982)

169. P.E.Pak,V.E.Privalov,Ya Fofanov, Opt. Spect. 51 5 (1981)

170. S.N.Bagaev,A.S.Dychkov,V.P.Chebotayev, Sov.Tech.Phy.Lett. 5 240 (1979)

171. P.Cerez,A.Brillet,C.Mann, Rev.App.Phys.(Fr.) 14 347 (1979)

172. V.M.Klementev,V.P.Chebotayev, Sov.Tech.Phy.Lett. 5 427 (1979)

173. V.P.Kapralov,V.E.Privalov,E.G.Chulyaev, Sov.J.Q.E. 10 1062 (1980)

174. S.N.Bagaev,L.S.Vasilenko,V.G.Goldort,A.K.Dmitriev, A.S.Dychkov,Sov. JQE 7 665 (1977), Sov.Tech.Phy.Lett.3 80 (1977)

175. A.Brillet,P.Cerez,S.Hajdukovic,F.Hartmann, Opt.Comm. 17 336 (1976)

176. N.B.Koshelyaevskii,Y.M.Malyshev,S.N.Ovchinnikov, Y.G.Rastorguev,V.M.Tatarenkov,A.N.Titov, Sov.JQE 9 288 (1979)

177. Y.M.Malyshev,S.N.Ovchinnikov,Y.G.Rastorguev,V.M.Tatarenkov, A.N.Titov, Sov.JQE 10 376(1980)

Shifts in HeNe Lasers

178. R.L.Barger,J.L.Hall, Phy.Rev.Lett 22 4 (1969)

179. K.Shimoda,Jap.J.App.Phy. 12 1393 (1973)

180. M.Ohi, Jap.J.App.Phy. 12 1377 (1973)

181. S.N.Bagaev,L.S.Vasilenko,Y.A.Matyugin,V.M.Klementev, B.Troshin,V.P.Chebotayev, Opt.Spec.32 422 (1972)

182. N.B.Koshelyaevskii,V.M.Tatarenkov,A.N.Titov, Sov.JQE 6 1244 (1976)

183. G.A.Mikhnenko,E.D.Protsenko,E.A.Sedoi, Opt.Spect. 32 425 (1972)

184. S.N.Bagaev,Y.D.Kolomnikov,V.Lisitsyn,V.P.Chebotayev, IEEE JQE 4 868 (1968)

185. S.N.Bagaev,E.V.Baklanov,V.P.Chebotayev, JETP Lett. 16 9 (1972)

186. S.N.Bagaev,V.P.Chebotayev, JETP Lett. 16 433 (1972)

187. S.N.Bagaev,A.S.Dychkov,V.P.Chebotayev, JETP Lett. 29 519 (1979)

188. S.N.Bagaev,A.S.Dychkov,A.K.Dmitriev,V.P.Chebotayev, JETP 52 586 (1980)

189. S.N.Bagaev,V.P.Chebotayev, JETP Lett. 16 243 (1972)

190. H.Goldring,A.Szoke,E.Zasmir,A.Ben-Reuven, JCP 49 4253 (1968)

191. N.D.Orlova,L.P.Platonova,JETP Lett. 31 8 (1980)

192. M.A.Gubin,V.V.Nikitin,V.N.Petrovskii,E.D.Protsenko, D.A.Tyurikov,L.P.Yatsenko, Sov.JQE 9 34 (1979)

193. S.N.Bagaev,V.Chebotayev,A.S.Dychkov,S.V.Maltsev, J.Phy.(Fr.) C8 42 C8-21 (1981)

194. S.N.Bagaev,S.V.Maltsev,V.P.Chebotayev, JETP Lett. 37 590 (1983)

195. W.G.Schweitzer,E.G.Kessler,R.D.Deslattes,H.P.Layer, J.R.Whetstone, App.Opt. 12 2927 (1973)

196. G.Flory,M.Broyer,J.Vigue,J.C.Lehman, Rev.Phy.App.(Fr.) 12 901 (1977)

197. P.Cerez,A.Brillet,F.Hartmann, IEEE Tran.Inst.Meas. 23 526 (1974)

198. A.J.Wallard, IEEE Tran.Inst.Meas. 23 532 (1974)

199. P.Cerez,A.Brillet,S.Hadjukovic,N.Man, Opt.Com. 21 332 (1977)

200. M.Glaser,Metrolog. 18 53 (1982), 'Nonlinear Frequency Shift', Conf. on Prec. Electomagnetic Measurements, June 28, 1982, Boulder Colorado

201. A.L.Bloom,D.L.Wright, App.Opt. 5 1528 (1966)

202. A.D.White, App.Phy.Lett. 10 24 (1967)

203. T.P.Sosnowski,W.B.Johnson, IEEE JQE 5 151 (1969)

204. V.N.Lisitsyn,V.P.Chebotayev, JETP 27 227 (1968)

205. I.M.Tkhek-De,A.P.Kazantsev,S.G.Rautian,E.B.Saprykin, A.M.Shalagin, Sov.JQE 4 234 (1974)

206. I.V.Dimitrieva,V.A.Kondrateva,E.N.Kotlikov,V.I.Tokarev, A.N.Khvostov, Opt.Spect.54 358 (1983)

207. F.Spieweck, IEEE Tran.Inst.Meas. 27 398 (1978), 29 361 (1980) (Ar+ and I-2 cell)

Recoil Effects

208. E.V.Baklanov, Opt.Spect. 38 352 (1975), Opt.Comm.13 54 (1975)

209. J.Shirley, J.Phys.B. 13 1537 (1980)

210. J.Shirley,S.Stenholm, J.Phy.A. 10 613 (1977)

211. E.A.Titov, Sov. JQE 6 242 (1976)

212. C.G.Aminoff,S.Stenholm,Phy.Lett.A 48 483 (1974)

Quadratic,Field,Transit Effects

213. E.V.Baklanov,B.Y.Dubetskii, Sov. JQE 5 1108 (1976)

214. N.B.Koshelyaevskii,V.M.Tatarenkov,A.N.Titov, Sov.JQE 6 222 (1976), JETP Lett., 15 326 (1972)

215. E.V.Baklanov,B.Y.Dubetskii,V.M.Semibalamut,E.A.Titov, Sov.JQE 5 1374 (1975)

216. E.A.Titov, Sov.JQE 5 1207 (1976)

217. E.B.Baklanov, Opt.Spect. 38 12,352 (1975)

218. S.N.Bagaev,L.S.Vasilenko,A.K.Dmitriev,M.N.Skvortsov, V.P.Chebotayev,JETP Lett.23 360 (1976)

219. V.M.Semibalamut,E.A.Titov, Sov. JQE 8 847 (1978)

220. V.A.Alekseev ,L.P.Yatsenko, JETP Lett. 29 389 (1979), JETP 50 1083(1979), J.Phy.(Fr.) C8 42 C8-29 (1981)

221. J.E.Thomas,M.J.Kelly,J.P.Monchalin,N.Kurnit,A.Javan, Phy.Rev.15 2356 (1977)

222. J.E.Thomas,W.Quivers, Phy.Rev.A 22 2115 (1980)

223. C.J.Borde,J.Hall,C.Kunasz,D.G.Hummer, Phy.Rev.A 14 236 (1976)

224. S.G.Rautian,G.I.Smirnov, Phy.Lett. 70A 387 (1979)

225. S.N.Bagaev,A.S.Dychkov,V.P.Chebotayev, JETP Lett. 29 570 (1979)

226. E.V.Baklanov,M.V.Belyaev, Opt. Spect. 49 354 (1980)

Hyperfine, Zeeman effects

227. Y.Baklanov,M.V.Belyayev, App.Phy. 14 389 (1977)

228. E.V.Baklanov,E.A.Titov, Sov. JQE 5 1029 (1976), Sov. JQE 5 967 (1976)

229. V.A.Alekseev,A.V.Malyugin, Sov. JQE 6 1075 (1977)

230. S.N.Bagaev,L.S.Vasilenko,V.G.Goldort,A.S.Dychkov, V.P.Chobotayev,App.Phy.13 291 (1977)

231. E.N.Kotlikov,V.I.Tokarev, Opt.Spect. 47 13 (1979)

232. S.N.Bagaev,M.V.Belyaev,A.K.Dmitriev,V.P.Chebotayev, App.Phys. 24 261 (1981), JETP Lett.32 661 (1980)

Experimental Observations

233. J.Hall,C.Borde, Phy.Rev.Lett. 30 1101 (1973)

234. J.Hall,C.Borde,K.Uehara, Phy.Rev.Lett. 37 1339 (1976)

235. J.Hall,C.Borde, App.Phy.Lett. 29 788 (1976)

236. K. Uehara,J.L.Hall, Opt.Lett. of 4 214 (1979)

237. E.E.Uzgiris,J.L.Hall,R.L.Barger, Phy.Rev.Lett. 26 289 (1971)

238. C.Borde,G.Camy,B.Decomps, Phy.Rev.A 20 254 (1979)

Experimental Observed Asymmetry

239. A.Szoke,A.Javan, Phy.Rev.Lett. 10 521 (1963), Phy. Rev.145 137 (1966)

240. P.Cerez,A.Brillet,S.Hajdukovic,N,Man, Opt.Comm. 21 332 (1977)

241. P.Kumar,G.O.Brink,S.Spence,H.S.Lakkaraju, Opt.Comm. 32 129 (1980)

242. A.Titov, Opt.Comm. 43 419 (1982)

243. A.LeFloch,R.LeNaour,G.Steph, Phy.Rev.Lett. 39 1611 (1977)

244. K.Shimoda,A.Javan ,J.App.Phy. 36 718 (1965)

245. C.Freed,H.Haus, IEEE JQE 9 219 (1973)

246. S.P.Koutsoyannis,K.Karamchati, IEEE JQE 4 912 (1968)

247. S.Rautian, I.Sobelman, IEEE JQE 2 446 (1966)

248. B.W.Peuse,M.G.Prentiss,S.Ezekiel, Phy.Rev.Lett. 49 269 (1982), Opt.Lett. 8 154 (1983)

Analysis of Asymmetry

249. A.N.Titov, Sov. JQE 11 1242 (1981)

250. A.LeFloch,R.LeNaour,J.M.Lenormand,J.P.Tache, Phy.Rev.Lett. 45 544 (1980) J Physique Lett.43 L-493 (1982)

251. A.LeFloch,J.Lenormand,G.Jezequel,R.LeNour, Opt.Lett. 6 48 (1981)

252. A.LeFloch,J.Lenormand,R.LeNaour,P.Brun, IEEE JQE 19 1474 (1983)

253. B.Couillard,A.Ducasse, Phy.Rev.Lett. 35 1276 (1975)

254. L.W.Casperson,A.Yariv, App.Opt. 11 462 (1972)

255. P.Cerez,A.Brillet, Metrol. 13 29 (1977)

Modulation Distortion and 3F Analysis

256. A.J.Wallard, J.Phy.E. 5 926 (1972)

257. A.M.Russell,D.A.Torchin, Rev. Sci.Instr. 33 42 (1962)

258. G.R.Hanes,K.M.Baird,J.DeRemigis, App.Opt. 12 1600 (1973)

259. D.P.Blair, App. Phy.Lett. 25 71 (1974)

260. G.Kramer,C.O.Weiss,J.Helmcke, Z.Naturforsch A 30 1128 (1975)

261. A.N.Vlasov,V.V.Teselkin, Sov.JQE 6 704 (1976)

262. B.P.J.vanOorshot, J.Phy.D. 10 1117 (1977)

263. R.LeNaour,A.LeFloch,G.Steph, Opt. and QE 10 119 (1978), App. Opt. 15 2673 (1976)

264. E.N.Bazarov,G.A.Gerasimov,V.P.Gubin,N.N.Starostin, V.V.Fomin, Sov. JQE11 916 (1981)

265. A.N.Vlasov,V.V.Teselkin, Sov. JQE 6 704 (1976)

Nonlinear Broadening

266. C.N.Bagaev,E.V.Baklanov,V.P.Chebotayev, JETP Lett. 16 9 (1972)

267. T.W.Meyer,C.K.Rhodes,H.A.Haus, Phy.Rev.A 12 1993 (1975)

268. P.Cahuzac,O.Robaux,R.Vetter, J.Phy.B 9 3165 (1976)

269. A.T.Mattick,N.A.Kurnit,A.Javan,Chem.Phy.Lett. 35 176 (1976)

270. C.J.Borde in Laser Spect.III,ed.J.L.Hall,J.L.Carlsten, Springer-Verlag, NY 1977, p. 121

271. I.Colomb,M.Dumont, Opt.Comm. 21 143 (1977)

272. C.N.Man,P.Cerez,A.Brillet,F.Hartman,J.Phy.Lett.(Fr.) 38 287 (1977)

273. J.L.LeGouet, J.Phy.B 11 3001 (1978)

274. P.Cahuzac, P.R.Damaschini, Opt.Comm. 22 251 (1980)

275. C.J.Borde,G.Camps,B.Decomps,J.D.Descombes, J.Phy.(Fr.) 42 1393 (1981)

276. M.V.Belyayev,V.P.Chebotayev,M.N.Skvortsov,L.S.Vasilenko, App.Phy.B 26 67 (1981)

277. R.Damaschini,J.Verges, Phy.Lett. 87A 27 (1981)

278. R.Roy,D.S.Elliot,D.Meschede,F.M.Pipkin,S.J.Smith, Chem.Phy.Lett. 93 603 (1982)

279. J.E.Thomas, MIT PhD Thesis, Physics Jan. 1979

280. M.J.Kelly, MIT PhD Thesis, Physics Feb. 1976

Lineshape References

281. A.A.Michelson, Astrophy.J. 2 251 (1895), H.A.Lorentz,K.Akad.(Neth.) Proc. 8 591 (1906)

282. W. Lenz , Z.Phy. 25 299 (1924),80 423 (1933), V.Weisskopf,Z.Phys. 75 287 (1932), 77 398 (1932)

283. E.Lindholm, Ark. Fys.A 32 1 (1945)

284. H.M.Foley, Phy.Rev. 69 616 (1946)

285. P.W.Anderson, Phy.Rev. 76 647 (1949), 86 809 (1952)

286. P.W.Anderson,T.D.Talman,Bell System,Tech.Publication 3117 (1956) Murray Hill, NJ

287. H.Margeneau, Rev. Mod.Phys. 11 1 (1939)

288. R.G.Breene, Rev.Mod.Phys. 29 94 (1957),"Shift and Shape of Spectral Lines", (1961) Pergamon Press, "Theory of Spectral Line Shape", J.Wiley (1981)

289. S.Y.Chen,M.Takeo, Rev. Mod.Phys. 26 20 (1957)

290. J. Cooper, Rev. Mod. Phys. 39 167 (1967)

291. J.Cooper, Line Broadening Lectures in Theoretical Physics,Vol. 11 p.241 (1968) Gordon and Breach, NY, Ed. by K.T.Mahanthappa,W.E.Brittin

292. M.Baranger, Phy.Rev. 111 481, 494 (1958), 112 885 (1958)

293. A.Jablonski, Phy.Rev. 68 78 (1945)

294. G.Birnbaum,Microwave Pressure Broadening and its Applications to Intermolecular Forces, Adv. In Chem. Phys., Vol. 12, 487 (1967)

295. H.Van Regemorter, Spectral Line Broadening, Atoms and Molecules in Astrophysics, p.85 (1972) ed. T.R.Carson,M.J.Roberts, Acad.Press.

296. H.Rabitz, Rotational and Rotation-Vibrational Pressure Broadened Spectral Lineshapes, Ann. Rev. of Phy.Chem.25 155 (1974)

297. I.I.Sobelman, "Introduction to Theory of Atomic Spectra", Pergamon Press, 1972

298. R.Friedberg,S.R.Hartmann, Phy.Rep.C 7 101 (1973)

299. A.Ben-Reuven, Adv.At.Mol.Phy. 11 201 (1969)

300. W.Behmenberg,Lineshapes,in Progress in Atomic Spectroscopy,ed. W.Hanle, H.Kleinpoppen,p.1187 (1972), Plenum Press, R.Schuller,W.Behmenberg, Phy.Rep.C 12 273 (1974)

301. E.L.Lewis, Phy. Rep.C 58 1 (1980)

302. A.Ben-Reuven, Adv. Chem.Phys. 33 235 (1975)

303. M.Baranger,Spectral Line Broadening in Plasmas, Atomic and Molecular Process, ed. D.R.Bates,p.493 (1962) Acad.Press.

304. W.R.Hindmarsh,J.M.Farr, Collisional Broadening of Spectral Lines, Prog. in Quant.Elect.2 143 (1972)

305. I.I.Sobelman,L.A.Vainshtein,E.A.Yukov,"Excitiation of Atoms and Broadening of Spectral Lines",Springer Verlag, NY (1981)

306. N.Allard,J.Kielkopf, Rev. Mod.Phy. 54 103 (1983)

Reviews of Nonlinear Spectroscopy

307. V.P.Chebotayev,L.S.Vasilenko, Prog. Quant.Elect. 8 79 (1983)

308. V.P.Chebotayev, Superhigh Resolution Spectroscopy, in Lasers and Applications, Ed.W.O.Guimaraes,C.T.Lin,A.Mooradian, Springer Verlag Vol 26, p. 105 (1981)

309. I.M.Beterov, R.I.Sokolovskii,Sov.Phy. Usp. 16 339 (1973)

310. V.P.Chebotayev,V.S.Letokhov, Prog. Quant.Elect. 4 111 (1975), "Nonlinear Laser Spectroscopy", Springer Verlag (1977)

311. K.Shimoda,Editor, "High Resolution Laser Spectroscopy", Spring Verlag (1976)

312. V.Letokhov,V.P.Chebotayev, Sov.Phy.Usp. 17 467 (1975)

313. J.Hall,The Lineshape Problem in Laser Saturated Molecular Absorption, Lectures in Theoretical Physics, Vol 12A,161 (1971),Ed. K.T.Mahanthappa, W.E.Brittin, Gordon and Breach NY

314. S.N.Bagaev,'Spectroscopic Studies into Elastic Scattering of Excited Particles', pg. 222, Laser Spectroscopy IV, Springer Verlag NY,1981

315. S.Stenholm, Phy.Rep.C 43 151 (1978)

316. H.Paul, Fortschritte der Physik 22 1 (1974)

317. M.Sargent III,Phy.Rep.C 43 223 (1978)

318. S.Stenholm, Prog. Quant.Elect. 1 189 (1971)

319. P.R.Berman,T.W.Mossberg,S.R.Hartman, Phy.Rev. 25 2550 (1982)

320. H.Greenstein, Phy.Rev. 175 438 (1968), J.App.Phy.43 1732 (1972), W.Culshaw, Phy.Rev. 164 329 (1967)

321. J.Shirley, Phy.Rev.A 8 347 (1973)

322. S.Stenholm, Phy.Rev.A 2 2089 (1970)

323. S.Haroche,F.Hartmann,Phy.Rev.A 6 1280 (1972)

324. E.V.Baklanov,V.P.Chebotayev, JETP 33 300 (1971),34 490 (1972),35 287 (1972)

325. L.Klein,M.Biraud,A.Ben-Reuven, Phy.Rev.A 16 289 (1977)

326. Proc.of Internat.School of Physics,Course LXIV, Nonlinear Spectroscopy, ed. N.Bloembergen, North Holland Publish., Amsterdam, 1977

327. V.S.Letokhov,B.D.Pavlik, Sov.JQE 1 36 (1971)

328. H.K.Holt, Phy.Rev.Lett. 29 1138 (1972), Phy.Rev.A2 233 (1970)

Collisional Redistribution

329. A.Omont,E.W.Smith,J.Cooper,Astrophy.J. 175 185 (1972)

330. K.Burnett,J.Cooper, Phy.Rev.A 22 2005,2022,2044 (1980)

331. G.Nienhuis,F.Schuller,Physica 92C 397 (1977)

332. J.L.Carlsten,A.Szoke,M.G.Raymer, Phy.Rev.A 15 1029 (1977)

333. G.Nienhuis, J.Phy.B 14 3117 (1981), J.Phy.B15 535 (1982)

334. H.F.Arnoldus,G.Nienhuis, J.Phy.B 16 2325 (1983)

335. K.Burnett,J.Cooper,P.D.Kleiber,A.Ben-Reuven, Phy.Rev.A 25 1345 (1982)

336. S.Reynaud,C.Cohen-Tannoudji, J.Phys.(Fr.) 43 1021 (1982)

337. G.Nienhuis, Comm.in At.Mol.Phy. 11 223 (1982)

338. P.D.Kleiver,J.Cooper,K.Burnett,C.V.Kunasz,M.G.Raymer, Phy.Rev.A 27 291 (1983)

339. K.Burnett, Comm.in At.Mol.Phy. 13 179 (1983)

340. P.R.Liao,J.E.Bjorkholm,P.R.Berman, Phy.Rev.A 20 1489 (1979)

Unified Theory

341. P.W.Anderson,J.D.Talman, Bell System Tech. Pub. No. 3117 29, Murray Hill NJ,(1956)

342. E.W.Smith,J.Cooper,L.Roszman, JQSRT 13 1523 (1973)

343. N.F.Allard,S.Sahal-Brechot,Y.G.Biraud,J.Phy.B 7 2158 (1974)

344. Y.Rabin,S.Mukamel,J.Phy.B 12 L-331 (1980)

345. F.Futrelle, Phy.Rev.A 5 2162 (1972)

346. J.Szudy,W.E.Baylis, JQSRT 15 641 (1975), 17 681 (1977)

347. J.Szudy, Acta.Phy.Pol. A 54 261, 841 (1978)

348. R.Lee, J.Phy.B 4 1640 (1971)

349. N.F.Allard,Y.G.Biraud, J.Phy.(Fr.) 44 935 (1983)

350. F.Schuller,G.Nienhuis, JQSRT 28 355 (1982)

351. J.Kielkopf J.Phy.B 9 1601 (1976)

352. A.Royer, J.Math.Phy. 24 380 (1983), Phy.Rev.A 22 1625 (1980)

CC thru IOS Theories

353. D.J.Kouri,D.F.Fitz, J.Phy.Chem. 86 2224 (1982)

354. A.S.Dickinson, Computer Phys.Comm. 17 51 (1979)

355. Atomic and Molecular Collision Theory, ed. R.B.Bernstein Plenum, NY 1979

356. T.A.Brunner,D.Pritchard,Dynamics of the Excited State,p.589 Ed.K.P.Lavley, J.Wiley, 1982

357. Franco A.Gianturco,The Transfer of Molecular Energies by Collisions, Lecture Note in Chemistry 11. Springer Verlag, 1979

358. R.Goldflam,S.Green,D.J.Kouri, JCP 67 4149 (1977)

359. G.Parker,R.T.Pack, JCP 68 1585 (1978)

360. S.Green, JCP 70 4686 (1979)

361. A.E.DePristo,H.Rabitz, JCP 69 902 (1978), Chem. Phy., 44 171 (1979)

362. V.Khare,D.J.Kouri,R.T.Pack, JCP 69 4419 (1978)

363. V.Khare,D.J.Kouri,D.K.Hoffman, JCP 74 2275 (1981)

364. R.J.Bieniek, JCP 73 851 (1980)

365. J.Jellinek,E.Pollack,JCP 78 3014 (1983)

366. G.A.Pfeffer,D.Secrest, JCP 78 3052 (1983)

367. B.Chang,L.Eno,H.Rabitz, JCP 73 820 (1980), 78 3027,4477 (1983)

ECS and Quantal Theories

368. A.E.DePristo, JCP 73 2145 (1980),74 36 (1981),74 5037 (1981)

369. A.DePristo,S.D.Augustin,R.Ramaswany,H.Rabitz, JCP 71 850 (1979)

370. R.J.Cross, JCP 76 931 (1981)

371. G.Jolicard,J.Bonamy, JCP 79 1248 (1983)

372. R.J.Cross, JCP 79 1272 (1983), 76 931 (1982), 77 1810 (11982)

373. L.Bonamy,P.N.M.Hoang, JCP 78 1673 (1983)

374. W.Miller,S.Shi, JCP 75 2258 (1981)

375. C.O.Trindle,K.H.Illinger, JCP 48 4415, 4427 (1968)

Combined Doppler and Pressure Broadening

376. J.Gerstein,H.Foley, JOSA 58 933 (1968)

377. L.Galatry, Phy.Rev. 122 1218 (1961)

378. S.G.Rautian,I.I. Sobelman, Sov.Phy.Usp. 9 701 (1967)

379. D.W.Ross, Ann.Phy.(USA) 36 458 (1966)

380. W.R.Chappell,J.Cooper,E.W.Smith,T.Dillion,J.Stat.Phy. 3 401 (1971)

381. G.Nienhuis, Physica 74 157 (1974),66 245 (1973)

382. J.Ward,J.Cooper,E.W.Smith, Physica 77 372 (1974)

383. H.K.Chen,S.S.Penner, JQSRT 14 239 (1974)

384. B.W.Fowler,C.C.Sung, JOSA 65 949 (1975)

385. J.Cooper,D.N.Stacey, Phy.Rev.A 12 2438 (1975), J.Phy.B7 2143 (1974)

386. P.L.Roney, JQSRT 15 361 (1975) 15 181 (1975)

387. S.Hess, Physica 61 80 (1972)

388. E.W.Smith,J.Cooper,W.R.Chappel,T.Dillon, JQSRT 11 1547,1567 (1971)

389. V.A.Alekseev,T.L.Andreeva,I.I.Sobelman,JETP 35 325 (1972)

390. E.Czuchaj,E.Paul,Act.Phy.Pol.A 56 547 (1979)

391. J.Fiutak,E.Paul,Act.Phy.Pol.A 49 773 (1976)

392. G.Nienhuis, JQSRT 20 275 (1978)

393. G.Nienhuis,F.Schuller Physica 92C 409 (1977)

394. B.Huttner,L.Knoll, Acta.Phy.Pol.A 52 135 (1977)

395. E.Bielicz,E.Czuchaj,J.Fiutak, Act.Phy.Pol.A 41 327 (1972)

396. D.R.A.McMahon, Aust.J.Phys. 34 639 (1981)

397. J.Ward,J.Cooper,E.W.Smith, JQSRT 14 555,591 (1974)

398. R.M.Herman,E.W.Weber, J.Phy.B 16 1323 (1983)

Semiclassical Nonperturbative Approach

399. R.G.Gordon,JCP 44 3083 (1966)

400. T.A.Dillon,E.W.Smith,J.Cooper,M.Mizushima, Phy.Rev.A 2 1839 (1970)

401. E.W.Smith,M.Giraud,J.Cooper, JCP 65 1256 (1976)

402. W.B.Neilsen,R.G.Gordon, JCP 58 4131, 4149 (1973)

403. D.E.Fritz,R.A.Marcus, JCP 59 4380 (1973), 62 3788 (1975)

404. S.C.Mehrota,J.E.Boggs, JCP 62 1453 (1975),64 2796 (1976)

405. C.Boulet,D.Robert, Chem.Phy.Lett. 60 162 (1978)

406. A.Turfa,D.E.Fritz,R.A.Marcus, JCP 67 4463 (1977)

ATC Theory

407. P.W.Anderson, Phy.Rev. 76 647 (1949)

408. C.J.Tsao,B.Curnutte, JQSRT 2 41 (1962)

409. J.Fiutak,J.VanKranendronk, Can.J.Phy. 40 1085 (1962),41 21,437 (1963)

410. M.Mizushima Supp.Prog.Theor.Phys. 40 207 (1967)

411. C.G.Gray, Can.J.Phy. 46 135 (1968)

412. J.VanKranendonk,D.M.Gass, Can.J.Phy. 51 2428 (1973)

413. P. Varanasi,S.Surangi,JQSRT 14 845 (1974)

414. A.Levy,C.Boulet, JQSRT 15 1067 (1975)

415. Krishnaji, J.Sci.Ind.Res. 32 168 (1973)

416. D.Robert,M.Giraud,L.Galatry, JCP 51 2192 (1969)

Curved Trajectory

417. S.C.Mehrotra, JCP 70 2024 (1979)

418. M.Berard,P.Lallemand, JQSRT 19 387 (1978)

Old HCl,HF, Diatomic Shift

419. G.A.Kuipers,J.Mol.Spect. 2 75 (1958)

420. S.Kimel,M.A.Hirshfeld,J.H.Jaffe, JCP 31 81 (1959)

421. D.H.Rank,W.B.Birtley,D.P.Eastman,T.A.Wiggins, JCP 32 296 (1960)

422. M.A.Hirshfeld,J.H.Jaffe,J.Kimel, JCP 32 297 (1960)

423. A.Ben-Reuven,S.Kimel,M.A.Hirshfeld,J.H.Jaffe, JCP 35 955 (1961)

424. W.F.Herget,W.E.Deeds,N.M.Gailar,R.J.Lovell,A.H.Nielson, JOSA 52 1113 (1962)

425. A.Ben-Reuven,H.Friedman,J.H.Jaffe, JCP 38 3021 (1963)

426. R.Sharma,G.C.Turrel, JCP 39 2638 (1963)

427. J.H.Jaffe,M.A.Hirshfeld,A.Ben-Reuven, JCP 40 1705 (1964)

428. J.H.Jaffe,A.Rosenberg,M.A.Hirshfeld,N.M.Gailar, JCP 43 1525 (1965)

429. A.Ben-Reuven, JCP 42 2037 (1965)

430. D.H.Rank,E.F.Gardner,P.Sitaram.W.A.Gilickman, T.A.Wiggins, J.Mol.Spect.13 87 (1964)

431. M.Giraud,D.Robert,L.Galatry JCP 53 352 (1970)

432. D.H.Rank,D.P.Eastman,B.S.Rao,T.A.Wiggins, J.Mol.Spect. 10 34 (1963)

433. R.D.Sharma,G.E.Caledonia, JCP 54 434 (1971)

434. U.G.Desai,N.M.Gailar,R.J.Lovell, JOSA 61 573 (1971)

435. B.Oskengorn, Spectrochem. Acta 19 541 (1963)

436. R.M.Herman, Phy.Rev. 132 262 (1963)

437. F.Schuller,B. Oskengorn, J.Mol.Phy. 5 573 (1962), J.Phys.(Fr.)30 531, 919 (1969), JQSRT9 185 (1969)

438. J.Szudy, Act.Phy.Pol.A 34 761 (1968)

439. F.Schuller, JQSRT 11 1725 (1971)

440. B.M.Shaw,R.J.Lovell, JOSA 59 1598 (1969)

441. T.A.Wiggins,N.C.Griffin,E.M.Arlin,D.L.Kerstetter,J. Mol.Spect. 36 77 (1970)

Recent HCl,HF,Rare Gas Shifts

442. R.H.Tipping,R.H.Herman, JQSRT 10 881,897 (1970)

443. A.Levy,E.Piollet-Mariel,C.Boulet, JQSRT 13 673, 953 (1973)

444. M.Giraud,D.Robert,L.Galatry, JCP 59 2204 (1973)

445. A.Levy,C.Boulet, JQSRT 15 1067 (1975)

446. D.Korff,R.P.Leavitt, Phy.Lett.A 53 351 (1975)

447. R.M.VanAalst,R.Spiekerman,J.VanderElsken, Phy.Lett.A 47 451 (1974)

448. J.Jarecki,R.M.Herman, JQSRT 15 707 (1975)

449. J.Jarecki, JCP 65 5318 (1976)

450. J.P.Houdeau,M.Larver,C.Haeusler, JQSRT 16 457 (1976)

451. D.Frenkel,J.Van Der Elsken, Chem.Phy.Lett. 50 116 (1977)

452. G.Guelachvili,M.A.Smith, JQSRT 20 35 (1978)

453. C.Boulet,D.Robert,L.Galatry, JCP 65 5302 (1976)

454. C.Boulet,D.Robert, Chem.Phy.Lett. 60 162 (1978)

455. E.T.Salesky,D.Korff, Phy.Lett.A 72 431 (1979)

456. D.Robert,J.Bonamy,F.Marsault-Herail,G.Levi,J.P.Marsault, Chem.Phy.Lett.74 467 (1980)

457. C.Boulet,D.Robert,L.Galatry, JCP 72 751 (1980)

458. C.Boulet,A.Rosenberg, J.Phys.(Fr.) 42 203 (1981)

459. J.P.Houdeau,C.Boulet, JQSRT 26 503 (1981)

460. C.Boulet,D.Robert, Chem.Phy.Lett. 60 162 (1978)

Microwave Shifts

461. I.C.Story,V.I.Metchnik,R.W.Parsons, J.Phy.B 4 593 (1971), Phy.Lett.A, 34 59 (1971)

462. R.P.Netterfield,R.W.Parsons,J.A.Roberts, J.Phy.B 5 146 (1972)

463. R.W.Parsons,V.Metchnik,I.C.Story, J.Phy.B 5 1221 (1972)

464. P.L.Hewitt,R.W.Parson, Phy.Lett. 45A 21 (1973)

465. R.B.Nerf, J.Mol.Spect. 58 451 (1975)

466. R.K.Kakar,R.L.Poynter, J.Mol.Spect. 54 475 (1975)

467. P.L.Hewitt, JQSRT 16 499 (1976)

468. W.R.MacGillivray, J.Phy.B 9 2511 (1976)

469. I.R.Dagg,J.A.Roberts,R.W.Parson, J.Mol.Spect. 63 241 (1976)

470. P.L.Hewitt, JQSRT 17 227 (1977)

471. W.Wensink,H.A.Dijkerman,R.W.Parsons, Phy.Lett.A 50A 331 (1974)

472. B.S.Frost,W.MacGillivray, J.Phy.B 10 3649 (1977)

473. W.A.Wensink,H.A.Dijkerman, J.Phy.B 10 L663 (1977)

474. J.P.Mathelin,P.Suzeau,B.Lamalle,J.Chanussot,Can.J.Phy. 56 882 (1978)

475. B.A.Andreev,S.P.Belov,A.F.Krupnov, Opt.Spect. 44 363 (1978)

476. W.A.Wensinki,C.Noorman,H.A.Dijkerman, J.Phy.B 12 1687 (1979)

477. G.Buffa,M.Martinelli,O.Tarrini,C.Umeton, J.Phy.B 12 743 (1979)

478. A.F.Krupnov, Radiophysic and QE 22 170, 628 (1979)

479. W.A.Winsink,C.Noorman,H.A.Dijkerman, J.Phy.B 13 4007 (1980)

480. R.C.Hom,S.L.Coy, JCP 74 5453 (1981)

481. S.P.Belov,L.I.Gershstein,A.F.Krupnov,A.Maslovskii, S.Urban,V.Spirko,D.Papousek,J.Mol.Spect.84 288 (1980)

482. W.A.Wensink,C.Noorman,H.A.Dijkerman, J.Phy.B 14 2813 (1981)

483. S.P.Belov,A.F.Krupnov,V.N.Markov,A.A.Melnikov, V.A.Skvortsov,M.V.Tretyakov,V.Kozakov, J.Mol.Spect.94 264 (1982), 101 258 (1983)

484. J.K.Messer,B.Khoobehi,J.Robert, JCP 76 2914 (1982)

485. G.Baldacchini,S.Marchetti,V.Montelatici, G.Buffa,O.Tarrini, JCP76 5271 (1982), JCP 78 665 (1983)

486. I.R.Dagg,P.S.Atherton,R.W.Parsons, J.Mol.Spect. 100 134 (1983)

487. M.O.Bulanin,Y.M.Ladvishchenko,E.B.Khodos, Opt.Spect. 53 119 (1982)

488. H.M.Pickett,R.L.Poynter,E.A.Cohen, JQSRT 26 197 (1981)

489. V.P.Kazakov,A.F.Krupnov,A.A.Melnikov,V.A.Skvortsov, Radiophysic and QE23 533 (1980)

490. A.F.Krupnov,A.A.Melnikov,V.A.Skvortsov,Radiophysics and QE 25 447 (1982)

491. G.Buffa,O.Tarrini, J.Mol.Spect. 101 271 (1983)

492. A.DiGiacomo,O.Tarrani, Nuovo Cimento 68B 165 (1970)

493. B.S.Frost, J.Phy.B 9 1001 (1976)

494. S.M.Luijendijk, J.Phy.B 10 1735, 1741 (1977)

495. S.C.Mehrotra,J.E.Boggs, JCP 66 5306 (1977)

Microwave Broadening Theory

496. J.Gerstein,H.M.Foley,Phy.Rev. 182 24 (1969)

497. M.Mizushima, Phy.Rev. 83 94 (1951)

498. Krishnaji,S.L.Srivastava, JCP 41 2266(1964), JCP 42 1546 (1965)

499. A.Ben-Reuven, Phy.Rev. 145 7 (1966)

500. G.Birnbaum,Phy.Rev. 150 101 (1966), JCP46 2455 (1967)

501. J.Murphy,J.Boggs, JCP 47 691, 4152 (1967),49 3333 (1968),50 3320 (1969),51 3891 (1969),54 2443 (1971)

502. G.D.Tejwani,P.Varanasi, JCP 55 1075 (1971)

503. G.Johri,S.Gupta, Ind.J.Pure.App.Phys. 20 508,510 (1982)

504. K.L.Petersen,JCP 75 5647,5655 (1981)

505. K.Petersen,R.H.Schwendendeman,JCP 75 5662 (1981)

506. R.H.Schwendendeman, JCP 73 4838 (1980)

507. W.K.Liu,R.A.Marcus, JCP 63 272,290 (1975)

CO Broadening and Shifts

508. J.P.Bouanich,C.Haeusler, JQSRT 12 695 (1972)

509. R.B.Nerf, M.A.Sonnenberg, J.Mol.Spect. 58 474 (1975)

510. C.Boulet,P.Isnard,A.Levy, JQSRT 13 911 (1973)

511. J.R.Bouanich, JQSRT 12 1609 (1972), 13 953 (1973), Can.J.Phys. 61 919 (1983)

512. J.R.Bouanich,C.Brodbeck, JQSRT 13 1 (1973), Rev. Phy.App., 9 475 (1974)

513. J.Bonamy,D.Robert,C.Boulet, JQSRT 31 23 (1984)

514. J.P.Bouanich,F.Farreno,C.Brodbeck, Can.J.Phy. 61 192 (1983)

515. C.R.Pollack,F.R.Petersen,D.A.Jenning,J.S.Wells,A.G.Maki, J.Mol.Spect.99 357 (1983)

Pressure Shifts in General

516. M.Fink,T.A.Wiggins,D.H.Rank, J.Mol.Spect. 18 384 (1965)

517. W.R.Hindmarsh,A.D.Petford,M.Smith,Proc. Roy.Soc.A 297 296 (1967)

518. J.M.Vaughan,G.Smith, Phy.Rev. 166 13,17 (1968)

519. I.M.Farr,W.R.Hindmarsh, J.Phy.B. 4 568 (1971)

520. N.F.Allard,S.Sahal-Brechot,Y.G.Biraud,J.Phy.B 7 2158 (1974)

521. R.Vetter,D.Reymann, J.Phy.B 7 323 (1974)

522. R.S.Eng,A.R.Calawa,T.C.Harman,P.L.Kelly,A.Javan, App.Phy. Lett.21 303 (1972)

523. R.S.Eng,P.L.Kelley,A.Mooradian,A.R.Calawa,R.C.Harman, Chem.Phy.Lett.19 524 (1973)

524. R.S.Eng,P.L.Kelley,A.R.Calawa,T.C.Harman,K.W.Nills, Mol.Phys.28 653 (1974)

525. H.J.Libe,M.C.Thompson,T.A.Dillon, JQRST 9 31 (1969)

526. E.Lisicki,J.Szudy,J.Wolnikowski,Acta Phy.Pol.A 56 557 (1979),58 105 (1980)

527. A.Bielski,R.Bobkowski,W.Dokurnov,J.Szudy,Z.Phy.A 302 1 (1981),59 107 (1981)

528. K.K.Innes,S.J.Jackling,T.W.Tolberts, JQSRT 16 443 (1976)

529. M.M.Salour, Phy.Rev.A 17 614 (1978)

530. V.D.Galkin, Opt.Spect. 46 106 (1979)

531. D.Schwamb, Phy.Lett.A 71 420 (1979)

532. C.Y.Wu,W.C.Stwalley, Phy.Rev. 18 1060 (1978),24 1117 (1981)

533. L.P.Giver,B.Gentry,G.Schwemmer.T.D.Wilkerson,JQSRT 27 423 (1982)

534. D.A.Jackson,JOSA 71 1064 (1981)

535. F.Rostas,J.L.LeMaire, J.Phy.B 14 555 (1971)

536. D.E.Gilbert,N.Allard,S.Y.Chen, JQSRT 23 201 (1980)

537. N.F.Allard,Y.G.Biraud, JQSRT 23 253 (1980)

538. K.Dietz,P,Dabkiewicz,H.Kluge,T.Kuhl,H.A.Schuessler, J.Phy.B13 2749 (1980)

539. W.C.Kreye,J.Phy.B 15 371 (1982)

540. R.W.Davies,B.A.Oli, JQSRT 20 95 (1978)

541. A.F.Krupnov,V.A.Skvortsov, Radiophysics and QE 25 200 (1982)

542. E.Lisicki,A.Bielski,R.S.Dygdala,J.Szudy,Acta.Phy.Pol.A 61 421 (1982)

543. E.Lisicki,A.Bielski,J.Szudy,Z.Naturforsch 35A 1249 (1980),36A 807 (1981),37A 93 (1982)

544. E.Weber ,Phy.Rev.A 20 2278 (1979)

545. M.Harris,N.Lwin,D.McCartan, J.Phy.B 15 L831 (1982)

546. P.Cahazac,R.Damaschini, Opt.Comm. 32 251 (1980)

547. E.W.Weber,J.Goldsmith, Phy.Lett.A 70A 95 (1979)

548. E.Weber,K.Jungman, Phy.Lett.A 81 223 (1981)

549. A.Bielski,R.Bobkowski,R.Dygdala,J.Wawrzynski,Act.Phy.Pol.A 63 411 (1983), Physica, 115C 261 (1983)

550. O.Vallee,E.Marie,N.TranMinh,R.Vetter, Phy.Rev.A 24 1391 (1981)

551. C.Belfrage,P.Grafstrom,S.Kroll,S.Svanberg, Phys.Scripta 27 367 (1983)

Rydberg Shifts,Highly Excited States Shift

552. B.P.Stoicheff,E.Weinberger, Phy.Rev.Lett. 44 733 (1980), and Laser Spectroscopy IV,Ed. H.Walther,K.W.Rothe, Springer Verlag 1979, p.264

553. H.Hohimer,J.Gee, Phy.Rev.A 25 1404 (1981)

554. W.Brillet,A.Gallagher, Phy.Rev.A 22 1012 (1981)

555. D.J.Krebs,L.D.Schearer, Phy.Rev.A 26 1473 (1982)

556. K.H.Weber,K.Niemax, Opt.Comm. 31 52 (1979), Z. Phys.A307 13 (1982)

557. Y.Rabin,F.Rebentrost, Opt.Comm. 40 257 (1982)

558. D.M.Bruce,M.Y.Mirza,W.W.Dudley, Opt.Comm. 40 347 (1982)

559. J.Kielkopf, J.Phy.B 16 3149 (1983)

Hyperfine Shifts

560. R.Freeman,D.Pritchard,D.Kleppner, Phy.Rev.A 13 907 (1976)

561. H.Ackerman,G.Putlitz,J.Schleusener.F.Sichart,J.Vetter, E.W.Weber,S.Winnik,Phy.Lett.A44 515 (1973)

562. S.Ray, Phy.Rev.A 12 2031 (1975)

563. C.W.Beer,R.A.Bernheim, Phy.Rev.A 13 1052 (1976)

564. R.D.Zwicker, J.Physic.Chem.Solid 39 445 (1978)

565. S.L.Izotova,A.Kantserov,M.S.Frish, Opt.Spect. 42 120 (1977), 46 646 (1979), 49 546 (1980), 51 107 (1981)

566. N.Beverini,F.Strumia,G.Rovera, Opt.Comm. 37 394 (1981)

567. V.Belov, Opt.Spect. 51 209 (1981)

568. J.Vanier,R.Kunski,N.Cry,J.Savard,M.Tetu, J.App.Phy. 53 5387 (1982)

569. K.Kondo, J.Phy.Soc.Jap. 52 2340 (1983)

570. Y.Fukuda,M.Tanigawa,T.Hashi,K.Kondo, Opt.Lett. 8 301 (1983)

571. V.V.Batygin,V.S.Zholnerov, Opt.Spect. 39 254 (1975)

572. V.V.Batygin,Y.G.Guzhva,B.G.Matisov,I.N.Toptygin,JETP 45 1104 (1977)

573. V.V.Batygin,M.B.Gornyi,B.G.Matisov, Opt.Spect. 43 479 (1977),46 572 (1979), Sov.Phy.Tech.Phy.22 1397 (1977),23 613, 1413 (1978),25 31, 657 (1980)

574. V.V.Batygin,V.M.Ostryakov,I.M.Sokolov, Sov.Phy.Tech.Phy. 25 969 (1980)

575. V.H.Rebane, Opt.Spect. 41 214 (1976),42 123 (1977),43 117,482 (1977),44 376 (1978),47 472 (1979)

Raman Lineshifts

576. A.D.May,V.Degen,J.S.Stryland,H.L.Welsch, Can.J.Phy. 39 1769 (1961)

577. A.D.May,G.Varghese,J.C.Stryland,H.L.Welsch, Can.J.Phy. 42 1058 (1964)

578. P.Lallemand,P.Simova,G.Brett, Phy.Rev.Lett. 17 1239 (1966)

579. P.Lallemand,P.Simova, J.Mol.Spect. 26 262 (1968)

580. V.G.Cooper,A.D.May,B.K.Gupta, Can.J.Phy. 48 725 (1970)

581. A.R.W.McKellar, Can.J.Phy. 51 389 (1973), Astroph.J., 185 L53 (1973)

582. J.R.Murray,A.Javan, J.Mol.Spect. 42 1 (1972)

583. C.Chackerian,L.P.Giver, J.Mol.Spect. 58 339 (1975)

584. T.Witkowicz,A.D.May, Can.J.Phy. 54 575 (1976)

585. R.Shafer,R.G.Gordon, JCP 58 5422 (1973)

586. E.C.Looi,J.C.Stryland,H.L.Welsch, Can.J.Phys. 56 1102 (1978)

587. G.E.Hahne,C.Chackerian, JCP 73 3223 (1980)

588. D.L.Tonks,J.B.Page, Chem.Phy.Lett. 79 247 (1981)

New Approaches to ATC Shift Theory

589. M.Cattani, Phy.Lett.A 38 147 (1972), Can.J.Phy.51 1388 (1973)

590. C.Gray,R.H.Tipping,Chem.Phy.Lett. 13 260 (1972)

591. R.D.Sharma, Chem.Phy.Lett. 8 428 (1971),13 261 (1972)

592. R.D.Scharma,J.Pasiack, Chem.Phy.Lett. 16 45 (1972)

593. R.Granier,J.Granier,F.Schuller, JQSRT 16 143 (1976)

594. R.P.Srivastava,H.R.Zaida, Can.J.Phy. 55 533 (1977)

595. A.Levy,C.Boulet, JQSRT 15 1067 (1975)

596. L.P.Kazachenko,E.K.Kruglik, J.App.Spect. 28 246 (1978)

597. G.K.Johri,S.L.Srivastava, Chem.Phy.Lett. 39 579 (1976), 45 364 (1977)

598. G.K.Johri, Ind.J.Phy. 55B 51 (1981)

599. Y.Yamamoto,M.Cattani, JQSRT 24 59 (1980)

600. E.T.Salesky,D.Korff, JQSRT 23 399 (1980)

601. J.Bonamy,L.Bonamy,D.Robert, JCP 67 4441 (1977)

602. D.Robert,J.Bonamy, J.Phy.(Fr.) 40 923 (1977)

603. R.P.Leavitt, JCP 72 3472 (1980)

604. R.P.Leavitt,D.Korff, JCP 74 2180 (1981)

605. R.P.Leavitt, JCP 73 5432 (1980)

CO-2 Broadening as Compared with ATC Theory

606. K.S.Jammy,G.E.St.Johm,H.L.Welsch, Can.J.Phy. 44 797 (1966)

607. C.G.Gray,J.Van Kranendonk, Can.J.Phy. 44 2411 (1966)

608. P.Arcas,L.Hochard-Demolliere, Can.J.Phy. 46 1697 (1968)

609. R.W.Boese,J.H.Miller,E.C.Y.Inn,L.P.Giver, JQSRT 8 1001 (1968)

610. T.K.McCubbin,T.R.Mooney, JQSRT 8 1255 (1968)

611. G.Yamamoto,M.Tanaka,T.Aoki,JQSRT 9 371 (1969)

612. C.Boulet,E.Arie,J.P.Bouanich,N.Lacombe,Can.J.Phy. 50 1800, 2178 (1972)

613. J. Bouanich, JQSRT 13 953 (1973)

614. C.Young,R.Chapman, JQSRT 14 679 (1974)

615. C.Boulet,P.Isnard,E.Arie, JQSRT 14 637 (1974)

616. J.Bouanich,C.Brodbeck, JQSRT 14 141 (1974)

617. M.Herpin,P.Lallemand, JQSRT 15 779 (1975)

618. R.P.Srivastiva,H.R.Zaidi, Can.J.Phy. 55 549 (1977)

J Dependent Linebroadening in CO-2

619. R.P.Madden, JCP 35 2083 (1961)

620. A.D.Devir,U.P.Oppenheim, JOSA 58 585 (1968), App.Opt. 8 2121 (1969)

621. D.E.Burch,D.A.Gryvnak,R.P.Patty,C.E.Barktky, JOSA 59 267 (1969)

622. L.D.Tubbs,D.William, JOSA 62 284 (1972)

623. H.G.Reichle,C.Young, Can.J.Phy. 50 2662 (1972)

624. V.A.Boldyrev,K.P.Vasilevskii, Opt.Spect. 35 476 (1973)

625. K.S.Jammu,G.E.St.John,H.W.Welsch, Can.J.Phy. 44 797 (1966)

626. E.Arie,N.Lacombe,C.Rossetti, Can.J.Phy. 50 1800 (1972)

627. F.P.J.Valero,C.B.Suarez,R.W.Boes, JQSRT 19 579 (1978), 23 337 (1980)

628. R.S.Eng,A.W.Mantz, J.Mol.Spect. 74 331 (1979)

629. R.T.Pack,JCP 70 3424 (1979)

630. H.Oodate,T.Fujioka, JCP 68 5494 (1978)

631. A.S.Biryukov,A.Y.Volkov,E.M.Kudryavtseev,R.I.Serikov, Sov. JQE 11 946 (1976)

632. M.O.Bulanin,V.P.Bulychev,E.B.Khodos, Opt.Spect. 48 486 (1980)

633. P.Arcas,E.Arie,P.Cardinet,A.Valentin,A.Henry,J.Mol.Spect. 81 262 (1980), 96 288 (1982)

Shifts in Carbon Dioxide

634. C.Freed,A.Javan, App.Phy.Lett. 17 53 (1970)

635. H.W.Mocker, App.Phy.Lett. 12 20 (1968)

636. L.S.Vasilenko,M.N.Skvortsov,V.P.Chebotayev,G.I.Shershneva, Opt.Spect.32 609 (1972)

637. P.T.Woods,B.W.Jolliffe, J.Phy.E 9 395 (1976)

638. P.Arcas,E.Arie,C.Boulet,Maillard, JCP 73 5383 (1980)

639. R.C.Hollins,D.L.Jordan, J.Phy.B 15 L491 (1982)

640. J.Geraedts,S.Stolte,J.Reuss, Chem.Phy.Lett. 97 152 (1983)

Anomalous Shifts

641. R.Vetter,D.Reymann, J.Phy.B 7 323 (1974)

642. E.W.Weber,J.E.M.Goldsmith, Phy.Lett.A 70 95 (1979)

643. P.Cahazac,R.Damaschini, Opt.Comm. 32 251 (1980)

644. E.Weber,K.Jungman, Phy.Lett.A 81 223 (1981)

645. A.Bielski,R.Bobkowski,R.Dygdala,A.Wawrynzski, Act.Phy.Pol.A 63 411 (1983)

CO-2 Measurements, Momentum Transfer

646. L.S.Vasilenko,A.A.Kovalev,A.S.Provorov,V.P.Chebotayev, Sov.JQE 5 1302 (1976)

647. L.S.Vasilenko,V.A.Kochanov,V.P.Chebotayev, Opt.Comm. 20 409 (1977)

648. Y.V.Brzhazvoskii,L.S.Vasilenko,V.P.Chebotayev, JETP 28 1108 (1969)

649. L.S.Vasilenko,V.P.Chebotayev,G.I.Shershneva, Opt. Spect. 29 107 (1970)

650. T.W.Meyer,C.K.Rhodes,H.A.Haus, Phy.Rev. A 12 1993 (1975)

651. T.W.Meyers,Line Broadening and Collisional Studies of CO_2 using the Techniques of Saturation Spectroscopy, UCRL-51561, Apr. 1974

652. T.Meyer,C.Rhodes,Phy.Rev.Lett. 32 637 (1974)

653. T.Meyer,W.Bischel,C.Rhodes, Phy.Rev.A 10 1433 (1974)

654. W.Bischel,C.Rhodes, Phy.Rev.A 14 176 (1976)

655. C.J.Borde,M.Ouhayon,A.VanLerberghe,C.Salamon, S.Avrillier,C.D.Cantreall,J.Borde,in Laser Spectroscopy IV, p. 142, Ed. H.Walther,K.W.Rother, Springer Verlag 1979

656. C.J.Borde,S.Avrillier,A.VanLerberghe,C.Salamon,D.Bassi, G.Scoles,J.Phy.(Fr.) C842 C8-15 (1981)

657. C.Salamon,C.Breant,C.J.Borde,R.L.Barger, J.Phy.(Fr.) C8 42 C8-3 (1981)

Kinetic and Collision (VCC) Theory

658. E.G.Pestov, J.App.Spect. 10 317 (1969)

659. T.L.Andreev, JETP 27 342 (1968)

660. V.A.Alekseev,T.L.Andreeva, I.I.Sobelman,JETP 35 325 (1972),37 413 (1973)

661. A.P.Kolchenko,S.G.Rautian,Y.Troitskii,A.M.Shalagin, JETP 39 414 (1974)

662. S.G.Rautian JETP 24 788 (1967)

663. A.P.Kolchenko,S.G.Rautian,R.I.Sokolovzkii, JETP 28 986 (1969)

664. E.G.Pestov,S.G.Rautian, JETP 29 488 (1969), 37 1025 (1973)

665. A.B.Kolchenko,S.G.Rautian, JETP 27 511 (1968)

666. A.P.Kolchenko,A.A.Pukhov,S.G.Rautian,A.M.Shalagin, JETP 36 619 (1973)

667. D.Kuhlke,E.Dopel,Czech.J.Phy.B 25 1084 (1975)

668. V.P.Kochanov,S.G.Rautian,A.M.Shalagin, JETP 45 714 (1977)

669. S.G.Rautian, Sov. JQE 8 970 (1978)

670. S.G.Rautian,Investigation of Collisions by Nonlinear Spectroscopy Methods, Atomic Physics 6, Ed. R.D.Damberg,O,Kukaine,Plenum Press, 1979

671. S.G.Rautian,A.M.Shalagin, Opt.Spect. 46 656 (1979)

672. S.G.Rautian,A.G.Rudavets,A.M.Shalagin, JETP 51 274 (1980)

673. E.V.Baklanov,M.V.Belyaev, Opt.Spect. 49 354 (1980)

674. V.P.Kochanov,S.G.Rautian,A.M.Shalagin,Sov.Phy.Tech.Phys. 24 1137 (1979)

675. K.Koura, JCP 72 268 (1980)

676. S.N.Atutov,S.G.Rautian,G.D.Rodionov,E.G.Saprykin, A.M.Shalagin,Sov.Tech.Phy.Lett.3 550 (1977),Opt.Spect. 49 569 (1980)

677. P.R.Berman, Phy.Rev.A 5 927 (1972),6 2157 (1972),9 2170 (1974),13 2191 (1976)

678. P.R.Berman, App.Phy.(Germ) 6 283 (1975), Phy. Report C 43 101 (1978)

679. P.R.Berman, Comments At.Mol.Phys. 5 19 (1975), 12 69 (1981)

680. P.R.Berman, Study of Collision by Laser Spectroscopy, Adv. Atom.Molec.Phys.13 57 (1977) ed. D.R.Bates,B.Bederson,Acad.Press

681. P.R.Berman,P.F.Liao,J.E.Bjorkholm, Phy.Rev.A 20 2389 (1979),21 1927 (1980)

682. J.LeGouet,P.R.Berman,Phy.Rev.A 24 1831 (1981)

683. P.R.Berman,T.W.Mossberg,S.R.Hartman,Phy.Rev.A 25 2550 (1982)

Velocity Changing Collisions,Experiments

684. A.Flushberg, Opt.Comm. 29 123 (1979)

685. P.R.Berman,J.M.Levy,R.G.Brewer, Phy.Rev.A 11 1668 (1975)

686. R.G.Brewer,R.L.Shoemaker, Phy.Rev.Lett. 27 631 (1971),Phy.Rev.A 6 2001 (1972)

687. J.Schmidt,P.R.Berman,R.G.Brewer, Phy.Rev.Lett. 31 1103 (1973)

688. P.R.Berman,J.M.Levy,R.G.Brewer, Phy.Rev.A 11 1668 (1975)

689. S.N.Jabr,W.R.Bennet, Phy.Rev.A 21 1518 (1980)

690. J-L.LeGouet,J.Phy.B 11 3001 (1978)

691. J.LeGouet,P.R.Berman,Phy.Rev.A 17 52 (1978)

692. P.Cahuzac,X.Drago, Opt.Comm. 24 63 (1978)

693. P.Cuhazac,J-L.LeGouet,P.E.Toschek,R.Vetter, Appl.Phy. 20 83 (1979)

694. M.Gorlicki, A.Peuriot,M.Dumont, J.Phy.Lett.(Fr.) 41 L-275 (1980)

695. M.Gorlicki,C.Lerminiaux,M.Dumont, Phy.Rev.Lett. 49 1394 (1982)

696. R.A.Forber, L.Spinelli,J.E.Thomas,M.S.Feld, Phy.Rev.Lett. 50 331 (1983)

697. T.Mossberg,R.Kachru,S.Hartmann, Phy.Rev.Lett. 44 73 (1980)

698. J. Schmidt,P.R.Berman, Phy.Rev.Lett. 31 1103 (1973)

699. P.R.Berman,J.Levy,R.Brewer,Phy,Rev.A 11 1668 (1975)

700. P.Cahuzac,E.Marie,O.Robaux,R.Vetter,P.R.Berman, J.Phy.B 11 645 (1978)

701. C.Brechnignac,R.Vetter,P.Berman, Phy.Rev.A 17 1609 (1978), J.Phy.B10 3443 (1977), J. Phy.Lett.(Fr.)39 L-231 (1978)

702. B.Comaskey,R.E.Scott,R.L.Shoemaker, Opt.Lett. 6 46 (1981)

703. P.Cahuzac,J.LeGouet,P.Toschek,R.Vetter, App.Phys. 20 83 (1979)

704. J.Tenenbaum,E.Miron,S.Lavi,J.Liran,M.Strauss,J.Oreg, G.Erez, J.Phy.B 16 4543 (1983)

Velocity Selective Optical Pumping

705. A.T.Mattick,N.A.Kurnit,A.Javan, Chem.Phy.Lett. 38 176 (1976)

706. A.T.Mattick,A.Sanchez,N.A.Kurnit,A.Javan, App.Phy.Lett. 23 675 (1973)

707. M.Pinard,C.G.Aminoff,F.Laloe, Phy.Rev.A 19 2366 (1979)

708. P.G.Pappas,R.A.Forber,W.W.Quivers,R.R.Dasari,M.S.Feld, D.E.Murnick,Phy.Rev.Lett.47 236 (1981), Laser Spectroscropy IV, p.186, Springer Verlag (1981)

709. M.S.Feld,M.M.Burn,T.W.Kuhl,P.Pappas,D.Murnick,Opt.Lett. 5 79 (1980), Phy.Rev.A21 1955 (1980)

710. C.G.Aminoff,M.Pinard, J.Phys.(Fr.) 43 263 (1982)

711. J.Bjorkholm,P.Liao,A.Wokaun, Phy.Rev.A 26 2643 (1982)

712. D.G.Steel,R.A.McFarlane, Opt.Lett. 8 33 (1983)

713. C.G.Aminoff, J.Javanainen,M.Kaivola, Phy.Rev.A 28 722 (1983)

More

714. P.R.Bevington,"Data Reduction and Error Analysis for the Physical Sciences", McGraw Hill, NY, 1969

APPENDIX 1 EIGENVALUE PROBLEM, MATRIX ELEMENTS

To calculate the pressure shifts in CO_2, the harmonic decomposition for each participating level must be obtained. Suzuki[11,12] and Chedin[1,7-9], as mentioned in Chapter 2, had worked extensively on diagonalizing the energy matrix for CO_2 and fitting the anharmonic potential constants to the measured spectroscopic constants for a large number of vibrational basis functions. A smaller vibrational energy problem was solved to obtain the desired harmonic decomposition. Here, the spectroscopic and anharmonic constants given by Chedin[1] were used in diagonalizing the energy matrix $|H - V| = 0$. As small a set of bases functions including those levels in Fermi resonance, was used in this problem.

Vibrational Bases for Energy Diagonalization

000	001
100	101
020	021
120	121
200	201
040	041

Assuming there was no coupling between the ν_3 state and with l=0, the bases included the above set of energy levels for the two separate diagonalization problems.

The diagonal matrix elements or the zero energy terms for each level (v_1,v_2,v_3) was taken to be:

$$E=\omega_1 v_1+\omega_2 v_2 +\omega_3 v_3+x_{11}v_1^2 +x_{12}v_1v_2+x_{13}v_1v_3 +x_{22}v_2^2+x_{23}v_2v_3+$$
$$+x_{33}v^2+y_{111}v_1^3 +y_{112}v_1^2v_2 +y_{113}v_1^2v_3 +y_{122}v_1v_2^2$$
$$+y_{123}v_1v_2v_3 +y_{133}v_1v_3^2 +y_{222}v_2^3 +y_{223}v_2^2v_3$$
$$+y_{233}v_2v_3^2 +y_{333}v_3^3$$

The 19 spectroscopic constants are listed in Table A7 and are labeled in the same order as given above, with X(1)= ω and X(19)= y_{333} and so forth. The anharmonic potential constants are listed in Table A8 with the corresponding subscripts 122 corresponding to f_{122} of the potential expansion $q_1q_2^2$ etc. The off diagonal matrix elements are given in Table A1 for the elements $\langle n|q^k|n'\rangle$ of the form $\langle n|q^k|n-m\rangle$. To obtain elements of the form $\langle n|q^k|n+m\rangle$, replace n→n+m in Table A1.

Here $\langle n|q^k|n'\rangle=\alpha^k f(k)$ where f(k) is given in the table and

$$\alpha=\sqrt{[h/(m\omega)]} \text{ and } \omega=\sqrt{(k/m)}.$$

Table A1 Harmonic Matrix Elements

k	n'	f(k)
1	n-1	$\sqrt{(n/2)}$
2	n	n+1/2
2	n-2	$0.5\sqrt{[n(n-1)]}$
3	n-1	$1.5n\sqrt{(n/2)}$
3	n-3	$\sqrt{[n(n-1)(n-2)/8]}$
4	n	$1.5(n+0.5)^2+0.375$
4	n-2	$(n-0.5)\sqrt{[n(n-1)]}$
4	n-4	$0.25\sqrt{[n(n-1)(n-2)(n-3)]}$

EIGEN2 is a computer program that diagonalized the |H-V| matrix to obtain the eigenvalues (vibrational energy levels) and the eigenvectors which are the anharmonic decomposition needed to calculate the harmonic matrix elements. Tables A2 to A5 list the most important components of the anharmonic decomposition of the $|0\rangle$, $|\nu_1\rangle$, $|2\nu_2\rangle$, $|\nu_3\rangle$ states. Table A6 gives the effective inertial B constants in the energy expansion for each vibrational-rotation level

$$E = \nu_o + B_{eff}J(J+1) - D_{eff}J^2(J+1)^2$$

where ν_o is the band center and D is the centrifugal distortion constant. Note that EIGEN2 solves a vibrational problem, ignoring any vibrational rotational coupling or any l-type coupling between matrix elements; this reduces the problem to block diagonalizing portions of the total energy problem which can be inaccurate if the above approximations are significant in determining the energy levels. Accordingly, EIGEN2 is a two pass diagonalization procedure in which the eigenvalue of the |0> state is subtracted off all diagonal elements to give a final solution such that the energy (eigenvalue) of |0> is 0. EIGEN2 is listed following Table A8.

Table A2

Vibrational Decomposition for Ground Level |0>

Isotope	|000>	|100>
16-12-16	-.996	-.084
16-13-16	-.996	-.083
18-12-18	-.996	-.084
18-13-18	-.996	-.082

Table A3

Vibrational Decomposition for Level $|\nu_3>$

Isotope	|001>	|101>
16-12-16	+.974	+.218
16-13-16	+.975	+.213
18-12-18	+.973	+.220
18-13-18	+.975	+.214

Table A4

Vibrational Decomposition of $|100,020>_I$ Level

Isotope	|000>	|020>	|100>	|200>
16-12-16	-.0488	+.5269	+.8423	+.0947
16-13-16	-.0636	+.7200	+.6780	+.1237
18-12-18	-.0313	+.3222	+.9437	+.0614
18-13-18	-.0414	+.4510	+.8873	+.0856

Table A5

Vibrational Decomposition of $|100,020\rangle_{II}$ Level

Isotope	|000>	|020>	|100>	|200>
16-12-16	+.0690	-.8284	+.5380	-.1328
16-13-16	+.0535	-.6676	+.7350	-.1036
18-12-18	+.0781	-.9280	+.3296	-.1493
18-13-18	+.0716	-.8730	+.4600	-.1377

Table A6

Inertial Constants for the Various Levels (cm^{-1})

Isotope	|000>	I	II	|001>
16-12-16	.39022	.39018	.39048	.38713
16-13-16	.39024	.38970	.39092	.38726
18-12-18	.34682	.34740	.34652	.34408
18-13-18	.34685	.34701	.34687	.34419

I and I refer to $(10°0,02°0)_I$ or $(10°0,02°0)_{II}$ levels

TABLE A7

SPECTROSCOPIC CONSTANTS

	16-12-16	16-13-16	18-12-18	18-13-18
X(1)	0.13358791D+04	0.13362871D+04	0.12597073D+04	0.12601008D+04
X(2)	0.66720435D+03	0.64834180D+03	0.65712964D+03	0.63795679D+03
X(3)	0.23616470D+04	0.22952388D+04	0.23262734D+04	0.22587644D+04
X(4)	-0.29926166D+01	-0.30001726D+01	-0.26482286D+01	-0.26563225D+01
X(5)	-0.52763777D+01	-0.51099873D+01	-0.49194612D+01	-0.47588396D+01
X(6)	-0.19140442D+02	-0.18674469D+02	-0.17666245D+02	-0.17216248D+02
X(7)	0.15800304D+01	0.14900103D+01	0.15366754D+01	0.14466181D+01
X(8)	-0.12541837D+02	-0.11756307D+02	-0.12280175D+02	-0.11494677D+02
X(9)	-0.12503301D+02	-0.11735859D+02	-0.12220226D+02	-0.11453855D+02
X(10)	0.24221286D-01	0.24221286D-01	0.20290442D-01	0.20290442D-01
X(11)	0.81591532D-02	0.68184081D-03	0.18347319D-01	0.10190055D-01
X(12)	-0.77356994D-01	-0.77514410D-01	-0.64929426D-01	-0.64802825D-01
X(13)	-0.51664598D-01	-0.44830598D-01	-0.53750541D-01	-0.46336126D-01
X(14)	0.95605195D-01	0.88849962D-01	0.89653730D-01	0.82977712D-01
X(15)	0.61423965D-01	0.62276449D-01	0.50754398D-01	0.51186886D-01
X(16)	-0.47088638D-02	-0.42258091D-02	-0.46422183D-02	-0.41535795D-02
X(17)	-0.20571679D-01	-0.20263821D-01	-0.17606616D-01	-0.17353672D-01
X(18)	0.18335227D-01	0.17034180D-01	0.17172657D-01	0.15910663D-01
X(19)	0.63136704D-02	0.56208000D-02	0.62550418D-02	0.55824965D-02

TABLE A8

ANHARMONIC POTENTIAL CONSTANTS

	16-12-16	16-13-16	18-12-18	18-13-18
111	-0.45515043D+02	-0.45515043D+02	-0.41658356D+02	-0.41658356D+02
122	0.75254423D+02	0.73112601D+02	0.71947569D+02	0.69834744D+02
133	-0.25635785D+03	-0.24906163D+03	-0.24509289D+03	-0.23789545D+03
1111	0.18266677D+01	0.18266677D+01	0.16232638D+01	0.16232638D+01
1122	-0.11770418D+02	-0.11435419D+02	-0.10925929D+02	-0.10605076D+02
1133	0.21536682D+02	0.20923726D+02	0.19991497D+02	0.19404423D+02
2222	0.26560930D+01	0.25070539D+01	0.25754118D+01	0.24263728D+01
2233	-0.28322220D+02	-0.26733000D+02	-0.27461908D+02	-0.25872688D+02
11122	0.84446700D+00	0.82044320D+00	0.67108200D+00	0.73873200D+00
12222	-0.10626600D+01	-0.10030300D+01	-0.10004100D+01	-0.94252100D+00
12233	0.57374400D+01	0.54155000D+01	0.54013700D+01	0.50888000D+01
3333	0.71057416D+01	0.67070234D+01	0.68898985D+01	0.64911803D+01
11133	-0.49721700D+00	-0.48306500D+00	-0.44812000D+00	-0.43496100D+00
14444	-0.93705600D+00	-0.88447600D+00	-0.88216800D+00	-0.83111700D+00

Eigenvalue Program and Matrix Elements

```
IMPLICIT REAL*8(A-H,O-Z)
REAL*8 B(91),X(19),Y(14),D(12),Z(12,12),EO,WK(120)
INTEGER I,J,K,I1,J1,I2,J2,I3,J3,L1,L2,L3,A(13,3)
REAL*8 L,M,N
A(1,1)=0
A(1,2)=0
A(1,3)=1
A(2,1)=1
A(2,2)=0
A(2,3)=1
A(3,1)=0
A(3,2)=2
A(3,3)=1
A(4,1)=2
A(4,2)=0
A(4,3)=1
A(5,1)=1
A(5,2)=2
A(5,3)=1
A(6,1)=0
A(6,2)=4
A(6,3)=1
A(7,1)=0
A(7,2)=0
A(7,3)=3
A(8,1)=1
A(8,2)=0
A(8,3)=3
A(9,1)=0
A(9,2)=2
A(9,3)=3
A(10,1)=2
A(10,2)=0
A(10,3)=3
A(11,1)=1
A(11,2)=2
A(11,3)=3
A(12,1)=0
A(12,2)=4
A(12,3)=3
A(13,1)=0
A(13,2)=0
A(13,3)=4
DO 55 K=1,19
READ(8,44) X(K)
```

```
55  CONTINUE
    DO 66 K=1,14
    READ(9,44) Y(K)
66  CONTINUE
44  FORMAT(2X,E20.8)
    C=0.
27  CONTINUE
    K=0
    DO 16 I=1,12
    DO 16 J=1,I
    K=K+1
    B(K)=0.
    I1=A(I,1)
    I2=A(I,2)
    I3=A(I,3)
    J1=A(J,1)
    J2=A(J,2)
    J3=A(J,3)
    L1=IABS(I1-J1)
    L2=IABS(J2-I2)
    L3=IABS(I3-J3)
    L=MAX(I1,J1)
    M=MAX(I2,J2)
    N=MAX(J3,I3)
47  FORMAT(2X,3I4,3E12.4)
    EO=X(1)*L+X(2)*M+X(3)*N+X(4)*L*L+X(5)*L*M+X(6)*L*N+X(7)*M*M+X(8)*M
   T*N+X(9)*N*N+X(10)*L*L*L+X(11)*L*L*M+X(12)*L*L*N+X(13)*L*M*M+X(14)*
   EL*N*M+X(15)*L*N*N+X(16)*M*M*M+X(17)*M*M*N+X(18)*M*N*N+X(19)*N*N*N
    EO=X(1)*L+X(2)*M+X(3)*N
    IF(L1.EQ.1.AND.I2.EQ.J2.AND.I3.EQ.J3)B(K)=B(K)+Y(1)*1.5*L*DSQRT(L/
   R2.)
    IF(L1.EQ.1.AND.L2.EQ.2.AND.I3.EQ.J3)B(K)=B(K)+Y(2)*DSQRT(L/2.)*.5*
   RDSQRT(M*(M-1.))
    IF(L1.EQ.1.AND.I2.EQ.J2.AND.I3.EQ.J3)B(K)=B(K)+Y(2)*DSQRT(L/2.)*(M
   R+.5)
    IF(L1.EQ.1.AND.I2.EQ.J2.AND.L3.EQ.2)B(K)=B(K)+Y(3)*DSQRT(L/2.)*.5*
   RDSQRT(N*(N-1.))
    IF(L1.EQ.1.AND.I2.EQ.J2.AND.I3.EQ.J3)B(K)=B(K)+Y(3)*DSQRT(L/2.)*(N
+.5)
    IF(L1.EQ.2.AND.I2.EQ.J2.AND.I3.EQ.J3)B(K)=B(K)+Y(4)*(L-.5)*DSQRT(L
   R*(L-1.))
    IF(L1.EQ.4.AND.I2.EQ.J2.AND.I3.EQ.J3)B(K)=B(K)+Y(4)*.25*DSQRT(L*(L
   R-1.)*(L-2.)*(L-3.))
    IF(I1.EQ.J1.AND.L2.EQ.2.AND.I3.EQ.J3)B(K)=B(K)+Y(5)*(L+.5)*.5*DSQR
   RT(M*(M-1.))
    IF(L1.EQ.2.AND.I2.EQ.J2.AND.I3.EQ.J3)B(K)=B(K)+Y(5)*.5*DSQRT(L*(L-
   R1.))*(M+.5)
    IF(L1.EQ.2.AND.L2.EQ.2.AND.I3.EQ.J3)B(K)=B(K)+Y(5)*.25*DSQRT(L*(L-
```

```
     R1.))*DSQRT(M*(M-1.))
      IF(L1.EQ.2.AND.I2.EQ.J2.AND.L3.EQ.2)B(K)=B(K)+Y(6)*.25*DSQRT(L*(L-
     R1.))*DSQRT(N*(N-1.))
      IF(I1.EQ.J1.AND.I2.EQ.J2.AND.L3.EQ.2)B(K)=B(K)+Y(6)*(L+.5)*.5*DSQR
     RT(N*(N-1.))
      IF(L1.EQ.2.AND.I2.EQ.J2.AND.I3.EQ.J3)B(K)=B(K)+Y(6)*.5*DSQRT(L*(L-
     R1.))*(N+.5)
      IF(I1.EQ.J1.AND.L2.EQ.2.AND.I3.EQ.J3)B(K)=B(K)+Y(7)*(M-.5)*DSQRT(M
     R*(M-1.))
      IF(I1.EQ.J1.AND.L2.EQ.4.AND.I3.EQ.J3)B(K)=B(K)+Y(7)*.25*DSQRT(M*(M
     R-1.)*(M-2.)*(M-3.))
      IF(I1.EQ.J1.AND.L2.EQ.2.AND.I3.EQ.J3)B(K)=B(K)+Y(8)*.5*DSQRT(M*(M
    -1.))*(N+.5)
      IF(I1.EQ.J1.AND.L2.EQ.2.AND.L3.EQ.2)B(K)=B(K)+Y(8)*.25*DSQRT(M*(M-
     R1.))*DSQRT(N*(N-1.))
      IF(I1.EQ.J1.AND.I2.EQ.J2.AND.L3.EQ.2)B(K)=B(K)+Y(8)*(M+.5)*.5*DSQR
     RT(N*(N-1.))
      IF(L1.EQ.1.AND.I2.EQ.J2.AND.I3.EQ.J3)B(K)=B(K)+Y(9)*1.5*L*DSQRT(L/
     R2.)*(M+.5)
      IF(L1.EQ.1.AND.L2.EQ.2.AND.I3.EQ.J3)B(K)=B(K)+Y(9)*1.5*L*DSQRT(L/2
     R.)*.5*DSQRT(M*(M-1.))
      IF(L1.EQ.1.AND.I2.EQ.J2.AND.I3.EQ.J3)B(K)=B(K)+Y(10)*DSQRT(L/2.)*
     R((6.*M+6.)*M+3.)/4.
      IF(L1.EQ.1.AND.L2.EQ.2.AND.I3.EQ.J3)B(K)=B(K)+Y(10)*DSQRT(L/2.)*(
     RM-.5)*DSQRT(M*(M-1.))
      IF(L1.EQ.1.AND.L2.EQ.4.AND.I3.EQ.J3)B(K)=B(K)+Y(10)*DSQRT(L/2.)*.2
     E5*DSQRT(M*(M-1.)*(M-2.)*(M-3.))
      IF(L1.EQ.1.AND.I2.EQ.J2.AND.L3.EQ.2)B(K)=B(K)+Y(11)*DSQRT(L/2.)*(M
     R+.5)*.5*DSQRT(N*(N-1.))
      IF(L1.EQ.1.AND.I2.EQ.J2.AND.I3.EQ.J3)B(K)=B(K)+Y(11)*DSQRT(L/2.)*(
     RM+.5)*(N+.5)
      IF(L1.EQ.1.AND.L2.EQ.2.AND.I3.EQ.J3)B(K)=B(K)+Y(11)*DSQRT(L/2.)*.5
     R*DSQRT(M*(M-1.))*(N+.5)
      IF(L1.EQ.1.AND.L2.EQ.2.AND.L3.EQ.2)B(K)=B(K)+Y(11)*DSQRT(L/2.)*.25
     R*DSQRT(M*(M-1.))*DSQRT(N*(N-1.))
      IF(I1.EQ.J1.AND.I2.EQ.J2.AND.I3.EQ.2)B(K)=B(K)+Y(12)*(N-.5)*DSQRT(
     RN*(N-1.))
      IF(I1.EQ.J1.AND.I2.EQ.J2.AND.I3.EQ.4)B(K)=B(K)+Y(12)*.25*DSQRT(N*(
     RN-1.)*(N-2.)*(N-3.))
      IF(L1.EQ.1.AND.I2.EQ.J2.AND.I3.EQ.J3)B(K)=B(K)+Y(13)*1.5*L*DSQRT(L
     R/2.)*(N+.5)
      IF(L1.EQ.1.AND.L2.EQ.2.AND.I3.EQ.J3)B(K)=B(K)+Y(13)*1.5*DSQRT(L/2.
     R)*.5*DSQRT(N*(N-1.))
      IF(L1.EQ.1.AND.I2.EQ.J2.AND.I3.EQ.J3)B(K)=B(K)+Y(14)*DSQRT(L/2.)*(
     R(6.*N+6.)*N+3.)/4.
      IF(L1.EQ.1.AND.L2.EQ.2.AND.I3.EQ.J3)B(K)=B(K)+Y(14)*DSQRT(L/2.)*(N
     R-.5)*DSQRT(N*(N-1.))
      IF(L1.EQ.1.AND.L2.EQ.4.AND.I3.EQ.J3)B(K)=B(K)+Y(14)*.25*DSQRT(L/2.
```

```
   T)*DSQRT(N*(N-1.)*(N-2.)*(N-3.))
    IF(I1.EQ.J1.AND.I2.EQ.J2.AND.I3.EQ.J3)B(K)=EO-C
16  CONTINUE
    NN=12
    IZ=12
    JOBN=2
2FORMAT(2X,E20.10)
    CALL EIGRS(B,NN,JOBN,D,Z,IZ,WK,IER)
    N2=NN/2
    N3=N2+1
34  FORMAT(10X,6E18.8)
    WRITE(6,33) (D(I),I=1,N2)
    WRITE(6,34) (D(I),I=N3,NN)
33  FORMAT(2X,6E18.8)
    SRT2=1.414213562
    DO  11 I=1,NN
    ANS=Z(1,I)*Z(2,I)+Z(3,I)*Z(5,I)+Z(7,I)*Z(8,I)+Z(9,I)*Z(11,I)+SRT2
   E*Z(2,I)*Z(4,I)+SRT2*Z(8,I)*Z(10,I)
    WRITE(6,37) I,ANS
11  CONTINUE
37  FORMAT(3X,I4,2X,E20.9)
    DO 32 I=1,NN
    WRITE(6,33) (Z(I,J),J=1,N2)
    WRITE(6,34) (Z(I,J),J=N3,NN)
32  CONTINUE
    IF(C.NE.0.0) GO TO 88
    C=D(1)-A(1,1)*X(1)-A(1,2)*X(2)-A(1,3)*X(3)
    IF(C.NE.0.0) GO TO 27
88  CONTINUE
    STOP
    END
```

APPENDIX 2 COMPUTER ANALYSIS AND LINESHAPE FITS

All the fluorescence linescan data were numerically reduced by fitting the data to the appropriate background and resonance dip. This appendix describes what equations the data was fitted to and also briefly describes the method and computer program used in the fit.

EXPRESSIONS FOR THE SATURATED LINESHAPE

The linescans taken in Chapter 5 were really a convolution of the laser power profile and the actual fluorescence signals. Initially in all the fits, the power profile is assumed to be negligible or its effect could be incorporated in the background signal by distorting the Gaussian background. In all the fits, the nonlinear standing wave resonance will be modeled as a Lorentzian of height A and FWHM $\Delta\nu_L$

$$L = \frac{A}{1+\{2(\nu-\nu_o)/\Delta\nu_L\}^2}$$

Even though it was emphasized that the lineshape appears asymmetric in many of the linescans and that this can also give rise to a 'suppposed' frequency shift, these factors are not taken into account in the lineshape fit. The reason is because one cannot trust the frequency shift obtained from such a coarse (coarse relative to the actual size 'real' 1 to 10 KHz shift) linescan where so many other factors including drift, noise, power error, offsets, and PZT hysteresis can easily influence the asymmetry and supposed shift. The asymmetry can be incorporated by assuming that the background peak and the Lorentzian peak do not coincide. (In actual measurements, they rarely coincide and hence the fit is to a Gaussian offset from an exact Lorentzian. To ease computations, the background Gaussian is expanded in first order as an offset parabola

$$G = A + B(\nu-\nu_o)+C(\nu-\nu_o)^2$$

Both the background approximation and the Lorentzian approximation were almost textbook exact since the least squares fit reconstructed the actual data over the entire laser scan except perhaps at the very edges of the lock. Thus the general expression of the shape of the fluorescence signal is

$$I= a_1 + a_2x + a_3x^2 - a_4/(1+4x^2/a^2_5)$$

(A2-1)

and the corresponding derivative signal is

$$I' = a_2 + 2_3x - 8xa_4/a^2{}_5/ (1+4x^2/a^2{}_5)^2 \qquad \text{(A2-2)}$$

where x is the detuning $\nu-\nu_o$.

As mentioned in Chapter 5, almost all the linescans that were taken were derivative linescans. Initially, the I' derivative scans were integrated to yield the I scans; these I scans were subsequently fit to five a_i parameters. As mentioned before, these numerically integrated lineshapes gave textbook perfect profiles of an offset parabola and the Lorentzian dip. But later on, as we became more aware of the asymmetry problem, most of the data reduction focused on the unaltered derivative signal. A different fitting procedure was used to try to get rid of the anomalous asymmetry and the amplitude variations caused by it. First a background line a_2+2a_3x was fitted to the derivative signal. This least squares fit line was subtracted off the real derivative data to provide a hopefully unbiased representation of the resonance signal. Then a standard Lorentzian was fitted to the resulting data points. During this data reduction process, the background slope, the supposed frequency zero offset, FWHM, and the variations

both in amplitude and in frequency of the + and - peaks of the derivative signals were recorded. As expected, large asymmetries gave large zero frequency offsets and also large frequency and amplitude variations in the + and - derivative peaks. Still, in almost all the fits,the dip was essentially a Lorenztian except perhaps at the tail while the background was almost exactly an offset parabola. Even though information on the slope error, the + and - derivative variations and the zero frequency offsets was obtained, the linescans were not a reliable way to correct for these errors because of the nature and drift and hysteresis associated with these linescans. These linescans cover a very large frequency range compared to the 1 or 10 KHz (equivalent to one scan data point) pressure shifts. Thus any attempts to correct the lineshift error using the offsets derived from the linescans can be grossly erroneous and variable. Effectively the errors are presented visually by these linescans and the results from the scans can only give typical values of the error and not the actual corrections.

COMPUTER FIT

All the linescans were fitted to their respective

lineshapes either by the standard least squares fit of a polynomial or else a nonlinear least squares fit of several adjustable parameters as in the case of the complete lineshape profile. All nonlinear least squares fit followed a two step Marquardt algorithm which is a hybrid between the Gauss and gradient methods. This method is described in detail in Bevington's book on "Data Reduction and Analysis" (714).

In the least squares problem, a fitting function f(x,a) is used to fit N data points (x,y) where a is a n-vector of parameters to be fit. The differences e_i are

$$e_i = |y_i - f(x_i,a)| \quad \text{and}$$

$$\chi^2 = \Sigma_i \, e^2_i$$

The only modification to the Marquardt method is to minimize

$$S = \chi^2 + \Sigma_i \, (\delta a_i)^2$$

Given an intial guess to the parameters a_o, each successive guess $a = a_o + \delta a$ is obtained so that is S is minimized. The following flowchart in Figure A1 summarizes the algorithm used in these fits. Note all the computer fits

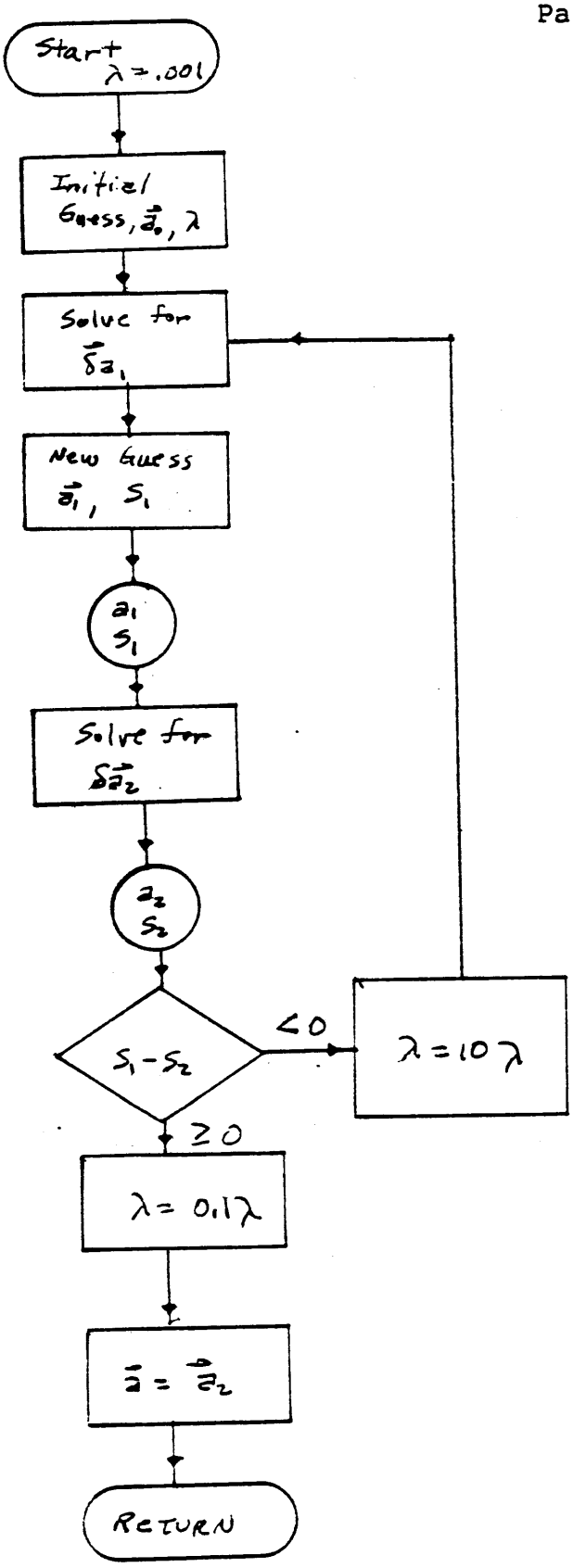

Figure A1

Flowchart for Nonlinear Least Squares Fit

were done on the HP 9825 computer system since all the data were recorded and stored either on tape or disk.

APPENDIX 3 SERVO LOCK SYSTEM

It was very evident from the measurements and from the standard deviation taken with an older servo lock system (referring to the system described in Reference 121) that the feedback servo electronics needed to be rebuilt and redesigned to meet the stringent requirements necessary to measure the pressure shifts in CO_2 In essence, the new feedback servo system must combine a phase sensitive detection system with a built in X400 gain servo amplifier system; this system should be detector noise limited and whose servo output have drift and stability of better than 1mv DC over days of continuous operation. It is the drift and stability requirements for the high voltage (-400V max) DC amplifier that made this system unique. Accordingly, precautions were taken with all the ground loops, leakage, high voltage components, construction components and overall design considerations to minimize the various sources of drift and leakage in the system.

The system is composed of Brower 261 preamplifiers and the extensively modified 131 Brower lockins as the front end detection system. The Brower 131 is used primarily as a

front end gain control unit which receives the signal and amplifies the signal to 1mv p-p via its front end buffer amplifier. This buffered signal is then feed into a separate servo chassis which contains all the electronics necessary to synchronously demodulate the buffered signal and then generate the necessary high voltage output to the PZT cylinder. After supplying the buffered signal, the 131 lockin functions as a normal lockin, analyzing the input signal in its own chassis plus providing an independent visual and analog output. The overload signals from the front end amplifier and buffer amplifier are also fed into the separate servo chassis from the 131 lockin. Thus,except for the preamplifier gain, the 131 lockin does not actively interfere with the actual servo electronics and thus cannot add any of its noise or drift into the feedback system.

The separate servo chassis serves two functions: it synchronously detects the actual signal and then integrates the rectified signal using a DC (-400V) chopper stabilized amplifier. Drift and stability due to voltage or current offsets are minimized and hopefully nulled out so that there is zero offset at the DC output (on the ±1mV level) Note that this system does not directly convert the rectified signal to a DC value to be used as the input of an RC

integrator; instead the rectified signal is fed directly into the DC chopper stabilized amplifier and thus eliminating another source of noise and drift in the servo path.

The signal processing is summarized in the block diagram in Figure A2. The buffered signal from the 131 lockin is first feed into a tuned amplifier. This bandpass amplifier is composed of cascaded lowpass and highpass filters both rolling off at -40 db/decade and has an overall gain of 80. Then the signal is inverted and both inverted and noninverted signals are AC coupled into an AC high voltage amplifier which has a gain of 50 and a 75:1 overload capability. This amplifier, with a -3db point at 10 Hz and 5KHz, was designed to operate at ±900V AC but is actually AC limited to a ±450 V output; thus the amplifier never suffers from saturation or phaseshift error or oscillations since it operates with such huge overload capabilities. This AC amplifier signal is further AC coupled to a special synchronous demodulation circuit. The resulting rectified output is fed into the DC chopper stabilized amplifier which supplies the output voltage to the PZT cyclinder. Special considerations must be taken with this DC amplifier. Any offset error from the synchronous rectifier and the rest of

the system could be nulled out by a current and/or voltage bucking scheme to bring the DC chopper stabilized output as close to zero mV as possible. The frequency for the chopper stabilized amplifier was taken off the 60 Hz line frequency so as not to introduce any addition frequencies to the detection electronics. Essentially in this DC amplifier, a miniature lockin system referenced at 30 Hz detects the error voltage on the - terminal of the DC amplifier and then injects a corresponding error servo voltage to the + terminal to keep the + and - terminal at equal voltages. Note, as an example of the precautions taken, there exist a separate AC signal ground in the input bandpass amplifier plus a separate DC signal ground in the synchronous rectifier in addition to the overall chassis ground.

In normal lock operations the input to the chopper stabilized amplifier is just the rectified output. Figure A3 gives a simplified diagram of the different servo modes. To get to lock operations, the system must first operate in search mode. In this mode, the DC amplifier acts like a normal inverting amplifier with a feedback R= 3.3M and a input R= 68K for a gain of ±15V(3.3M/68K)= 500V when the input search voltage covers ±15V. By adjusting a search potientiometer connected to the ±15V, the output voltage to

the PZT cylinder can be adjusted until the resonance dip is reached; then the system is switched into lock mode where the feedback resistor is dropped out and only 600V polystyrene capacitors are used in the feedback path of the amplifier. Thus the effective AC time constant is RC where R = 3.3M and C are the polystyrene capacitors. An external ramp voltage, taking the place of the feedback error voltage, can also drive the output voltage of the DC amplifier. In the ramp mode operation, the servo is positioned in the search mode and the search potentiometer is adjusted until the desired starting DC voltage is reached. Then a ±15V max ramp voltage (from an external ramp generator with adjustable time duration) is added to this search voltage, driving the DC output voltage to follow the ramp input. This is used to generate the frequency locked linescan or just a regular ramp line scan since the laser frequency is adjusted to follow the DC output voltage.

In this system, as in the normal Brower 131 lockin system, there exist BNC monitors of the rectified signal and the chopper stabilized reference output plus the option to calibrate the whole system by injecting a test signal at the preamp input and then monitoring the final analog output

and rectified signals. In addition, a separate overload light monitors the overloads in the buffer amp, bandpass filter, and the AC and DC outputs.

In light of all the special precautions to eliminate noise and extraneous signals at the reference frequency, a separate oscillator box was built containing all the synchronous reference frequencies for the rectifier cards and the modulation circuit. Thus one 555 timer configuration provides one reference signal from which all the correct phasing and modulation frequencies originated for both lasers. There is one reference frequency source but two separate adjustable lockin channels for the left and right lasers. Thus this separate box provides two sets of in phase and out of phase demodulation reference signals, one set for the 131 lockin and one set for the upper serve chassis for both left and right channels.

Given the reference frequency from the 555 timer, correctly phased square waves have to be provided for the rectifier monitors. Thus a quadrant select MUX and a variable delay provides a four quadrant, 0-120° phase adjustment for each square wave demodulation reference signal. In the modulation board a square wave trigger from

the 555 oscillator is converted into a sinusoid using two consecutive double pole bandpass state filters, BB-UAF-31. Then two independent, variable phase, variable voltage amplitude, current boosted (by the BB3302/03 amplifiers) sinewaves were generated to provide the two PZT stack voltages. The variable phase and variable voltage capability is very important since each individual PZT has its own separate hysteresis history and frequency response such that separate phase and voltage adjustments are necessary to null out as much as possible the frequency modulation on the final beat signal ($\nu_1 - \nu_2$)

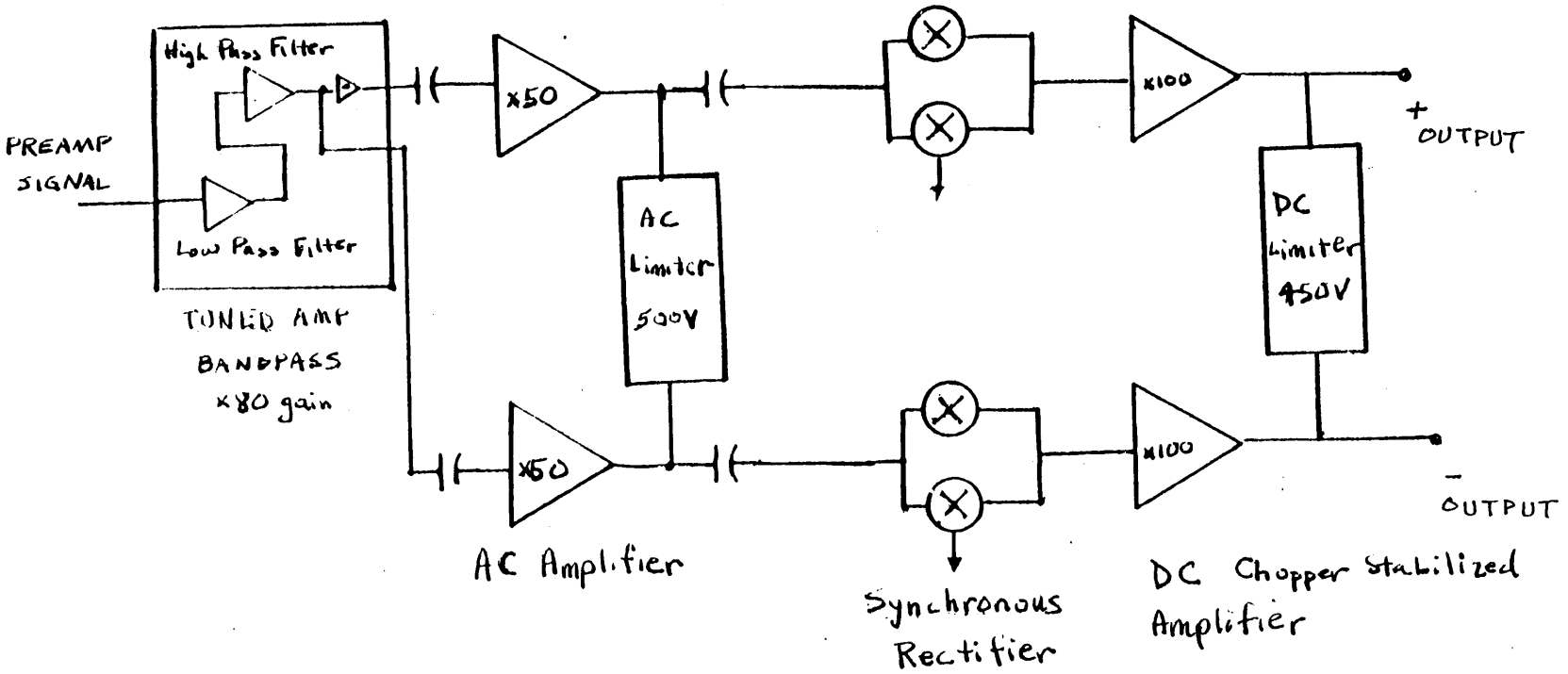

Figure A2 Block Diagram of Servo Electronics

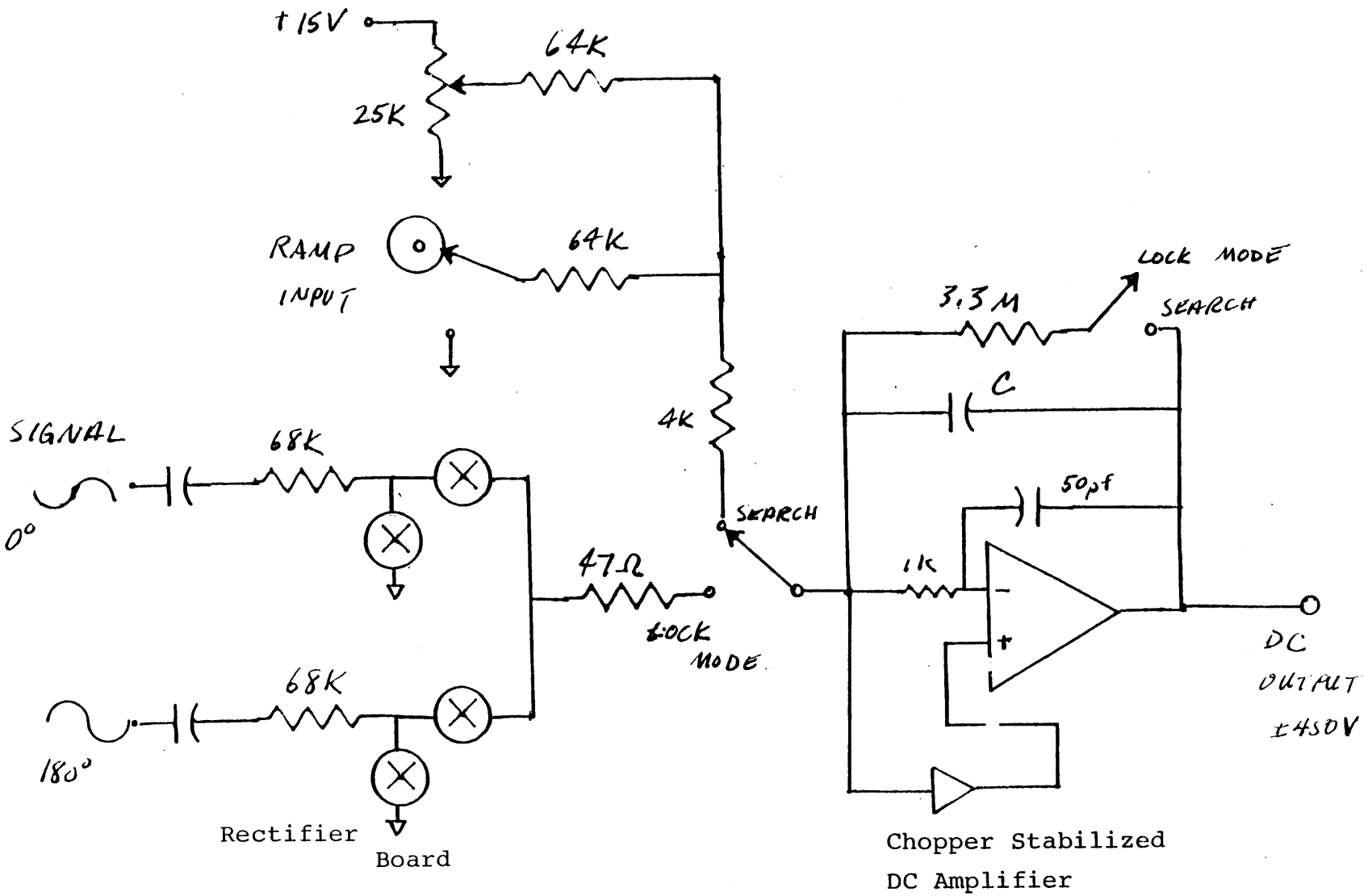

Figure A3 Block Diagram of Search,Lock and Ramp Modes

APPENDIX 4 LINESCAN LOCK BOX

The phase lock and frequency lock box used in all the linescan experiments was designed to lock a raw input frequency with a reference LO signal by creating the desired error phase and frequency servo voltages needed to lock the lasers. All frequency and phase discriminators were done digitally using TTL logic; the error TTL signals were then converted into analog ±15V signals to be fed into the appropriate feedback loop.

The lock box consists of three basic blocks built on three different component boards; these included the frequency discriminator board, the phase discriminator board and the servo compensation board. A total block diagram and separate block diagram follow this appendix in Figures A4 to A5. Basically the reference and the raw frequency (beat signal) are both fed into the frequency and phase boards. The corresponding frequency and phase errors are fed into the servo compensation board which generates the servo error voltages that are fed either into the PZT stack (phase error) or into the ramp (frequency error) input and then to the PZT cylinder.

In the frequency board, the absolute frequencies of the LO reference signal and the raw beat signals are compared to find which signal is high, low or if they are both equal; an appropriate difference amplifier logically combines this high or low information and feeds an error frequency signal to the servo board. In terms of the actual components, each input signal triggers two cascaded dual 4 bit binary counters (74393) which count continously throughout the operation. The 16 bit output for each input channel is compared against the other input channel using four cascaded 4 bit (7485) magnitude comparators. The final comparator triggers a set of flipflops (7475) which updates the high, low or equal counting signals. When any one counter triggers the 15th bit, a 74121 monostable generates a one shot reset pulse so that the 74393 counters start the counting sequence over again. Thus a continuous + or - frequency discriminator error signal is obtained from this frequency discriminator board.

In contrast, the phase discriminator board works only when the frequency of the two inputs signals are very close together. In the phase compensation board, each signal, after passing through a pulse forming LC network, is divided down several times to 'spread' out and emphasize the phase

difference between the two signals. Then by NANDing the two 'lower' frequencies together, a variable length 'pulse train' proportional to the relative phase error is integrated and amplified as the final phase error signal from the phase compensation board. In the phase board, the relative degree of phase matching (dividing down by 2,4,8,16) is controlled by choosing the appropriate 7493 counter output to be NANDed via the 7415 multiplexer. Further phase enhancement is achieved by counting down with the dual 74393 counter before NANDing the signals together. Thus an effective means of obtaining the digital phase error is achieved with this process.

The servo board takes the frequency and phase error voltages for the final amplification and integration. The phase error is amplified and then current boosted; it is then transformer coupled with the modulation voltage so that both voltages could be fed into the PZT stack. The frequency error is also amplified and integrated and then fed as the ramp input for the high voltage DC amplifier. In actual operations of the frequency lock system, the PZT cyclinder voltage is tuned until the system is very close to frequency lock. Then the short across the integrating amplifier is lifted via a toggle switch and the frequency

error servo system produces the ramp input voltage that controls the frequency locking and tracking. An extra toggle switch changes the polarity of the frequency error signal in case the error voltage is of the wrong polarity; this is very useful because all the frequency sweeps were done with the same conventions for Laser 1 and Laser 2. Thus the polarity of the servo errors will differ if $\nu_1-\nu_2$ is positive or negative.

In this system, the frequency response was limited not by the TTL response but rather by how large a raw beat signal could be obtained; this was especially true since a minimun of +0 to +5 db beat signal was needed for the TTL to work properly. Thus the beat amplifiers and the beat detector response imposed a limit on the scan frequencies to at most ±9 MHz off line center before the frequency lock would drop out.

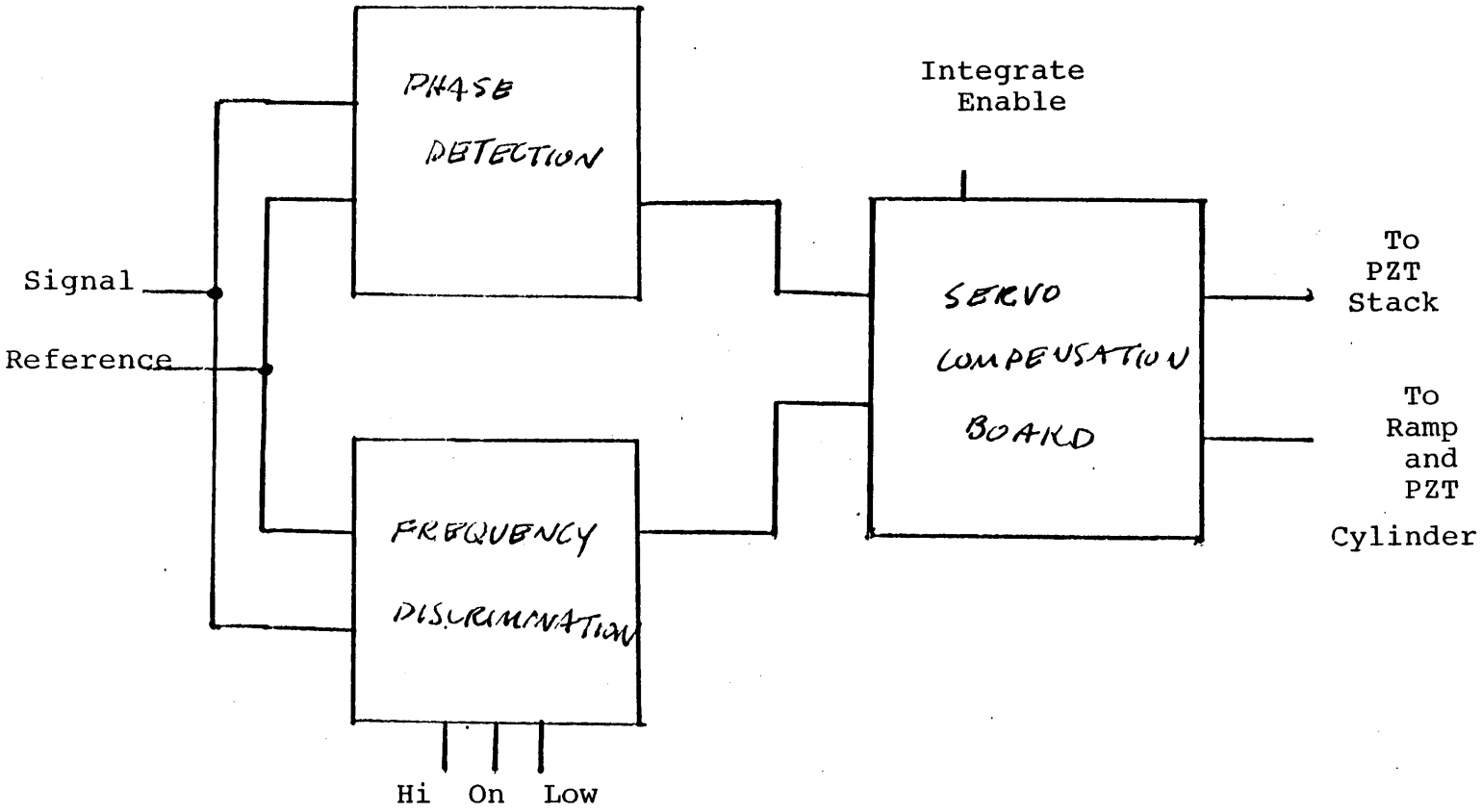

Figure A4 Block Diagram of Linescan Locking Box

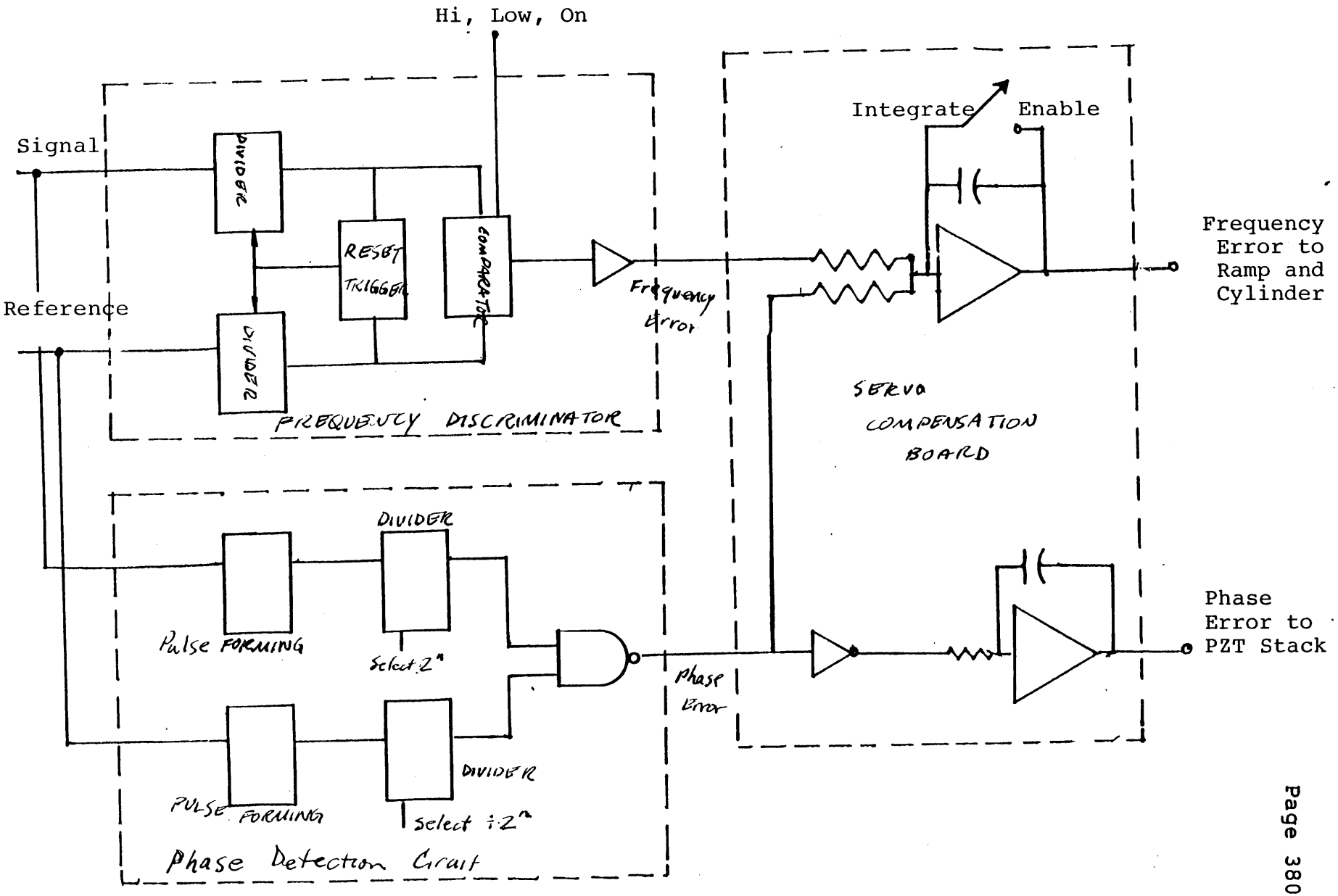

Figure A5 Components of Linescan Locking Box

APPENDIX 5 SPECTROSCOPIC CONSTANTS AND BEAT FREQUENCIES

This appendix lists the rotational spectroscopic constants used in determining the frequencies for any J of the P or R branch transitions. The constants are given in the same format as was tabulated in Reference 121 and as utilized in the HPL programs listed in Appendix 6. Specifically, the energy for each vibrational-rotation level $E(\nu_o,J)$ is of the form

$$E= \nu_o+BJ(J+1)-DJ^2(J+1)^2 +HJ^3(J+1)^3+LJ^4(J+1)^4$$

The values of ν_o and B,D,H, and L are given in Table A9 for the participation levels (001) and $(100,020)_I$ and $(100,020)_{II}$ Note that the constants for the (001) level are given directly while the constants for the I and II levels are given as the difference of the (001) and the I or II level constants, B(001-II) or B(001-II). Accordingly, the energies for any P(J→J-1) or R(J→J+1) transition is obtained by using these spectroscopic constants in their appropriate J polynomial. The HPL subroutine 'Pnum' and 'Rnum' in the main programs Sfine, and Go list the J polynomial that results from using this specific form of the spectroscopic constants when calculating the lasing energies for any J

value in the P or R branch, respectively. Table A9 lists the particular rotational spectroscopic constants for 9 different isotopes, including those of the recently measured 16-13-18 and 17-12-17 isotopes; these constants were obtained by using the same least square procedure described in Reference 121. The beat frequency listings in the extended Table A10 gives the predicted IF obtained by heterodyning Laser 1 with Laser 2 (ν_1-ν_2); only those beats frequencies which are less than 17 GHz are listed. All the various combinations of the beat frequencies for the four isotopes measured in this experiment are tabulated in the extended Table A10.

	16-12 16	8-12-18	16-13-16
	2.88088138342E 07	2.[illegible]85970802E 07	2.73837925886E 07
V[II]	3.18899601577E 07	3.24891929454E 07	3.05086592233E 07
B[001]	1.16062071900E 04	1.03155592200E 04	1.16101646718E 04
B[I]	-9.13625419912E 01	-9.93347620330E 01	-7.32767445844E 01
B[II]	-1.00157630847E 02	-7.29682192958E 01	-1.09200019653E 02
D[001]	3.98845161191E-03	3.15004934426E-03	3.98470179950E-03
D[I]	5.42070167380E-04	3.82409281260E-04	3.80127894[illegible]E-04
D[II]	-7.23338791102E-04	-3.67727110371E-04	-7.62738718133E-04
H[001]	6.72072683569E-10	3.33609879393E-11	5.53511834999E-10
H[I]	-5.19291746705E-09	-2.29457166683E-09	-5.82792197848E-09
H[II]	-6.52083347268E-09	-4.50166579399E-09	-7.80325212117E-09
L[001]	-4.15682419638E-14	4.35724889876E-14	-1.62979749364E-14
L[I]	-1.19279139010E-14	1.88284759227E-14	-8.48818164176E-14
L[II]	2.19528352777E-14	4.22478294609E-14	8.36158200610E-14

	16-14-16	18-13-18	18-14-18
V[I]	2.59659174866E 07	2.78385511435E 07	2.66579399406E 07
V[II]	2.94600024006E 07	3.07858843541E 07	2.94562833798E 07
B[001]	1.16136686727E 04	1.03190957315E 04	1.03222230409E 04
B[I]	-6.10562229704E 01	-8.43777868664E 01	-6.91773597[illegible]8E 01
B[II]	-1.13385278095E 02	-7.98866179900E 01	-8.79480466163E 01
D[001]	3.98175513257E-03	3.14833491578E-03	3.14696652761E-03
D[I]	2.04619398164E-04	4.30235978289E-04	3.75553944409E-04
D[II]	-8.41650276208E-04	-5.08869653060E-04	-5.71407958761E-04
H[001]	6.99622105610E-10	4.38995121869E-10	6.94775269808E-10
H[I]	-2.68085579720E-09	-2.78510671054E-09	-1.59481859995E-09
H[II]	-1.25551060029E-08	-4.82603954234E-09	-4.38628081524E-09
L[001]	-8.89463886033E-14	-3.01708191654E-14	-1.86351676467E-14
L[I]	-2.45786063941E-13	-8.42186171791E-15	-4.75176593840E-13
L[II]	1.02186990066	9.7312988556[illegible]	1.10970861369E-14

Table A9 Rotational Spectroscopic Constants

	16-12-18	16-13-18	17-12-17
V[I]	2.89680123538E 07	2.76916621439E 07	2.89495325081E 07
V[II]	3.21583506379E 07	3.06109627486E 07	3.21484618132E 07
B[001]	1.09510226695E 04	1.09541711784E 04	1.09215332679E 04
B[I]	-9.67017939109E 01	-7.89188133422E 01	-9.68116333072E 01
B[II]	-8.49817956709E 01	-9.42084780179E 01	-8.45643740682E 01
D[001]	3.55094183510E-03	3.55102057777E-03	3.52544585511E-03
D[I]	4.86099795138E-04	4.55642089419E-04	4.80888418282E-04
D[II]	-5.45023624953E-04	-6.53963727003E-04	-5.39728401486E-04
H[001]	1.96979502613E-10	3.04246767642E-09	-5.37587993972E-09
H[I]	-2.81552958256E-09	1.69637589541E-09	-3.31442538068E-09
H[II]	-3.97211398701E-09	-1.31737610363E-08	-6.66954150231E-09
L[001]	1.00681516587E-14	-9.74242336202E-13	1.91589731334E-12
L[I]	-4.99483494754E-14	-3.02382249221E-12	3.20957621469E-14
L[II]	-7.72640242034E-13	3.74752072610E-12	3.44234276459E-13

Table A9 Rotational Spectroscopic Constants (continued)

Table A10 Calculated Beat Frequencies

16-13-16		18-12-18		
	Frequency (MHz)		Frequency (MHz)	Beat (MHz)
1R- 2	27453013.47210	1P-58	27449958.79270	3054.6794
1R- 4	27498426.55600	1P-56	27514420.98350	-15994.4275
1R- 8	27587486.03510	1P-54	27578044.11750	9441.9176
1R-10	27631129.94820	1P-52	27640832.02090	-9702.0727
1R-14	27716638.80370	1P-50	27702788.33720	13850.4665
1R-16	27758500.36900	1P-48	27763916.53000	-5416.1610
1R-20	27840428.18720	1P-46	27824219.88490	16208.3023
1R-22	27880490.13730	1P-44	27883701.51160	-3211.3743
1R-26	27958798.16360	1P-42	27942364.34650	16433.8171
1R-28	27997038.96510	1P-40	28000211.15490	-3172.1898
1R-32	28071679.68330	1P-38	28057244.53180	14435.1515
1R-34	28108073.28900	1P-36	28113466.90560	-5393.6166
1R-38	28178989.84210	1P-34	28168880.53830	10109.3038
1R-40	28213505.35890	1P-32	28223487.52890	-9982.1700
1R-44	28280630.79860	1P-30	28277289.81380	3340.9848
1R-46	28313232.06660	1P-28	28330289.16890	-17057.1023
1R-48	28345186.23220	1P-28	28330289.16890	14897.0633
1R-50	28376488.41100	1P-26	28382487.21170	-5998.8007
1R-54	28437116.07010	1P-24	28433885.40180	3230.6683
1R-56	28466430.55650	1P-22	28484485.04340	-18054.4869
1R-58	28495071.04860	1P-22	28484485.04340	10586.0052
1R-60	28523031.37900	1P-20	28534287.28530	-11255.9063
2R-22	30987471.96490	2P-60	30991695.46640	-4223.5015
2R-26	31059009.22600	2P-58	31049479.89620	9529.3298
2R-28	31093488.45840	2P-56	31106752.54080	-13264.0824
2R-32	31159883.67480	2P-54	31163509.49330	-3625.8185
2R-36	31222884.94380	2P-52	31219746.91520	3138.0286
2R-40	31282524.18230	2P-50	31275461.04190	7063.1404
2R-44	31338837.09930	2P-48	31330648.18640	8188.9129
2R-48	31391863.00760	2P-46	31385304.74340	6558.2642
2R-52	31441644.62390	2P-44	31439427.19360	2217.4303
2R-56	31488227.85850	2P-42	31493012.10810	-4784.2496
2R-58	31510335.25010	2P-42	31493012.10810	17323.1420
2R-60	31531661.60020	2P-40	31546056.15100	-14394.5508
2P-24	29886344.53070	1R-60	29875439.61430	10904.9164
2P-26	29828925.55000	1R-54	29822756.78260	6168.7674
2P-26	29828925.55000	1R-56	29841192.61690	-12267.0669
2P-28	29770668.18480	1R-48	29762259.68590	8408.4989
2P-28	29770668.18480	1R-50	29783285.56320	-12617.3784
2P-30	29711577.07330	1R-42	29694074.31740	17502.7559
2P-30	29711577.07330	1R-44	29717649.83610	-6072.7628
2P-32	29651657.11190	1R-38	29644401.94420	7255.1677
2P-32	29651657.11190	1R-40	29669657.08640	-17999.9745
2P-34	29590913.44920	1R-34	29591392.29950	-478.8503
2P-36	29529351.48260	1R-30	29535072.48870	-5721.0061
2P-38	29466976.85050	1R-26	29475467.03000	-8490.1795
2P-40	29403795.42940	1R-22	29412597.90400	-8802.4746
2P-42	29339813.32610	1R-18	29346484.59840	-6671.2723
2P-44	29275036.87260	1R-14	29277144.14590	-2107.2733
2P-46	29209472.61980	1R-10	29204591.15820	4881.4616
2P-48	29143127.33110	1R- 6	29128837.85260	14289.4785
2P-50	29076007.97620	1R- 4	29089764.24920	-13756.2730
2P-52	29008121.72400	1R- 0	29009228.18600	-1106.4620
2P-54	28939475.93600	1P- 2	28946738.92180	-7262.9858
2P-56	28870078.16040	1P- 6	28860640.35640	9437.8040
2P-58	28799936.12380	1P- 8	28816400.49790	-16464.3741
2P-60	28729057.72540	1P-12	28725539.89410	3517.8313

	16-12-16		18-13-18	
	Frequency (MHz)		Frequency (MHz)	Beat (MHz)
1R-20	29257658.52990	2P-60	29264508.38340	-6849.8535
1R-24	29333861.15920	2P-58	29323720.01050	10141.1487
1R-26	29370829.61990	2P-56	29382386.96300	-11557.3431
1R-30	29442483.32000	2P-54	29440503.88350	1979.4365
1R-34	29511066.68320	2P-52	29498065.52410	13001.1591
1R-36	29544196.33660	2P-50	29555066.75200	-10870.4154
1R-40	29608108.16120	2P-48	29611502.55550	-3394.3943
1R-44	29668855.85290	2P-46	29667368.04960	1487.8033
1R-48	29726394.79400	2P-44	29722658.48030	3736.3137
1R-52	29780676.06540	2P-42	29777369.23060	3306.8345
1R-56	29831646.25670	2P-40	29831495.82450	150.4322
1R-60	29879247.26410	2P-38	29885033.93230	-5786.6682
1P- 2	28761840.93830	1R-58	28759727.66920	2113.2691
1P- 2	28761840.93830	1R-60	28779899.81180	-18058.8735
1P- 4	28714137.73010	1R-54	28717086.70000	-2948.9699
1P- 6	28665704.61050	1R-48	28647468.43800	18236.1725
1P- 6	28665704.61050	1R-50	28671421.57830	-5716.9678
1P- 8	28616541.77240	1R-46	28622775.01320	-6233.2408
1P-10	28566649.19820	1R-42	28571186.38790	-4537.1897
1P-12	28516026.66070	1R-38	28516691.86710	-665.2064
1P-14	28464673.72070	1R-34	28459324.49430	5349.2264
1P-16	28412589.72630	1R-30	28399114.28010	13475.4462
1P-16	28412589.72630	1R-32	28429572.98300	-16983.2567
1P-18	28359773.81060	1R-28	28367951.67550	-8177.8649
1P-20	28306224.89070	1R-24	28303527.02370	2697.8670
1P-22	28251941.66470	1R-20	28236321.77690	15619.8878
1P-22	28251941.66470	1R-22	28270270.66260	-18328.9979
1P-24	28196922.61020	1R-18	28201682.77320	-4760.1630
1P-26	28141165.98100	1R-14	28130343.18050	10822.8005
1P-28	28084669.80430	1R-12	28093646.55040	-8976.7461
1P-30	28027431.87840	1R- 8	28018208.25420	9223.6242
1P-32	27969449.76820	1R- 6	27979469.53800	-10019.7698
1P-34	27910720.80260	1R- 2	27899959.09570	10761.7069
1P-36	27851242.06990	1R- 0	27859189.32240	-7947.2525
1P-38	27791010.41430	1P- 2	27796768.57910	-5758.1648
1P-42	27668274.46310	1P- 8	27667374.62740	899.8357
1P-44	27605762.59380	1P-10	27622895.05580	-17132.4620
1P-46	27542482.64400	1P-14	27531912.68330	10569.9607
1P-48	27478430.16590	1P-16	27485409.01510	-6978.8492
1P-52	27347988.45570	1P-22	27341839.33470	6149.1210
1P-54	27281588.93250	1P-24	27292626.45900	-11037.5265
1P-58	27146404.63510	1P-30	27140899.66160	5504.9735
1P-60	27077607.79190	1P-32	27088955.59030	-11347.7984
2P- 6	31746483.77240	2R-58	31733347.37080	13136.4016
2P- 6	31746483.77240	2R-60	31756153.77870	-9670.0063
2P- 8	31697061.40880	2R-54	31685990.38300	11071.0258
2P- 8	31697061.40880	2R-56	31709960.95480	-12899.5460
2P-10	31646843.37160	2R-50	31636280.73000	10562.6416
2P-10	31646843.37160	2R-52	31661431.61610	-14588.2445
2P-12	31595831.74030	2R-46	31584187.51130	11644.2290
2P-12	31595831.74030	2R-48	31610533.92080	-14702.1805
2P-14	31544028.86790	2R-42	31529681.84110	14347.0268
2P-14	31544028.86790	2R-44	31557237.95470	-13209.0868
2P-16	31491437.37900	2R-40	31501515.90200	-10078.5230
2P-18	31438060.16840	2R-36	31443342.20660	-5282.0382
2P-20	31383900.39760	2R-32	31382693.71760	1206.6800
2P-22	31328961.49370	2R-28	31319549.82410	9411.6696
2P-24	31273247.14520	2R-26	31287036.38430	-13789.2391
2P-26	31216761.29950	2R-22	31220116.58630	-3355.2868
2P-28	31159508.15930	2R-18	31150661.72370	8846.4356
2P-30	31101492.17870	2R-16	31114980.13260	-13487.9539
2P-32	31042718.05940	2R-12	31041703.22970	1014.8297
2P-34	30983190.74610	2R- 8	30965869.69660	17321.0495
2P-36	30922915.42240	2R- 6	30926993.03420	-4077.6118
2P-38	30861897.50530	2R- 2	30847319.28710	14578.2182
2P-40	30800142.64080	2R- 0	30806522.53300	-6379.8922
2P-42	30737656.69810	2P- 2	30744128.77050	-6472.0724
2P-44	30674445.76350	2P- 6	30658703.58490	15742.1786
2P-46	30610516.13630	2P- 8	30615036.06980	-4519.9335
2P-50	30480527.01970	2P-14	30480230.43500	296.5847
2P-54	30347743.73540	2P-20	30339758.29130	7985.4441
2P-56	30280322.09530	2P-22	30291685.25840	-11363.1631
2P-60	30143455.97710	2P-28	30143756.40690	-300.4298

16-12-16		16-13-16		
	Frequency (MHz)		Frequency (MHz)	Beat (MHz)
1R- 2	28877902.45180	2P-56	28870078.16040	7824.2914
1R- 4	28923046.44420	2P-54	28939475.93600	-16429.4918
1R- 8	29011133.01850	2P-52	29008121.72400	3011.2945
1R-14	29137736.12160	2P-48	29143127.33110	-5391.2095
1R-18	29218430.69000	2P-46	29209472.61980	8958.0702
1R-20	29257658.52990	2P-44	29275036.87260	-17378.3427
1R-24	29333861.15920	2P-42	29339813.32610	-5952.1669
1R-28	29407038.25060	2P-40	29403795.42940	3242.8212
1R-32	29477160.86430	2P-38	29466976.85050	10184.0138
1R-34	29511066.68320	2P-36	29529351.48260	-18284.7994
1R-36	29544196.33660	2P-36	29529351.48260	14844.8540
1R-38	29576545.14020	2P-34	29590913.44920	-14368.3090
1R-40	29608108.16120	2P-34	29590913.44920	17194.7120
1R-42	29638880.21350	2P-32	29651657.11190	-12776.8984
1R-44	29668855.85290	2P-32	29651657.11190	17198.7410
1R-46	29698029.37160	2P-30	29711577.07330	-13547.7017
1R-48	29726394.79400	2P-30	29711577.07330	14817.7207
1R-50	29753945.86890	2P-28	29770668.18480	-16722.3159
1R-52	29780676.06510	2P-28	29770668.18480	10007.8803
1R-56	29831646.25670	2P-26	29828925.55000	2720.7067
1R-60	29879247.26410	2P-24	29886344.53070	-7097.2666
1P-12	28516026.66070	1R-60	28523031.37900	-7004.7183
1P-14	28464673.72070	1R-56	28466430.55650	-1756.8358
1P-16	28412589.72630	1R-52	28407133.48000	5456.2463
1P-18	28359773.81060	1R-48	28345186.23220	14587.5784
1P-18	28359773.81060	1R-50	28376488.41100	-16714.6004
1P-20	28306224.89070	1R-46	28313232.06660	-7007.1759
1P-22	28251941.66470	1R-42	28247387.08450	4554.5802
1P-24	28196922.61020	1R-38	28178989.84210	17932.7681
1P-24	28196922.61020	1R-40	28213505.35890	-16582.7487
1P-26	28141165.98100	1R-36	28143844.54790	-2678.5669
1P-28	28084669.80430	1R-32	28071679.68330	12990.1210
1P-30	28027431.87840	1R-30	28034667.16050	-7235.2821
1P-32	27969449.76820	1R-26	27958798.16360	10651.6046
1P-34	27910720.80260	1R-24	27919947.64730	-9226.8447
1P-36	27851242.06990	1R-20	27840428.18720	10813.8827
1P-38	27791010.41430	1R-18	27799764.18770	-8753.7734
1P-40	27730022.43140	1R-14	27716638.80370	13383.6277
1P-42	27668274.46310	1R-12	27674181.40860	-5906.9455
1P-44	27605762.59380	1R- 8	27587486.03510	18276.5587
1P-46	27542482.64400	1R- 6	27543251.13280	-768.4888
1P-50	27413600.43720	1R- 0	27407012.90200	6587.5352
1P-52	27347988.45570	1P- 2	27336912.38330	11076.0724
1P-54	27281588.93250	1P- 4	27289446.60440	-7857.6719
1P-58	27146404.63510	1P-10	27143540.18440	2864.4507
1P-60	27077607.79190	1P-12	27093735.73280	-16127.9409
1P- 4	28714137.73010	2P-60	28729057.72540	-14919.9953
2P-14	31544028.86790	2R-60	31531661.60020	12367.2677
2P-16	31491437.37900	2R-56	31488227.85850	3209.5205
2P-18	31438060.16840	2R-52	31441644.62390	-3584.4555
2P-20	31383900.39760	2R-46	31365758.33720	18142.0604
2P-20	31383900.39760	2R-48	31391863.00760	-7962.6100
2P-22	31328961.49370	2R-42	31311094.05600	17867.4377
2P-22	31328961.49370	2R-44	31338837.09930	-9875.6056
2P-24	31273247.14520	2R-40	31282524.18230	-9277.0371
2P-26	31216761.29950	2R-36	31222884.94380	-6123.6443
2P-28	31159508.15930	2R-32	31159883.67480	-375.5155
2P-30	31101492.17870	2R-28	31093488.45840	8003.7203
2P-32	31042718.05940	2R-26	31059009.22600	-16291.1666
2P-34	30983190.74610	2R-22	30987471.96490	-4281.2188
2P-36	30922915.42240	2R-18	30912478.65990	10436.7625
2P-38	30861897.50530	2R-16	30873680.38800	-11782.8827
2P-40	30800142.64080	2R-12	30793471.81780	6670.8230
2P-42	30737656.69810	2R-10	30752058.84870	-14402.1506
2P-44	30674445.76350	2R- 6	30666611.00580	7834.7577
2P-46	30610516.13630	2R- 4	30622575.18230	-12059.0460
2P-48	30545874.32040	2R- 0	30531879.53670	13994.7837
2P-52	30414481.13060	2P- 4	30413595.23070	885.8999
2P-54	30347743.73540	2P- 6	30364755.63410	-17011.8987
2P-56	30280322.09530	2P-10	30264469.08490	15853.0104
2P-58	30212223.64360	2P-12	30213026.14200	-802.4984
2P-60	30143455.97710	2P-14	30160719.90730	-17263.9302

	16-12-16		18-12-18	
	Frequency (MHz)		Frequency (MHz)	Beat (MHz)
1R- 8	29011133.01850	1R- 0	29009228.18600	1904.8325
1R-10	29054072.71290	1R- 2	29049894.07300	4178.6399
1R-12	29096274.40410	1R- 4	29089764.24920	6510.1549
1R-14	29137736.12160	1R- 6	29128837.85260	8898.2690
1R-16	29178455.68270	1R- 8	29167113.87450	11341.8082
1R-18	29218430.69000	1R-10	29204591.15820	13839.5318
1R-20	29257658.52990	1R-12	29241268.39950	16390.1304
1R-22	29296136.37060	1R-16	29312216.79580	-16080.4252
1R-24	29333861.15920	1R-18	29346484.59840	-12623.4392
1R-26	29370829.61990	1R-20	29379945.65200	-9116.0321
1R-28	29407038.25060	1R-22	29412597.90400	-5559.6534
1R-30	29442483.32000	1R-24	29444439.14940	-1955.8294
1R-32	29477160.86430	1R-26	29475467.03000	1693.8343
1R-34	29511066.68320	1R-28	29505679.03250	5387.6507
1R-36	29544196.33660	1R-30	29535072.48870	9123.8479
1R-38	29576545.14020	1R-32	29563644.57250	12900.5677
1R-38	29576545.14020	1R-34	29591392.29950	-14847.1593
1R-40	29608108.16120	1R-34	29591392.29950	16715.8617
1R-40	29608108.16120	1R-36	29618312.52550	-10204.3643
1R-42	29638880.21350	1R-38	29644401.94420	-5521.7307
1R-44	29668855.85290	1R-40	29669657.08640	-801.2335
1R-46	29698029.37160	1R-42	29694074.31740	3955.0542
1R-48	29726394.79400	1R-44	29717649.83610	8744.9579
1R-48	29726394.79400	1R-46	29740379.67250	-13984.8785
1R-50	29753945.86890	1R-46	29740379.67250	13566.1964
1R-50	29753945.86890	1R-48	29762259.68590	-8313.8170
1R-52	29780676.06510	1R-48	29762259.68590	18416.3792
1R-52	29780676.06510	1R-50	29783285.56320	-2609.4981
1R-54	29806578.56490	1R-52	29803452.81700	3125.7479
1R-54	29806578.56490	1R-54	29822756.78260	-16178.2177
1R-56	29831646.25670	1R-54	29822756.78260	8889.4741
1R-56	29831646.25670	1R-56	29841192.61690	-9546.3602
1R-58	29855871.72960	1R-56	29841192.61690	14679.1127
1R-58	29855871.72960	1R-58	29858755.29660	-2883.5670
1R-60	29879247.26410	1R-60	29875439.61430	3807.6498
1R- 0	28832026.23260	1P- 8	28816400.49790	15625.7347
1R- 2	28877902.45180	1P- 6	28860640.35640	17262.0954
1P- 2	28761840.93830	1P-10	28771367.04190	-9526.1036
1P- 4	28714137.73010	1P-12	28725539.89410	-11402.1640
1P- 6	28665704.61050	1P-14	28678918.81140	-13214.2009
1P- 8	28616541.77240	1P-16	28631503.40170	-14961.6293
1P-10	28566649.19820	1P-18	28583293.12370	-16643.9255
1P-12	28516026.66070	1P-20	28534287.28530	-18260.6246
2R-30	32516543.62030	2R- 0	32509824.05120	6719.5691
2R-32	32550429.15530	2R- 2	32550648.16440	-219.0091
2R-34	32583536.62670	2R- 4	32590887.74530	-7351.1186
2R-36	32615869.68910	2R- 6	32630542.43580	-14672.7467
2R-38	32647432.23120	2R- 6	32630542.43580	16889.7954
2R-40	32678228.37060	2R- 8	32669612.01860	8616.3520
2R-42	32708262.44820	2R-10	32708096.41680	166.0314
2R-44	32737539.02260	2R-12	32745995.69230	-8456.6697
2R-46	32766062.86390	2R-14	32783310.04570	-17247.1818
2R-48	32793838.94850	2R-14	32783310.04570	10528.9028
2R-50	32820872.45130	2R-16	32820039.81440	832.6369
2R-52	32847168.73990	2R-18	32856185.47210	-9016.7322
2R-54	32872733.36770	2R-18	32856185.47210	16547.8956
2R-56	32897572.06610	2R-20	32891747.62640	5824.4397
2R-58	32921690.73800	2R-22	32926727.01740	-5036.2794
2R-60	32945095.44940	2R-22	32926727.01740	18368.4320
2R-60	32945095.44940	2R-24	32961124.51570	-16029.0663
2R- 0	31913172.55610	2P-26	31901961.30230	11211.2538
2R- 2	31958996.05030	2P-24	31950570.76810	8425.2822

2R- 4	32004017.37210	2P-22	31998614.15670	5403.2154
2R- 6	32048236.24130	2P-20	32046089.25980	2146.9815
2R- 8	32091652.65500	2P-18	32092993.99760	-1341.3426
2R-10	32134266.88640	2P-16	32139326.42040	-5059.5340
2R-12	32176079.48360	2P-14	32185084.71110	-9005.2275
2R-14	32217091.26870	2P-12	32230267.18700	-13175.9183
2R-16	32257303.33550	2P-10	32274872.30060	-17568.9651
2R-20	32335334.03700	2P- 8	32318898.64200	16435.3950
2R-22	32373156.19950	2P- 6	32362344.93960	10811.2599
2R-24	32410185.69410	2P- 4	32405210.06080	4975.6333
2R-26	32446424.93840	2P- 2	32447493.01320	-1068.0748
2P- 2	31842934.53680	2P-28	31852788.09330	-9853.5565
2P- 4	31795108.65790	2P-30	31803053.59900	-7944.9411
2P- 6	31746483.77240	2P-32	31752760.39740	-6276.6250
2P- 8	31697061.40880	2P-34	31701911.18530	-4849.7765
2P-10	31646843.37160	2P-36	31650508.77340	-3665.4018
2P-12	31595831.74030	2P-38	31598556.08490	-2724.3446
2P-14	31544028.86790	2P-40	31546056.15100	-2027.2831
2P-16	31491437.37900	2P-42	31493012.10810	-1574.7291
2P-18	31438060.16840	2P-44	31439427.19360	-1367.0252
2P-20	31383900.39760	2P-46	31385304.74340	-1404.3458
2P-22	31328961.49370	2P-48	31330648.18640	-1686.6927
2P-24	31273247.14520	2P-50	31275461.04190	-2213.8967
2P-26	31216761.29950	2P-52	31219746.91520	-2985.6157
2P-28	31159508.15930	2P-54	31163509.49330	-4001.3340
2P-30	31101492.17870	2P-56	31106752.54080	-5260.3621
2P-32	31042718.05940	2P-58	31049479.89620	-6761.8368
2P-34	30983190.74610	2P-60	30991695.46640	-8504.7203

	16-13-16 Frequency (MHz)		18-13-18 Frequency (MHz)	Beat (MHz)
1R-28	27997038.96510	1R- 6	27979469.53800	17569.4271
1R-30	28034667.16050	1R- 8	28018208.25420	16458.9063
1R-32	28071679.68330	1R-10	28056267.72210	15411.9612
1R-34	28108073.28900	1R-12	28093646.55040	14426.7386
1R-36	28143844.54790	1R-14	28130343.18050	13501.3674
1R-38	28178989.84210	1R-16	28166355.88630	12633.9558
1R-40	28213505.35890	1R-18	28201682.77320	11822.5857
1R-42	28247387.08450	1R-20	28236321.77690	11065.3076
1R-44	28280630.79860	1R-22	28270270.66260	10360.1360
1R-46	28313232.06660	1R-24	28303527.02370	9705.0429
1R-48	28345186.23220	1R-26	28336088.27970	9097.9525
1R-50	28376488.41100	1R-28	28367951.67550	8536.7355
1R-52	28407133.48000	1R-30	28399114.28010	8019.1999
1R-54	28437116.07010	1R-32	28429572.98300	7543.0871
1R-56	28466430.55650	1R-34	28459324.49430	7106.0622
1R-58	28495071.04860	1R-36	28488365.34140	6705.7072
1R-60	28523031.37900	1R-38	28516691.86710	6339.5119
1R- 0	27407012.90200	1P-20	27390373.28210	16639.6199
1R- 2	27453013.47210	1P-18	27438229.49990	14783.9722
1R- 4	27498426.55600	1P-16	27485409.01510	13017.5409
1R- 6	27543251.13280	1P-14	27531912.68330	11338.4495
1R- 8	27587486.03510	1P-12	27577741.19110	9744.8440
1R-10	27631129.94820	1P-10	27622895.05580	8234.8924
1R-12	27674181.40860	1P- 8	27667374.62740	6806.7812
1R-14	27716638.80370	1P- 6	27711180.08870	5458.7150
1R-16	27758500.36900	1P- 4	27754311.45580	4188.9132
1R-18	27799764.18770	1P- 2	27796768.57910	2995.6086
1P- 2	27336912.38330	1P-22	27341839.33470	-4926.9514
1P- 4	27289446.60440	1P-24	27292626.45900	-3179.8546
1P- 6	27241395.76100	1P-26	27242733.28270	-1337.5217
1P- 8	27192760.21600	1P-28	27192158.25820	601.9578
1P-10	27143540.18440	1P-30	27140899.66160	2640.5228
1P-12	27093735.73280	1P-32	27088955.59030	4780.1425
1P-14	27043346.77800	1P-34	27036323.96160	7022.8164
1P-16	26992373.08530	1P-36	26983002.50970	9370.5756
1P-18	26940814.26710	1P-38	26928988.78480	11825.4823
1P-20	26888669.78000	1P-40	26874280.14950	14389.6305
1P-22	26835938.92290	1P-42	26818873.77720	17065.1457
1P-38	26392844.02100	1P-56	26411214.01430	-18369.9933
1P-40	26334776.60590	1P-58	26350100.30890	-15323.7030
1P-42	26276106.35460	1P-60	26288254.41640	-12148.0618
2R-12	30793471.81780	2R- 0	30806522.53300	-13050.7152
2R-14	30834011.93310	2R- 2	30847319.28710	-13307.3540
2R-16	30873680.38800	2R- 4	30887476.20840	-13795.8204
2R-18	30912478.65990	2R- 6	30926993.03420	-14514.3743
2R-20	30950408.50690	2R- 8	30965869.69660	-15461.1897
2R-22	30987471.96490	2R-10	31004106.32180	-16634.3569
2R-24	31023671.34410	2R-12	31041703.22970	-18031.8856
2R-26	31059009.22600	2R-12	31041703.22970	17305.9963
2R-28	31093488.45840	2R-14	31078660.93220	14827.5262
2R-30	31127112.15180	2R-16	31114980.13260	12132.0192
2R-32	31159883.67480	2R-18	31150661.72370	9221.9511
2R-34	31191806.64900	2R-20	31185706.78610	6099.8629
2R-36	31222884.94380	2R-22	31220116.58630	2768.3575
2R-38	31253122.67170	2R-24	31253892.57510	-769.9034
2R-40	31282524.18230	2R-26	31287036.38430	-4512.2020
2R-42	31311094.05600	2R-28	31319549.82410	-8455.7681
2R-44	31338837.09930	2R-30	31351434.88220	-12597.7829
2R-46	31365758.33720	2R-30	31351434.88220	14323.4550
2R- 0	30531879.53670	2P-12	30525797.87030	6081.6664
2R- 2	30577664.60830	2P-10	30570733.65550	6930.9528
2R- 4	30622575.18230	2P- 8	30615036.06980	7539.1125
2R- 6	30666611.00580	2P- 6	30658703.58490	7907.4209
2R- 8	30709772.11790	2P- 4	30701734.86540	8037.2525
2R-10	30752058.84870	2P- 2	30744128.77050	7930.0782
2P-14	30160719.90730	2P-28	30143756.40690	16963.5004
2P-16	30107553.10420	2P-30	30093220.26360	14332.8406
2P-18	30053528.73930	2P-32	30042076.32500	11452.4143
2P-20	29998650.09970	2P-34	29990328.12770	8321.9720
2P-22	29942920.75050	2P-36	29937979.37490	4941.3756
2P-24	29886344.53070	2P-38	29885033.93230	1310.5984
2P-26	29828925.55000	2P-40	29831495.82450	-2570.2745
2P-28	29770668.18480	2P-42	29777369.23060	-6701.0458
2P-30	29711577.07330	2P-44	29722658.48030	-11081.4070
2P-32	29651657.11190	2P-46	29667368.04960	-15710.9377

	18-12-18		18-13-18	
	Frequency (MHz)		Frequency (MHz)	Beat (MHz)
1R-14	29277144.14590	2P-60	29264508.38340	12635.7625
1R-16	29312216.79580	2P-58	29323720.01050	-11503.2147
1R-20	29379945.65200	2P-56	29382386.96300	-2441.3110
1R-24	29444439.14940	2P-54	29440503.88350	3935.2659
1R-28	29505679.03250	2P-52	29498065.52410	7613.5084
1R-32	29563644.57250	2P-50	29555066.75200	8577.8205
1R-36	29618312.52550	2P-48	29611502.55550	6809.9700
1R-40	29669657.08640	2P-46	29667368.04960	2289.0368
1R-44	29717649.83610	2P-44	29722658.48030	-5008.6442
1R-46	29740379.67250	2P-44	29722658.48030	17721.1922
1R-48	29762259.68590	2P-42	29777369.23060	-15109.5447
1R-50	29783285.56320	2P-42	29777369.23060	5916.3326
1R-54	29822756.78260	2P-40	29831495.82450	-8739.0419
1R-56	29841192.61690	2P-40	29831495.82450	9696.7924
1R-60	29875439.61430	2P-38	29885033.93230	-9594.3180
1P-10	28771367.04190	1R-58	28759727.66920	11639.3727
1P-10	28771367.04190	1R-60	28779899.81180	-8532.7699
1P-12	28725539.89410	1R-54	28717086.70000	8453.1941
1P-12	28725539.89410	1R-56	28738788.00610	-13248.1120
1P-14	28678918.81140	1R-50	28671421.57830	7497.2331
1P-14	28678918.81140	1R-52	28694629.40960	-15710.5982
1P-16	28631503.40170	1R-46	28622775.01320	8728.3885
1P-16	28631503.40170	1R-48	28647468.43800	-15965.0363
1P-18	28583293.12370	1R-42	28571186.38790	12106.7358
1P-18	28583293.12370	1R-44	28597346.12350	-14052.9998
1P-20	28534287.28530	1R-38	28516691.86710	17595.4182
1P-20	28534287.28530	1R-40	28544300.22720	-10012.9419
1P-22	28484485.04340	1R-36	28488365.34140	-3880.2980
1P-24	28433885.40180	1R-32	28429572.98300	4312.4188
1P-26	28382487.21170	1R-28	28367951.67550	14535.5362
1P-26	28382487.21170	1R-30	28399114.28010	-16627.0684
1P-28	28330289.16890	1R-26	28336088.27970	-5799.1108
1P-30	28277289.81380	1R-22	28270270.66260	7019.1512
1P-32	28223487.52890	1R-20	28236321.77690	-12834.2480
1P-34	28168880.53830	1R-16	28166355.88630	2524.6520
1P-36	28113466.90560	1R-14	28130343.18050	-16876.2749
1P-38	28057244.53180	1R-10	28056267.72210	976.8097
1P-40	28000211.15490	1R- 8	28018208.25420	-17997.0993
1P-42	27942364.34650	1R- 4	27940052.79880	2311.5477
1P-44	27883701.51160	1R- 2	27899959.09570	-16257.5841
1P-48	27763916.53000	1P- 4	27754311.45580	9605.0742
1P-50	27702788.33720	1P- 6	27711180.08870	-8391.7515
1P-52	27640832.02090	1P-10	27622895.05580	17936.9651
1P-54	27578044.11750	1P-12	27577741.19110	302.9264
1P-56	27514420.98350	1P-14	27531912.68330	-17491.6998
1P-58	27449958.79270	1P-18	27438229.49990	11729.2928
1P-60	27384653.53450	1P-20	27390373.28210	-5719.7476
2P-32	31752760.39740	2R-60	31756153.77870	-3393.3813
2P-34	31701911.18530	2R-54	31685990.38300	15920.8023
2P-34	31701911.18530	2R-56	31709960.95480	-8049.7695
2P-36	31650508.77340	2R-50	31636280.73000	14228.0434
2P-36	31650508.77340	2R-52	31661431.61610	-10922.8427
2P-38	31598556.08490	2R-46	31584187.51130	14368.5736
2P-38	31598556.08490	2R-48	31610533.92080	-11977.8359
2P-40	31546056.15100	2R-42	31529681.84110	16374.3099
2P-40	31546056.15100	2R-44	31557237.95470	-11181.8037
2P-42	31493012.10810	2R-40	31501515.90200	-8503.7939
2P-44	31439427.19360	2R-36	31443342.20660	-3915.0130
2P-46	31385304.74340	2R-32	31382693.71760	2611.0258
2P-48	31330648.18640	2R-28	31319549.82410	11098.3623
2P-50	31275461.04190	2R-26	31287036.38430	-11575.3424
2P-52	31219746.91520	2R-22	31220116.58630	-369.6711

APPENDIX 6 COMPUTER PROGRAM

This appendix gives the computer listing of some of the important programs utilized in this thesis. Most of the data collection and analysis programs were written in HPL, a Hewlett Packard BASIC language, on the HP9820 desktop computer. The theoretical analysis was written in FORTRAN for use on the IBM VM system. The main IBM program sets up the shift expression to be integrated using the various integration routines. It calls FUNK which calculates the S_2 and S_1 expressions and returns the integrand to the main program. FUNK calls up FAC and FOC which calculate the quadrupole summation along with FE3 and FEI3 which calculates the $f_3(k)$ resonance functions.

The HPL programs include Start and Go which initializes and takes the pressure shift data, and Sfine which controls the phase and frequency locked linescan sweeps. Dipdi analyzes the linescans obtained from Sfine while Qer does the two power fit to the shift and background slope. Pltt plots the pressure shift data and the resulting power slope correction and then applies a least squares fit to the appropriate points.

Fortran Program to Calculate Shift
Integration $\int 2\pi bdb$

```
      IMPLICIT REAL*8(A-H,O-Z)
      INTEGER J2,JI,JF,MO
      REAL*8 W(2400),OMEG
      INTEGER IW(904)
      COMMON /BL/JI,JF,J2
      COMMON /US/VC,RS2I,RS2F,RS2M,S2II,S2IF,S1,SUN
      COMMON /COM/MO
      COMMON /LL/ U1,U2,Q1,Q2,A1,A2,H1,H2,B,HV,ALLL1,
     qALLL2,APER1,APER2
      COMMON /KK/ UAVG, C6,C12,AD,C8,C10,SIG,EP,Y12,PI
      COMMON /JJ/VZ,VY,DELQ,WGT,BF,R0,BI
      EXTERNAL D01BAX,FUNK
      PI=3.14159265358979
      U1=0.0
      U2=0.0
      WRITE(6,30)
      READ(5,10) WGT
10    FORMAT(F9.3)
      WRITE(6,10) WGT
      WRITE(6,31)
      READ(5,12) BF
      WRITE(6,12) BF
      WRITE(6,32)
      READ(5,12) DELQ
12    FORMAT(F11.6)
      WRITE(6,12) DELQ
      WRITE(6,37)
      READ(5,12) VZ
      WRITE(6,12) VZ
37    FORMAT(2X,'ENTER VZ')
      WRITE(6,34)
      READ(5,12) BI
      WRITE(6,12) BI
      WRITE(6,38)
      READ(5,12) VY
      WRITE(6,12) VY
      WRITE(6,11)
      READ(5,17) JI
      WRITE(6,17) JI
      WRITE(6,13)
      READ(5,17) JF
      WRITE(6,17) JF
11    FORMAT(2X,'ENTER JI')
13    FORMAT(2X,'ENTER JF')
34    FORMAT(2X,'ENTER BI')
```

```
 17   FORMAT(I3)
 30   FORMAT(2X,'ENTER REDUCE MASS')
38    FORMAT(2X,'ENTER C6')
 31   FORMAT(2X,'ENTER B COEF')
 32   FORMAT(2X,'ENTER DELQ')
      Q1=2.6767
      Q2=2.6768
      A1=16.0
      A2=15.83
      H1=.208
      H2=.2421
      HV=2.4546E-4*DSQRT(22./WGT)
      ALLL1=0.0
      ALLL2=0.0
      APER1=0.0
      APER2=0.0
      UAVG=.5065
      C6=8.07
      C12=1.57D6
      C8=1533.D0
      C10=18135.D0
      AD=11.3
      EP=5.9518E-4
      SIG= 6.57633D0
      Y12=1.69
      AN=0.0
 18   FORMAT(2X,I3,2X,2D15.5,D15.5)
      AM=0.0
      R0=.968428*SIG*(Y12**(1./6.))
      Y=1.595**2
      J2=24
      DO 27 JT=1,2,1
      BI=BI+.5
      XX=1.8758E-3*J2*(J2+1.)
      PJ2=2.*(2.*J2+1.)*1.8758E-3*DEXP(-XX)
 33   FORMAT(10D12.4)
 19   FORMAT(2X,I4,6D19.8)
      EPS=0.01
      RER=1.0E-3
      A=R0-0.0
      B=120.0
      INF=1
      IF=1
      OMEG=1.0+3.7E-2*(DELQ+VZ)/2.0
      CALL D01AJF(FUNK,A,B,EPS,RER,ANS,ABS,W,2400,IW,902,IF)
      AN=PJ2*ANS+AN
      ANT=PJ2*ANS
      WRITE(6,19) J2,PJ2,BI,ANS,ANT
```

```
27   CONTINUE
53   CONTINUE
     STOP
     END


     DOUBLE PRECISION FUNCTION FUNK(X)
     IMPLICIT REAL*8(A-H,O-Z)
     REAL*8 S2,X,RC,RR,Y,SUN,S1
     INTEGER L1,L2,NUM,JA,JI,JF,MO,K
     COMMON /BL/JI,JF,J2
     COMMON /US/VC,RS2I,RS2F,RS2M,S2II,S2IF,S1,SUN
     COMMON /COM/MO
     COMMON /LL/ U1,U2,Q1,Q2,A1,A2,H1,H2,B,HV,ALLL1,
    eALLL2,APER1,APER2
     COMMON /KK/UAVG, C6,C12,AD,C8,C10,SIG,EP,Y12,PI
     COMMON /JJ/ VZ,VY,DELQ,WGT,BF,R0,BI
     PI=3.14159265358979
     RC=X
     Y=1.595**2
     RR=SIG/RC
     V=1.53875E-4*DSQRT(22./WGT)*DSQRT(Y)
     IF(RC.LT.R0) GO TO 45
31   FORMAT(9D12.4)
     VC=V
     VV=1.0
     MO=0
     RS2I=16./25.*(Q1*Q2/VC)**2*(1./RC**8)*FAC(RC,VC,JI)
     RS2F=16./25.*(Q1*Q2/VC)**2*(1./RC**8)*FAC(RC,VC,JF)
     RS2M=16./25.*(Q1*Q2/VC)**2*(1./RC**8)*FOC(RC,VC)
     MO=1
32   FORMAT(10D12.4)
     S2II=16./25.*(Q1*Q2/VC)**2*(1./RC**8)*FAC(RC,VC,JI)
     S2IF=16./25.*(Q1*Q2/VC)**2*(1./RC**8)*FAC(RC,VC,JF)
     S1=9.7277D-4/VC*DELQ*RR**5*(21.*Y12/32.*RR**6-1.)
     SUN=DEXP(-(RS2I+RS2F+RS2M))*DSIN(S1+S2IF-S2II)
     FUNK=2.*PI*RC*SUN
27   FORMAT(10D12.4)
     RETURN
45   FUNK=0.0
     RETURN
     END


     DOUBLE PRECISION FUNCTION FAC(RC,VC,JR)
     IMPLICIT REAL*8(A-H,O-Z)
     REAL*8 CONS(3),CON(3)
     INTEGER JN,JM,KK,LL,K2,L2
```

```
      REAL*8 CL,E,EK,RC,VC,AB
      INTEGER MO, JI,JF,JR,J2
      COMMON /COM/ MO
      COMMON /BL/ JI,JF,J2
      COMMON /JJ/VZ,VY,DELQ,WGT,BF,R0,BI
      CONS(2)=JR*(JR+1.)/((2.*JR+3.)*(2.*JR-1.))
      CONS(1)=3.*JR*(JR-1.)/(2.*(2.*JR+1.)*(2.*JR-1.))
      CONS(3)=3.*(JR+1.)*(JR+2.)/(2.*(2.*JR+3.)*(2.*JR+1.))
      CON(1)=3.*J2*(J2-1.)/(2.*(2.*J2+1.)*(2.*J2-1.))
      CON(2)=J2*(J2+1.)/((2.*J2+3.)*(2.*J2-1.))
      CON(3)=3.*(J2+1.)*(J2+2.)/(2.*(2.*J2+3)*(2.*J2+1.))
      CL=0.
12    FORMAT(10D12.4)
      DO 55 LL=1,3
      DO 55 KK=1,3
      K2=2*KK
      L2=2*LL
      JN=JR*(JR+1)-(JR-4+K2)*(JR-4+K2+1)
      JM=J2*(J2+1)-(J2-4+L2)*(J2-4+L2+1)
      E=RC*4.5563E-6*BF*((JN)+(JM))/VC
      EK=DABS(E)
      IF(MO.EQ.0) AB=FE3(EK)
      IF(MO.EQ.1) AB=FE3I(EK)
      CL=CL+CONS(KK)*CON(LL)*AB
55    CONTINUE
33    FORMAT(4I4,6D14.4)
      FAC=CL
      RETURN
      END


      DOUBLE PRECISION FUNCTION FOC(RC,VC)
      IMPLICIT REAL*8(A-H,O-Z)
      REAL*8 CON(3),CONSI,CONSF
      INTEGER JN,JM,KK,LL,K2,L2
      REAL*8 CL,E,EK,RC,VC,AB,DD,D
      INTEGER MO, JI,JF,JR,J2
      COMMON /COM/ MO
      COMMON /BL/ JI,JF,J2
      COMMON /JJ/ VZ,VY,DELQ,WGT,BF,R0,BI
      CONSI=JI*(JI+1.)/((2.*JI+3.)*(2.*JI-1.))
      CONSF=JF*(JF+1.)/((2.*JF+3.)*(2.*JF-1.))
      CON(1)=3.*J2*(J2-1.)/(2.*(2.*J2+1.)*(2.*J2-1.))
      CON(2)=J2*(J2+1.)/((2.*J2+3.)*(2.*J2-1.))
      CON(3)=3.*(J2+1.)*(J2+2.)/(2.*(2.*J2+3)*(2.*J2+1.))
      CL=0.
      DO 60 LL=1,3
      L2=2*LL
```

```
      JM=J2*(J2+1)-(J2-4+L2)*(J2-4+L2+1)
      JN=
      E=RC*4.5563E-6*BF*((JM))/VC
      EK=DABS(E)
      CL=CL+CON(LL)*FE3(EK)
60    CONTINUE
      D=(-1)**(JI+JF)*2*DSQRT((2.*JI+1.)*(2.*JF+1.)
     9*CONSI*CONSF)*DD(1)
      FOC=D*CL
      RETURN
      END


      DOUBLE PRECISION FUNCTION DD (J)
      IMPLICIT REAL*8(A-H,O-Z)
      REAL *8 X,S,Y,P,AF,AI
      INTEGER JI,JF,J
      COMMON/BL/JI,JF,J2
      COMMON /COM/MO
      AI=JI
      AF=JF
      P=J
      S=J+JI+JF
      X=AI*(AI+1.)+AF*(AF+1.)-P*(P+1.)
      IF(JI.LT.1) GO TO 11
      IF(JF.LT.1) GO TO 11
      DD=2.*(3.*X*(X-1.)-4.*AI*(AI+1.)*
     4AF*(AF+1.))/DSQRT((2.*AI-1.)*2.*A
     RI*(2.*AI+1.)*(2.*AI+2.)*(2.*AI+3.)*
     4(2.*AF-1.)*2.*AF*(2.*JF+1.)*(2.
     R*AF+2.)*(2.*AF+3.))
      RETURN
11    DD=0.0
      RETURN
      END


      DOUBLE PRECISION FUNCTION FE3(X)
      IMPLICIT REAL*8 (A-H,O-Z)
      REAL*8 FK,F
      Y=DABS(X)
      IF(Y.GT.80.0) GO TO 55
      A0=0.999994
      A1=2.00007
      A2=2.05531
      A3=1.44491
      A4=0.787502
      A5=0.362692
```

```
      A6=0.152717
      A7=8.72664E-2
      IF(Y.LT.8.0) GO TO 33
      A0=0.997971
      A1=2.00119
      A2=2.05474
      A3=1.44514
      A4=0.787443
      A5=0.362701
      A6=0.152716
      A7=8.72665E-2
33    CONTINUE
      FK=((((((A7*Y+A6)*Y+A5)*Y+A4)*Y+A3)*Y+A2)*Y+A1)*Y+A0)
      F=DEXP(-2.*Y)*FK
      FE3=F
      RETURN
55    FE3=0.
      RETURN
      END


      DOUBLE PRECISION FUNCTION FE3I(X)
      IMPLICIT REAL*8 (A-H,O-Z)
      REAL*8 FK,Y
      Y=DABS(X)
      A0=9.41518E-6
      A1=-2.39063E-4
      A2=2.38037E-3
      A3=-1.26200E-2
      A4=4.03733E-2
      A5=-8.24909E-2
      A6=1.06973E-1
      A7=-6.58886E-2
      A8=2.10596E-2
      A9=-3.45731E-3
      A10=2.32499E-4
      IF(Y.LT.2.0) GO TO 33
      A0=-2.09943
      A1=5.15269
      A2=-5.16147
      A3=2.60896
      A4=-6.41119E-1
      A5=5.31282E-2
      A6=9.87050E-3
      A7=-3.14478E-3
      A8=3.62788E-4
      A9=-2.03940E-5
      A10=4.65103E-7
```

```
33  CONTINUE
    FK=(((((((((A10*Y+A9)*Y+A8)*Y+A7)*Y+A6)*Y+A5)
   y*Y+A4)*Y+A3)*Y+A2)*Y0+A1)*Y+A0)
    FE3I=FK
    IF(Y.GT.7.5)FE3I=FK3I(X)
    RETURN
    END
```

```
0: "Go, Frequency Measurement Program":
1: files Const:0,Isot:0,Dat:1,Count1:0
2: dim I$[9],H$[1],O$[10,9],K$[1],A$[9]
3: dim B$[15],C$[15],D$[35],E$[10],F$[10],G$[25],J$[35],Z$[3],Y$[2],L$[2]
4: dsp "enter Isotope I";ent "",I$
5: fmt 1,c14
6: wrt 706.1,"Isotope 1",I$
7: for S=1 to 10
8: rread 2,S,O$[S]
9: if I$=O$[S];S)I
10: next S
11: fmt 7,2x,f4.1,2x,f20.5,"  MHz"
12: dsp "enter band 1 or 2";ent "",K
13: dsp "enter Transition R or P";ent "",H$
14: dsp "enter J number";ent "",M
15: fmt 2,"Transition",f4.0,"-",c2,"(",f2.0,")"
16: dsp "enter cell pressure in mtorr";ent "",O
17: wrt 706.2,K,H$,M
18: fmt 4,f8.4,"  mtorr"
19: wrt 706.4,"Cell Pressure:  ",O
20: if H$="R";cll 'Rnum'(I,K,M,1,R);R)F;gto "second"
21: if H$="P";cll 'Pnum'(I,K,M,1,P);P)F;gto "second"
22: "second":
23: wrt 706.7,M,F
24: dsp "enter Isotope 2";ent "",A$
25: wrt 706.1,"Isotope 2",A$
26: for S=1 to 10
27: rread 2,S,O$[S]
28: if A$=O$[S];S)C
29: next S
30: dsp "enter band 1 or 2";ent "",E
31: dsp "enter Transition R or P";ent "",K$
32: dsp "enter J number";ent "",N
33: wrt 706.2,E,K$,N
34: dsp "enter cell pressure in mtorr";ent "",A
35: wrt 706.4,"Cell Pressure:  ",A
36: if K$="R";cll 'Rnum'(C,E,N,2,R);R)G;gto "beat"
37: if K$="P";cll 'Pnum'(C,E,N,2,P);P)G;gto "beat"
38: "beat":
39: wrt 706.7,N,G
40: F-G)B
41: fmt 3,f21.6,"  MHz"
42: wrt 706.3,"Beat Frequency (1-2):",B
43: abs(B))B
44: 1)D
45: if B>=1.85e4 and B<=3.7e4;2)D
46: if B>=3.7e4 and B<=5.55e4;3)D
47: if B>7.4e4;wrt 706,"Beat is > 4th Harmonic"
48: if B>=5.55e4 and B<=7.4e4;4)D
49: fmt 8,1/,2x,f4.0,f20.5," MHz"
50: dsp "Enter offset Frq in Mhz";ent "",L
51: wrt 706.8,"The ",D,"th Harmonic Frequency is",B
52: (B-L)/D)B
53: fmt 5,2x,f20.8,2x,"MHz"
54: wrt 706.5,"The Mixer 8672 Frequency is ",B
55: wrt 706.5,"The Offset Mixed Freq",B*D
56: int(B))X
57: frc(B))Y
58: cll 'freq'(X,Y)
59: if B<10000000;"Q"&B$&C$)D$
60: lcl 719
61: dsp "Enter Guess Frequency";ent "",L
62: rem 719
```

```
63: int(L))X
64: frc(L))Y
65: cll 'freq'(X,Y)
66: dsp "DifferentFreq?";ent "",Z$
67: if Z$="y";gto -6
68: fmt 6,e20.7,"  Hz"
69: lcl 719
70: rread 4,1,X,Y  -
71: dsp "Is this a new set of runs?";ent "",Z$
72: if Z$="Y";Y+1)Y
73: rprt 4,1,X,Y
74: rprt 3,1,X,Y,I,K,H$,M,O,F,C,E,K$,N,A,G,L,D
75: wrt 706.5,"The Guess Frequency is",L
76: getk "Four"
77: get "Star"
78: end
79: "Pnum":
80: if p4=2;gto +2
81: dim P[60],V[2],B[2],D[2],H[2],L[2],T$[8],R[0:60]
82: rread 1,p1,T$,V[1],V[2],B,B[1],B[2],D,D[1],D[2],H,H[1],H[2],L,L[1],L[2]
83: for J=2 to 60 by 2
84: if p3#100;p3)J
85: B[p2]J^2-(2B-B[p2])J-D[p2](J^4+J^2)+(2D-D[p2])2J^3)P[J]
86: V[p2]-(2H-H[p2])(3J^5+J^3)-(2L-L[p2])(4J^7+4J^5)+P[J])P[J]
87: L[p2](J^8+6J^6+J^4)+H[p2](J^6+3J^4)+P[J])P[J])p5=
88: if p3#100;gto "out"
89: fmt 9,2x,f4.1,5x,f20.5,"  MHz"
90: wrt 706.9,J,P[J]
91: next J
92: ret
93:
94: "out":
95: fmt 2x,f4.1,2x,e20.11
96: ret
97: "Rnum":
98: if p4=2;gto +2
99: dim R[0:60],V[2],B[2],D[2],H[2],L[2],T$[8],P[60]
100: rread 1,p1,T$,V[1],V[2],B,B[1],B[2],D,D[1],D[2],H,H[1],H[2],L,L[1],L[2]
101: for J=0 to 60 by 2
102: if p3#100;p3)J
103: (2B-B[p2])(J+1)+B[p2](J+1)^2-D[p2]((J+1)J)^2-4D(J+1)^3+V[p2])R[J]
104: H[p2]((J+1)J)^3+H(6J^5+30J^4+62J^3+66J^2+36J+8)+R[J])R[J]
105: L(8J^7+56J^6+176J^5+320J^4+360J^3+248J^2+96J+16)+R[J])R[J]
106: L[p2]((J+1)J)^4+R[J])R[J])p5
107: if p3#100;gto "out"
108: fmt 9,2x,f4.1,5x,f20.5,"  MHz"
109: wrt 706.9,J,R[J]
110: next J
111: ret
112:
113: "out":
114: fmt 2x,f4.1,5x,e20.11
115: ret
116:
117:
118: "freq":fmt "P",fz9.3,"Z9K0L3";wrt 719,int(p1)+.002
119: 1+(p1)=6200)+(p1)=12400))p4
120: 10(int(.1p1)modp4)+10frc(.1int(p1))+frc(p2))p3
121: 30-p3/p4+10int(.1p3/p4))p0
122: fmt "FU1FR",f13.9,"MHAM0DB";wrt 717,p0;ret
*25174
```

```
0: "Start":
1: "Frequency Measurement Controller Program":
2: fmt 1,"Sigma y(tau) pgm (het) 05390-16002 rev B"
3:
4: files Dat:1,Data:1,Count:0
5: dim Z[5];0)Z[3]
6: "bf":5)Z[4]
7: gto "init"
8: "pe":beep;fxd 0;dsp "PGM error",p1;stp
9: ret
10:
11:
12: "INITILIZATION  770615.1330":
13: "INITILIZATION  770615.1330":
14:
15:
16: "init":
17: "da":dev "prtr",706)r0,"cntr",710,"msd",712,"msp",713,"clk",714,"bus",731
18: dim M$[80],T$[18],N,B$[16],F,C,X[8],Y[8],C[3],Q,R
19: dim A$[20],Y$[2],T[5],K$[1],H$[1],S$[1]
20: 5)L
21: dim B,M,R[L],M[0:L],S[0:L],L$[1],P$[1]
22: "83")Y$[1,2]
23: 10)R[1];10)N;"100khz")B$;3e7)F;\2)C
24: 1e-3)X[1];1e3)X[2];8.5)X[5];.6)X[6];.4)X[7]
25: 1e-14)Y[1];1e-7)Y[2];11)Y[5];1.25)Y[6];1.25)Y[7]
26: 120)C[1];46)C[2];43)C[3]
27: 1)J
28: 10)R
29: R)R[1]
30:
31: "MEAS & REC. DATA  770615.1330":
32:
33: "meas":
34: dim Z$[1],U[4],Q$[1]
35: rread 3,1,X,Y
36: rread 1,1,X,Y,I,K,H$,T,O,H,L,E,K$,Q,A,G,U,D
37: dsp "enter  cell pressure";ent "",O
38: ent "enter Power",P
39: fmt 3,1/,f8.3
40: rprt 1,1,X,Y,I,K,H$,T,O,H,L,E,K$,Q,A,G,U,D,P
41: wait 400
42: wrt 706.3,"Power is",P
43: wait 1000
44: wrt 706.3,"Cell Pressure is",O
45: ent "ent number of avg",N
46: fmt 9x,c
47: wait 200
48: wrt "prtr"," F R A C T I O N A L   F R E Q U E N C Y   D E V I A T I O N"
49: wait 700
50: cll 'rapt';A$)T$
51: cmd "cntr","I2G5E1<E:E8I1";fmt ;red "cntr",B;red 731,B
52: wait 300
53: fmt 3x,"number of samples averaged",f6.0;wrt "prtr",N
54: wait 600
55: fmt 4x,4"----------  ";wrt "prtr"
56:
57: "Trial":1)W;0)V;0)H;0)P;"N")Q$
58: "start":0)M;0)H
59: "rpt":
60: cmd "cntr","I2E;G5E1<E8I1"
61: cmd "msp","HG1G3G4F1";rds("msp"))r1
62: fmt 9,3e20.11
```

```
63: for J=1 to 1
64: fmt 4x,f8.2,2x,z;wrt "prtr",R[J]
65: if R[J]<=.99/B;fmt "not measurable";0)S[J];gto "nt"
66: prnd(R[J]*B,0)/B)M[J]
67: if M[J]=M[M];wrt "prtr","duplicate,not measured";gto "nt"
68: M[J])M[M+1)M]
69: prnd(log(5e8*M[M]),0)+1)D
70: fmt "T",f.0,"N",f.0,"D0",z;wrt "msp",D,N+5
71: (.95/B+M[M])*1e6-7-1.7*D)G
72: if G<100;fmt "M",f.0,"E0KRI";wrt "bus",G;gto +2
73: fmt "M",e.2,"KRI",z;wrt "bus",G*1e-2
74: fmt ;red "msd",T,E
75: 0)X;red "bus",T,E;E/T)Z
76: 0)F
77: red "bus",T,E;E/T)Y;Y+H)H
78: dsp F,(Y-Z)*5e8
79: (Z-Y)^2+X)X;Y)Z;1)F
80: for I=2 to N
81: "read":
82: if F-I>3;gto "stop"
83: if F=N+3;gto "stop"
84: fmt ;red "bus",T,E;E/T)Y;1+F)F
85: max(8*(X+.45*(Y-Z)^2)/I,3.6e-13))C
86: dsp F,I,5e8*(Y-Z)
87: if (Z-Y)^2>C;dsp "Random Error",5e8(Z-Y),F,I;gto "read"
88: if F-I>3;gto "stop"
89: (Z-Y)^2+X)X;Y)Z;Y+H)H
90: next I
91: fmt 6,f4.1
92: if F-N>0;wrt 706.6,"Exist Random Error Trials",F-N
93: gto "cont"
94: 0)S
95: if F<N+3;fmt ;red "bus",T,E;E/T)Y;1+F)F;1+S)S
96: dsp F,5e8*(Y-Z)
97: Y)Z
98: if F<N+3;gto -3
99: if 3-S>0;wrt 706.6,"Exist Random Error Trials",3-S
100: rds("msp"))r1;if r1#96;cll 'pe'(5)
101: "cont":
102: \(X/(2*N))*5e8)S[M];H/N*5e8)H
103: "nt":next J
104: beep;beep;beep
105: H)T[W];S[M])U[W]
106: rread 1,1,X,Y,I,K,H$,T,O,H,L,E,K$,Q,A,G,U,D,C
107: wrt 706.9,"Freq",T[W]," Sigma",S[M]
108: beep;beep;beep
109: fmt 8,3e15.8
110: gto +2
111: "stop":wrt 706,"Random Errors";"N")S$;gto +3
112: dsp "Test OK?";ent "",S$
113: if S$#"N";gto +3
114: if S$="N";wrt 706,"VOID TRIAL";gto "start"
115: fmt 7,f7.2
116: W+1)W;if W<=3 and Q$#"Y";gto "start"
117: dsp "Another Trial?";ent "",Q$
118: if Q$="Y";dsp "Trial?";ent "",W
119: if W#1 or 2 or 3;dsp "Repeat W?";ent "",W
120: if Q$="Y";wrt 706,"Replace Trial",W;gto "start"
121: for J=1 to 3
122: T[J]+V)V;U[J]+P)P
123: next J
124: V/3)V;P/3)P
125: fmt 1,f9.4
126: V)T[4];P)T[5]
127: wait 1330
128: wrt 706.9,"Count Average",V
```

```
129: wait 400
130: wrt 706.9,"Sigma Average",P
131: wait 500
132: wrt 706.9,"Laser Beat Freq ",(abs(H-G)-U)*1e6+V*D)S
133: fmt 6,3f20.6
134: rread 3,1,X,Y
135: dsp "Accept Run?";ent "",Z$
136: if Z$#"N";X+1)X
137: rprt 3,1,X,Y
138: wrt 706.6,"TEST X=",X," Y=",Y,T[4]
139: if Z$="N";gto +4
140: rprt 2,X,X,Y,I,K,H$,T,O,L,E,K$,Q,A,S,T[*],C,T$
141: wait 800
142: wrt 706,"Run is saved"
143: if flg9;fmt c,z;wrt "prtr","END ";cll 'rapt'
144: end
145:
146: "rapt":
147: fmt ;red "clk";"  ")A$
148: wti 0,7;rdi 4)D;wait 100;if iof7;gto +2
149: cfg 9;ent "ent date/time MM,DD,hh:mm:ss",A$[3,16];gto +2
150: sfg 9;red "clk",A$
151: Y$&A$[1,16])A$
152: fmt 3x,"DATE ",c2,"/",c2,"/",c2,"  TIME  ",c
153: wait 300
154: wrt "prtr",A$[1,2],A$[5,6],A$[8,9],A$[11,18];ret
155:
156: "rpad":
157: ent "enter record file #",r1
158: if 'cf'(r1);gto -1
159: L)Q;rcf r1,M$,T$,N,B$,F,C,X[*],Y[*],C[*],Q,R
160: if 'cf'(r1+1);gto -3
161: rcf r1+1,B,M,R[*],M[*],S[*]
162: gto "ex"
163:
164: "cf":
165: fdf p1
166: idf p2,p3,p4,p5,p6
167: if p4#0;fxd 0;dsp p1,"used.type",p3,"ok to destroy?";gto +2
168: ret 0
169: ent "",A$
170: if A$[1,2]="ye";ret 0
171: if A$[1,2]="no";ret 1
172: cll 'pe'(8);gto -3
*16459
```

```
0: "Pltt":
1: "Plot Routine and Power Corrections":
2: files Isot:0,Const:0,Data:1,Count1:0
3: dim T[5],Q[200],P[200],K$[1],H$[1],T$[18],O$[10,9]
4: dsp "enter first record";ent "",D
5: dsp "enter last record";ent "",G
6: dsp "Enter Test Run #  Y";ent "",Y
7: D)r0;G)r1;Y)r3
8: fmt 3," Records",f4.0," To ",f4.0," Run ",f4.0
9: wrt 706.3,D,G,Y
10: Y)W;-1)U
11: for Z=D to G
12: rread 3,Z,X,Y,I,K,H$,M,O,C,E,K$,N,A,B,T[*],V,T$
13: if Y=W;U+1)U;O)P[3*U+1])P[3*U+2])P[3*U+3];X)F
14: if Y=W;T[1]-3.2e8)Q[3*U+1];T[2]-3.2e8)Q[3*U+2];T[3]-3.2e8)Q[3*U+3]
15: next Z
16: 3*U+3)U
17: dim B[U],W[U],A[4,5],K[1]
18: for Z=1 to U
19: Q[Z]/1000)W[Z];P[Z])B[Z]
20: next Z
21: rread 1,I,O$[I];I)Q
22: rread 1,C,O$[C]
23: fmt 5," Isotope",c10,f2.0,c2,"-",f3.0
24: wrt 706.5,O$[I],K,H$,M;K)Z;M)V
25: fmt 6,"Fit from ",f7.2," To ",f7.2
26: wrt 706.6,P[1],P[U]
27: pclr
28: max(W[*]))R
29: min(B[*]))S
30: min(W[*]))O
31: max(B[*]))P
32: S-10)I
33: P+10)P
34: prnd(R,0)+1)R
35: fxd 0
36: prnd(O,0)-1)K
37: scl 0,160,K,K+8
38: xax K,10,0,160,10
39: yax 0,1,K,K+8,6
40: 0)D)H)L)B)A)F)G)C)E)I
41: plt 100,K+8,1
42: 4)N
43: lbl O$[Q],Z,H$,V,"(X=",r0,r1,")"," Y=",r3
44: plt 100,K+7.6,1
45: lbl T$[1,2],"/",T$[5,6],"/",T$[8,9]
46: fmt 1,"Test",9x,"Pressure",9x,"Frequency"
47: 0)K
48: for J=1 to U
49: fmt 2,2x,f3.0,2x,2e20.11
50: cll 'move'(B[J],W[J])
51: cll 'plot'(B[J],W[J])
52: next J
53: dsp "enter slope";ent "",r6
54: dsp "enter lock2";ent "",r11
55: dsp "enter power";ent "",r15
56: 4.2e0)r1
57: 2.486e2^2)r16
58: 0)r14
59: r7*r6/r11)K[1]
60: for J=1 to U
61: if B[J]#r14;dsp "ent lock";ent "",r7
62: B[J])r14;r7*r6/r11)K[1]
```

```
63: gsb "FUNC1"
64: -Z+W[J])W[J]
65: next J
66: for J=1 to U
67: cll 'move'(B[J],W[J])
68: cll 'plot'(B[J],W[J])
69: next J
70: dsp "ent first record fit";ent "",E
71: dsp "ent last record fit";ent "",K
72: 3*(E-r0)+1)r2
73: 3*(K-r0)+3)r3
74: 3*(K-E+1))U
75: for J=r2 to r3
76: B[J]^2+D)D
77: B[J]+L)L
78: W[J]^2+B)B
79: W[J]+H)H
80: B[J]^3+F)F
81: B[J]^4+G)G
82: B[J]*W[J]+A)A
83: next J
84: U*D-L^2)V
85: U*B-H^2)W
86: U*A-L*H)Q
87: Q/V)M
88: H/U-M*L/U)O
89: abs(Q/\(V*W)))F
90: fmt 9,2x,f20.11
91: wrt 706.6,B[r3],B[r2]
92: wrt 706.9,"Correlation is ",F
93: pen
94: for X=B[r3] to B[r2]
95: plt X,M*X+O
96: next X
97: fmt 3,2x,"Least Squares Fit ",f10.4,"x + ",e10.4
98: wrt 706.3,M,O
99: for Z=B[r2] to B[r3]
100: plt Z,M*Z+O
101: next Z
102: fmt 4,2x,"Fit",e15.9," +",f15.9,"x +",f15.9,"x2+",f15.9,"x3"
103: pen
104: end
105:
106: "move":
107: pen;plt p1,p2,1;ret
108:
109: "plot":
110: cplt -.33,-.3
111: lbl "+"
112: cplt -.67,.3;iplt 0,0;ret
113: "SOLVE":cfg 4;0)I
114: if (I+1)I)=N;gto +15
115: I-1)K;0)B
116: if (K+1)K)>N;gto +3
117: if (abs(A[K,I]))T)>B;T)B;K)R
118: gto -2
119: if B=0;sfg 4;dsp "DET=0";ret
120: I)J;if I=R;gto +2
121: A[I,J])T;A[R,J])A[I,J];T)A[R,J];jmp (J+1)J)>N+1
122: I+1)J;A[I,I])B
123: A[I,J]/B)A[I,J];jmp (J+1)J)>N+1
124: I)K
125: if (K+1)K)>N;gto -11
126: I+1)J
127: A[K,J]-A[K,I]A[I,J])A[K,J];jmp (J+1)J)>N+1
128: gto -3
129: if A[N,N]=0;0)B;gto -10
130: dim X[N];A[N,N+1]/A[N,N])X[N];N)I
131: if (I-1)I)<1;ret
132: 0)S;N)K
133: A[I,K]X[K]+S)S;jmp (K-1)K)<=I
134: A[I,N+1]-S)X[I];gto -3
135:
136:
137: "FUNC1":
138: B[J])r4
139: r16*r15/(r1*r4)^2)r5
140: .5+.5*\(1+2*r5)+\(1+r5))r8
141: (r1*r4)^2*((4*r5^2-4(1+r5)(r8*r8)+r8^4)/(4*(1+r5)-r8*r8)))r9
142: (\(1+2r5)-1)/(2*\(1+r5)-\(1+2r5)-1))r10
143: K[1]*r9*r10/8)Z
144: ret
```

```
0: "Qer, Fit Two Power Pressure Shifts to get":
1: "Linear Slope and Instrumental Error":
2: files Isot:0,Const:0,Data:1,Count1:0
3: dim X[200],Z[200],F[200],O$[10,9]
4: dim T[5],Q[200],W[200],K$[1],H$[1],T$[18],S$[1],C$[1]
5: "One":
6: dsp "enter first record";ent "",D
7: dsp "enter last record";ent "",G
8: dsp "Enter Test Run #  Y";ent "",Y
9: fmt 3,"  Records",f4.0," To ",f4.0," Run ",f4.0
10: wrt 706.3,D,G,Y
11: Y)W;-1)U;1e9)R
12: for Z=D to G
13: rread 3,Z,X,Y,I,K,H$,M,O,C,E,K$,N,A,B,T[*],P,T$
14: if Y=W;U+1)U;O)W[3*U+1])W[3*U+2])W[3*U+3]
15: if Y=W;T[1]-3.2e8)Q[3*U+1];T[2]-3.2e8)Q[3*U+2];T[3]-3.2e8)Q[3*U+3]
16: if min(T[1],T[2],T[3])-3.2e8<=R;min(T[1],T[2],T[3])-3.2e8)R
17: next Z
18: R)r14
19: 3*U+3)U
20: fmt 2,2x,f5.2
21: dsp "Enter Power";ent "",P
22: P)r15
23: wrt 706.2,"Power is",P
24: U)r11
25: for Z=1 to U
26: Q[Z]/1000)Z[Z];W[Z])K[Z]
27: next Z
28: "Two":
29: dsp "ent first rec";ent "",F
30: dsp "ent last rec";ent "",H
31: dsp "ent test no";ent "",L
32: wrt 706.3,F,H,L
33: L)W;-1)U;1e9)R
34: for Z=F to H
35: rread 3,Z,X,Y,I,K,H$,M,O,C,E,K$,N,A,B,T[*],P,T$
36: if L=W;U+1)U;O)W[3*U+1])W[3*U+2])W[3*U+3]
37: if L=W;T[1]-3.2e8)Q[3*U+1];T[2]-3.2e8)Q[3*U+2];T[3]-3.2e8)Q[3*U+3]
38: if min(T[1],T[2],T[3])-3.2e8<=R;min(T[1],T[2],T[3])-3.2e8)R
39: next Z
40: dsp "Enter Power";ent "",P
41: P)r12
42: wrt 706.2,"Power is",P
43: 3*U+3)U)r13
44: min(R,r14))r14
45: for Z=1 to U
46: Q[Z]/1000)Z[r11+Z];W[Z])X[r11+Z]
47: next Z
48: rread 1,I,O$[I];I)Q
49: K)Z;M)V;N)F
50: fmt 6,"Fit from ",f7.2," To ",f7.2
51: wrt 706.6,X[r11+1],X[r13+r11]
52: r14/1000)r14
53: wrt 706.6,X[1],X[r11]
54: fmt 1,2x,2f5.1
55: if Z[r11])Z[1];max(Z[*]))r14
56: "Begin":
57: r11+r13)M)N
58: pclr
59: for J=1 to N
60: Z[J]-r14)Z[J]
61: next J
62: max(Z[*]))R
```

```
63: min(Z[*])>O
64: max(X[*])>Y
65: Y+10)Y
66: prnd(R,1)+10)R
67: prnd(O,1))K
68: scl 0,Y,K,R
69: xax K,10,0,Y,2
70: yax 0,5,K,R,2
71: plt .8*Y,.3*R,1
72: fxd 0
73: lbl "Test",O$[Q],Z,H$,V
74: plt Y,O,1
75: pen
76: "+")C$
77: for J=1 to r11
78: fmt 2,2x,f3.0,2x,2e20.11
79: cll 'move'(X[J],Z[J])
80: cll 'plot'(X[J],Z[J])
81: next J
82: pen
83: plt 0,R,1
84: for J=r11+1 to r11+r13
85: cll 'move'(X[J],Z[J])
86: cll 'plot'(X[J],Z[J])
87: next J
88: pen
89: dim P[10],S[2]
90: dim B[10,10],V[10],A[10],D[10],K[10],R[10,10]
91: "Starr":
92: rread 1,Q,O$[Q]
93: rread 1,C,O$[C]
94: fmt 2,"Isotope ",c14
95: wrt 706.2,O$[Q]
96: fmt 3,f4.0,"-",c2,"(",f2.0,")"
97: wrt 706.3,Z,H$,V
98: fmt 4,f6.2
99: wrt 706.2,O$[C]
100: wrt 706.3,E,K$,F
101: 3.95e-2)r0
102: 1.91)r19
103: .795)r18
104: 4.2e0)r1
105: r11+r13)N)M
106: 2)Q
107: 500)A[1]
108: 1)r3
109: 8e-6/7)A[2]
110: 2.468e2^2)r16
111: .001)L
112: "Start":
113: gsb "SR2"
114: gsb "SR5"
115: for I=1 to Q
116: A[I]+V[I])A[I]
117: next I
118: fmt 2,"Initial guesses are",6e20.11
119: wrt 706.2,A[1],A[2]
120: gsb "SR6"
121: S)Y
122: gsb "SR2"
123: gsb "SR5"
124: for I=1 to Q
125: A[I])K[I]
126: A[I]+V[I])A[I]
127: next I
128: gsb "SR6"
```

```
129: fmt 7,3e15.6
130: wrt 706.7,Y,S,L
131: 1+r3)r3
132: if Y-S<0;10*L)L;gto "Add"
133: if Y-S>=0;.1*L)L;gto "Ad"
134: "Add":
135: for I=1 to Q
136: K[I])A[I];next I
137: "Ad":
138: if L<1e-6 or r3>8;gto "Re"
139: gto "Start"
140: "Re":
141: fmt 3,"Final Guesses are ",6e20.11
142: dsp "Plot last Fit";ent "",A
143: wrt 706.3,A[1],A[2]
144: cll 'RPLOT1'
145: fmt 9,2f4.1
146: end
147:
148:
149: "SR2":
150: for J=1 to Q
151: 0)P[J]
152: for K=1 to J
153: 0)R[J,K]
154: next K
155: next J
156: for I=1 to N
157: gsb "FDER1"
158: gsb "FUNC1"
159: for J=1 to Q
160: P[J]+(Z[I]-Z)*D[J])P[J]
161: for K=1 to J
162: R[J,K]+D[J]*D[K])R[J,K]
163: next K
164: next J
165: next I
166: for J=1 to Q
167: for K=1 to J
168: R[J,K])R[K,J]
169: if J=K;R[J,K]+L)R[J,K]
170: next K
171: next J
172: ret
173:
174: "SR5":
175: for I=1 to Q
176: for J=1 to Q
177: P[I])B[I,Q+1]
178: R[I,J])B[I,J]
179: next J
180: next I
181: Q)O
182: gsb "SOLVE"
183: ret
184:
185:
186: "SR6":
187: 0)S
188: for I=1 to Q
189: S+V[I]^2)S
190: next I
191: gsb "CHISQ1"
192: L*S+C)S
193: ret
194:
```

```
195:
196: "FDER1":
197: if I<=N;r12)r17
198: if I<=r11;r15)r17
199: X[I])D[1]
200: 350/X[I]+r0*X[I])r2
201: r2*r18*X[I]+r2*r2)r20
202: r19*(r2+.07*r18*X[I])*X[I]+.07*(1-.07)*(r18*X[I])^2)r5
203: r16/(r1*X[I])*r17/(r2+r19*X[I]+(1-.07)*r18*X[I]))r4
204: .0785*r4/\(1+r4))r7
205: .0785*r4/\(1+2*r4))r6
206: r6/(1+r5/r20*r6))r8
207: r7/(1+r5/r20*r7))r9
208: (r1*X[I])^2*(r8/(r9-r8))/8)D[2]
209: ret
210:
211:
212: "FUNC1":
213: if I<=N;r12)r17
214: if I<=r11;r15)r17
215: 350/X[I]+r0*X[I])r2
216: r2*r18*X[I]+r2*r2)r20
217: r19*(r2+.07*r18*X[I])*X[I]+.07*(1-.07)*(r18*X[I])^2)r5
218: r16/(r1*X[I])*r17/(r2+r19*X[I]+(1-.07)*r18*X[I]))r4
219: .07853*r4/\(1+r4))r7
220: .07853*r4/\(1+2*r4))r6
221: r6/(1+r5*r6/r20))r8
222: r7/(1+r5*r7/r20))r9
223: A[1]*X[I]+A[2]*(r1*X[I])^2*(r8/(r9-r8))/8)Z
224: ret
225: "Der":
226: gsb "FUNC1"
227: A[2]*r9*r10/8)r14
228: 1.05*r5)r5
229: .5+.5+\(1+2r5)+\(1+r5))r8
230: (r1*X[I])^2((4*r5^2-4(1+r5)(r8*r8)+r8^4)/(4(1+r5)-r8^2)))r9
231: (\(1+2r5)-1)/(2\(1+r5)-\(1+2r5)-1))r10
232: (A[2]*r9*r10/8-r14)/(.05*A[3]))T
233: ret
234: --
235:
236: "CHISQ1":
237: 0)C
238: for I=1 to N
239: gsb "FUNC1"
240: C+(Z[I]-Z)^2)C
241: ret
242:
243:
244: "SOLVE":cfg 4;0)I
245: if (I+1)I)=0;gto +15
246: I-1)K;0)B
247: if (K+1)K))0;gto +3
248: if (abs(B[K,I]))T))B;T)B;K)R
249: gto -2
250: if B=0;sfg 4;dsp "DET=0";ret
251: I)J;if I=R;gto +2
252: B[I,J])T;B[R,J])B[I,J];T)B[R,J];jmp (J+1)J))0+1
253: I+1)J;B[I,I])B
254: B[I,J]/B)B[I,J];jmp (J+1)J))0+1
255: I)K
256: if (K+1)K))0;gto -11
257: I+1)J
258: B[K,J]-B[K,I]B[I,J])B[K,J];jmp (J+1)J))0+1
259: gto -3
260: if B[0,0]=0;0)B;gto -10
```

```
261: B[0,0+1]/B[0,0]>V[0];0>I
262: if (I-1)I><1;ret
263: 0>H;0>K
264: B[I,K]V[K]+H>H;jmp (K-1>K><=I
265: B[I,0+1]-H>V[I];gto -3
266:
267:
268: "RPLOT1":
269: for I=1 to N
270: gsb "FUNC1"
271: "*">C$
272: Z>F[I]
273: cll 'move'(X[I],F[I])
274: cll 'plot'(X[I],F[I])
275: next I
276: pen
277: ret
278:
279: "move":
280: pen;plt p1,p2,-2;ret
281:
282: "plot":
283: cplt -.33,-.3
284: lbl "+"
285: cplt -.67,.3;iplt 0,0;ret
*12193
```

```
 0: "Sfine, Compputer Controlled Frequency Sweep":
 1: "Frequency and Phased Locked Lineshape Sweep":
 2: files Const:0,Isot:0,Dat:1,Count3:0
 3: dim X,Y,I,K,H$[1],M,O,F,C,E,K$[1],N,A,G,B,D,M$[16],X[275],Z[275]
 4: dim I$[9],O$[10,9],A$[9],L$[13]
 5: dim B$[15],C$[15],D$[35],E$[10],F$[10],G$[25],J$[35],Z$[3]
 6: cll 'rapt'
 7: "front":
 8: fmt 3,"FU1FR",f5.0,"KHAM3VO"
 9: wrt 717.3,8500
10: lcl 719
11: dsp "Push to cont";ent "",A
12: wrt 710,"I2E8E9G0E:I1"
13: wrt 710,"J1"
14: red 710,A;red 731,A
15: fmt 4,1/,2x,f20.11,1/
16: 10500)W
17: fmt 1,"FU1AM3VOST",f5.0,"KHSP",f5.0,"KHTI30SESSSS"
18: wrt 717.1,8500,10500
19: wait 32000
20: wait 12000
21: for J=1 to 275
22: 3)T
23: if J>125;3)T
24: if J>135;.5)T
25: if J>165;3)T
26: if J>195;6.25)T
27: if J>215;12.5)T
28: if J>235;25)T
29: if J>255;50)T
30: if J<125;3)T
31: if J<80;6.25)T
32: if J<60;12.5)T
33: if J<40;25)T
34: if J<20;50)T
35: W)U
36: U-T)W
37: fmt 2,"ST",f7.1,"KHSP",f7.1,"KHTI.10SESSSS"
38: wrt 717.2,U,W;trg 723;red 723,V
39: if J>215;wait 1000
40: if J<60;wait 1000
41: wait 1300
42: wrt 710,"I2E8E9G0E:I1"
43: 0)P
44: wrt 710,"J1";for D=1 to 10
45: trg 723;red 723,V
46: V+P)P
47: next D
48: P/10)Z[J]
49: red 710,A;red 731,A
50: A)X[J]
51: next J
52: rread 4,1,X,Y
53: dsp "Is this new set of run";ent "",Z$
54: if Z$="Y";Y+1)Y
55: dsp "Accept this run";ent "",Z$
56: if Z$="Y";X+1)X
57: fmt 5,"X= ",f3.0,"Y=  ",f3.0
58: rprt 4,1,X,Y
59: wrt 706.5,X,Y
60: dsp "Which trk";ent "",J
61: trk J
62: rread 3,1,X,Y,I,K,H$,M,O,F,C,E,K$,N,A,G,B,D
```

```
63: rread 4,1,X,Y
64: rcf X,X,Y,I,K,H$,M,O,F,C,E,K$,N,A,G,B,D,M$,X[*],Z[*]
65: fmt 6,2x,f3.0,2x,f20.2,3x,f20.7,2x,f20.7
66: dsp "Continue this run?";ent "",Z$
67: if Z$="N";gto "back"
68: dsp "enter new pressure";ent "",O
69: cll 'rapt'
70: wrt 706.4,"Cell Pressure ",O
71: rprt 3,1,X,Y,I,K,H$,M,O,F,C,E,K$,N,A,G,B,D
72: gto "front"
73: "back":
74: end
75: "Pnum":
76: if p4=2;gto +2
77: dim P[60],V[2],B[2],D[2],H[2],L[2],T$[8],R[0:60]
78: rread 1,p1,T$,V[1],V[2],B,B[1],B[2],D,D[1],D[2],H,H[1],H[2],L,L[1],L[2]
79: for J=2 to 60 by 2
80: if p3#100;p3)J
81: B[p2]J^2-(2B-B[p2])J-D[p2](J^4+J^2)+(2D-D[p2])2J^3)P[J]
82: V[p2]-(2H-H[p2])(3J^5+J^3)-(2L-L[p2])(4J^7+4J^5)+P[J])P[J]
83: L[p2](J^8+6J^6+J^4)+H[p2](J^6+3J^4)+P[J])P[J]>p5
84: if p3#100;gto "out"
85: fmt 9,2x,f4.1,5x,f20.5,"  MHz"
86: wrt 706.9,J,P[J]
87: next J
88: ret
89:
90: "out":
91: ret
92: "Rnum":
93: if p4=2;gto +2
94: dim R[0:60],V[2],B[2],D[2],H[2],L[2],T$[8],P[60]
95: rread 1,p1,T$,V[1],V[2],B,B[1],B[2],D,D[1],D[2],H,H[1],H[2],L,L[1],L[2]
96: for J=0 to 60 by 2
97: if p3#100;p3)J
98: (2B-B[p2])(J+1)+B[p2](J+1)^2-D[p2]((J+1)J)^2-4D(J+1)^3+V[p2])R[J]
99: H[p2]((J+1)J)^3+H(6J^5+30J^4+62J^3+66J^2+36J+8)+R[J])R[J]
100: L(8J^7+56J^6+176J^5+320J^4+360J^3+248J^2+96J+16)+R[J])R[J]
101: L[p2]((J+1)J)^4+R[J])R[J])>p5
102: if p3#100;gto "out"
103: fmt 8,2x,f4.1,5x,f20.5,"  MHz"
104: wrt 706.8,J,R[J]
105: next J
106: ret
107:
108: "out":
109: ret
110: "rapt":
111: fmt ;red 714;"  ")M$
112: red 714,M$
113: wrt 706,M$
114: ret
*24270
```

```
0: "Dipdi, LSF of Derivative  Lineshape":
1: "Include Backgrnd Slope":
2: files Dati:0,Datti:0,Count4:0,Isot:0
3: dim X,Y,I,K,H$[1],M,O,F,C,E,K$[1],N,A,G,B,D,M$[16],X[275],Z[275],F[275]
4: dim G[100],H[100],C[10],P[10],S[2]
5: dim B[10,10],V[10],A[10],D[10],T[10],R[10,10],Y$[25],C$[1]
6: dim J[8],A$[1],O$[10,9]
7: dsp "enter first file";ent "",S[1]
8: dsp "enter last file ";ent "",S[2]
9: dsp "Which track?";ent "",J
10: trk J
11: "Starr":
12: ldf S[1],X,Y,I,K,H$,M,O,F,C,E,K$,N,A,G,B,D,M$,X[*],Z[*]
13: rprt 1,1,X,Y,I,K,H$,M,O,F,C,E,K$,N,A,G,B,D,M$
14: fmt 1,1/,1x,4f4.1
15: wrt 706.1,"Run X= ",X," Y= ",Y," from tape ",S[1]," on trk ",J
16: rread 4,I,O$[I]
17: rread 4,C,O$[C]
18: fmt 2,"Isotope ",c14
19: wrt 706.2,O$[I]
20: fmt 3,f4.0,"-",c2,"(",f2.0,")"
21: wrt 706.3,K,H$,M
22: fmt 4,f6.2
23: wrt 706.4,"Cell Pressure ",O
24: wrt 706.2,O$[C]
25: wrt 706.3,E,K$,N
26: wrt 706.4,"Cell Pressure ",A
27: pclr
28: pen
29: 275)M
30: for J=1 to 137
31: X[J])X;Z[J])Y;X[276-J])E;Z[276-J])A
32: X)X[276-J];E)X[J];Y)Z[276-J];A)Z[J]
33: next J
34: max(Z[*]))Q;min(Z[*]))P
35: for J=1 to 275
36: if Z[J]=Q;J)L
37: if Z[J]=P;J)S
38: next J
39: int(abs(L+S)/2))V
40: (X[L]+X[S])/2)C
41: 275)M
42: fmt 9,"The Center Point",f9.2," Is the Pair",f15.3,f15.5
43: for I=1 to M
44: X[I]-C)X[I]
45: next I
46: min(X[*]))E
47: 275)N
48: for J=1 to N
49: min(abs(E),abs(X[J])))E
50: next J
51: V)T
52: for J=1 to N
53: if abs(X[J])=E;J)T
54: next J
55: wrt 706.9,T,X[T],Z[T]
56: cll 'PLOT'
57: fmt 1,"Compare ",f15.5,"with  ",f15.5," FHHM is ",f15.5
58: fmt 3,"Compare ",e15.5,"with  ",e15.5," FWHM is ",e15.5
59: fmt 2,"Compare middle",f5.0,"with  ",2f4.0,/
60: wrt 706.1,Z[L],Z[S],abs(Z[L]-Z[S])
61: wrt 706.3,X[L],X[S],abs(X[L]-X[S])*\3
62: wrt 706.2,V,L,S
```

```
63: for J=1 to 8
64: Z[J]>H[J]
65: X[J]>G[J]
66: next J
67: for I=9 to 16
68: X[I+259]>G[I]
69: Z[I+259]>H[I]
70: next I
71: 16>P
72: 0>A>B>C>D>E>F>G
73: for I=1 to P
74: A+G[I]>A
75: E+H[I]>E
76: B+G[I]^2>B
77: F+H[I]*G[I]>F
78: next I
79: P>B[1,1];A>B[2,1]
80: A>B[1,2];B>B[2,2]
81: 2>O
82: E>B[1,3];F>B[2,3]
83: gsb "SOLVE"
84: for J=1 to 2
85: V[J]>A[J]
86: next J
87: 275>N
88: fmt 1,"The initial guesses are",3e20.11
89: wrt 706.1,A[1],A[2]
90: 1>r0
91: if A[2]>0;-1>r0
92: "begin":
93: fmt 4,"The Center Shift is",e12.5
94: cll 'REPLOT1'
95: -A[1]/A[2]>G
96: wrt 706.4,G
97: for J=1 to N
98: Z[J]-A[1]>Z[J]
99: next J
100: cll 'REPLOT'
101: 0>A[1]
102: 4>Q
103: abs((X[L]-X[S])*\3)>A[4]
104: (Z[L]+A[2]*A[4]/2/\3)*A[4]*4/9*\3>A[3]
105: 1>r1
106: .001>L
107: "Start":
108: gsb "SR2"
109: gsb "SR5"
110: for I=2 to Q
111: A[I]+V[I]>A[I]
112: next I
113: fmt 2,"Initial guesses are",6e20.11
114: wrt 706.2,A[1],A[2],A[3],A[4],A[5]
115: gsb "SR6"
116: S>Y
117: gsb "SR2"
118: gsb "SR5"
119: A[1]>T[1];A[2]>T[2]
120: for I=2 to Q
121: A[I]>T[I]
122: A[I]+V[I]>A[I]
123: next I
124: gsb "SR6"
125: fmt 7,3e15.6
126: wrt 706.7,Y,S,L
127: 1+r1>r1
128: if Y-S<0;10*L>L;gto "Add"
```

```
129: if Y-S>=0;.1*L>L;gto "Add"
130: "Add":
131: for I=2 to Q
132: T[I]>A[I];next I
133: "Ad":
134: if L<1e-5 or r1>3;gto "Re"
135: gto "Start"
136: "Re":
137: fmt 3,"Final Guesses are ",6e20.11
138: wrt 706.3,A[1],A[2],A[3],A[4]
139: cll 'RPLOT1'
140: fmt 5,"The Doppler Width is",f20.6
141: for J=1 to 4
142: A[J]>J[J]
143: next J
144: "Y">A$
145: if A$="N";gto +7
146: rread 1,1,X,Y,I,K,H$,M,O,F,C,E,K$,N,A,G,B,D,M$
147: rread 3,1,Z,W
148: rprt 2,Z,X,Y,I,K,H$,M,O,F,C,E,K$,N,A,G,B,D,M$,J[*]
149: rprt 3,1,Z+1,Y
150: fmt 9,2f6.1
151: wrt 706.9,"Count Z= ",Z,"Count Y= ",Y
152: S[1]+1>S[1];if S[1]<=S[2];gto "Starr"
153: end
154:
155:
156: "SR2":
157: for J=1 to Q
158: 0>P[J]
159: for K=1 to J
160: 0>R[J,K]
161: next K
162: next J
163: for I=1 to N
164: gsb "FDER1"
165: gsb "FUNC1"
166: for J=1 to Q
167: P[J]+(Z[I]-Z)*D[J]>P[J]
168: for K=1 to J
169: R[J,K]+D[J]*D[K]>R[J,K]
170: next K
171: next J
172: next I
173: for J=1 to Q
174: for K=1 to J
175: R[J,K]>R[K,J]
176: if J=K;R[J,K]+L>R[J,K]
177: next K
178: next J
179: ret
180:
181:
182:
183: "SR5":
184: for I=1 to Q
185: for J=1 to Q
186: P[I]>B[I,Q+1]
187: R[I,J]>B[I,J]
188: next J
189: next I
190: Q>0
191: gsb "SOLVE"
192: ret
193:
194:
```

```
"SR6":
0)S
for I=1 to Q
S+V[I]^2)S
next I
gsb "CHISQ1"
L*S+C)S
ret


"FDER1":
X[I])r6
r6*2/A[4])r8
1)D[1]
r6)D[2]
1+r8^2)r7
r0*8*r6/(A[4]*r7)^2)D[3]
-2*D[3]*A[3]/A[4]+16*A[3]*D[3]*r6*r6/(A[4]^3*r7))D[4]
ret


"FUNC1":
X[I])r4
A[3]/(1+4*r4^2/A[4]^2)^2)r5
A[1]+r4*A[2]+r0*r5*8*r4/A[4]^2)Z
ret


"CHISQ1":
0)C
for I=1 to N
gsb "FUNC1"
C+(Z[I]-Z)^2)C
ret
"FS1":
X[I])r1
A[1]+A[2]*r1)W
ret


"SOLVE":cfg 4;0)I
if (I+1)I)=0;gto +15
I-1)K;0)B
if (K+1)K))0;gto +3
if (abs(B[K,I]))T))B;T)B;K)R
gto -2
if B=0;sfg 4;dsp "DET=0";ret
I)J;if I=R;gto +2
B[I,J])T;B[R,J])B[I,J];T)B[R,J];jmp (J+1)J))0+1
I+1)J;B[I,I)B
B[I,J]/B)B[I,J];jmp (J+1)J))0+1
I)K
if (K+1)K))0;gto -11
I+1)J
B[K,J]-B[K,I]B[I,J])B[K,J];jmp (J+1)J))0+1
gto -3
if B[0,0]=0;0)B;gto -10
B[0,0+1]/B[0,0])V[0];0)I
if (I-1)I)<1;ret
0)H;0)K
B[I,K]V[K]+H)H;jmp (K-1)K)<=I
B[I,0+1]-H)V[I];gto -3


"INT":1)I
```

```
261: if (I+1)I)>N-1;gto +3
262: .5(X[I]-X[I-1])X)/(X[I+1]-X[I-1])H))K[I]
263: 2(((Z[I+1]-Z[I])/(X[I+1]-X[I])-(Z[I]-Z[I-1])/X)/H)T))S[I];3T)F[I];gto -2
264: 0)S[1])S[N];8-4^3)W
265: 0)U;2)I
266: W(-S[I]-K[I]S[I-1]-(.5-K[I])S[I+1]+F[I]))T
267: if (abs(T))H))>U;H)U
268: S[I]+T)S[I]
269: if I#N-1;I+1)I;gto -3
270: if U)=E;gto -5
271: 0)I)A
272: if (I+1)I)>N-1;ret
273: A+(.5(X[I+1]-X[I])H)(Z[I]+Z[I+1])-(1/24)H^3(S[I]+S[I+1])))A;gto -1
274:
275:
276: "PLOT":
277: max(Z[*]))H
278: max(X[*]))P
279: min(Z[*]))T
280: min(X[*]))U
281: scl prnd(U,5),prnd(P,5),T-1,H+1
282: xax T,1e6,prnd(U,5),prnd(P,5),3
283: yax prnd(U,5),1,T,H,1
284: "+")C$
285:
286: for J=1 to M
287: cll 'move'(X[J],Z[J])
288: cll 'plot'(X[J],Z[J])
289: next J
290: pen
291: ret
292: "REPLOT1":
293: for I=1 to N
294: gsb "FS1"
295: W)F[I]
296: cll 'move'(X[I],F[I])
297: cll 'plot'(X[I],F[I])
298: next I
299: pen
300: ret
301:
302: "RPLOT1":
303: for I=1 to N
304: gsb "FUNC1"
305: Z)F[I]
306: cll 'move'(X[I],F[I])
307: cll 'plot'(X[I],F[I])
308: next I
309: pen
310: ret
311:
312: "REPLOT":
313: for J=1 to N
314: cll 'move'(X[J],Z[J])
315: cll 'plot'(X[J],Z[J])
316: next J
317: pen
318: ret
319: "move":
320: pen;plt p1,p2,2;ret
321:
322: "plot":
323: cplt -.33,-.3
324: "+")C$
325: lbl C$
326: cplt -.67,.3;ret
```

APPENDIX 7 RESONANCE FUNCTIONS

This appendix calculates and tabulates the real and imaginary parts of the resonance functions[453,605] normally encountered in dealing with the electrostatic,dispersive, and inductive forces in the familiar ATC theory. The imaginary component was calculated by using the Hilbert transform (NAG routine D01AQF). The Hilbert transform is given as

$$f(k)= 1/\pi P.P.\int dk' f(k')/(k-k')$$

where P.P. stands for the principle part of the integral from the limits $-\infty$ to ∞.

Since $\chi=\chi'+ i\chi''$,the real and imaginary parts of the dispersion can be related by the Kramers-Kronig relationship:

$$\chi''= -1/\pi\int d\omega' \chi'(\omega)/ (\omega'-\omega)$$

$$=-2\omega/\pi \int d\omega' \chi'(\omega)/ (\omega'^2-\omega^2)$$

where the integration runs from 0 to ∞. The last form of the integral was used in the NAG routine D01AJF to obtain the imaginary part of the resonance function using the Hilbert transform. Most of these imaginary functions have not been tabulated in the previous literature but are needed in calculated certain forms of the dispersive, inductive and

electrostatic contributions to the pressure shift. The resonance functions are listed and plotted in this appendix. Note that there exist a very good polynomial approximation (484) to many of the resonance functions so that repeated evaluations of the modified Bessel functions can be avoided. The approximation for the $f_3(k)$ resoance function is given in the FORTRAN listing FE3 and FEI3 in Appendix 6.

Table A11 is a list of the real parts of the f(k) and g(k) resonance function as expressed in Leavitt(605).

$$f_1(k) = \tfrac{1}{4} k^4 [K_2(k)^2 + 4K_1(k)^2 + 3K_0(k)^2] ,$$

$$f_2(k) = \tfrac{1}{64} k^6 [K_3(k)^2 + 6K_2(k)^2 + 15K_1(k)^2 + 10K_0(k)^2] ,$$

$$f_3(k) = \tfrac{1}{2304} k^8 [K_4(k)^2 + 8K_3(k)^2 + 28K_2(k)^2 + 56K_1(k)^2 + 35K_0(k)^2] ,$$

$$f_4(k) = \tfrac{1}{840} k^3 e^{-k} [2(27k + 27k^2 + 14k^3 + 5k^4) K_0(k)$$
$$+ 3(45 + 45k + 33k^2 + 18k^3 + 5k^4) K_1(k) + 6(15k + 15k^2 + 6k^3 + k^4) K_2(k) + (105 + 105k + 45k^2 + 10k^3 + k^4) K_3(k)] ,$$

$$f_5(k) = \tfrac{1}{5040} k^4 e^{-k} [(27 + 27k + 39k^2 + 30k^3 + 35k^4) K_0(k) + 8(9k + 9k^2 + 10k^3 + 7k^4) K_1(k)$$
$$+ 4(15 + 15k + 27k^2 + 22k^3 + 7k^4) K_2(k) + 8(15k + 15k^2 + 6k^3 + k^4) K_3(k) + (105 + 105k + 45k^2 + 10k^3 + k^4) K_4(k)] ,$$

$$g_1(k) = \tfrac{1}{63} e^{-2k} (63 + 126k + 126k^2 + 84k^3 + 39k^4 + 12k^5 + 2k^6) ,$$

$$g_2(k) = \tfrac{1}{5031} e^{-2k} (5031 + 10\,062k + 10\,296k^2 + 7176k^3 + 3876k^4 + 1740k^5 + 668k^6 + 216k^7 + 54k^8) ,$$

$$g_3(k) = \tfrac{1}{225} e^{-2k} (225 + 450k + 414k^2 + 228k^3 + 81k^4 + 18k^5 + 2k^6) ,$$

$$g_4(k) = \tfrac{1}{3825} e^{-2k} (3825 + 7650k + 7848k^2 + 5496k^3 + 2892k^4 + 1176k^5 + 364k^6 + 80k^7 + 10k^8) ,$$

$$g_5(k) = \tfrac{1}{900} e^{-2k} (900 + 1800k + 1818k^2 + 1236k^3 + 627k^4 + 246k^5 + 74k^6 + 16k^7 + 2k^8) ,$$

$$g_6(k) = \tfrac{1}{321\,975} e^{-2k} (321\,975 + 643\,950k + 654\,642k^2 + 450\,684k^3 + 236\,988k^4$$
$$+ 102\,024k^5 + 37\,656k^6 + 12\,264k^7 + 3558k^8 + 900k^9 + 180k^{10}) ,$$

$$g_7(k) = \tfrac{1}{1575} e^{-2k} (1575 + 3150k + 3060k^2 + 1920k^3 + 870k^4 + 300k^5 + 80k^6 + 16k^7 + 2k^8) .$$

Table A11 Real and Imaginary Resonance Functions

REAL F(K) RESONANCE VALUES

K	F1(K)	F2(K)	F3(K)	F4(K)	F5(K)
0.1000	0.10052E+01	0.10013E+01	0.10006E+01	0.10018E+01	0.10002E+01
0.3000	0.10447E+01	0.10120E+01	0.10051E+01	0.10155E+01	0.10018E+01
0.5000	0.11023E+01	0.10359E+01	0.10146E+01	0.10407E+01	0.10051E+01
0.7000	0.11481E+01	0.10738E+01	0.10303E+01	0.10738E+01	0.10100E+01
0.9000	0.11624E+01	0.11222E+01	0.10533E+01	0.11099E+01	0.10169E+01
1.1000	0.11386E+01	0.11736E+01	0.10845E+01	0.11442E+01	0.10258E+01
1.3000	0.10798E+01	0.12187E+01	0.11237E+01	0.11716E+01	0.10370E+01
1.5000	0.99424E+00	0.12491E+01	0.11686E+01	0.11880E+01	0.10511E+01
1.7000	0.89176E+00	0.12587E+01	0.12159E+01	0.11905E+01	0.10685E+01
1.9000	0.78168E+00	0.12446E+01	0.12608E+01	0.11774E+01	0.10897E+01
2.1000	0.67157E+00	0.12070E+01	0.12985E+01	0.11484E+01	0.11152E+01
2.3000	0.56691E+00	0.11484E+01	0.13244E+01	0.11046E+01	0.11451E+01
2.5000	0.47123E+00	0.10728E+01	0.13351E+01	0.10477E+01	0.11795E+01
2.7000	0.38638E+00	0.98515E+00	0.13286E+01	0.98055E+00	0.12176E+01
2.9000	0.31300E+00	0.89028E+00	0.13042E+01	0.90583E+00	0.12584E+01
3.1000	0.25082E+00	0.79271E+00	0.12627E+01	0.82650E+00	0.13002E+01
3.3000	0.19906E+00	0.69624E+00	0.12058E+01	0.74529E+00	0.13411E+01
3.5000	0.15661E+00	0.60383E+00	0.11362E+01	0.66462E+00	0.13788E+01
3.7000	0.12224E+00	0.51763E+00	0.10569E+01	0.58648E+00	0.14110E+01
3.9000	0.94731E-01	0.43899E+00	0.97113E+00	0.51243E+00	0.14356E+01
4.1000	0.72933E-01	0.36862E+00	0.88192E+00	0.44356E+00	0.14507E+01
4.3000	0.55816E-01	0.30669E+00	0.79209E+00	0.38059E+00	0.14549E+01
4.5000	0.42482E-01	0.25301E+00	0.70399E+00	0.32386E+00	0.14471E+01
4.7000	0.32169E-01	0.20707E+00	0.61954E+00	0.27344E+00	0.14272E+01
4.9000	0.24246E-01	0.16823E+00	0.54016E+00	0.22918E+00	0.13952E+01
5.1000	0.18195E-01	0.13574E+00	0.46683E+00	0.19075E+00	0.13518E+01
5.3000	0.13599E-01	0.10883E+00	0.40012E+00	0.15773E+00	0.12983E+01
5.5000	0.10126E-01	0.86726E-01	0.34027E+00	0.12961E+00	0.12359E+01
5.7000	0.75129E-02	0.68725E-01	0.28725E+00	0.10589E+00	0.11664E+01
5.9000	0.55561E-02	0.54174E-01	0.24080E+00	0.86023E-01	0.10916E+01
7.0000	0.10048E-02	0.13490E-01	0.81849E-01	0.25135E-01	0.65875E+00
9.0000	0.38084E-04	0.82503E-03	0.80167E-02	0.19983E-02	0.15925E+00
11.0000	0.12525E-05	0.39963E-04	0.56996E-03	0.12166E-03	0.24011E-01
13.0000	0.37440E-07	0.16530E-05	0.32564E-04	0.61510E-05	0.25970E-02
15.0000	0.10448E-08	0.61012E-07	0.15880E-05	0.27135E-06	0.22012E-03
17.0000	0.27682E-10	0.20663E-08	0.68699E-07	0.10786E-07	0.15495E-04
19.0000	0.70439E-12	0.65432E-10	0.27060E-08	0.39488E-09	0.94266E-06
21.0000	0.17351E-13	0.19631E-11	0.98847E-10	0.13527E-10	0.50986E-07
23.0000	0.41615E-15	0.56343E-13	0.33941E-11	0.43861E-12	0.25035E-08
25.0000	0.97619E-17	0.15584E-14	0.11067E-12	0.13582E-13	0.11338E-09

IMAGINARY F(K) RESONANCE VALUES

K	F1(K)	F2(K)	F3(K)	F4(K)	F5(K)
0.1000	0.43792E-03	0.89647E-06	0.86333E-09	0.12679E-03	-0.72534E-15
0.3000	0.16558E-01	0.30040E-03	0.25821E-05	0.32789E-02	0.42338E-10
0.5000	0.72721E-01	0.36083E-02	0.85445E-04	0.14463E-01	0.10718E-07
0.7000	0.17030E+00	0.16287E-01	0.74936E-03	0.37553E-01	0.35793E-06
0.9000	0.29446E+00	0.45712E-01	0.34442E-02	0.74904E-01	0.44535E-05
1.1000	0.42619E+00	0.96873E-01	0.10794E-01	0.12716E+00	0.30835E-04
1.3000	0.54927E+00	0.17057E+00	0.26254E-01	0.19327E+00	0.14477E-03
1.5000	0.65289E+00	0.26347E+00	0.53347E-01	0.27069E+00	0.51551E-03
1.7000	0.73171E+00	0.36925E+00	0.94791E-01	0.35579E+00	0.14929E-02
1.9000	0.78466E+00	0.48028E+00	0.15184E+00	0.44439E+00	0.36830E-02
2.1000	0.81360E+00	0.58899E+00	0.22397E+00	0.53222E+00	0.79943E-02
2.3000	0.82199E+00	0.68894E+00	0.30899E+00	0.61537E+00	0.15632E-01
2.5000	0.81397E+00	0.77539E+00	0.40336E+00	0.69062E+00	0.28024E-01
2.7000	0.79365E+00	0.84541E+00	0.50275E+00	0.75553E+00	0.46694E-01
2.9000	0.76478E+00	0.89777E+00	0.60254E+00	0.80862E+00	0.73085E-01
3.1000	0.73050E+00	0.93268E+00	0.69840E+00	0.84919E+00	0.10837E+00
3.3000	0.69333E+00	0.95137E+00	0.78657E+00	0.87732E+00	0.15332E+00
3.5000	0.65520E+00	0.95573E+00	0.86413E+00	0.89366E+00	0.20812E+00
3.7000	0.61749E+00	0.94804E+00	0.92913E+00	0.89928E+00	0.27237E+00
3.9000	0.58115E+00	0.93066E+00	0.98050E+00	0.89553E+00	0.34508E+00
4.1000	0.54676E+00	0.90590E+00	0.10180E+01	0.88389E+00	0.42469E+00
4.3000	0.51467E+00	0.87583E+00	0.10422E+01	0.86587E+00	0.50925E+00
4.5000	0.48502E+00	0.84227E+00	0.10540E+01	0.84292E+00	0.59651E+00
4.7000	0.45781E+00	0.80674E+00	0.10547E+01	0.81637E+00	0.68410E+00
4.9000	0.43295E+00	0.77047E+00	0.10459E+01	0.78740E+00	0.76969E+00
5.1000	0.41031E+00	0.73439E+00	0.10293E+01	0.75700E+00	0.85110E+00
5.3000	0.38972E+00	0.69920E+00	0.10063E+01	0.72602E+00	0.92642E+00
5.5000	0.37100E+00	0.66539E+00	0.97867E+00	0.69512E+00	0.99411E+00
5.7000	0.35395E+00	0.63329E+00	0.94762E+00	0.66482E+00	0.10530E+01
5.9000	0.33842E+00	0.60307E+00	0.91436E+00	0.63549E+00	0.11023E+01
7.0000	0.27345E+00	0.47113E+00	0.72859E+00	0.49938E+00	0.12023E+01
9.0000	0.20508E+00	0.33692E+00	0.49689E+00	0.35281E+00	0.95094E+00
11.0000	0.16517E+00	0.26584E+00	0.37851E+00	0.27604E+00	0.67944E+00
13.0000	0.13860E+00	0.22093E+00	0.30948E+00	0.22854E+00	0.52205E+00
15.0000	0.11952E+00	0.18947E+00	0.26320E+00	0.19564E+00	0.42956E+00
17.0000	0.10511E+00	0.16606E+00	0.22952E+00	0.17127E+00	0.36801E+00
19.0000	0.93834E-01	0.14790E+00	0.20374E+00	0.15243E+00	0.32317E+00
21.0000	0.84759E-01	0.13338E+00	0.18330E+00	0.13739E+00	0.28866E+00
23.0000	0.77294E-01	0.12148E+00	0.16667E+00	0.12509E+00	0.26113E+00
25.0000	0.71045E-01	0.11156E+00	0.15286E+00	0.11484E+00	0.23858E+00

IMAGINARY G(K) RESONANCE VALUES

K	G1(K)	G2(K)	G3(K)	G4(K)	G5(K)	G6(K)	G7(K)
0.1000	0.26576	0.38313	0.44514	0.11834	0.16736	0.65616	0.28641
0.3000	0.80854	0.11676	0.13236	0.36402	0.50796	0.20236	0.85752
0.5000	0.13802	0.20197	0.21672	0.63603	0.86571	0.35794	0.14235
0.7000	0.19877	0.30186	0.29546	0.94953	0.12503	0.55303	0.19807
0.9000	0.26264	0.42828	0.36676	0.13160	0.16687	0.82153	0.25254
1.1000	0.32817	0.59695	0.42917	0.17419	0.21244	0.12168	0.30532
1.3000	0.39326	0.82586	0.48174	0.22278	0.26162	0.18164	0.35596
1.5000	0.45556	0.11323	0.52400	0.27679	0.31387	0.27235	0.40393
1.7000	0.51280	0.15294	0.55595	0.33510	0.36823	0.40627	0.44868
1.9000	0.56308	0.20234	0.57798	0.39612	0.42340	0.59693	0.48965
2.1000	0.60501	0.26117	0.59086	0.45797	0.47790	0.85741	0.52631
2.3000	0.63779	0.32827	0.59554	0.51867	0.53020	0.11985	0.55821
2.5000	0.66121	0.40170	0.59315	0.57632	0.57884	0.16273	0.58498
2.7000	0.67552	0.47895	0.58488	0.62918	0.62253	0.21454	0.60639
2.9000	0.68139	0.55722	0.57188	0.67587	0.66027	0.27488	0.62239
3.1000	0.67975	0.63366	0.55526	0.71536	0.69134	0.34274	0.63302
3.3000	0.67169	0.70565	0.53604	0.74703	0.71538	0.41659	0.63852
3.5000	0.65836	0.77095	0.51508	0.77065	0.73232	0.49451	0.63922
3.7000	0.64091	0.82783	0.49315	0.78633	0.74235	0.57431	0.63555
3.9000	0.62041	0.87514	0.47085	0.79445	0.74591	0.65369	0.62803
4.1000	0.59781	0.91224	0.44868	0.79564	0.74360	0.73044	0.61720
4.3000	0.57396	0.93905	0.42700	0.79067	0.73612	0.80252	0.60364
4.5000	0.54954	0.95590	0.40609	0.78040	0.72425	0.86821	0.58790
4.7000	0.52512	0.96344	0.38615	0.76572	0.70878	0.92612	0.57051
4.9000	0.50113	0.96261	0.36729	0.74750	0.69047	0.97531	0.55196
5.1000	0.47790	0.95446	0.34956	0.72660	0.67004	0.10152	0.53269
5.3000	0.45565	0.94014	0.33300	0.70376	0.64815	0.10456	0.51308
5.5000	0.43453	0.92080	0.31758	0.67967	0.62536	0.10668	0.49346
5.7000	0.41463	0.89754	0.30328	0.65492	0.60217	0.10790	0.47407
5.9000	0.39598	0.87138	0.29002	0.62998	0.57899	0.10830	0.45514
7.0000	0.31436	0.71038	0.23300	0.50337	0.46282	0.99803	0.36432
9.0000	0.22877	0.48690	0.17266	0.35265	0.32565	0.70978	0.26009
11.0000	0.18181	0.36847	0.13834	0.27290	0.25272	0.51640	0.20370
13.0000	0.15162	0.30015	0.11583	0.22477	0.20842	0.40904	0.16874
15.0000	0.13031	0.25483	0.99759	0.19191	0.17809	0.34241	0.14452
17.0000	0.11436	0.22201	0.87670	0.16776	0.15575	0.29603	0.12657
19.0000	0.10195	0.19697	0.78225	0.14916	0.13852	0.26137	0.11268
21.0000	0.91994	0.17714	0.70636	0.13435	0.12480	0.23430	0.10158
23.0000	0.83831	0.16103	0.64399	0.12227	0.11359	0.21249	0.92507
25.0000	0.77009	0.14765	0.59181	0.11221	0.10425	0.19450	0.84936

REAL G(K) RESONANCE VALUES

K	G1(K)	G2(K)	G3(K)	G4(K)	G5(K)	G6(K)	G7(K)
0.1000	1.00000	1.00047	0.99840	1.00052	1.00020	1.00033	0.99943
0.2000	0.99993	1.00187	0.99362	1.00205	1.00078	1.00133	0.99771
0.3000	0.99966	1.00425	0.98571	1.00454	1.00172	1.00301	0.99486
0.4000	0.99898	1.00764	0.97474	1.00792	1.00294	1.00539	0.99086
0.5000	0.99762	1.01208	0.96083	1.01206	1.00438	1.00849	0.98571
0.6000	0.99530	1.01761	0.94411	1.01682	1.00591	1.01233	0.97943
0.7000	0.99174	1.02429	0.92476	1.02202	1.00743	1.01697	0.97200
0.8000	0.98666	1.03214	0.90297	1.02745	1.00878	1.02244	0.96343
0.9000	0.97981	1.04116	0.87894	1.03291	1.00981	1.02878	0.95372
1.0000	0.97098	1.05134	0.85291	1.03814	1.01035	1.03603	0.94288
1.1000	0.96000	1.06261	0.82513	1.04290	1.01023	1.04425	0.93090
1.2000	0.94677	1.07487	0.79585	1.04694	1.00928	1.05345	0.91781
1.3000	0.93123	1.08797	0.76532	1.05002	1.00731	1.06368	0.90360
1.4000	0.91338	1.10170	0.73380	1.05189	1.00417	1.07493	0.88830
1.5000	0.89328	1.11582	0.70156	1.05233	0.99971	1.08721	0.87193
1.6000	0.87102	1.13005	0.66884	1.05114	0.99379	1.10048	0.85453
1.7000	0.84674	1.14408	0.63587	1.04814	0.98630	1.11468	0.83612
1.8000	0.82063	1.15755	0.60288	1.04320	0.97715	1.12975	0.81675
1.9000	0.79288	1.17011	0.57009	1.03619	0.96628	1.14555	0.79648
2.0000	0.76373	1.18141	0.53767	1.02704	0.95363	1.16195	0.77536
2.1000	0.73342	1.19111	0.50580	1.01570	0.93922	1.17878	0.75347
2.2000	0.70220	1.19888	0.47464	1.00217	0.92304	1.19584	0.73087
2.3000	0.67031	1.20440	0.44431	0.98648	0.90515	1.21291	0.70765
2.4000	0.63800	1.20744	0.41494	0.96867	0.88561	1.22973	0.68390
2.5000	0.60552	1.20776	0.38661	0.94885	0.86451	1.24606	0.65970
2.6000	0.57307	1.20519	0.35941	0.92711	0.84196	1.26162	0.63515
2.7000	0.54087	1.19961	0.33339	0.90361	0.81808	1.27614	0.61035
2.8000	0.50912	1.19096	0.30859	0.87850	0.79301	1.28935	0.58540
2.9000	0.47797	1.17921	0.28504	0.85195	0.76691	1.30098	0.56039
3.0000	0.44759	1.16440	0.26275	0.82414	0.73993	1.31078	0.53542
3.1000	0.41810	1.14659	0.24172	0.79527	0.71224	1.31852	0.51059
3.2000	0.38961	1.12592	0.22196	0.76552	0.68399	1.32399	0.48597
3.3000	0.36220	1.10254	0.20342	0.73511	0.65535	1.32702	0.46167
3.4000	0.33595	1.07664	0.18610	0.70421	0.62649	1.32745	0.43775
3.5000	0.31092	1.04843	0.16994	0.67302	0.59756	1.32517	0.41429
3.6000	0.28712	1.01815	0.15493	0.64171	0.56869	1.32010	0.39136
3.7000	0.26459	0.98606	0.14100	0.61047	0.54005	1.31219	0.36903
3.8000	0.24334	0.95242	0.12811	0.57944	0.51174	1.30143	0.34733
3.9000	0.22334	0.91748	0.11622	0.54878	0.48389	1.28785	0.32632
4.0000	0.20459	0.88153	0.10526	0.51862	0.45661	1.27150	0.30603
4.1000	0.18707	0.84482	0.09520	0.48907	0.42999	1.25247	0.28651
4.2000	0.17074	0.80760	0.08597	0.46026	0.40411	1.23088	0.26777
4.3000	0.15556	0.77012	0.07752	0.43226	0.37905	1.20686	0.24982
4.4000	0.14148	0.73262	0.06981	0.40516	0.35486	1.18059	0.23269
4.5000	0.12846	0.69529	0.06277	0.37902	0.33158	1.15223	0.21638

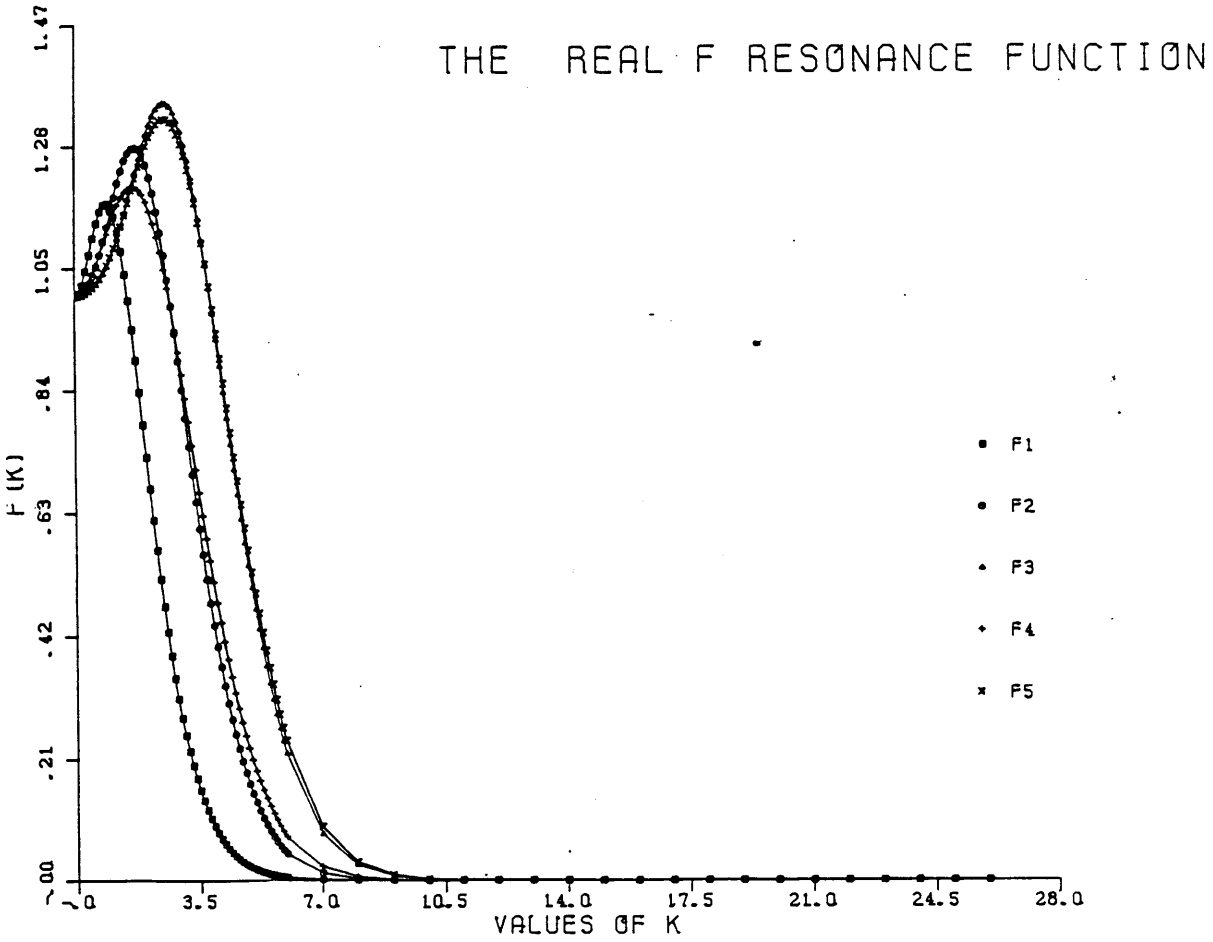

Figure A6 Resonance Functions

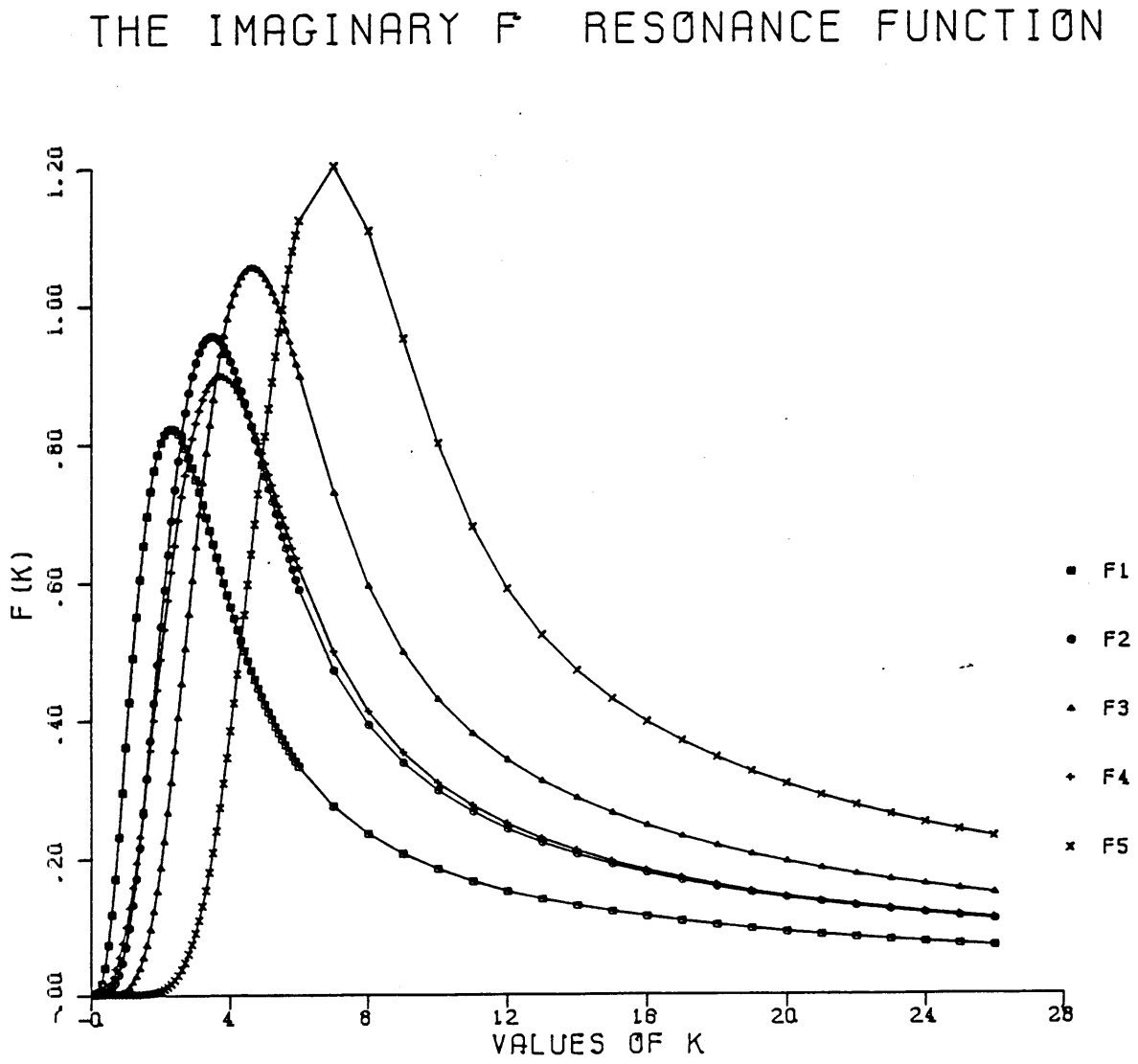

Figure A7 Resonance Functions

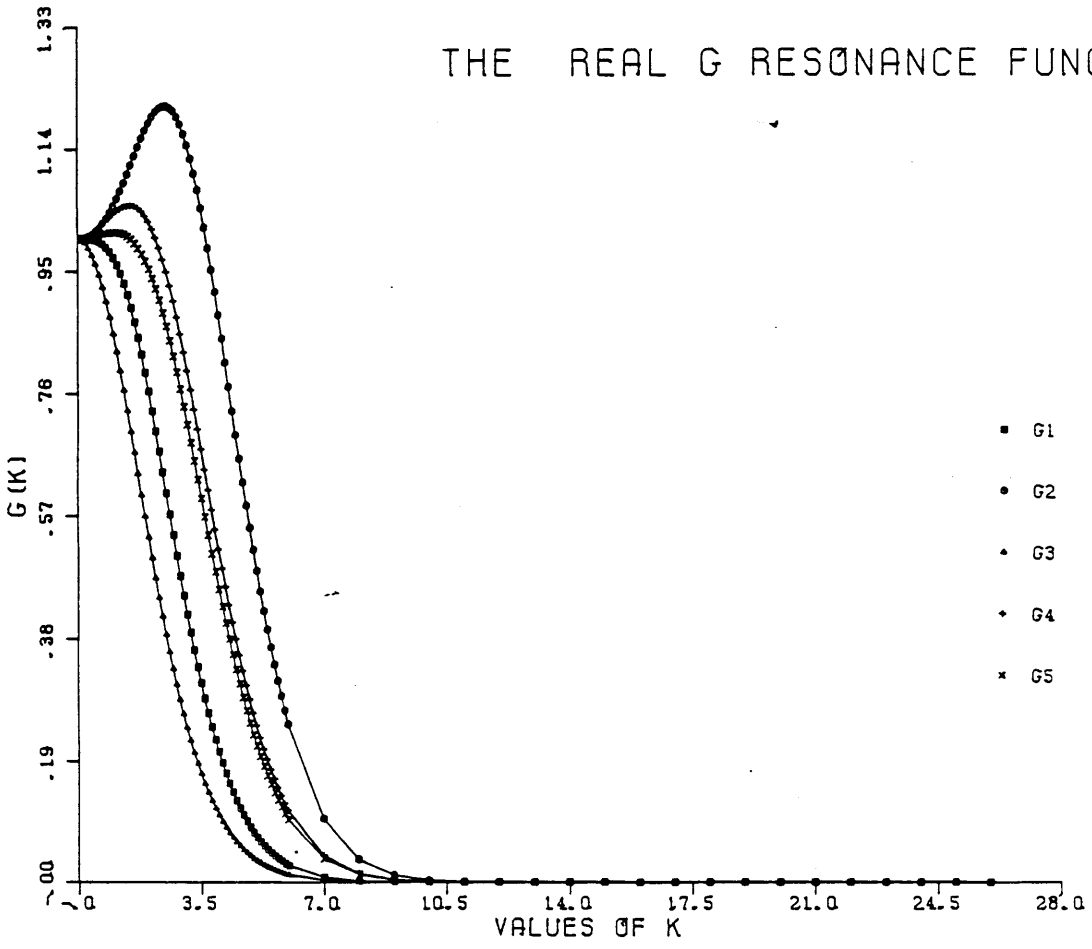

Figure A8 Resonance Functions

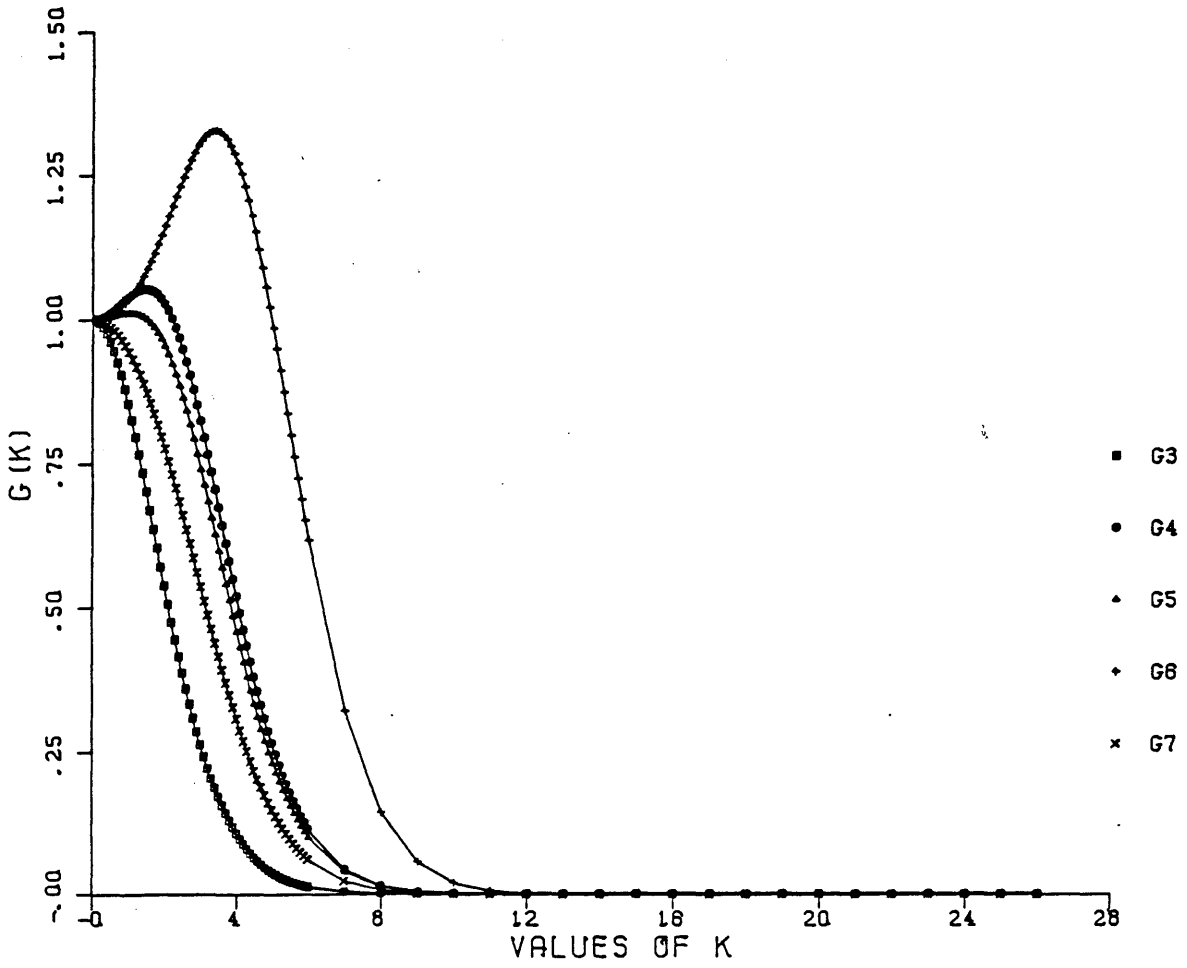

Figure A9 Resonance Functions

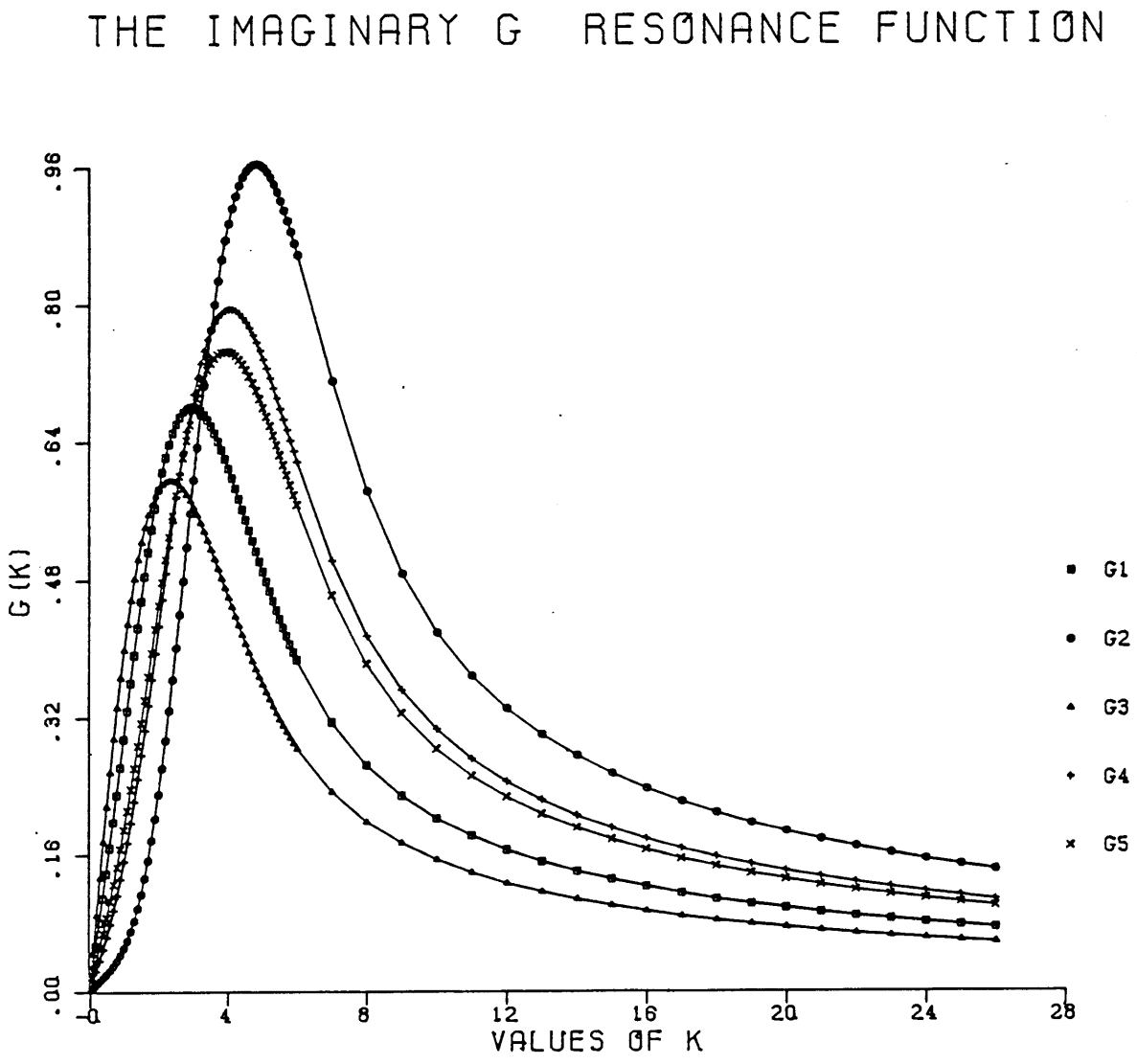

Figure A10 Resonance Functions

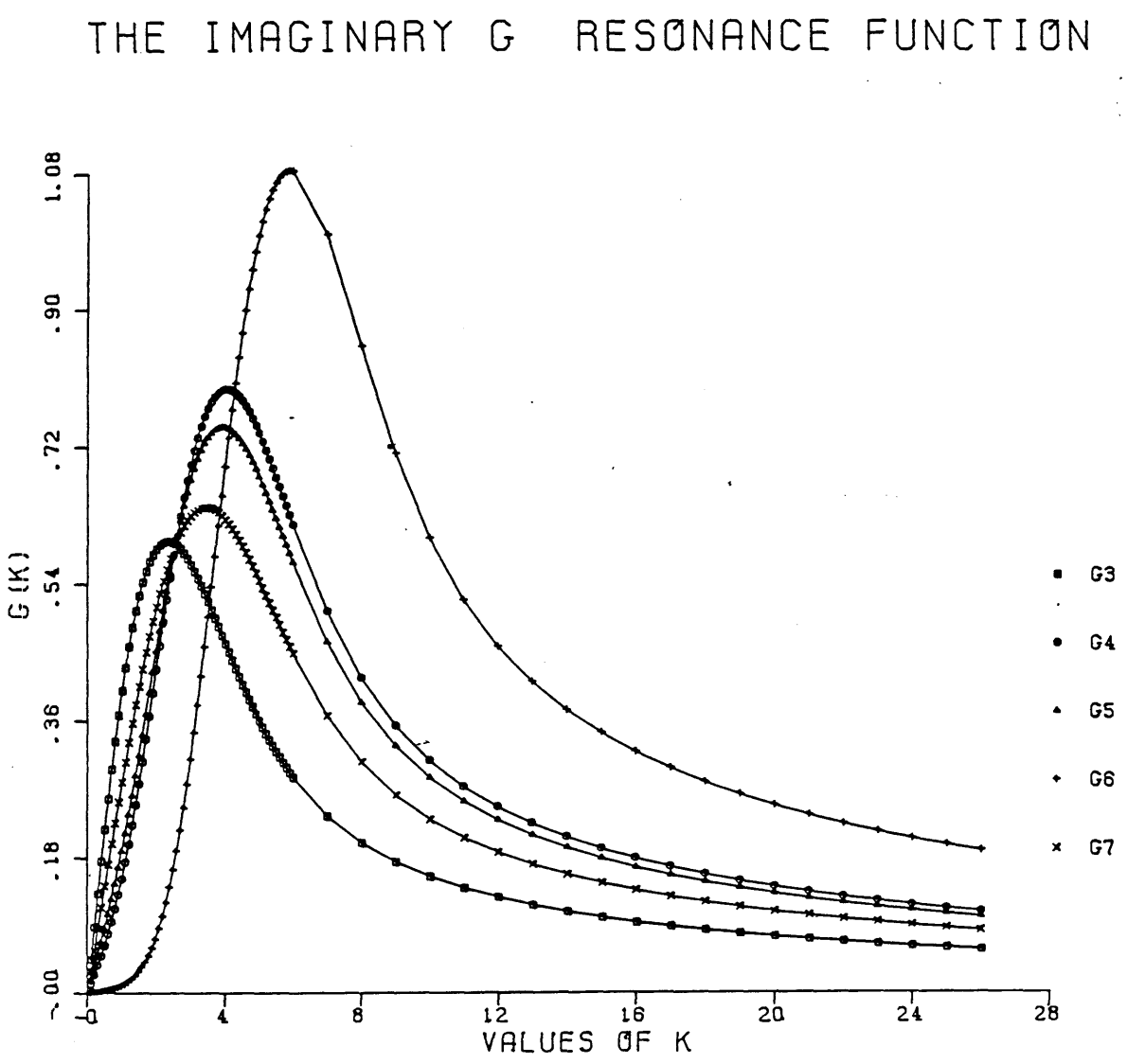

Figure A11 Resonance Functions